ICES REPORT ON OCEAN CLIMATE 2019

Volume 350 I December 2020

ICES COOPERATIVE RESEARCH REPORT

RAPPORT
DES RECHERCHES
COLLECTIVES

ICES INTERNATIONAL COUNCIL FOR THE EXPLORATION OF THE SEA
CIEM CONSEIL INTERNATIONAL POUR L'EXPLORATION DE LA MER

International Council for the Exploration of the Sea
Conseil International pour l'Exploration de la Mer

H. C. Andersens Boulevard 44–46
DK-1553 Copenhagen V
Denmark
Telephone (+45) 33 38 67 00
Telefax (+45) 33 93 42 15
www.ices.dk
info@ices.dk

Series editor: Emory Anderson
Prepared under the auspices of the ICES Working Group for Oceanic Hydrography (WGOH)

http://doi.org/10.17895/ices.pub.7537
ISBN number: 978-87-7482-310-0
ISSN number: 2707-7144 I © 2020 International Council for the Exploration of the Sea

ICES Cooperative Research Report

Volume 350 I December 2020

ICES Report on Ocean Climate 2019

Prepared by the ICES Working Group on Oceanic Hydrography (WGOH)

Editors

Cesar González-Pola • Karin M. H. Larsen • Paula Fratantoni • Agnieska Beszczynska-Möller

Recommended format for purpose of citation:

González-Pola, C., Larsen, K. M. H., Fratantoni, P., and Beszczynska-Möller, A. (Eds.). 2020. ICES Report on Ocean Climate 2019. ICES Cooperative Research Reports No. 350. 136 pp. https://doi.org/10.17895/ices.pub.7537

ICES International Council for the Exploration of the Sea
CIEM Conseil International pour l'Exploration de la Mer

Contents

I Foreword

Like most of the world, the International Council for the Exploration of the Sea (ICES) Working Group on Ocean Hydrography (WGOH) was challenged by the onset of the COVID-19 global pandemic in 2020. The pandemic forced the last-minute cancelation of our annual in-person meeting, which was replaced by a much shorter video conference. In addition, many collaborative tasks were significantly delayed by the unusual working conditions, which affected contributors to different degrees.

The production of the 2019 ICES Report on Ocean Climate (IROC 2019) suffered as well. Many of the improvements planned for the report were postponed in order to focus on the timely publication of an updated issue. Despite the exceptional circumstances, the majority of the regional time-series were updated, highlighting the strong commitment of the international community to this collaborative product. With this publication, the IROC 2019 finally sees the light, providing marine scientists and environmental managers with the interpretation of current ocean conditions for the North Atlantic.

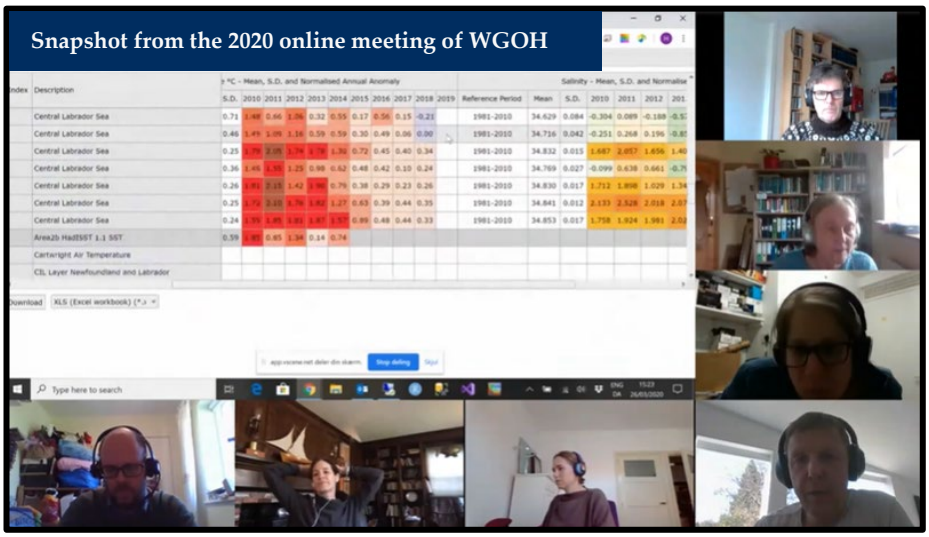

Snapshot from the 2020 online meeting of WGOH

The IROC 2019 was written by the following members of WGOH: Jon Albretsen (IMR, Bergen); Wilken-Jon von Appen (AWI, Bremerhaven); Barbara Berx (MSS, Aberdeen); Agnieszka Beszczynska-Möller (IOPAN, Sopot); Léon Chafik (MISU, Stockholm); Boris Cisewski (TI-SF, Bremerhaven); Caroline Cusack (Marine Institute, Galway); Frédéric Cyr (DFO, St. John's); Magnus Danielsen (MFRI, Iceland); Damien Desbruyères (IFREMER/LOPS, Brest); Stephen Dye (CEFAS, Lowestoft); Almudena Fontán (AZTI, San Sebastián); Paula Fratantoni (NOAA, Woods Hole); Peter Galbraith (DFO, Mont-Joli); César González-Pola (IEO, Gijón); Hjálmar Hátún (FAMRI, Tórshavn); David Hebert (DFO, Dartmouth); Jenny Hindson (MSS, Aberdeen); N. Penny Holliday (NOC, Southampton); Randi Ingvaldsen (IMR, Bergen); Sam Jones (SAMS, Oban); Holger Klein (BSH, Hamburg); Manuela Köllner (BSH, Hamburg); Nicolas Kolodziejczyk (UBO, Brest); Karin Margretha H. Larsen (FAMRI, Tórshavn);

K. Latarius (BSH, Hamburg); C. Layton (DFO, Dartmouth); Taavi Liblik (TalTech, Tallinn); Johanna Linders (SMHI, Göteborg); Peter Loewe (BSH, Hamburg); Kieran Lyons (Marine Institute, Galway); Kjell-Arne Mork (IMR, Bergen); Sólveig R. Ólafsdóttir (MFRI, Iceland); Hjalte Parner (ICES, Cophenhagen); Ricardo Sánchez-Leal (IEO, Cadiz); Tim Smyth (PML, Plymouth); Alexander Trofimov (PINRO, Murmansk); Victor Valencia (AZTI, San Sebastián); Pedro Vélez-Belchí (IEO, Tenerife); Tycjan Wodzinowski (MIR-PIB, Gdynia) and Svein Østerhus (NORCE, Bergen).

For a list of authors by section, including full affiliation and contact details, see Annex 2. For a complete list of data providers, see Annex 1.

Technical assistance for the assembly of the IROC 2019 was provided by Rocio Graña (IEO, Spain).

1 Introduction

Long time-series of ocean properties are rare in the surface ocean and even more uncommon in the deep ocean. The North Atlantic region is unique, having a relatively large number of locations where oceanographic data have been collected repeatedly for multiple years or decades. The longest records extend back more than a century.

The ICES Report on Ocean Climate (IROC) combines decades of ocean observations across the North Atlantic ICES region to describe the current status of sea temperature, salinity, and atmospheric conditions as well as observed trends and recent variability. The IROC is produced by ICES Working Group on Oceanic Hydrography (WGOH; Gonzalez-Pola *et al*., 2019).

Section 1 synthesizes information from a selection of the longest available time-series into an overview of changes across the ICES Area. The main focus of this report is the observed variability of the upper ocean (upper 1000 m), and a summary of upper ocean conditions is provided in Section 2. Section 2.3 provides gridded fields constructed by optimal analysis of Argo float data, distributed by the Coriolis data centre in France, while Section 2.4 continues to provide an estimate of the Subpolar Gyre Index. Sections 4 and 5 contain short regional summaries on the variability of North Atlantic upper ocean, and intermediate and deep waters, respectively. A new section has been added this year, reporting for the first time on the conditions in the Gulf of St Lawrence (Section 4.4). The focus of the report is on temperature and salinity measurements. However, additional complementary datasets are included throughout the report, such as sea level pressure (SLP), air temperature, and ice cover.

The data presented here represent an accumulation of knowledge collected by many individuals and institutions over decades of observations. A list of contacts for each dataset is provided in Annex 1, including e-mail addresses for the individuals who provided information and the data centres at which full archives are maintained. Much of the data included in this report, and additional data, are available to download via the IROC web tool[1]. A more detailed overview of a particular region and a full description of some of the datasets used to develop the time-series presented in this report can be found in the WGOH annual meeting reports[2].

WGOH met via video conference on March 26, 2020 to review oceanographic conditions in the North Atlantic in 2019. The following highlights emerged from the joint analysis of the available hydrographic time-series.

1.1 Highlights for the North Atlantic in 2019

- The fresh anomaly that has persisted within the eastern North Atlantic sector in recent years has weakened in the Subpolar Gyre, while strengthening in the subtropical region to the south and Arctic regions to the north.

[1] http://ocean.ices.dk/iroc

[2] https://www.ices.dk/community/groups/Pages/WGOH.aspx

- A large-scale latitudinal pattern of warming–cooling–warming, observed in the surface layers (0–100 m) of the subtropical, subpolar, and Nordic seas since 2002, reversed to a pattern of cooling–warming–cooling in 2018/2019, as corroborated by the array of Argo profiling floats.
- Bottom ocean temperatures in the western North Atlantic were warmer than normal along the northeast US continental shelves, including record highs in the deep basins of the central Scotian Shelf and in the deep channels of the Gulf of St Lawrence. Surface temperatures were above normal on the Labrador Shelf, near-to-above-normal on the Newfoundland Shelf, western Scotian Shelf and northeast US continental shelves, and below normal in the Gulf of St Lawrence and on the eastern Scotian Shelf.
- The eastern subpolar North Atlantic remained fresh in 2019, but is recovering from the extreme minimum values observed in 2016/2017. Surface waters were anomalously warm during summer throughout the region.
- Widespread freshening continued in the northeast Subtropical Gyre, including in the Bay of Biscay, West Iberia, Gulf of Cadiz, and Canaries regions. This was coupled with continued cooling in most areas, and particularly in the southern regions. In contrast, the temperature stabilized above 300 m in Biscay and Western Iberia. The upwelling system extending from the Gulf of Cadiz to the Canaries was the coldest and freshest observed since 2000.
- While still warmer than average, Atlantic Water (AW) tended to be cooler and fresher along its route through the Norwegian Sea and into the Barents Sea and Fram Strait. In contrast, deep waters in the Greenland Sea were warmer and saltier than in previous years.
- Conditions in the North Sea and Baltic Sea were generally warm. Fresh conditions were observed in the North Sea, due to fresher inflows from the North Atlantic, and in the eastern Baltic Sea. Severe hypoxic conditions were prevalent in the Baltic Sea, similar to those observed in 2018.

1.2 Highlights for the North Atlantic atmosphere in winter 2018/2019

- The North Atlantic Oscillation (NAO) index remained positive for a sixth successive winter. The index was the strongest observed since 2015, but the associated pattern of sea level pressure was most evident in the eastern areas of the region.
- Air temperatures were relatively warm across Europe, the Nordic seas, and the Labrador Sea.
- Colder-than-normal winter air temperatures were limited to a region stretching from Nova Scotia to east of the Flemish Cap.
- Windspeeds across the region were generally lower than average, particularly east of Newfoundland, from south of Cape Farewell to the northern North Sea, and in a band stretching across the Nordic seas from Scoresby Sund in Greenland to the North Cape of Norway.

1.3 Beyond 2019: initial assessment of the North Atlantic atmosphere in winter 2019/2020

- The NAO index for winter 2019/2020 will likely be more strongly positive than the previous winter, with a more typical NAO sea level pressure anomaly pattern extending across the region.
- A region from the west of Ireland, and across the UK, North Sea and southern Scandinavia will experience particularly strong southwesterly winds throughout December–February.
- Experimental seasonal forecasts predict that, in summer 2020, surface temperatures are likely to be warmer than average across the region. However, the surface temperatures in the Subpolar Gyre to the west of Ireland and Iceland, and southeast of Cape Farewell, are more likely to be near average than in other areas.

Waves in the Atlantic. Photo: Tomasz Szumski, Marine Institute, Galway, Ireland

2 Summary of upper ocean conditions in 2019

This section summarizes conditions in the upper layers of the North Atlantic during 2019 using data from (i) a selected set of sustained observations, (ii) gridded sea surface temperature (SST) data, and (iii) gridded vertical profiles of temperature and salinity from Argo floats.

2.1 *In situ* stations and sections

Normalized anomalies (see Information Box 2.1) are provided for *in situ* section and station data in the summary tables and figures for ease of trend comparison across regions (Figure 2.1 and Figure 2.2, Table 2.1).

Information Box 2.1 - Definitions

Sustained observations or time-series: regular measurements of ocean temperature and salinity made over 10–100 years. Most measurements are taken 1–4 times a year, but some are made more frequently.

Anomalies: the mathematical differences between each individual measurement and the average value of temperature, salinity, or other variables at each location and time. Positive anomalies in temperature and salinity imply warm or saline conditions, respectively; negative anomalies imply cool or fresh conditions.

Normalized anomalies: anomalies that have been normalized by dividing the values for a given year by the standard deviation (s.d.) of the 1981–2010 data (or the closest time-period available). A value of +2 thus represents temperature or salinity data measuring 2 s.d. higher than normal.

Seasonal cycle: the short-term changes at the surface of the ocean brought about by the passing of the seasons – the ocean surface is cold in winter and warms through spring and summer. Temperature and salinity changes caused by the seasonal cycle are usually much greater than the prolonged year-to-year changes we describe here.

Fog over Cape Spear. Photo: Frédéric Cyr, Fisheries and Oceans Canada

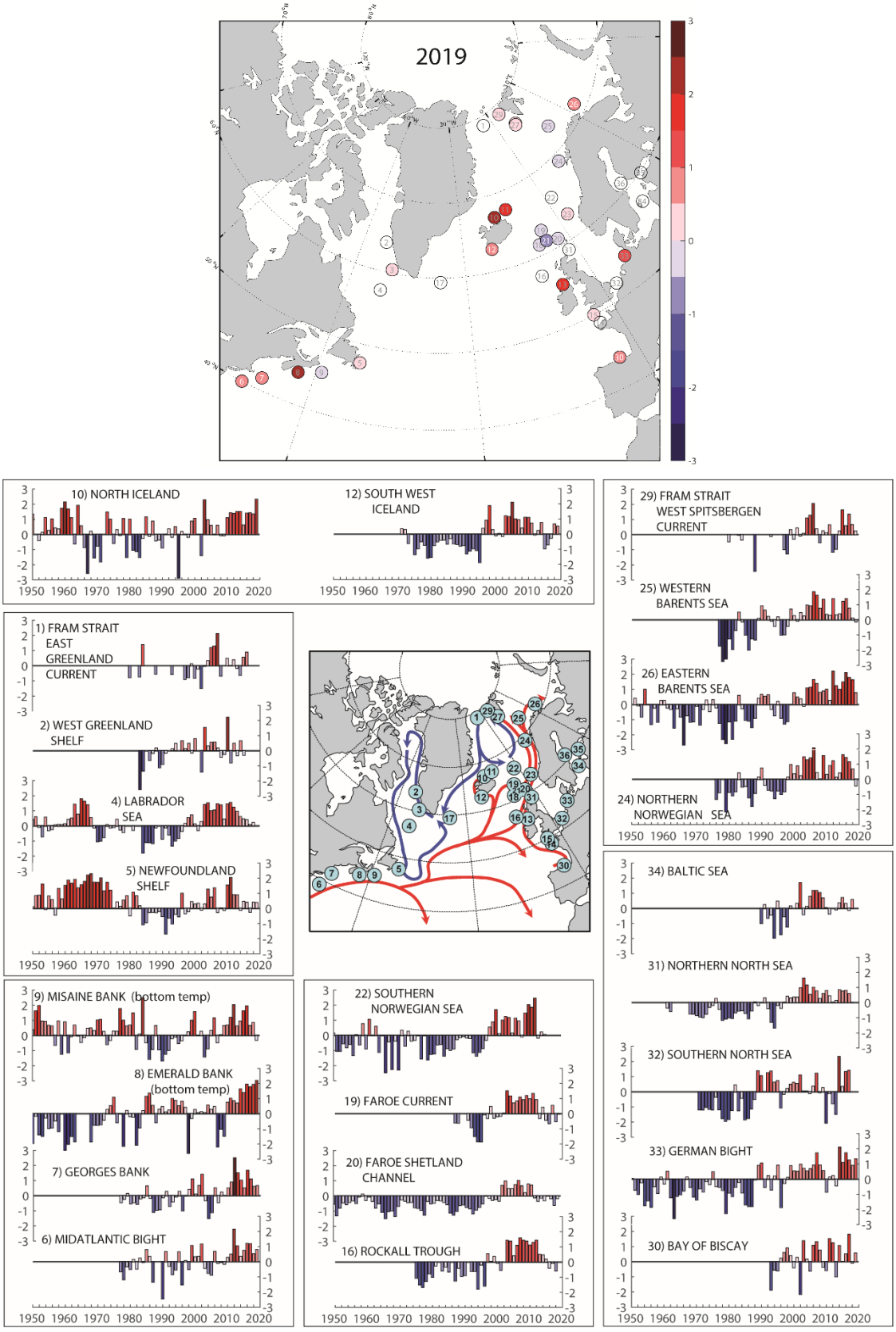

Figure 2.1. Upper ocean temperature anomalies at selected locations across the North Atlantic. The anomalies are normalized with respect to the standard deviation (s.d.; e.g. a value of +2 indicates 2 s.d. above normal). Upper panel: map of the conditions in 2019. Lower panels: time-series of normalized anomalies at each of the selected stations. Colour intervals: 0.5 s.d.; red: positive/warm; blue: negative/cool. More details can be found in Section 4.

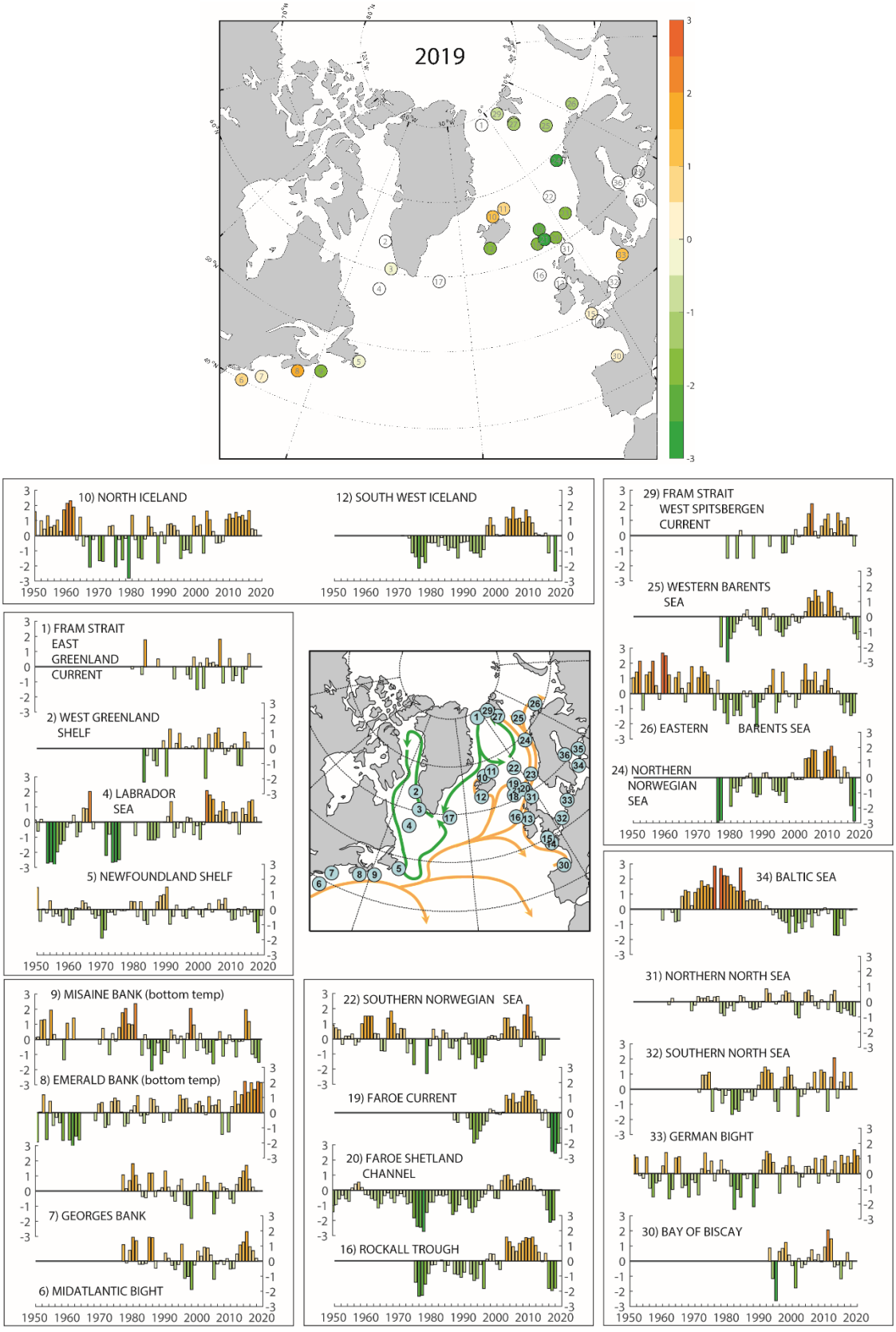

Figure 2.2. Upper ocean salinity anomalies at selected locations across the North Atlantic. The anomalies are calculated relative to a long-term mean and normalized with respect to the s.d. (e.g. a value of +2 indicates 2 s.d. above normal). Upper panel: map of conditions in 2019. Lower panels: time-series of normalized anomalies at each of the selected stations. Colour intervals: 0.5 s.d.; orange: positive/saline; green: negative/fresh. More details can be found in Section 4.

Table 2.1. Changes in temperature (upper panel) and salinity (lower panel) at selected stations in the North Atlantic region during the past decade, 2010–2019. The index numbers on the left can be used to cross-reference each point with information in figures 2.1 and 2.2 and in Table 2.2. Unless specified, these are upper-layer anomalies. The anomalies are normalized with respect to the s.d. (e.g. a value of +2 indicates that the data observation of temperature or salinity for that year was 2 s.d. above normal). Blank boxes indicate that data were unavailable for a particular year at the time of publication. Note that no salinity data are available for station 13. Colour intervals: 0.5 s.d.; red: warm; blue: cold; orange: saline; green: fresh.

	2010	2011	2012	2013	2014	2015	2016	2017	2018	2019
1	0.49	0.01	0.40	-0.18	-0.64	0.58	0.91			
2	2.22	-0.81	0.50	-0.33	0.67	-0.30				
3	1.15	0.57	1.28	0.18	0.83	-0.47	-0.41			0.39
4	1.46	1.55	1.25	0.98	0.62	0.48	0.42	0.10	0.24	
5	1.55	2.04	0.91	0.90	-0.14	0.46	0.40	-0.26	0.42	0.39
6	0.29	0.51	2.15	1.06	0.36	0.76	1.22	1.19	0.54	0.81
7	0.51	0.90	2.51	1.51	1.03	0.51	1.68	1.11	0.62	0.67
8	0.76	1.02	0.87	0.71	1.64	1.40	1.95	1.79	1.94	2.21
9	0.69	1.20	2.05	0.64	0.96	1.63	1.95	0.67	0.87	-0.33
10	1.10	1.43	1.38	1.52	1.52	0.63	1.41	1.44	1.36	2.34
11	0.30	1.03	0.64	0.79	1.89	0.89	1.15	2.62	2.78	1.99
12	1.11	0.73	-0.07	0.24	0.77	-0.98	-0.72	-0.28	0.67	0.54
13	0.40	1.04	0.62	0.42	1.72	0.73	1.59	1.96	0.42	1.96
14	-1.95	0.06	0.38	-0.83	1.58	1.04	0.61			
15	0.02	0.05	0.59	-0.26	0.70	0.25	0.19	0.63	0.56	0.16
16	1.13	1.31	1.45	0.52	0.48	0.20	-0.41	-0.09	-0.59	
17	0.55	0.69	-0.29		-0.01	-0.43	-0.75		-0.43	
18	0.73	1.29	-0.03	0.04	0.56	0.13	-0.02	0.22	-0.60	-0.19
19	0.98	1.34	0.93	-0.32	0.42	-0.45	-0.66	0.55	-0.54	-0.04
20	0.80	0.72	-0.14	-0.36	-0.15	-0.32	0.03	-0.19	-0.62	-0.18
21	1.23	0.83	0.31	0.41	0.50	0.15	-0.12	0.13	-0.07	-0.78
22	2.05	1.87	2.47	-0.19	0.23	0.06				
23	0.86	1.12	0.44	0.55	0.33	0.52	0.38	0.76	-0.55	0.41
24	0.33	0.91	1.23	0.14	0.43	1.63	1.43	1.16	0.69	-0.45
25	0.37	0.30	1.41	0.33	0.41	1.24	1.41	0.78	0.13	-0.13
26	1.02	0.28	2.20	1.25	1.00	1.50	2.12	1.79	1.64	0.79
27	0.40	1.02	0.90	0.03	1.12	0.95	1.42	1.50	1.46	0.30
28	-0.01		0.60	-0.23	1.17		0.88	2.35	1.10	0.41
29	0.13	0.65	-1.17	-0.97	0.25	1.64	0.59	1.36	0.66	0.25
30	-0.60	1.53	1.25	-1.00	1.07	0.02	0.53	1.82	-0.10	0.59
31	0.80	0.45	0.04	0.15	0.86	0.77	0.81	0.61	0.00	
32	-2.08	-0.12	-0.79	-1.49	2.35	0.36	1.35	1.42		
33	-0.87	0.15	0.24	-0.45	2.12	1.11	1.75	1.27	0.91	1.35
34	0.05	-0.38		-0.11	0.37	0.72	0.33	-0.14	0.59	
35	0.38	-0.36	0.74	1.08	0.07	0.29	1.07	0.99	0.97	
36	-0.53	-1.16	-0.17	0.02	1.46	1.42	1.60	1.16	0.54	

	2010	2011	2012	2013	2014	2015	2016	2017	2018	2019
1	0.54	-0.93	-0.60		-1.08	-0.17	0.86			
2	0.17	0.31	-1.12	-1.15	1.07	0.42				
3	0.07	1.20	-0.14	0.80	-0.47	0.15	-1.28			-0.03
4	-0.10	0.64	0.66	-0.80	0.91	0.51	1.36	1.47	0.33	
5	-0.70	-0.65	0.08	-0.42	0.18	-0.31	-0.16	-0.79	-1.52	-0.38
6	-0.53	-0.49	0.47	1.07	1.26	1.95	0.95	0.70	0.19	0.74
7	-0.52	-0.81	0.44	0.89	1.33	1.70	0.78	0.26	0.00	0.00
8	0.42	1.42	0.56	1.19	2.07	1.35	1.98	1.54	2.05	1.99
9	0.29	-0.13	-1.16	-0.13	-0.11	1.96	1.18	-0.98	-1.21	-1.52
10	1.43	1.16	1.54	1.24	1.34	1.01	1.65	0.44	0.38	1.20
11	0.99	1.13	1.55	1.22	-0.04	0.90	1.06	1.01	-0.10	0.84
12	1.24	0.85	0.17	0.06	-0.04	0.17	-1.14	-3.22	-2.35	-1.61
13										
14	-0.11	0.87	1.17	0.11	-0.54	0.46	0.36			
15	0.46	1.31	0.76	0.79	0.46	1.43	0.85	1.37	-0.23	0.14
16	1.49	1.57	1.02	0.58	-0.05	0.50	-1.82	-1.97	-1.80	
17	1.39	0.85	0.46		0.35	0.71	0.49		-0.08	
18	1.51	1.39	0.30	0.45	-0.09	0.31	-1.53	-2.28	-2.77	-1.76
19	1.41	1.19	0.85	0.22	-0.49	0.20	-0.97	-2.55	-2.67	-2.02
20	0.83	0.76	0.30	-0.04	0.06	-0.34	-1.30	-2.12	-1.98	-1.58
21	1.43	0.91	0.79	0.20	-0.42	-0.45	-1.43	-2.35	-2.76	-2.95
22	2.23	1.45	0.48	0.18	-1.42	-1.08				
23	1.82	1.53	0.69	0.30	-0.63	0.17	-0.97	-2.57	-3.07	-1.90
24	1.85	2.07	1.40	0.49	-0.36	0.71	0.34	-1.86	-2.87	-3.24
25	1.73	1.60	0.68	0.35	0.55	-0.20	0.23	-0.10	-1.12	-1.50
26	0.88	1.60	0.34	-0.02	0.16	-0.74	-1.28	-0.56	-1.46	-1.28
27	0.95	1.74	1.71	0.98	1.57	0.67	1.02	1.02	0.26	-0.98
28	0.82		1.45	1.00	1.74		1.21	0.95	-0.74	-1.05
29	1.08	1.42	0.45	0.18	1.50	0.97	0.76	1.18	0.05	-0.69
30	0.93	2.05	1.47	-0.38	-0.26	-1.18	-0.32	0.56	-0.52	0.03
31	-0.53	0.47	0.74	-0.65	-0.76	-0.43	-0.58	-0.86	-0.95	
32	-1.47	0.80	2.07	-0.60	0.47	1.13	0.20	1.13		
33	-0.15	0.25	0.82	-0.58	1.21	0.67	1.15	0.70	1.57	1.19
34	0.08	-0.29	0.03	-1.71	-1.74	-0.61	-1.08		-0.06	
35	0.78	-0.85	-1.12	0.57	0.20	-0.27	-0.04	0.76	0.93	
36	2.17	2.18	1.03	0.40	1.01	-0.65	-0.20	1.33	2.40	

Table 2.2. Details of the datasets included in figures 2.1 and 2.2 and in Table 2.1. Blank boxes indicate that no information was available for the area at the time of publication. T: temperature, S: salinity. Some data are calculated from an average of more than one station; in such cases, the latitudes (Lat.) and longitudes (Lon.) presented here represent a nominal midpoint along that section.

Index	Description	Section	Measurement depth	Reference period	Lat.	Lon.	Mean T	s.d.	Mean S	s.d.
1	Fram Strait East Greenland Current	4.21	50–500 m	1983–2010	78.83	-6.00	0.69	0.57	34.650	0.135
2	Fylla Section – Station 4 – Greenland Shelf	4.1	0–50 m	1983–2010	63.88	-53.37	2.64	1.10	33.162	0.392
3	Cape Desolation Section – Station 3 – Greenland Shelf	4.1	75–200 m	1983–2010	60.47	-50.00	5.72	0.66	34.923	0.062
4	Central Labrador Sea	4.2	15–50 m	1981–2010	57.07	-50.92	4.68	0.69	34.635	0.176
5	Station 27 – Newfoundland Shelf Temperature – Canada	4.3	0–175 m	1981–2010	47.55	-52.59	0.33	0.39	31.946	0.166
6	NE US continental shelf – Northern Middle Atlantic Bight	4.5	1–30 m	1981–2010	40.00	-71.00	11.36	0.94	32.710	0.430
7	NE US continental shelf – Northwest Georges Bank	4.5	1–30 m	1981–2010	41.50	-68.30	10.00	0.79	32.580	0.270
8	Emerald Basin – Central Scotian Shelf – Canada	4.4	250 m (Near Bottom)	1981–2010	44.00	-63.00		0.83		0.151
9	Misaine Bank – Northeast Scotian Shelf – Canada	4.4	100 m (Near Bottom)	1981–2010	45.00	-59.00		0.63		0.134
10	Siglunes Station 2–4 – North Iceland – North Icelandic Irminger Current – Spring	4.6	50–150 m	1981–2010	67.00	-18.00	3.41	0.98	34.859	0.108
11	Langanes Station 2–6 – Northeast Iceland – East Icelandic Current – Spring	4.6	0–50 m	1981–2010	67.50	-13.50	1.22	0.61	34.729	0.067
12	Selvogsbanki Station 5 – Southwest Iceland – Irminger Current – Spring	4.6	0–200 m	1981–2010	63.00	-21.47	7.88	0.47	35.187	0.049
13	Point 33 – Astan	4.10	5 m	1998–2010	48.78	-3.94	12.79	0.34	35.206	0.112
14	Western Channel Observatory (WCO) – E1 – UK	4.10	0–40 m	1981–2010	50.03	-4.37	12.43	0.93	35.200	0.100
15	Malin Head Weather Station	4.11	Surface	1981–2010	55.37	-7.34	10.25	0.57		
16	Ellett Line – Rockall Trough – UK (Section Average)	4.12	30–800 m	1981–2010	56.75	-11.00	9.35	0.28	35.351	0.036
17	Central Irminger Sea Sub Polar Mode Water	4.15	200–400 m	1991–2010	59.40	-36.80	4.35	0.53	34.900	0.031

Table 2.2 (continued)

Index	Description	Section	Measurement depth	Reference period	Lat.	Lon.	Mean T	s.d.	Mean S	s.d.
18	Faroe Bank Channel – West Faroe Islands	4.16	Upper Layer High Salinity Core	1988–2010	61.40	-8.30	8.80	0.36	35.302	0.043
19	Faroe Current – North Faroe Islands (Modified North Atlantic Water)	4.16	Upper Layer High Salinity Core	1987–2010	63.00	-6.00	8.11	0.39	35.249	0.043
20	Faroe Shetland Channel – Shetland Shelf (North Atlantic Water)	4.16	Upper Layer High Salinity Core	1981–2010	61.00	-3.00	9.95	0.47	35.398	0.051
21	Faroe Shetland Channel – Faroe Shelf (Modified North Atlantic Water)	4.16	Upper Layer High Salinity Core	1981–2010	61.50	-6.00	8.32	0.54	35.256	0.055
22	Ocean Weather Station Mike	4.19	50 m	1981–2010	66.00	2.00	7.71	0.44	35.176	0.036
23	Southern Norwegian Sea – Svinøy Section – Atlantic Water	4.19	50–200 m	1981–2010	63.00	3.00	8.04	0.39	35.234	0.039
24	Central Norwegian Sea – Gimsøy Section – Atlantic Water	4.19	50–200 m	1981–2010	69.00	12.00	6.89	0.34	35.154	0.031
25	Fugløya – Bear Island Section – Western Barents Sea – Atlantic Inflow	4.19	50–200 m	1981–2010	73.00	20.00	5.55	0.46	35.078	0.035
26	Kola Section – Eastern Barents Sea	4.20	0–200 m	1981–2010	71.50	33.50	4.22	0.52	34.771	0.056
27	Greenland Sea section – West of Spitsbergen 76.5N	4.19	200 m	1996–2010	76.50	10.50	3.19	0.61	35.058	0.043
28	Northern Norwegian Sea – Sorkapp Section – Atlantic Water	4.19	50–200 m	1981–2010	76.33	10.00	4.08	0.60	35.073	0.038
29	Fram Strait – West Spitsbergen Current	4.21	50–500 m	1983–2010	78.83	7.00	3.11	0.69	35.027	0.038
30	Santander Station 6 (Shelf Break) – Bay of Biscay – Spain	4.7	0–30 m	1993–2010	43.71	-3.78	15.74	0.32	35.460	0.160
31	Fair Isle Current Water (Waters entering North Sea from Atlantic)	4.17	0–100 m	1981–2010	59.00	-2.00	9.93	0.61	34.874	0.132
32	Section Average – Felixstowe – Rotterdam – 52 N	4.17	Surface	1981–2010	52.00	3.00		0.72		0.212
33	North Sea – Helgoland Roads	4.17	Surface	1981–2010	54.18	7.90	10.26	0.75	32.096	0.568
34	Baltic Proper – East of Gotland – Baltic Sea	4.18	Surface T Surface S	1990–2010 1987–2010	57.50	19.50	9.27	1.03	7.172	0.196
35	Baltic – LL7 – Baltic Sea	4.18	70 m	1991–2010	59.51	24.50	3.97	0.73	7.961	0.666
36	Baltic – SR5 – Baltic Sea	4.18	110 m	1991–2010	61.05	19.35	3.27	0.58	6.428	0.141

2.2 Sea surface temperature

Satellites have been measuring SST for approximately 40 years, which has allowed the creation of gridded datasets. Figure 2.3 shows seasonal SST anomalies for 2019 extracted from the Optimum Interpolation SST dataset version 2 (OISST.v2) provided by the National Oceanic and Atmospheric Administration (NOAA; USA) – Cooperative Institute for Research in Environmental Sciences (CIRES; USA) Climate Diagnostics Center. The data may be less reliable at high latitudes, where *in situ* data are sparse and satellite data are hindered by cloud cover. Regions with > 50% ice cover over the averaging period appear blank.

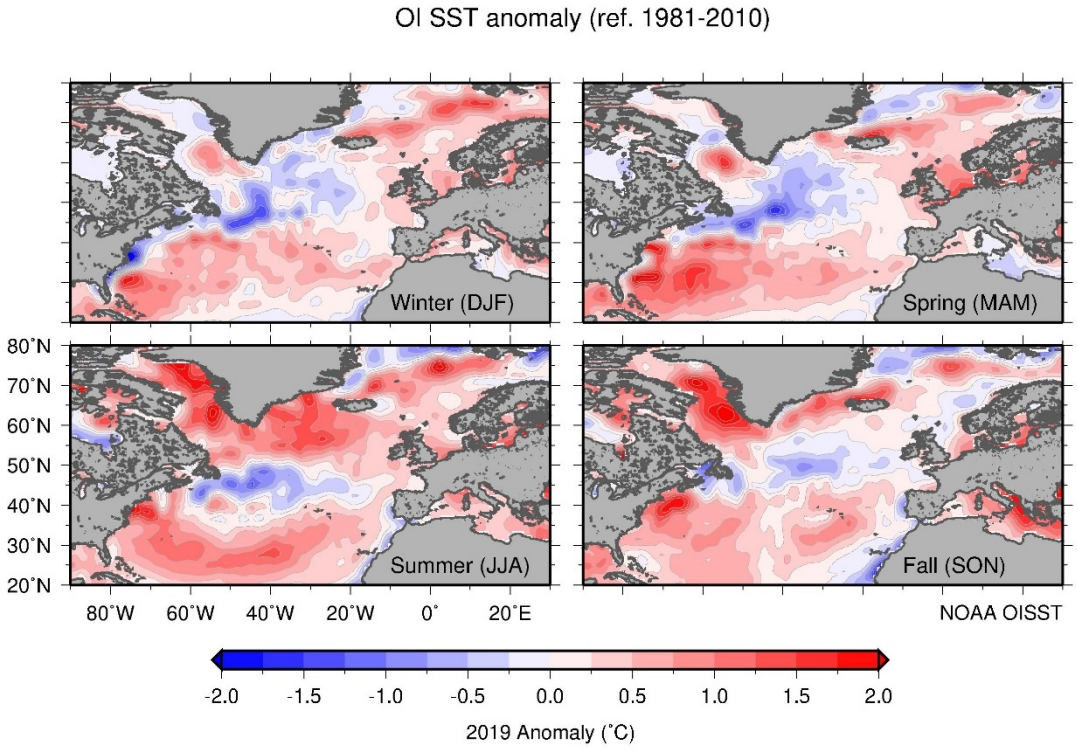

Figure 2.3. Maps of seasonal sea surface temperature anomalies (°C) over the North Atlantic for 2019 from the NOAA OISST.v2 dataset provided by the NOAA-CIRES Climate Diagnostics Center, USA. The data are produced on a 1° grid from a combination of satellite and *in situ* temperature data. The colour-coded temperature scale is the same in all panels, and the anomaly is calculated with respect to mean conditions for 1981–2010. Regions with ice cover for > 50% of the averaging period appear blank

2.3 ARGO gridded temperature and salinity fields

N. Kolodziejczyk and D. Desbruyères

The ARGO network of profiling floats has been set up to monitor large-scale global ocean variability (http://www.argo.ucsd.edu). Argo data are transmitted in real time and rapidly made available by the two Global Data Assembly Centres (Argo-GDAC). Delayed-mode data undergo expert calibration and are delivered later. In the North Atlantic, temperature and salinity conditions have been adequately described over the upper 2000 m since 2002. The dataset is thus suitable for an overview of oceanographic conditions in this basin and provides the general context for the data collected at stations and sections, mostly located at the periphery of the basin.

2.3.1 ISAS: Gridded temperature and salinity fields

Temperature and salinity gridded fields are estimated on a regular 0.5° grid using the *In Situ* Analysis System (ISAS; Gaillard *et al.*, 2016). The dataset used for generating ISAS gridded fields is downloaded from the Coriolis Argo GDAC1. It should be noted that Coriolis assembles many types of data transmitted in real time, merging the Argo dataset with data collected by the Global Telecommunications System[1] (GTS), such as data from moorings and CTDs, and data on marine animals. However, the Argo dataset remains the main contributor to the ISAS gridded fields in the open ocean. The optimal interpolation (OI) procedure is as follows: the *in-situ* temperature and salinity profiles are vertically interpolated on 152 standard levels between the surface and 2000 m depth. The horizontal mapping to produce gridded fields is performed at each standard level independently. The mapping method is based on an optimal estimation algorithm and includes a horizontal smoothing through specified covariance scales. The results presented here were produced with the last version of ISAS. The reference state used in the OI process was computed as the mean of a 2005–2012 analysis (using ISAS13; Gaillard *et al.*, 2016) and the *a priori* variances were computed from the same dataset. Two ISAS gridded temperature and salinity products are used:

- For the period 2002–2015, ISAS15 product is used (Kolodziejczyk *et al.*, 2017). For this period, only delayed mode *in situ* data are used, and ISAS15 product is the highest quality product in Delayed Mode. Moreover, data are preprocessed, and extra quality control is applied to *in situ* profiles before they are included in the analysis.
- The last years of the analysed series, i.e. 2016–2019, use the Near Real Time (NRT) dataset prepared by Coriolis at the end of each month from real-time data. For this period, data are interpolated using ISAS v6 including only real-time mode data (i.e. only from automatic QC processing). Because Argo salinity data require advanced quality checks and validation, NRT salinity fields have to be used with caution. Therefore, time-series of monthly

[1] https://www.wmo.int/pages/prog/www/TEM/GTS/index_en.html

salinity anomalies are not considered herein, and the focus is rather made on their seasonally averaged and annually averaged patterns.

The ISAS interpolated fields are used to compute seasonal to interannual maps of temperature and salinity anomalies averaged within an upper layer (0–100 m depth) and an intermediate layer (800–1200 m depth). Note that the temperature and salinity anomalies throughout this section are computed using the climatological ISAS15 fields (2006–2015). This approach differs from the Argo sections of previous IROC reports, which described anomalies referenced to the long-term pre-Argo era (World Ocean Atlas, 2005). In order to compute temperature and salinity anomalies, the climatological monthly temperature and salinity fields are removed from each monthly ISAS field over the period 2002–2019. Note that the temperature and salinity fields are blanked in regions with water depths exceeding 1000 m, where the Argo coverage is either too sparse or unavailable. A criterion of > 80% of explained variance provided by the objective analysis was chosen to further discard the undersampled grid points, which are mostly found within shallow shelf regions. The seasonal time-windows are defined as winter (December–March), spring (April–June), summer (July–September), and autumn (October–December).

IN THE NORTH ATLANTIC SECTOR, THE SURFACE LAYER (0–100 M) OF THE SUBTROPICAL OCEAN, SUBPOLAR OCEAN, AND THE NORDIC SEAS HAD BEEN TRENDING WARMER, COOLER, AND WARMER, RESPECTIVELY SINCE 2002. IN THE MOST RECENT YEARS (2018–2019), THOSE TRENDS HAVE REVERSED, PRESUMABLY SIMULTANEOUSLY, AND A COOLING – WARMING – COOLING LATITUDINAL PATTERN IS NOW BEING OBSERVED BY THE ARRAY OF ARGO PROFILING FLOATS.

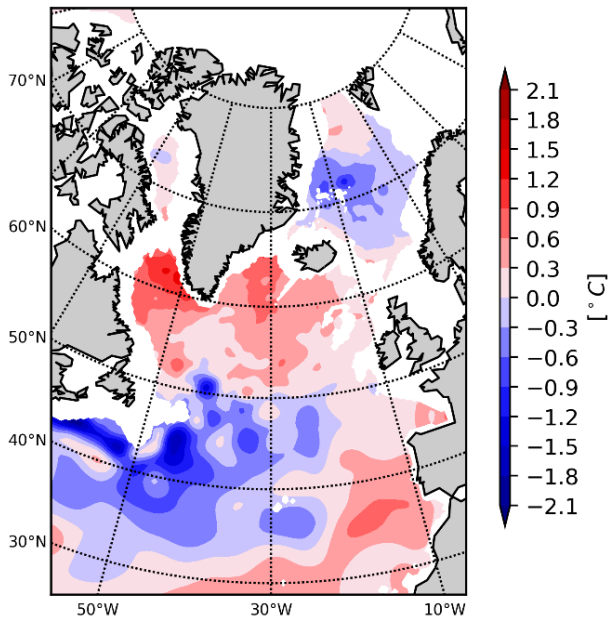

Figure 2.4. 2019 minus 2018 temperature difference in the upper layer (0–100 m).

2.3.2 Surface layers

Seasonal cycle

The broad pattern of temperature and salinity anomalies in 2019 (with respect to the 2006–2015 climatological mean) shows a relatively warm and salty subtropical region, a relatively cold and fresh subpolar region, and relatively warm and salty Nordic seas. However, there were significant subregional and intra-annual changes in each of these regions (Figure 2.6). The warm subtropical anomalies appear to originate in winter in a confined area encompassing the Gulf Stream path south of the Grand Banks. They subsequently spread eastward and southward in the subsequent seasons following the general anticyclonic circulation of the gyre. A similar, although less marked, pattern is observed for salinity. In the subpolar region, negative temperature anomalies were significant within two centres of action, the Irminger Sea and the Newfoundland area, and peaked in both regions in spring, after which the former faded away, while the latter started to propagate eastward toward the Iceland Basin. Interestingly, a warm and salty anomaly gradually developed in the northern Labrador Sea, reaching a peak amplitude in autumn while being advected southward by the Labrador Current along the upper North American continental slope. In the Nordic seas, warm anomalies primarily developed within the western portion of the domain (Iceland and Greenland seas), while cold anomalies developed along the eastern margin (Norwegian Sea). This asymmetric pattern is less visible for salinity, but still present (salty in the west and fresh in the east). The 2019 seasonal cycles of temperature and salinity, averaged within five boxes representative of the main area of the North Atlantic domain, are put into context relative to the long-term 2002–2019 context in Figure 2.7.

- In the Eastern Atlantic (Figure 2.5 and Figure 2.7), the 2019 surface layer temperature exhibited a seasonal cycle similar to the 2006–2015 average. In contrast, during 2014–2018, the surface layer was consistently cooler than normal throughout the year.
- In the Irminger Sea (Figure 2.5 and Figure 2.7), the surface layer temperature was cooler than normal throughout the seasonal cycle, especially during winter season. Nevertheless, during summer, temperatures were warmer than during the 2014–2018 period.
- The surface layer temperatures in the Labrador Sea (Figure 2.5 and Figure 2.7) were warmer than normal over the whole seasonal cycle.
- The surface layer in the Greenland Sea (Figure 2.5 and Figure 2.7) was also warmer than normal throughout the year, comparable to the period 2015–2018.
- The surface layer of the Gulf Stream region (Figure 2.5 and Figure 2.7) was warmer than normal. However, the warming tendency appears to have declined in comparison to the four previous warmest years (2015–2018).

In conclusion, the observed 2019 seasonal cycle supports the reversal of the warming–cooling–warming pattern observed in the subtropical-subpolar-Nordic seas region

(Gulf Stream, and Irminger and Greenland seas), towards a more average situation (referred to the 2006–2015 climatology).

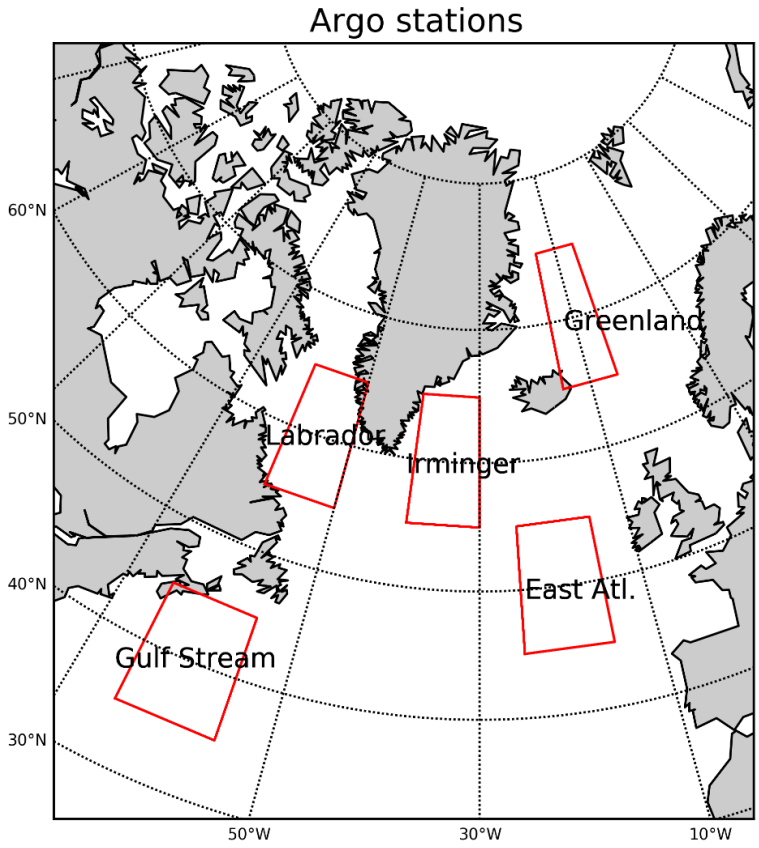

Figure 2.5. Location of five boxes in the North Atlantic basin: Eastern Atlantic, Irminger Sea, Labrador Sea, Gulf Stream region, and Greenland Sea. Those areas are used for temperature and salinity diagnosis (time-series).

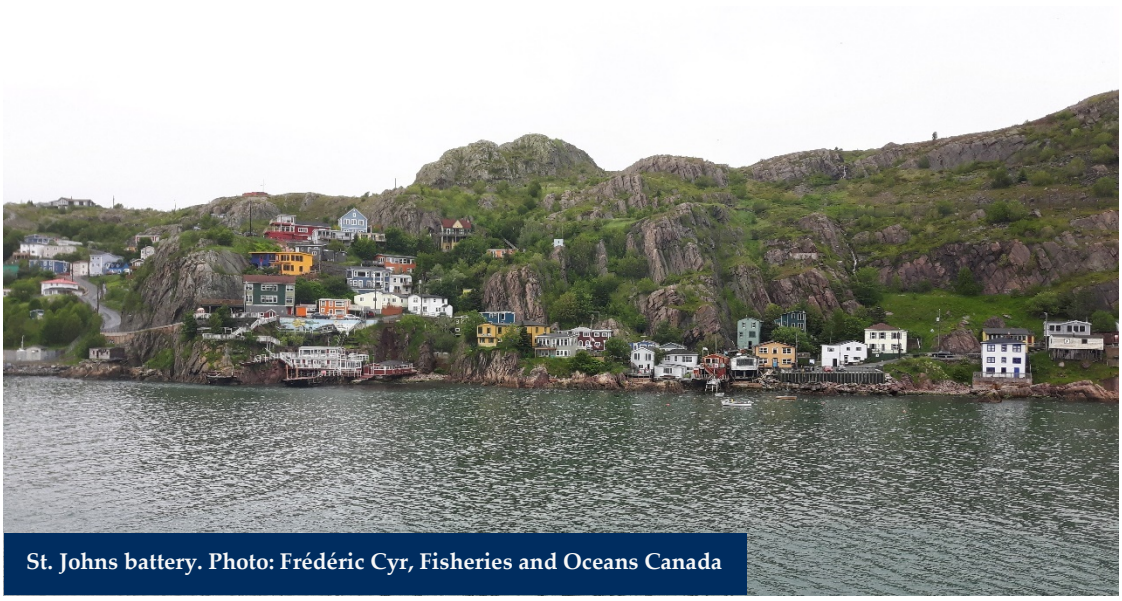

St. Johns battery. Photo: Frédéric Cyr, Fisheries and Oceans Canada

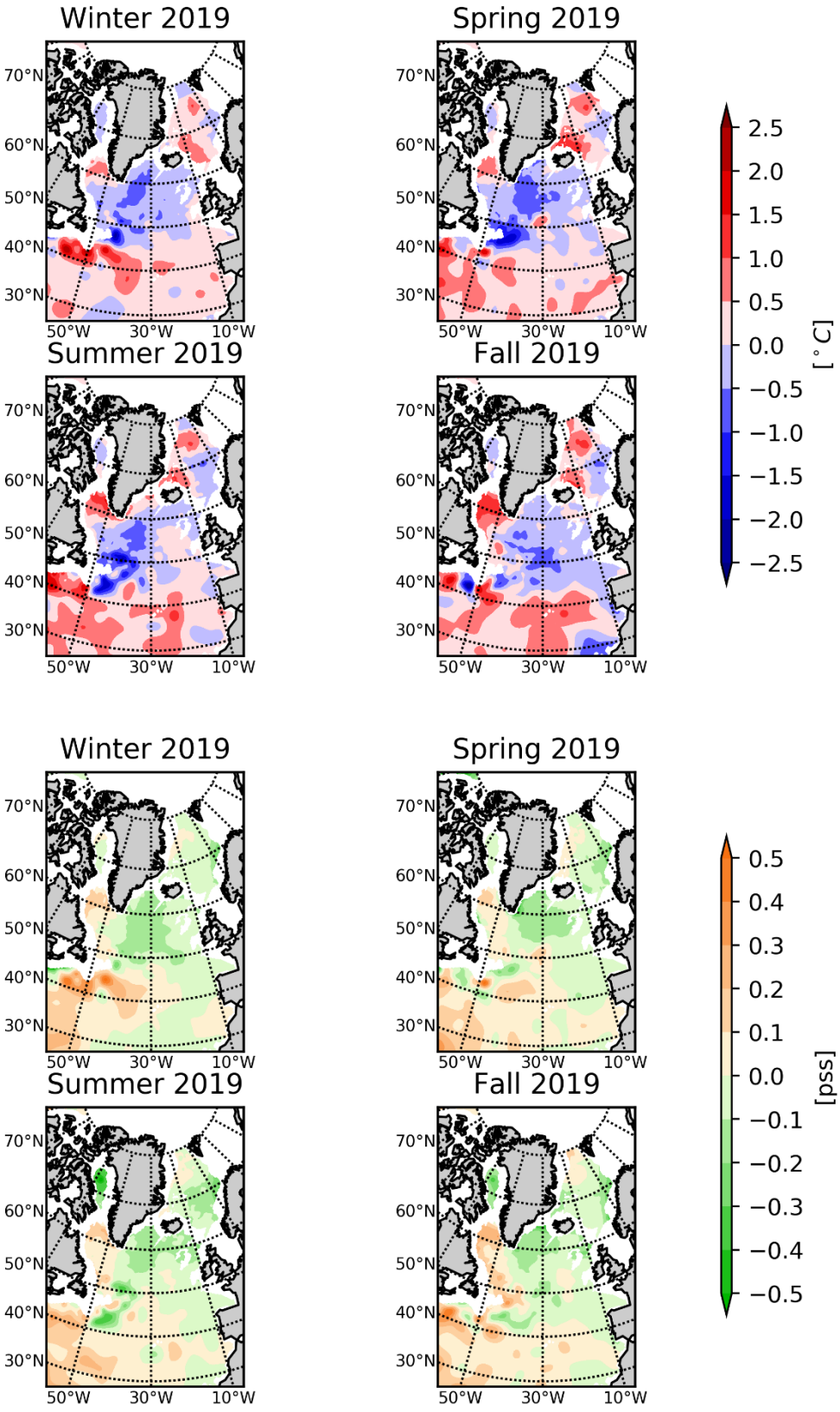

Figure 2.6. Maps of 2019 seasonal temperature (upper) and salinity (lower) anomalies within the upper layer (0–100 m) of the North Atlantic. Anomalies are the differences between the ISAS monthly mean values and the reference climatology ISAS15 2006–2015. The colour-coded scale is the same in all panels. Data prepared from the Coriolis, ISAS monthly analysis of Argo data.

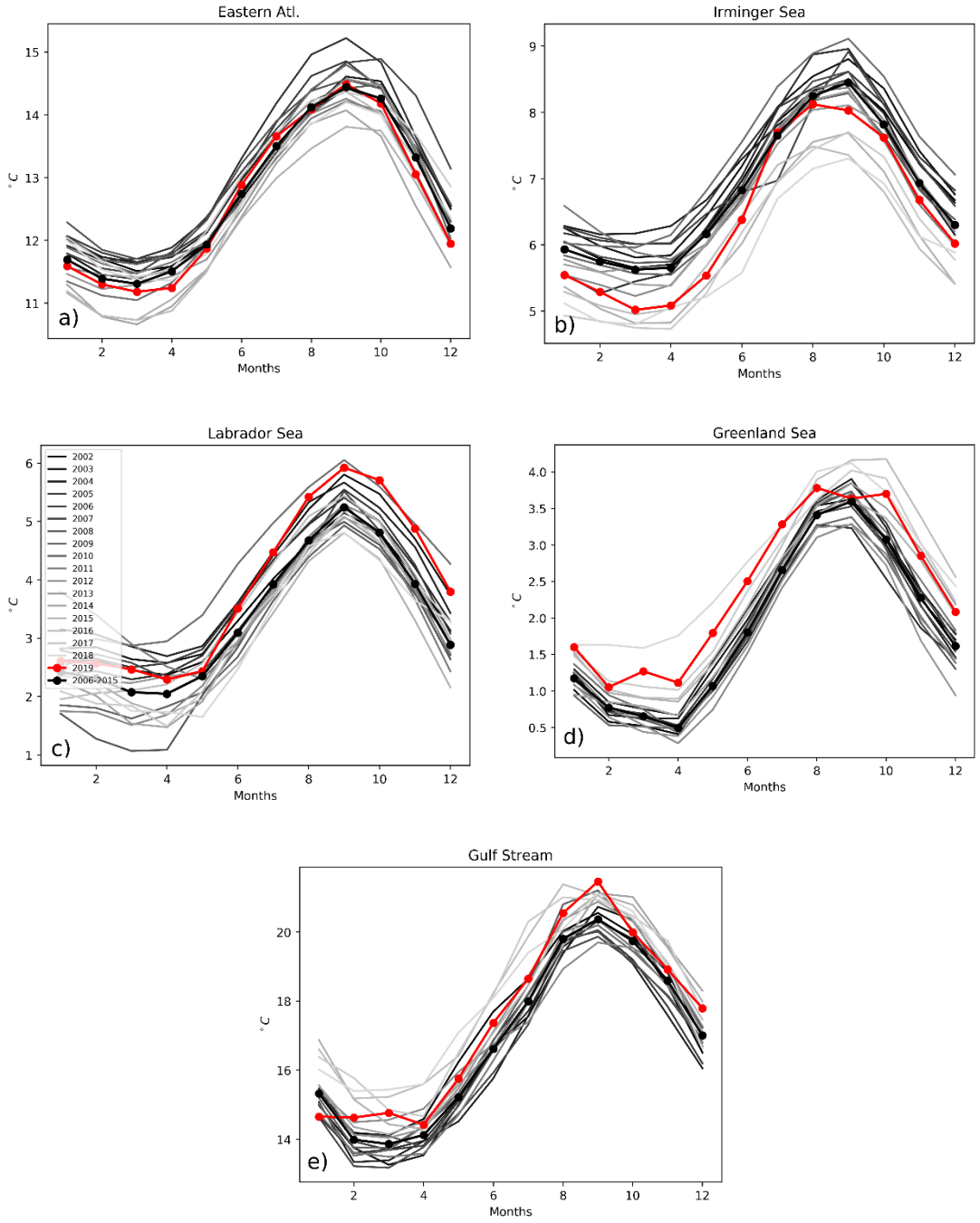

Figure 2.7. Seasonal cycle for upper temperature (0–100 m layer) as averaged within five boxes in the North Atlantic basin (see stations in Figure 2.3). (a) Eastern Atlantic; (b) Irminger Sea; (c) Labrador Sea; (d) Greenland Sea, and (e) Gulf Stream region. The year 2019 is shown in thick red, the 2006–2015 climatology in thick black, and other curves show the individual years 2002–2018.

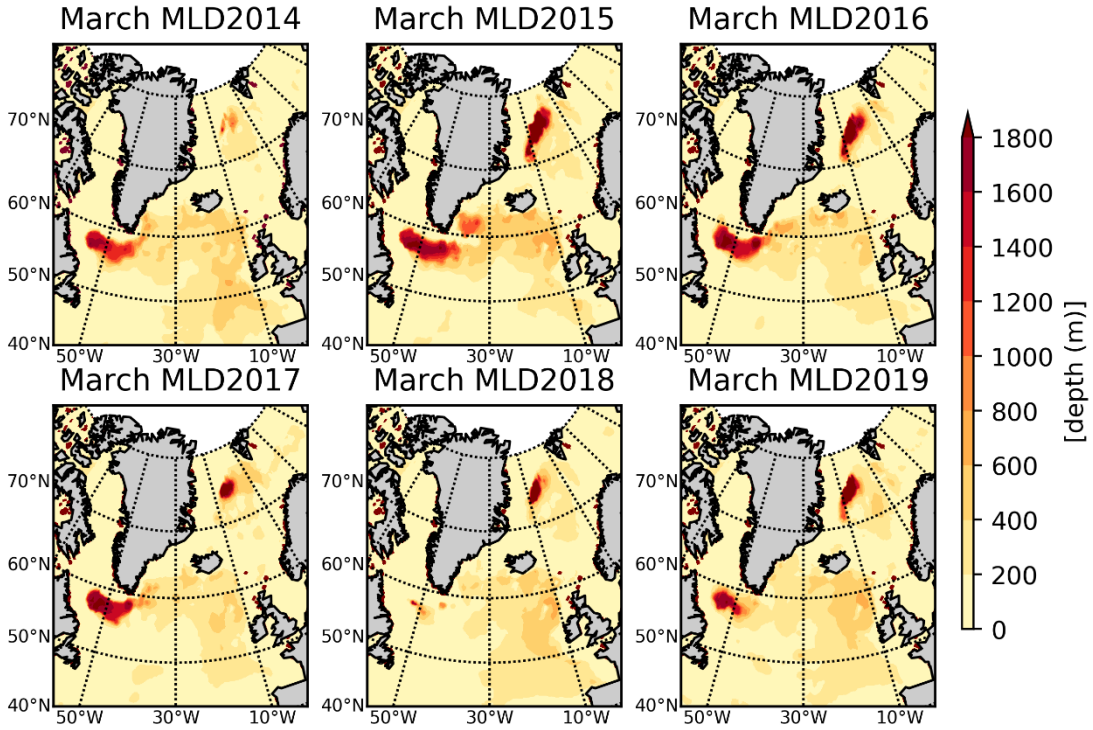

Figure 2.8. Maps of North Atlantic winter (March) mixed-layer depths (MLD) for 2014–2019. From the ISAS monthly analysis of Argo data. The mixed-layer depth is defined as the depth at which the density has increased by more than 0.03 kg m^{-3} from the density at 10 m depth. This criterion is able to represent MLD in areas where there are both effects of temperature and salinity (ice melting).

Interannual variability

The interannual variability of upper layer (0–100 m) temperature in the North Atlantic is illustrated by annual maps of temperature anomaly (Figure 2.9) and regional average time-series (Figure 2.10). When compared to the long-term 2006–2015 mean, the subtropical region was generally warmer during recent years, with anomalies increasing in intensity and being particularly strong over the Gulf Stream / North Atlantic Current (NAC) path (Newfoundland basin) in 2016 and 2018. On average, the subpolar region was colder than the long-term mean in recent years, with anomalies peaking in 2015, 2016, and 2018 over the NAC pathways towards the eastern basins.

The most noticeable large-scale change occurred between 2018 and 2019 when the anomalous subtropical–subpolar–Nordic seas tripole weakened from its 2018 peak. This significant change characterizing the most recent years (2018/2019) is best illustrated through the time-series of regional-average upper temperatures (Figure 2.10), where a clear transition to cooling, warming, and cooling trends has taken place in the subtropical (Gulf Stream panel), subpolar (Irminger Sea panel), and Nordic seas (Greenland Sea panel) regions, respectively. This reversal event is also evident for salinity, although it is less striking. The spatial pattern associated with this trend reversal is shown in Figure 2.4.

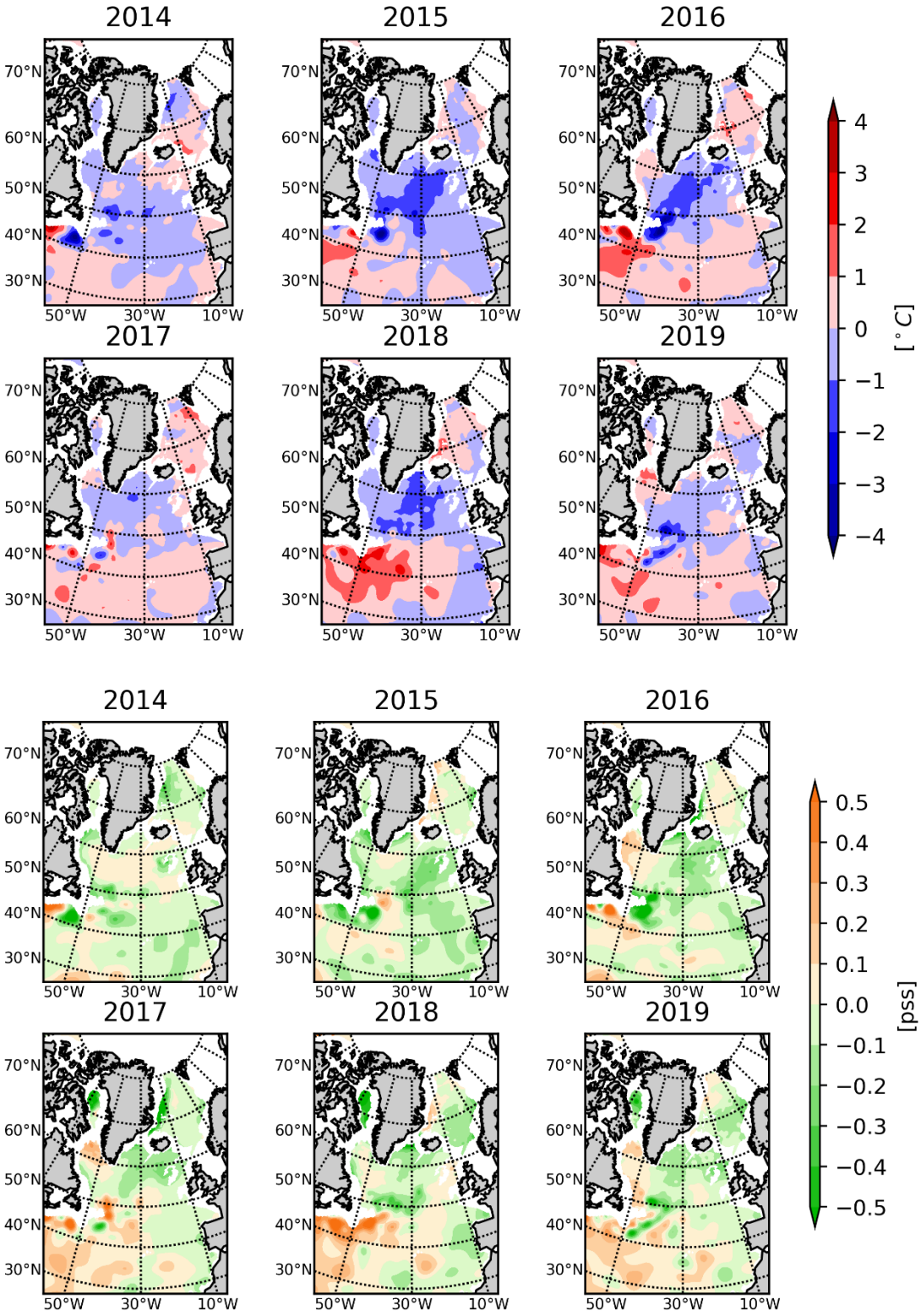

Figure 2.9. Maps of annual temperature (upper) and salinity (lower) anomalies averaged within 0–100 m in the North Atlantic for the period 2014–2019. Anomalies are the differences between the ISAS monthly mean values and the reference climatology ISAS15 2006–2015. The colour-coded scale is the same in all panels. Data prepared from the Coriolis, ISAS monthly analysis of Argo data.

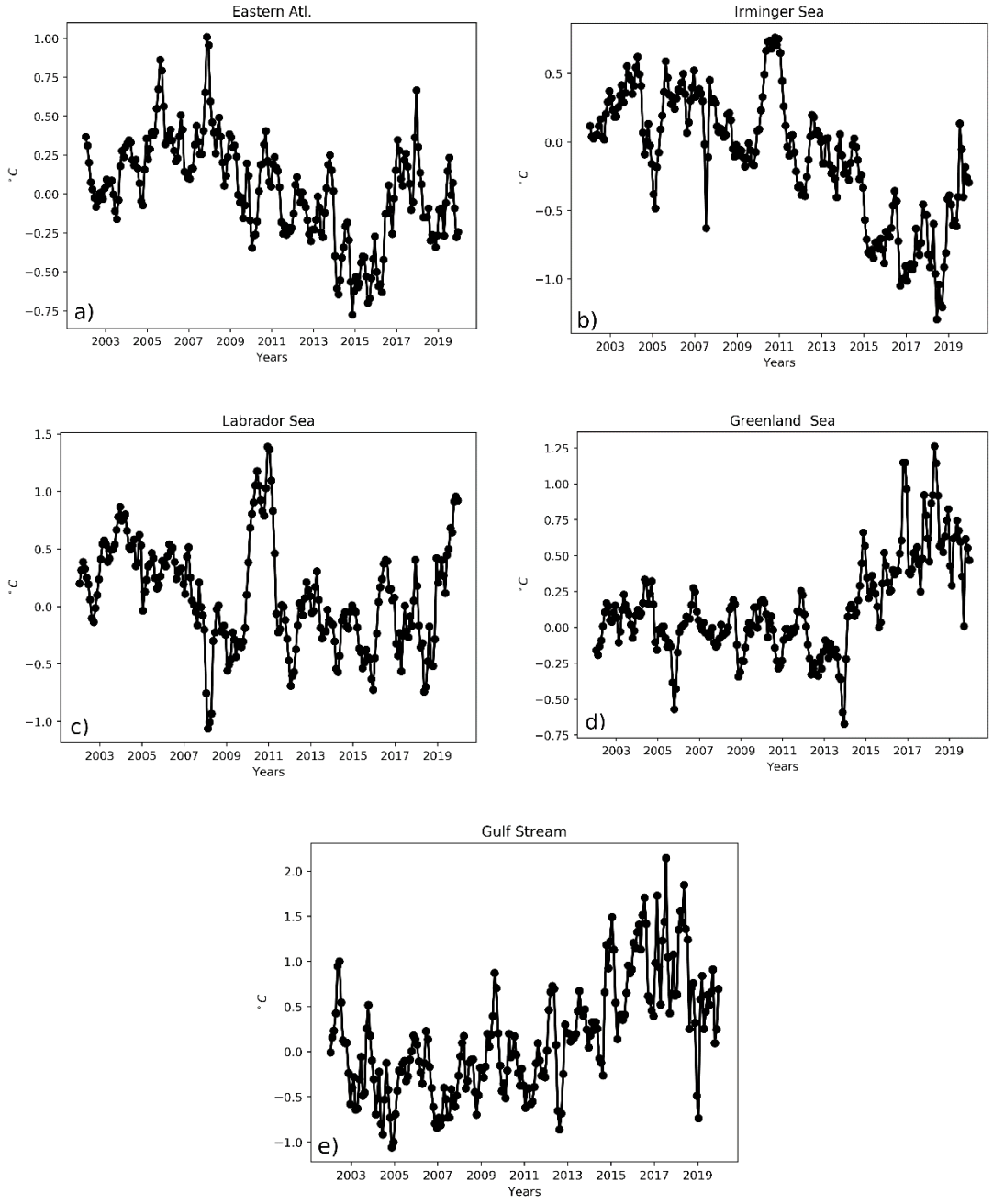

Figure 2.10. Time-series of temperature anomalies (using 2006–2015 as reference) averaged over the 0–100 m layer and in (a) Eastern Atlantic, (b) Irminger Sea,(c) Labrador Sea, (d) Greenland Sea, and (e) Gulf Stream region over the period 2002–2019.

Mixed-layer depth

The mixed-layer depth is an indicator of winter convection intensity in the North Atlantic and Nordic seas. Winter heat and freshwater fluxes control the buoyancy loss (increase of density) of the ocean surface layers and trigger deep convection. In order to compare all areas throughout the decade, the mixed-layer depth is defined here as the level at which density changes by more than 0.03 kg m^{-3} with respect to the 10 m depth value. This is a common criterion used for the global ocean (de Boyer Montegut *et al.*, 2004). Given the stratification in the North Atlantic and Nordic seas, it is probably not the optimal criterion to define the mixed layer in this region. However, adopting this definition allows the comparison of the relative winter mixed-layer depth across multiple years. The month of March has been selected as being the common period for maximum mixed-layer depth, is at the end of the winter season, and comes before spring re-stratification. However, this is not always true, since the time-point when the deepest mixed layer occurs can vary from year-to-year at a single location and might not occur at the same time of year across the whole basin (between February and March in the North Atlantic).

The 2019 winter was characterized by a noticeable increase in mixed-layer depths in both the Labrador and Greenland seas (> 1600 m). This reflects both an important recovery of atmospherically driven convective mixing in those regions since the 2018 winter and its very shallow mixed layers. The spatial extent of 2019 mixed layers was still relatively small when compared to those observed during the highly convective period of 2014–2016.

2.3.3 Deep layers

The interannual variability of temperature anomalies in the intermediate layer (800–1200 m) during 2014–2019 is provided in Figure 2.11 as maps for the years 2014–2019, and in Figure 2.12 as time-series for the period 2002–2019. In this layer, the gross spatial pattern in recent years is for a relatively warm subtropical region, a relatively cold subpolar region, and relatively warm Nordic seas (when compared to the 2006–2015 climatological period). This tripole pattern characterizing the intermediate layer has progressively intensified over the years and has a reached its current peak in amplitude in 2018/2019. The strongest centres of action are located in the western Subtropical Gyre, where the Gulf Stream/NAC area are found, in the Irminger and Labrador seas, and in the Greenland Sea. The contrasting behaviour of temperature in those regions is striking (Figure 2.12). Since 2012, the Gulf Stream area has warmed nearly 0.1°C, and the subpolar area (Labrador and Irminger seas) has cooled nearly 0.4°C. In contrast to those two latter regions, temperatures in the intermediate layer of the Greenland Sea have been characterized by a long-term positive trend (increase of about 0.25°C since 2002). A similar intensifying tripole pattern can be seen in the salinity fields in recent years, with a relatively salty subtropical region, fresh subpolar region, and salty Nordic seas, although the picture is less clear than for temperature.

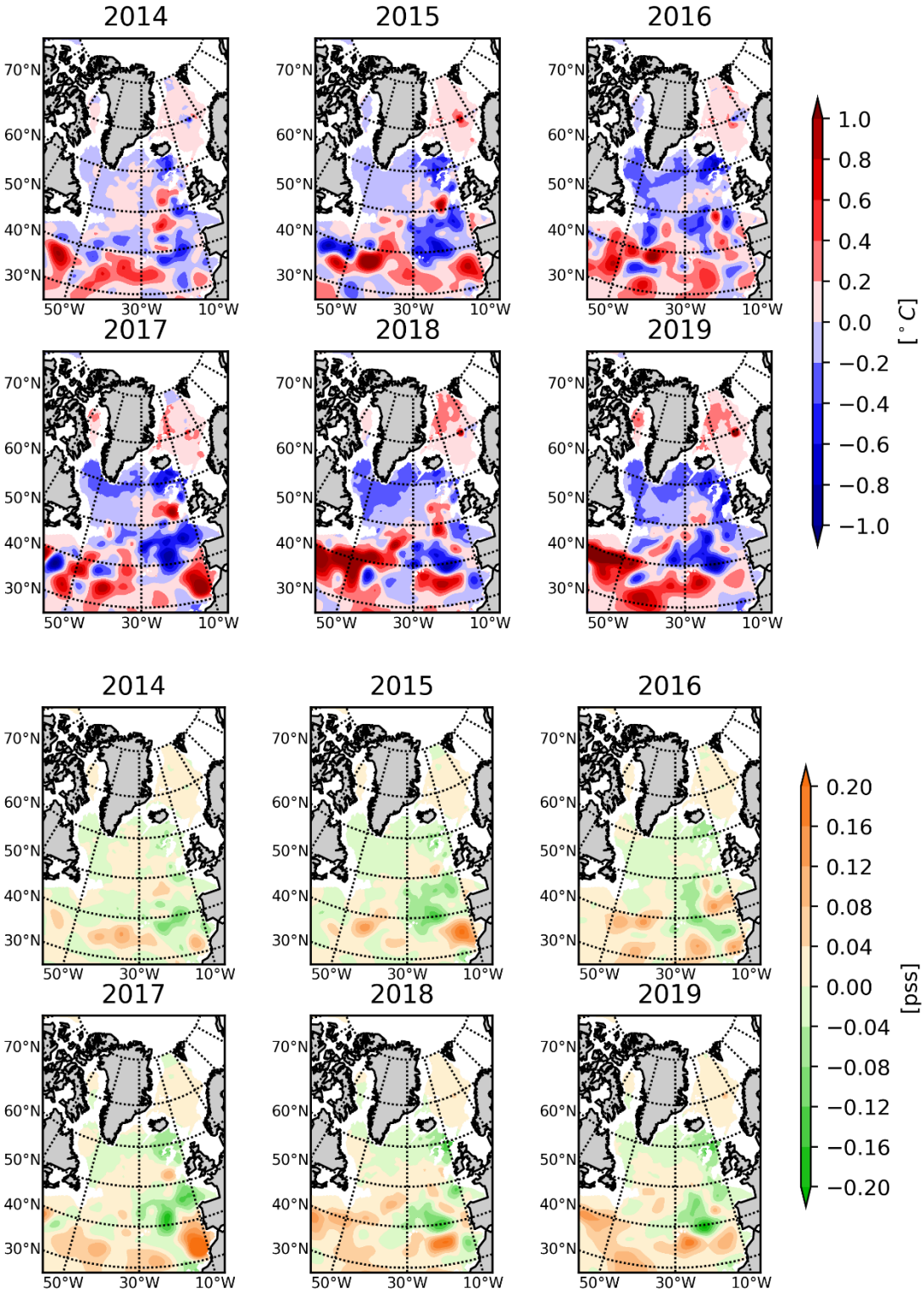

Figure 2.11. Maps of annual temperature (upper) and salinity (lower) anomalies at 1000 m depth in the North Atlantic for the period 2014–2019. Anomalies are the differences between the ISAS monthly mean values and the reference climatology, World Ocean Atlas 05 (WOA5). The colour-coded scale is the same in all panels. Data prepared from the Coriolis, ISAS monthly analysis of Argo data.

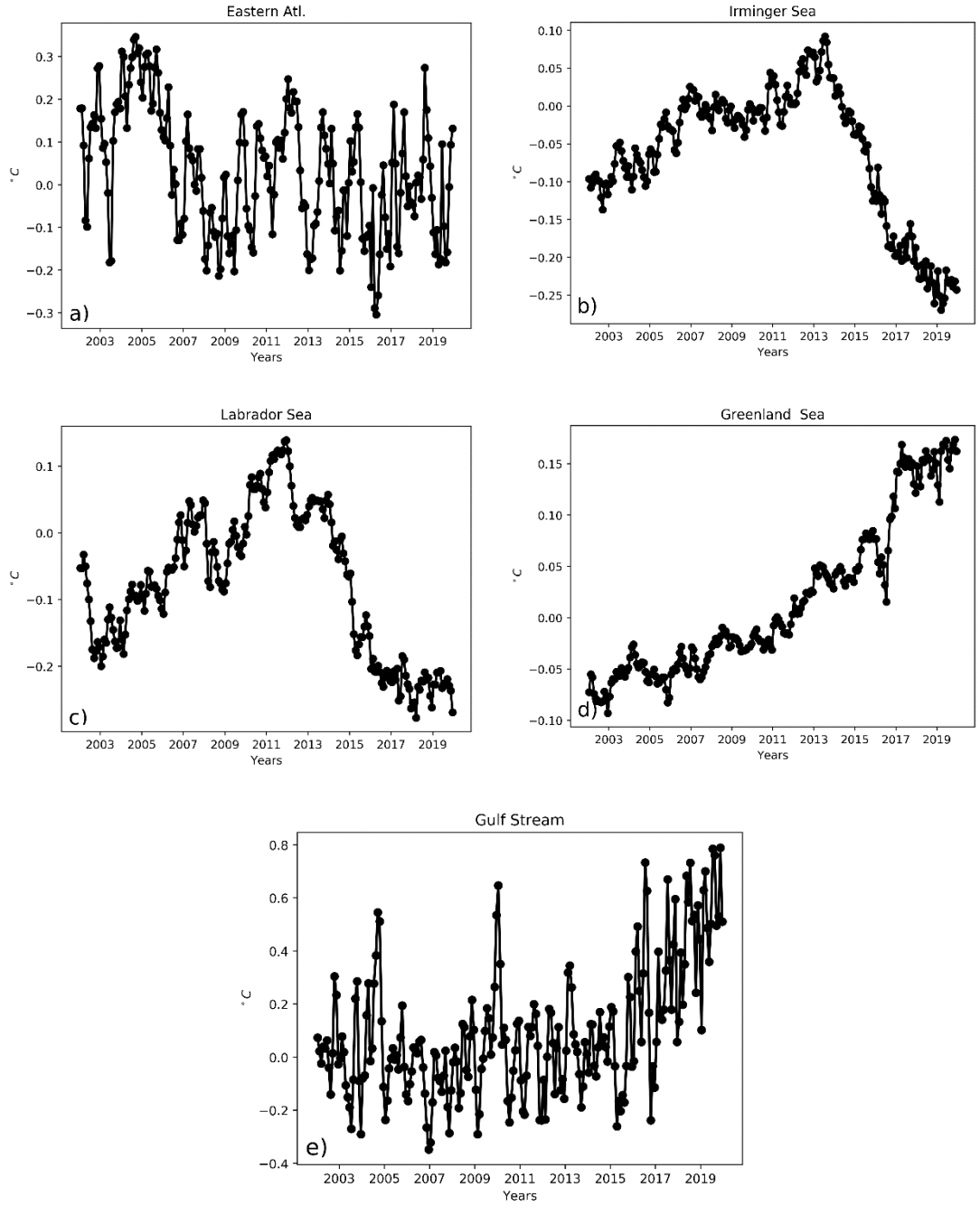

Figure 2.12. Time-series of temperature anomalies (using 2006–2015 as reference) averaged over the 800–1200 m layer and in (a) Eastern Atlantic, (b) Irminger Sea, (c) Labrador Sea, (d) Greenland Sea, and (e) Gulf Stream region over the period 2002–2019.

2.4 Subpolar Gyre index

L. Chafik, B. Berx, and H. Hátún

The Subpolar Gyre is strongly affected by the atmospheric circulation of the North Atlantic and is often characterized by the NAO. However, using the Subpolar Gyre index for ocean research has the advantage over the NAO index of integrating the oceanic imprint of the various atmospheric drivers. It thus has more direct implications for the marine climate and ecosystems in the subpolar North Atlantic.

In the early 1990s, the Subpolar Gyre index was negative, reflecting a period of strong gyre circulation (anomalously low sea surface heights, Figure 2.13). This phenomenon was intensified by the anomalously strong atmospheric forcing, as represented by the very high NAO index during the late 1980s–early 1990s (Delworth *et al.*, 2016). A rapid reversal of the westerly winds that occurred during winter 1995/1996 switched the NAO index in 1996 and was followed by a period with average or negative NAO values. As a result, the Subpolar Gyre index transitioned to a positive phase, indicating a weaker and contracted gyre circulation (anomalously high sea surface heights, Figure 2.13). This modified gyre shape, most notably in the eastern North Atlantic, permitted a larger contribution of warm, saline, and nutrient-poor subtropical waters to Atlantic inflows towards the Arctic, which ultimately accessed the central Subpolar Gyre, further weakening its strength.

Since 2014, strong atmospheric forcing and winter convection, associated with a positive NAO index (e.g. Yashayaev and Loder, 2017), has resulted in a return of the Subpolar Gyre to a very strong and expanded circulation, similar to the early 1990s. This is clearly illustrated by a switch to negative gyre index values in the past few years (Figure 2.13). The Subpolar Gyre index remained negative in 2019, but less so than the 2017–2018 period.

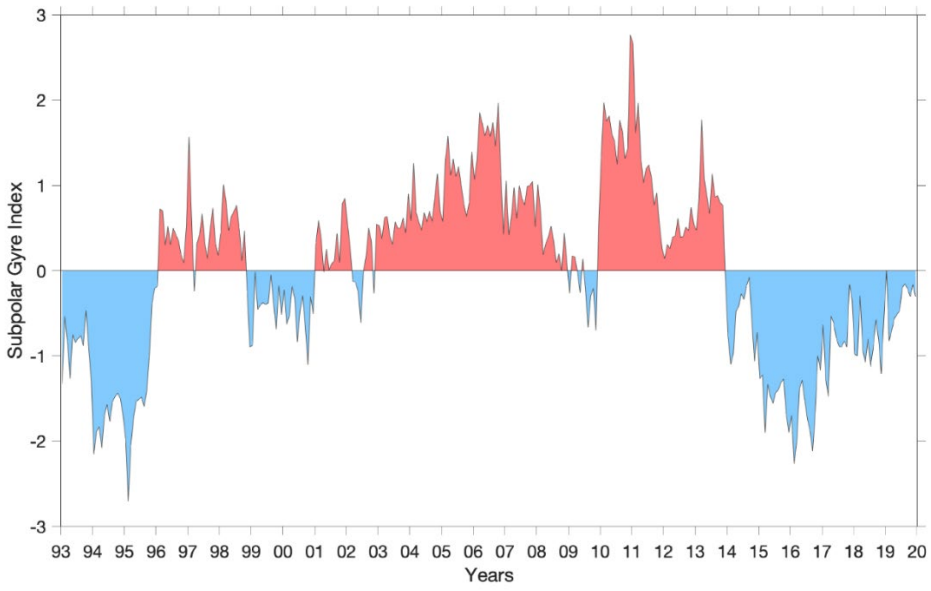

Figure 2.13. The monthly gyre index (second principal component) from January 1993 until December 2019. Data source: altimetry data were obtained through the Copernicus Marine Environment Monitoring Service (http://marine.copernicus.eu).

3 The North Atlantic atmosphere

S. R. Dye

The NAO is a pattern of atmospheric variability that has a significant impact on oceanic conditions. It affects windspeed, precipitation, evaporation, and the exchange of heat between ocean and atmosphere, and its effects are most strongly felt in winter. The NAO index is a simple device used to describe the state of the NAO. It is a measure of the strength of the sea level air pressure gradient between Iceland and Lisbon, Portugal. When the NAO index is positive, there is a strengthening of the Icelandic low-pressure system and the Azores high-pressure system. This produces stronger mid-latitude westerly winds, with colder and drier conditions over the western North Atlantic and warmer and wetter conditions in the eastern North Atlantic. When the NAO index is negative, there is a reduced pressure gradient, and the effects tend to be reversed.

There are several slightly different versions of the NAO index calculated by climate scientists. The Hurrell winter (December/January/February/March, or DJFM) NAO index (Hurrell *et al.*, 2003) is the most commonly used and is particularly relevant to the eastern North Atlantic. Note that although we may think of winter as coming at the end of the year, here the 'winter season' spans an annual boundary and precedes the year of interest, so winter of December 2019 to March 2020 sets up conditions for summer 2020.

The NAO is the dominant pattern of atmospheric pressure variability in the North Atlantic. However, when the NAO itself is weak (i.e. the dominant atmospheric pattern is not an NAO type pattern), this may be because a different pattern is occurring. Two other dominant atmospheric regimes have been identified as useful descriptors: (i) the Atlantic Ridge mode, when a strong anticyclonic ridge develops off western Europe (similar to the East Atlantic pattern); and (ii) the Blocking regime, when the anticyclonic ridge develops over Scandinavia. The four regimes (positive NAO, negative NAO, Atlantic Ridge, and Blocking) have all been occurring at around the same frequency (20–30% of all winter days) since 1950 (Hurrell and Deser, 2010). For this reason, we also include maps of sea level pressure, windspeed, and air temperature as this offers a more detailed understanding of the North Atlantic atmospheric variability than the NAO Index alone.

3.1 The North Atlantic Oscillation NAO index

The Hurrell NAO index underwent a long period of increase from an extreme and persistent negative phase in the 1960s to a most extreme and persistent positive phase during the late 1980s and early 1990s. This was followed by a large and rapid decrease during winter 1995/1996. In many of the years between 1996 and 2009, the Hurrell winter NAO index was fairly weak and a less useful descriptor of atmospheric conditions, mainly because the sea-level pressure patterns were not typical for the NAO. In winter 2009/2010, the index was strongly negative (Figure 3.1), and its anomaly pattern exerted a dominant influence on atmospheric conditions. This was the strongest negative anomaly since 1969 and the second strongest negative value for the Hurrell winter NAO index on record (starting in 1864). Winter 2014/2015 saw the strongest NAO index since 1995 and the fourth most positive NAO index in the last

110 years (Hurrell and National Center for Atmospheric Research Staff (Eds.), 2019). In winter 2016/2017, the NAO index was strong and positive (+1.47) for the fourth consecutive winter, the first such positive run since 1992–1995. Winter 2017/2018 experienced a positive, but near neutral (+0.30), NAO index, while in winter 2018/2019, the index has returned to a strong positive value (+2.09).

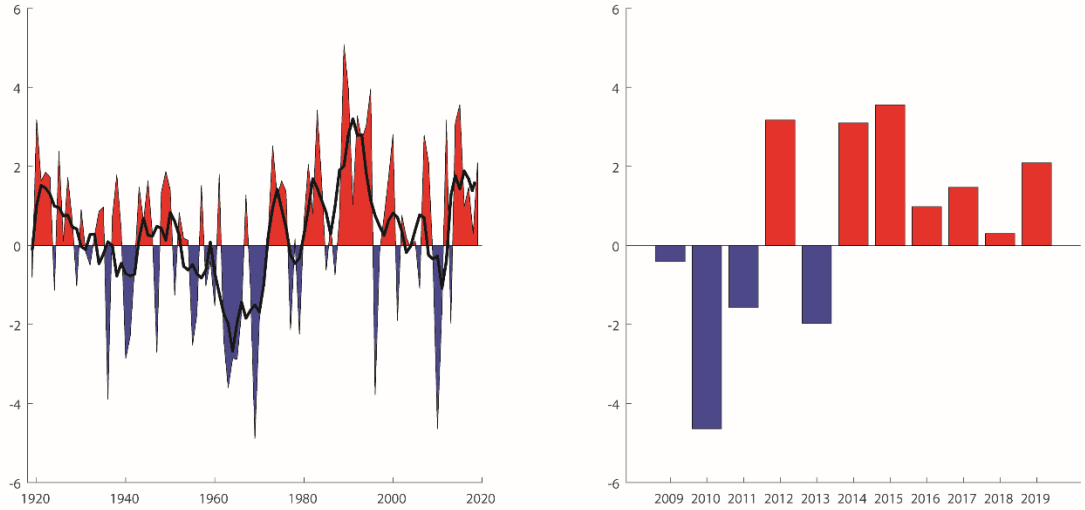

Figure 3.1. The Hurrell winter (DJFM) NAO index for the past 100 years with a two-year running mean applied (left panel) and for the current decade (right panel). Data source: NAO Index Data provided by the Climate Analysis Section, NCAR, Boulder, USA, (Hurrell and National Center for Atmospheric Research Staff (Eds.), 2019).

3.2 Sea level pressure and windspeed

The spatial pattern of atmospheric conditions indicated by a particular NAO index value are more understandable when the anomaly fields are mapped. Impacts on ocean properties are particularly dominated by winter conditions; hence, the inclusion of SLP and windspeed maps for the winter period (Figure 3.2 and Figure 3.3).

The top panel of Figure 3.2 shows the winter SLP averaged over 30 years (1981–2010). The dominant features (action centres) are the Iceland Low, situated southwest of Iceland, and the Azores High, west of Gibraltar. The middle panel of Figure 3.2 shows the mean SLP for winter 2018/2019 (December 2018 through March 2019), and the bottom panel shows the 2018/2019 winter SLP anomaly (i.e. the difference between the top and middle panels).

The pattern of SLP is closely related to wind patterns. The geostrophic or gradient wind blows parallel to the isobars, with lower pressure to the left in the northern hemisphere. The closer the isobars are, the stronger the wind is. The strength of the winter-mean surface wind averaged over the 30-year period (1981–2010) is shown in the upper panel of Figure 3.3, while the middle panel shows the mean surface wind for winter 2018/2019 and the lower panel the anomaly in winter 2018/2019.

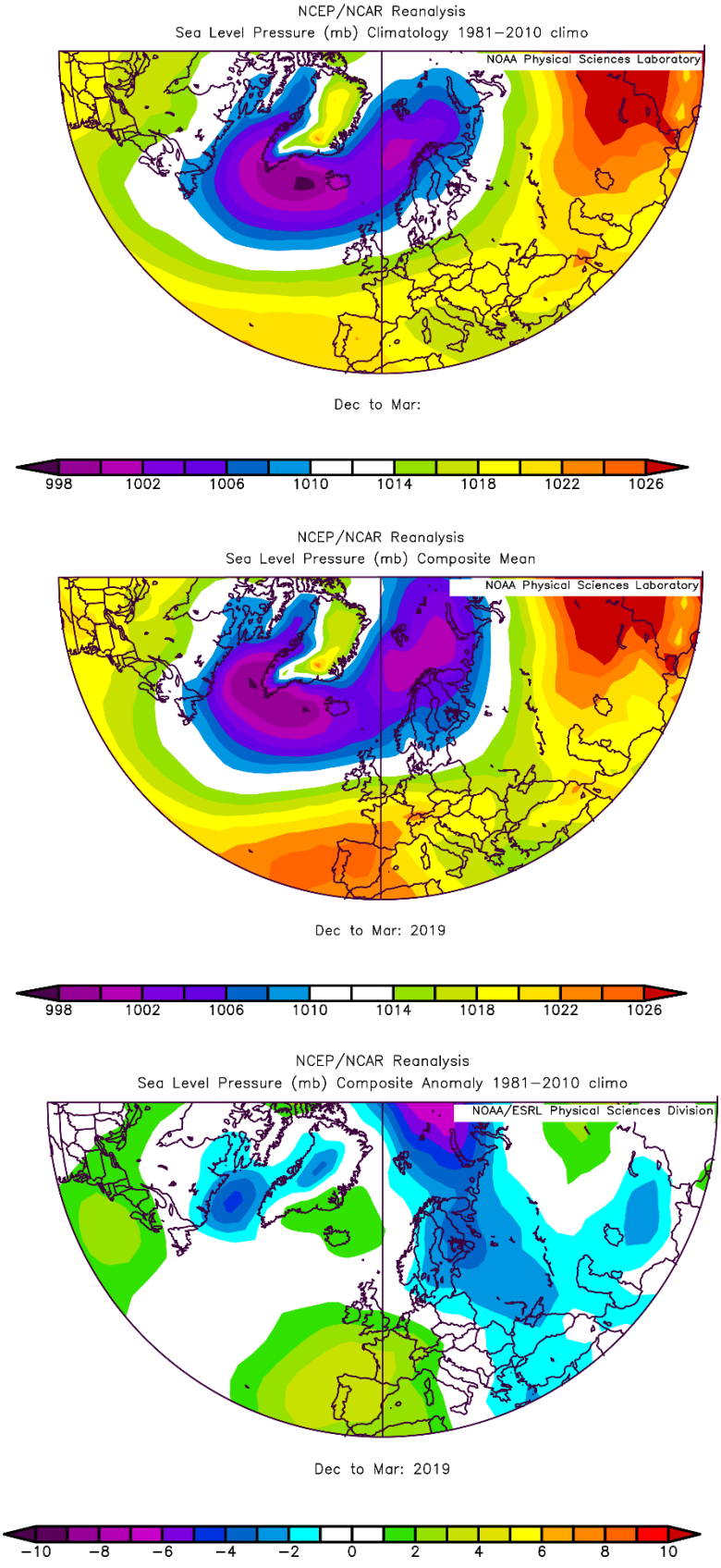

Figure 3.2. Winter (DJFM) sea level pressure fields. Top panel: sea level pressure averaged over 30 years (1981–2010). Middle panel: sea level pressure in winter 2018/2019. Bottom panel: winter 2018/2019 sea level pressure anomaly, calculated as the difference between the top and middle panels. Images provided by the NOAA/ESRL Physical Sciences Division, Boulder, CO, USA.

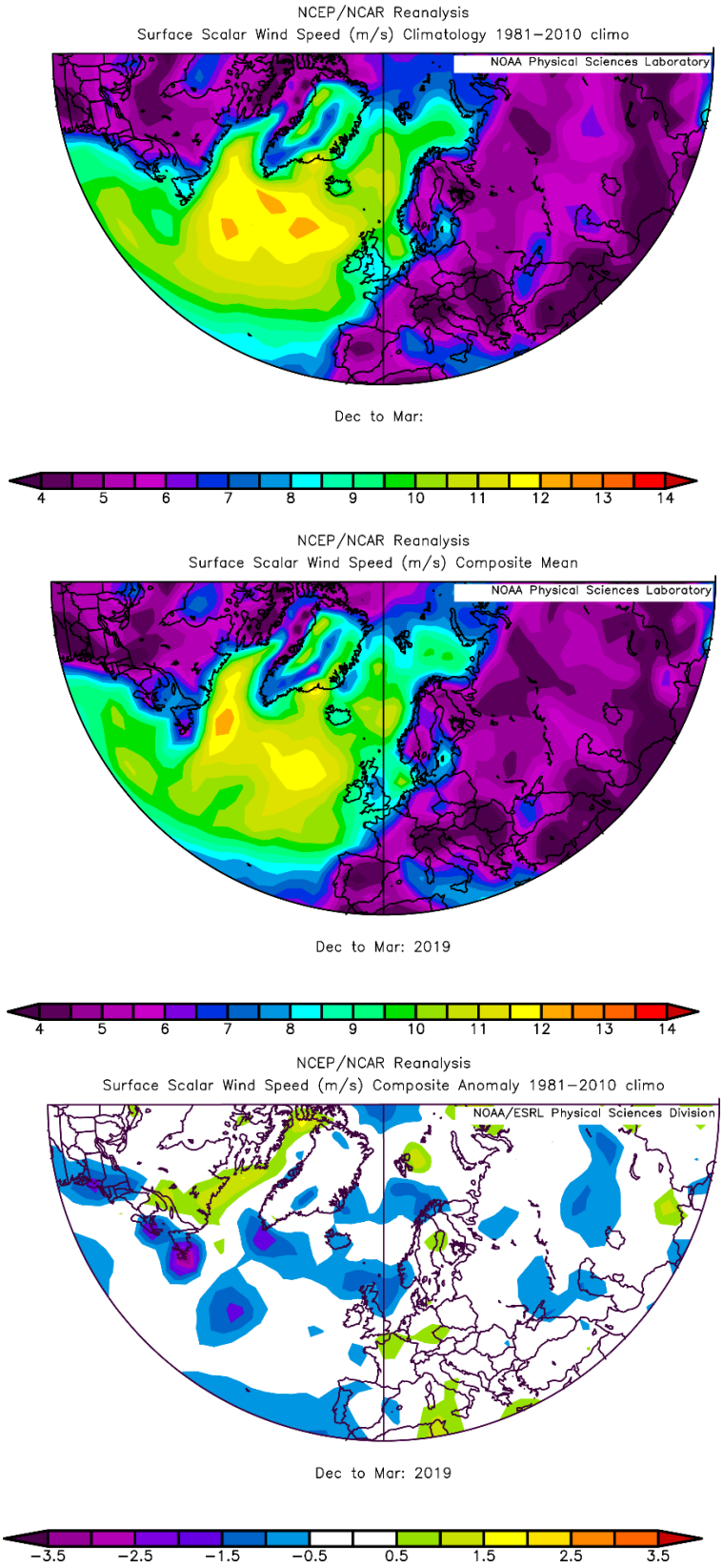

Figure 3.3. Winter (DJFM) windspeed fields. Top panel: scalar windspeed averaged over 30 years (1981–2010). Middle panel: scalar windspeed in winter 2018/2019. Bottom panel: winter 2018/2019 scalar windspeed anomaly, calculated as the difference between the top and middle panels. Images provided by the NOAA/ESRL Physical Sciences Division, Boulder, CO, USA.

The SLP anomaly for winter 2018/2019 (Figure 3.2) did not resemble a typical positive NAO pattern despite the strong positive NAO. A high-pressure (anticyclonic) anomaly was present across western Europe, but limited to the area between the Azores in the west, Germany in the east, and Ireland in the north. A weak anticyclonic anomaly was present over Iceland, instead of the low-pressure (cyclonic) anomaly that might have been expected. Lower SLP was evident over the Labrador Sea and in an extended system that stretched from the Arctic across the Barents Sea and Scandinavia and into eastern Europe.

The influence of this atypical SLP anomaly during a strong positive NAO index is seen in windspeeds (Figure 3.3). Strengthening of the prevailing southwesterlies in the east of the region might have been expected. However, in reality, the windspeeds across the region in winter 2018/19 were generally lower than average, particularly east of Newfoundland, from south of Cape Farewell across to the northern North Sea, and in a band stretching across the Nordic seas from Scoresby Sund in Greenland to the North Cape of Norway.

3.3 Surface air temperature

North Atlantic winter mean surface air temperatures are shown in Figure 3.4 (Kalnay *et al.*, 1996). The 1981–2010 mean conditions (Figure 3.4, top panel) show warm temperatures penetrating far to the north on the eastern side of the North Atlantic and the Nordic seas caused by the northward movement of warm oceanic water. The middle panel of Figure 3.4 shows the conditions in winter 2018/2019, and the bottom panel shows the difference between the two.

Over most of the main body of the North Atlantic ocean, away from the shelves and marginal seas, air temperature was near average. Winter air temperatures were warmer than the 1981–2010 average across Europe (apart from Spain and Portugal), the Nordic seas, and the Labrador Sea. Colder-than-normal winter air temperatures were limited to a region stretching from Nova Scotia to east of Flemish Cap.

Waves in the Atlantic. Photo: Tomasz Szumski, Marine Institute, Galway, Ireland

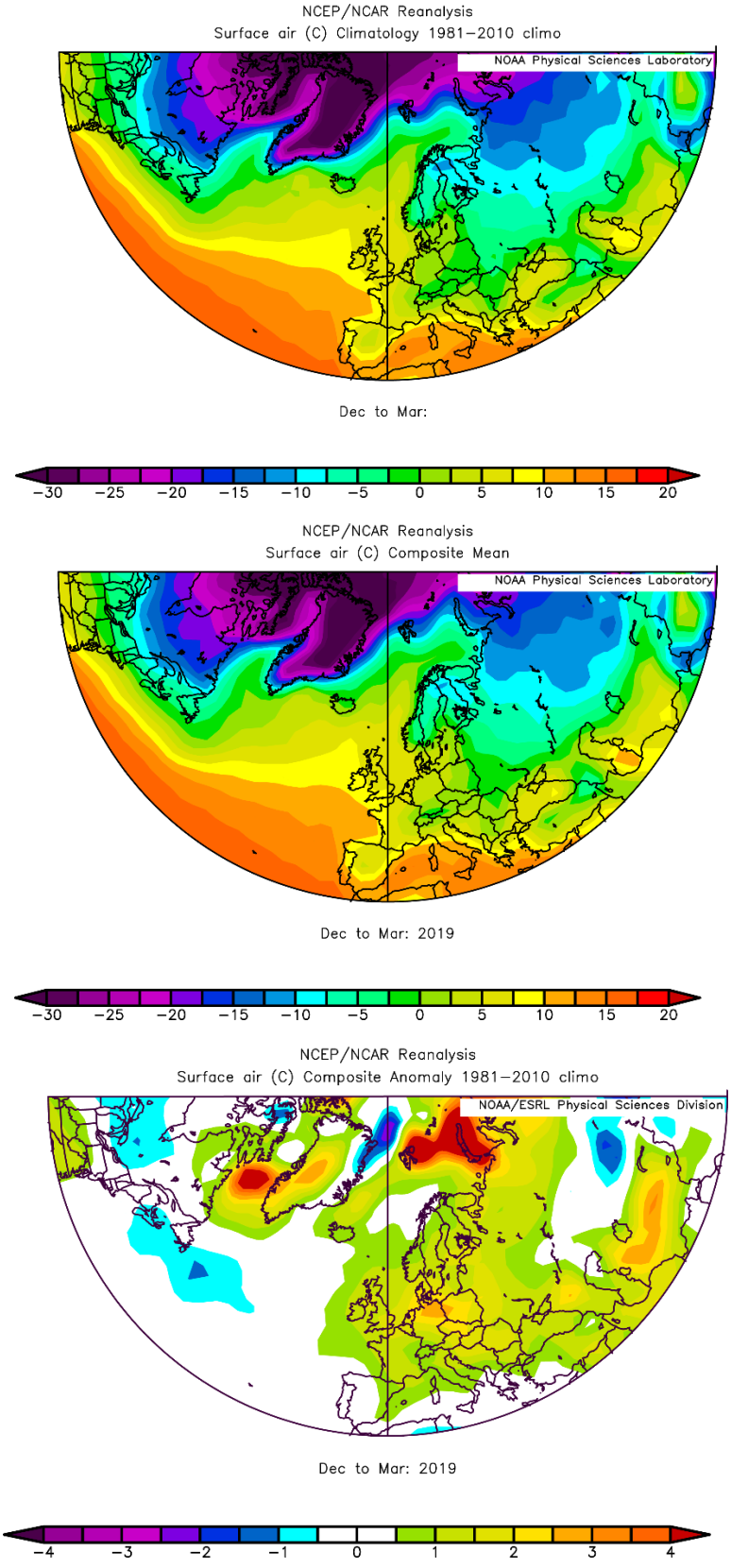

Figure 3.4. Winter (DJFM) surface air temperature fields. Top panel: surface air temperature averaged over 30 years (1981–2010). Middle panel: surface air temperatures in winter 2018/2019. Bottom panel: winter 2018/2019 surface air temperature anomaly, calculated as the difference between the top and middle panels. Images provided by the NOAA/ESRL Physical Sciences Division, Boulder, CO, USA (available online at http://www.cdc.noaa.gov/).

3.4 Outlook beyond 2019

An initial assessment of the North Atlantic atmosphere at the end of the IROC year is included. Atmospheric conditions during winter are a determining factor for oceanic conditions the following year. Therefore, this outlook offers some predictive capability for spring–autumn 2020.

The SLP pattern for December 2019–March 2020 suggests a second consecutive strong positive NAO index winter. In contrast to the previous winter, the SLP anomaly pattern has been closer to what would be expected during a strong positive NAO, with strong zonal extension in both the Azores High and Icelandic Low centres of action. A region from the west of Ireland across the UK, North Sea, and southern Scandinavia experienced particularly strong southwesterly winds through much of winter. Air temperatures were relatively warm across Europe, northeast America, the Nordic seas, and Labrador Sea, with colder-than-normal air temperatures over the central North Atlantic where average windspeeds are greatest.

Recent advances in understanding the predictability of the NAO are showing significant skill in seasonal predictions of the European winter through predictability of the winter NAO (Scaife *et al.*, 2014), Arctic Oscillation (AO), and Sudden Stratospheric Warming (SSW) events (Scaife *et al.*, 2015). Results published by the Met Office suggest that there is even significant skill in predicting the winter NAO index one year ahead (Dunstone *et al.*, 2016), with a correlation coefficient (r) between observed and predicted NAO of about 0.4 for the second winter, comparing well with that of about 0.6 for the first winter (Scaife *et al.* 2014).

Experimental forecasts from the US over seasonal periods[1] suggest that summer 2020 surface temperatures are likely to be warmer than average across the region, but that the Subpolar Gyre to the west of Ireland and Iceland and southeast of Cape Farewell is more likely to be near average than other areas, possibly even cooler than average. Forecasts over the next five years from the UK (Met Office Decadal forecast January 2020) suggest a warmer outlook for the Subpolar Gyre region than has been seen in the last few cold anomaly years. As experimental forecasts are at an early stage, these are noted here so that we can track their performance and gauge their utility as they develop.

[1] www.cpc.ncep.noaa.gov/products/NMME/

4 Detailed area descriptions, part I: the upper ocean

Introduction

This section presents time-series from sustained observations in each of the ICES areas shown in Figure 4.1. The general pattern of oceanic circulation in the upper layers of the North Atlantic in relation to the areas described here is shown in Figure 4.2. In addition to temperature and salinity, other indices are presented where available, such as air temperature and sea ice extent. The regional context of the sections and stations are summarized, noting any significant changes.

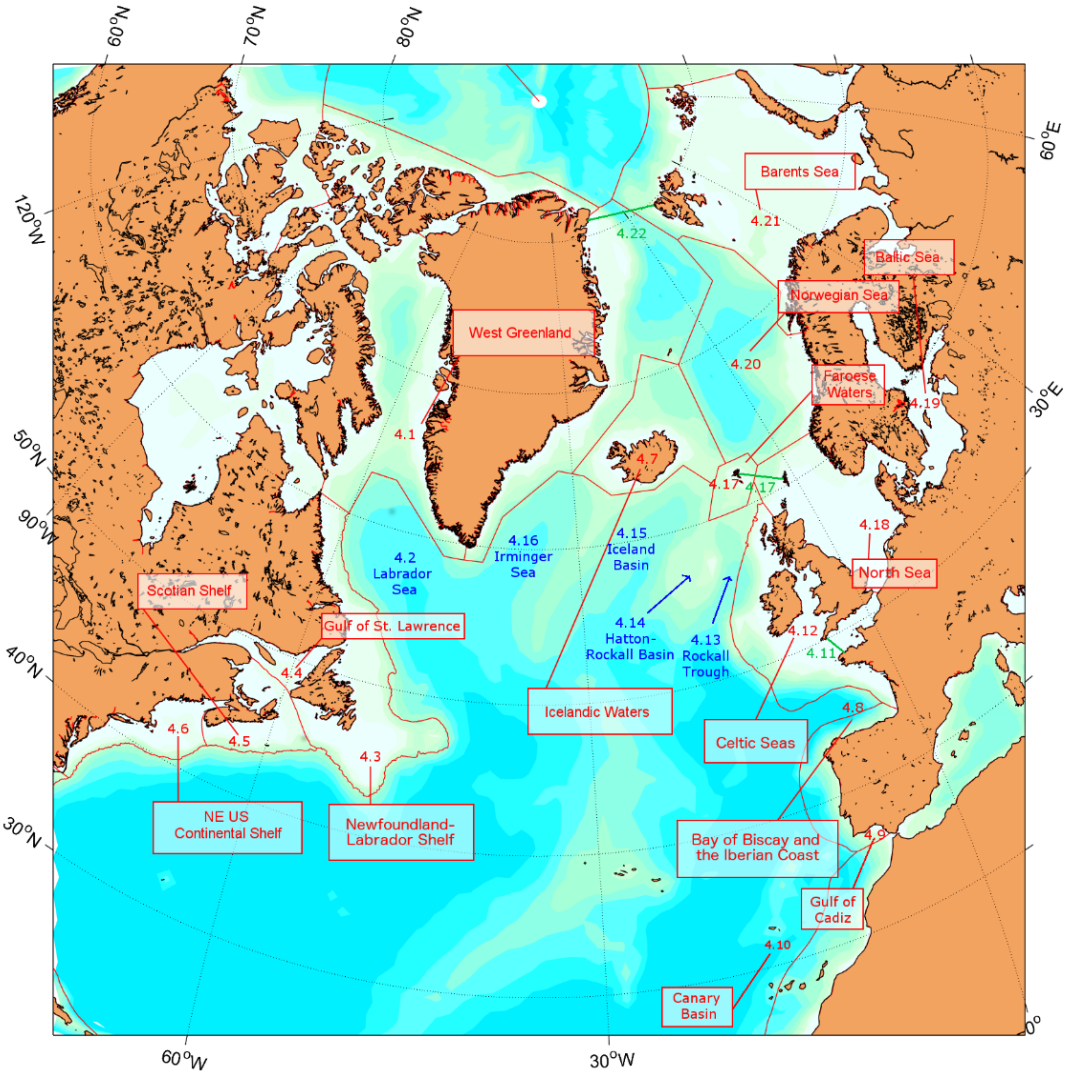

Figure 4.1. Schematic of marine areas used to organize data presented in this section. Numbers refer to the section number. Regions are labelled in red. Ocean basins are labelled in blue. Straits are labelled in green. NOAA Large Marine Ecosystems boundaries (http://www.lme.noaa.gov/) are shown as background reference, but hydrographic regions are loosely defined so they do not perfectly overlap.

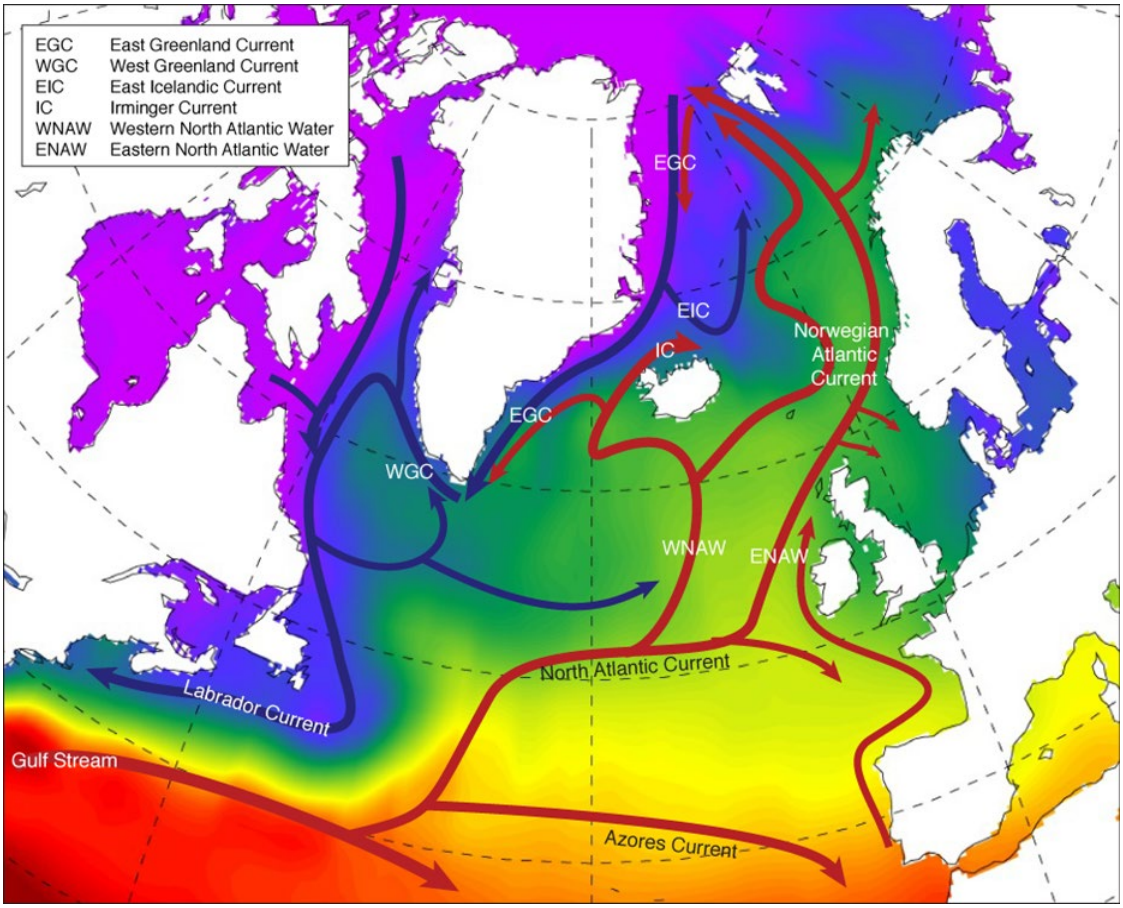

Figure 4.2. Schematic of the general circulation of the upper ocean (0–1000 m) in the North Atlantic. Blue arrows: movement of cooler waters of the Subpolar Gyre; red arrows: movement of warmer waters of the Subtropical Gyre.

Most standard sections or stations are sampled annually or more frequently. Many of the time-series presented here have been extracted from larger datasets and have been chosen as indicators of the conditions in a particular area. Where appropriate, data are presented as anomalies to demonstrate how the values compare with the average or "normal" conditions (usually the long-term mean of each parameter during 1981–2010). For datasets that do not extend as far back as 1981, the average conditions have been calculated from the start of the dataset through to 2010.

In places, the seasonal cycle has been removed from a dataset either by calculating the average seasonal cycle during 1981–2010 or by drawing on other sources, such as regional climatology datasets. Smoothed versions of most time-series are included using a "Loess smoother", a locally weighted regression with a two- or five-year window (chosen depending on which was the most appropriate to each time-series).

In some areas, data are sampled regularly enough to allow a good description of the seasonal cycle. Where possible, monthly data from 2019 are presented and compared with the average seasonal conditions and statistics.

Although there are no real boundaries in the ocean, it is intended that the data presented represent conditions in a particular area. This section groups datasets into areas based on existing definitions. The NOAA Large Marine Ecosystems (LMEs)[1] serve as an overall reference as they cover all regions. However, ICES Marine Ecoregions[2], the bathymetry of ocean basins[3], and the general pattern of ocean circulation are also taken into account (Figure 4.2). While the data we present offer the best available indicative time-series within a region, consideration should be given to how representative these data are of the whole ecoregion in large areas with complex circulation patterns.

Viking Buoy. Photo: S. Snook

[1] http://lme.edc.uri.edu/index.php/lme-briefs

[2] http://www.ices.dk/advice/ICES%20ecoregions%20and%20advisory%20areas/Pages/ICES-ecosystems-and-advisory-areas.aspx

[3] http://www.gebco.net/data_and_products/undersea_feature_names/

4.1 West Greenland

B. Cisewski

The NOAA Large Marine Ecosystems project identifies the ecosystem of the Canadian Eastern Arctic–Western Greenland as a single LME. Here, only conditions in the Western Greenland portion of the region are examined. The hydrographic conditions presented are monitored at two oceanographic sections across the continental slope of West Greenland in the southwestern part of the ecoregion at a position that is influenced by the West Greenland Current (WGC; Figure 4.3). The WGC carries water northward along the west coast of Greenland and consists of two components: a cold, fresh inshore component, which is a mixture of Polar Water and melt water, and a warmer, saltier offshore component, which is called Irminger Sea Water. Being part of the cyclonic Subpolar Gyre, the WGC is subject to hydrographic variations on time-scales associated with variability in the gyre.

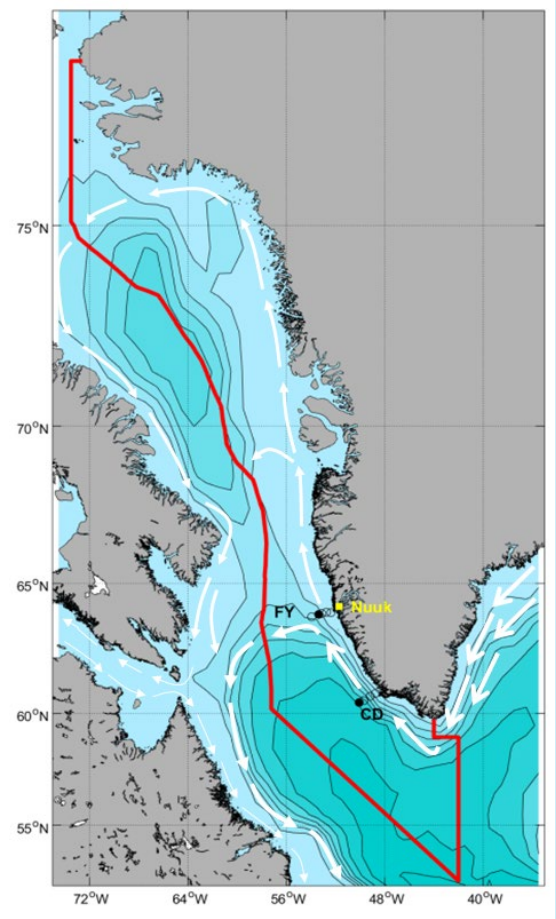

Figure 4.3. Circulation schematic for the Labrador Sea and Davis Strait. The location of Nuuk is marked in yellow. White arrows show the path of the surface circulation. The thick arrows are the WGC. The red lines show the extent of NAFO Area 1a, Western Greenland. Circles labelled 'FY' are the stations of the Fyllas Bank hydrographic section; station 4 is marked as a black circle. Circles labelled 'CD' are the stations of the Cape Desolation hydrographic section; station 3 is marked as a black circle.

In winter 2018/2019, the NAO index was positive (+2.09) for the sixth consecutive winter. The annual mean air temperature at Nuuk Weather Station in West Greenland was 0.4°C in 2019, which was 1.8°C above the 1981–2010 long-term mean (Figure 4.4).

Hydrographic conditions are monitored at two oceanographic NAFO–ICES sections, which span the western shelf and continental slope of Greenland near Cape Desolation (Figure 4.6) and Fyllas Bank (Figure 4.5). Two offshore stations at each section have been chosen to document changes in hydrographic conditions off West Greenland. However, in autumn 2019, the Fyllas Bank section had to be abandoned due to time constraints. In November 2019, water temperature in the 75–200 m layer at Cape Desolation Station 3 was 5.98°C and salinity was 34.92, 0.26°C above and 0.004 below the long-term means, respectively.

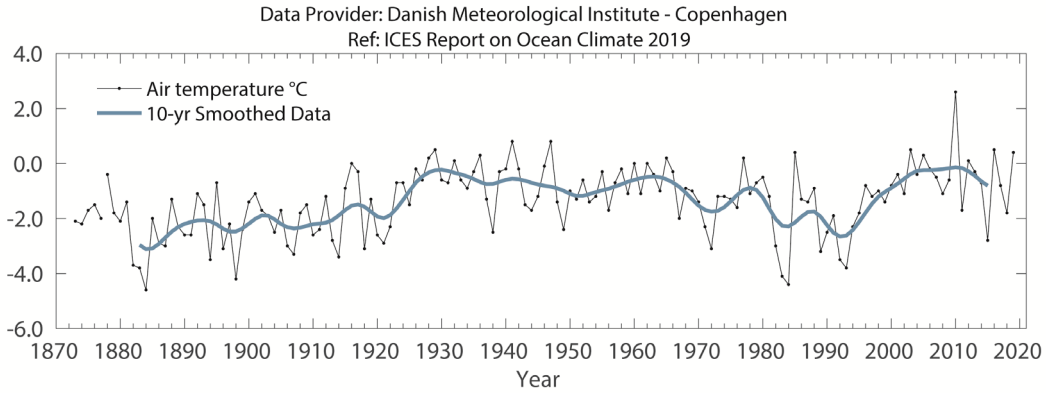

Figure 4.4. West Greenland. Annual mean air temperature at Nuuk station (64.16°N51.75°W). Data source: Cappelen (2020).

CTD and zooplankton net. Photo: Svanhildur Egilsdottir, Marine and Freshwater Institute, Iceland

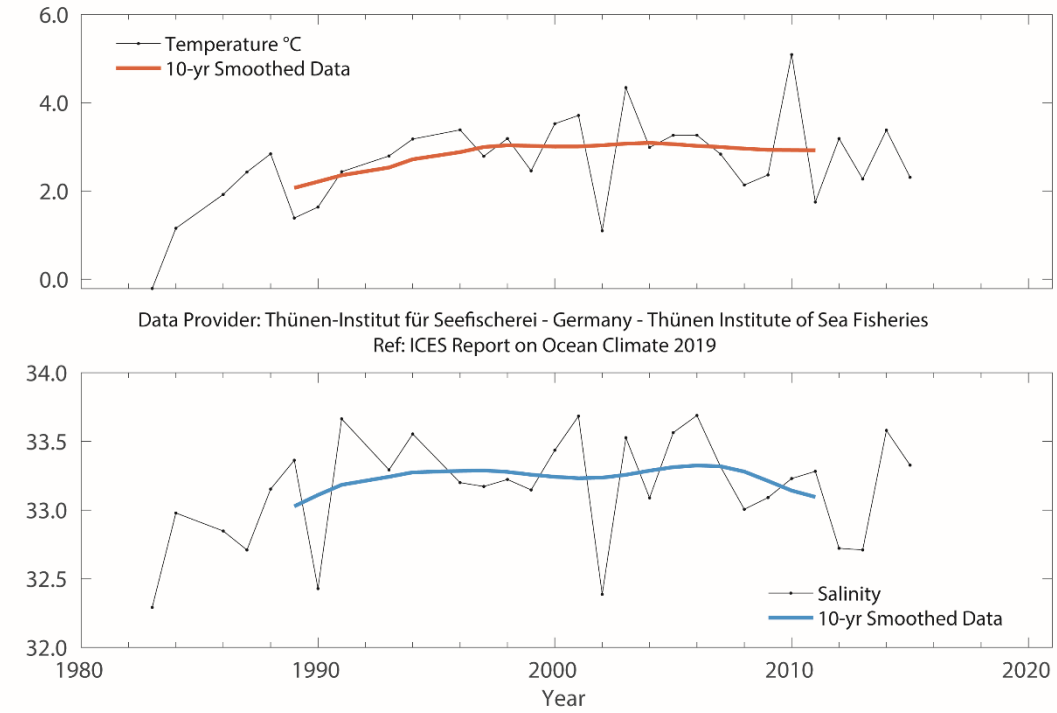

Figure 4.5. West Greenland. Mean temperature (upper panel) and salinity (lower panel) in the 0–50 m water layer at Fyllas Bank Station 4 (63.88°N 53.37°W). Data until 2015.

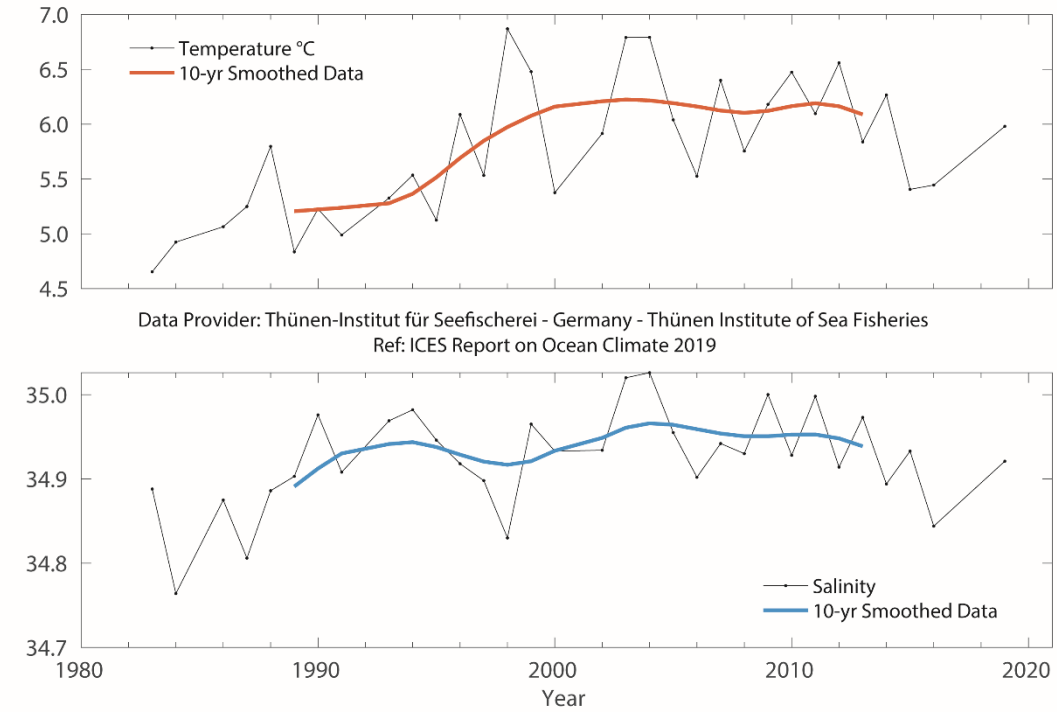

Figure 4.6. West Greenland. Temperature (upper panel) and salinity (lower panel) in 75–200 m water layer at Cape Desolation Station 3 (60.47°N 50°W).

4.2 Labrador Sea

I. Yashayaev

THERE IS NO 2019 UPDATE FOR THE LABRADOR SEA.

For the most recent regional overview, please see Section 4.2 in the IROC 2018 (González-Pola *et al.*, 2018).

The Labrador Sea is located between Greenland and the Labrador coast of eastern Canada. Its deep semi-enclosed basin is bounded by the West Greenland and Newfoundland–Labrador shelves. Cold, low-salinity waters of polar origin circle the Labrador Sea in a counterclockwise current system that includes both the north-flowing WGC on the eastern side and the south-flowing Labrador Current on the western side. Patches of warmer and saltier AW, typically found under the offshore extension of the WGC, can be traced to their origin in the low latitudes of the North Atlantic by following the NAC and Gulf Stream. The AW mixes with other water masses and progressively becomes colder and fresher as it flows north into the Labrador Sea, following its eastern boundary, and eventually circuits the sea's northern and western peripheries.

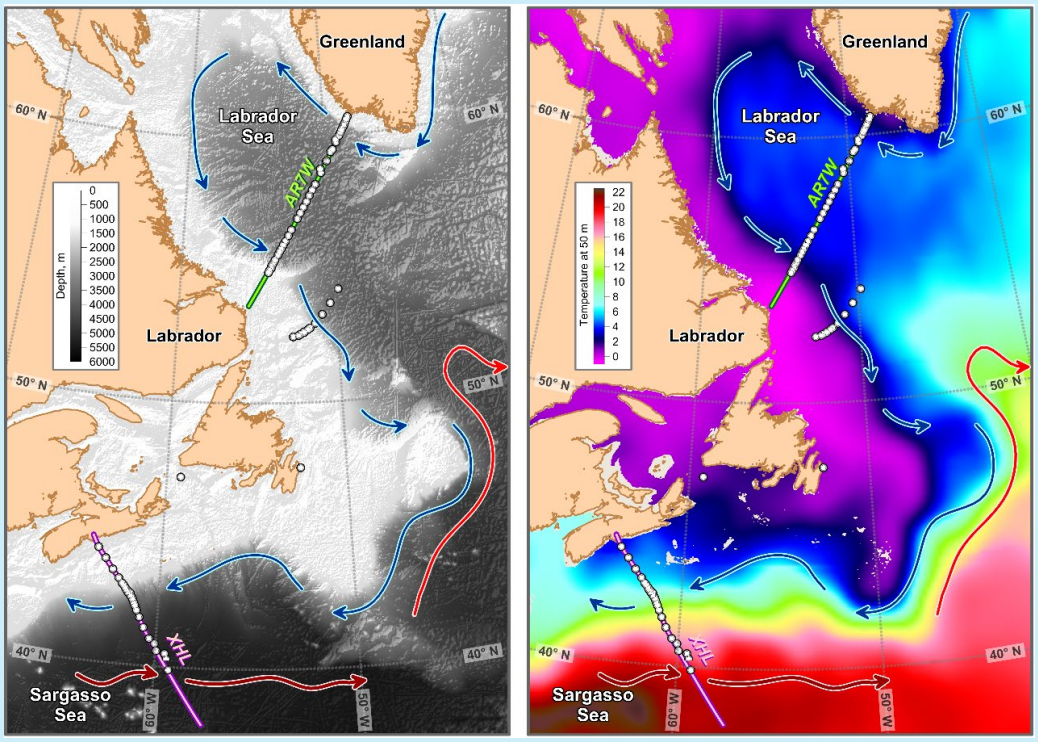

Figure 4.7. Labrador Sea. Topography, surface currents, and temperature at 50 m in the Atlantic Zone Offshore Monitoring Program (AZOMP) domain. Standard sampling (CTD stations, AR7W, and Extended Halifax lines) are shown in both panels.

Interannual changes in the hydrographic conditions of the Labrador Sea are controlled by a number of factors, including annual heat loss to the atmosphere, heat and salt gain from the AW, freshwater gain from the Arctic outflow, sea ice melt, precipitation, and continental run-off. In addition, instantaneous conditions and process development depend on the cumulative effect of past heat, salt, and freshwater gains, and their respective temperature, salinity, and density changes, also termed ocean preconditioning (Yashayaev and Loder, 2017). In the Labrador Sea, surface heat losses in winter result in the formation of dense intermediate-depth waters (200–2500 m). This process makes the Labrador Sea the primary region in the northern hemisphere for the atmospheric ventilation of the Atlantic Ocean's intermediate-depth waters. Through winter cooling of surface and subsurface waters and their subsequent mixing and sinking to depths of 500–2500 m (depending on winter severity), a relatively dense and deep intermediate water mass is formed known as Labrador Sea Water. This water spreads over the Atlantic Ocean ventilating its deep layers and feeding and driving the global ocean's overturning circulation or ocean conveyor belt.

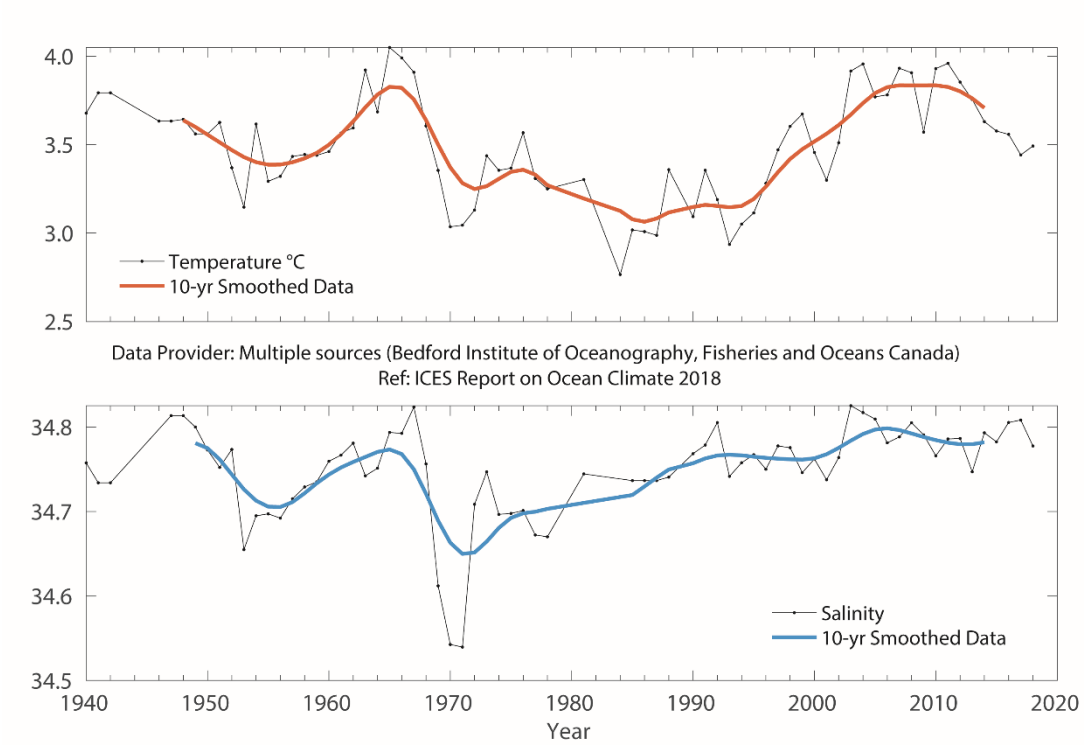

Figure 4.8. Labrador Sea. Potential temperature (upper panel) and salinity (lower panel) anomalies at 50–200 m, from CTD and Argo data in the west-central Labrador Sea (centred at 56.7°N 52.5°W). Estimates of seasonal cycle (derived from all data in the timeseries) have been removed from the observations Data until 2018.

4.3 Newfoundland–Labrador Shelf

F. Cyr and P. Galbraith

THE REGIONAL CLIMATE IN NEWFOUNDLAND AND LABRADOR WAS NORMAL IN 2019, CONTRASTING TO THE COLDER-THAN-AVERAGE CONDITIONS THAT MOSTLY PREVAILED DURING THE PERIOD 2014–2017.

The Newfoundland–Labrador Shelf region is situated on the western side of the Labrador Sea stretching from the Hudson Strait to the tail of the Grand Banks. It is dominated by shallow banks separated by deeper channels or saddles. The circulation is dominated by the south-flowing Labrador Current, which brings cold and fresh waters from the north, as well as sea ice and icebergs, to southern areas of the Grand Banks.

Hydrographic conditions in the region are determined, in part, by the strength of the winter atmospheric circulation over the Northwest Atlantic (e.g. winter NAO index), advection by the Labrador Current, cross-shelf exchange with warmer continental slope water, and bottom topography. Superimposed are large seasonal and interannual variations in solar heat input, sea ice cover, and storm-forced mixing. The resulting water mass on the shelf exhibits large annual cycles with strong horizontal and vertical temperature and salinity gradients.

The winter NAO index, a key indicator of the direction and intensity of the winter windfield patterns over the Northwest Atlantic, was positive for the sixth consecutive year. Despite this, the regional climate in Newfoundland and Labrador was mostly normal in 2019, contrasting to the colder-than-average conditions that mostly prevailed during 2014–2017.

Annual air temperature across the Northwest Atlantic was about normal, but characterized by warmer-than-normal temperatures in the north (e.g. +1.3 s.d. in Iqaluit, Baffin Island) and colder-than-normal temperatures on Newfoundland, especially during the first half of the year. At Cartwright, located in southern Labrador, the annual air temperature was normal at 0.1 s.d. (Figure 4.10). The seasonal (DJFMAMJ) mean sea ice volume was below normal at −0.8 and −0.9 s.d. on the Labrador and the Newfoundland shelves, respectively (Figure 4.9). This was characterized by a large negative anomaly in March–April, which also led to an early sea ice retreat on the Newfoundland shelf. A large number of icebergs (1515) also drifted south of 48°N, the seventh largest number since 1900.

At the standard monitoring site off eastern Newfoundland (Station 27), the depth-averaged annual water temperature has experienced a progressive cooling since the record-high temperatures of 2011 when it was +1.4°C (+2.8 s.d.) above normal (Figure 4.11). This warmer-than-average period generally coincided with fresher-than-average conditions that culminated in 2018, the freshest anomaly year since 1970, at −1.5 s.d. In 2019, however, both temperature and salinity were normal.

A robust index of ocean climate conditions in eastern Canadian waters is the areal extent of the cold intermediate layer (CIL), defined as the continental shelf waters < 0°C (Figure 4.12). After its formation during winter, the CIL remains isolated between the seasonally heated upper layer and the warmer shelf–slope water throughout summer and early autumn. During the 1960s, when the NAO was at its most negative phase of the 20th century, the volume of CIL water was at a minimum (warmer-than-normal conditions), and during the high NAO years of the early 1990s, the CIL volume reached near-record high values (colder-than-normal conditions). Since the late 1990s, as a consequence of increased ocean temperatures, the area of CIL water experienced a shrinking trend that lasted until 2011. However, since then, the CIL area has expanded and reached, in 2015, its highest level since 1970 on the Grand Bank during spring (+2.2 s.d.). In 2019, the CIL area was normal off southern Labrador (–0.3 s.d.) and below normal (–1.5 s.d.) off eastern Newfoundland during summer, the latter being the most negative anomaly since 2011.

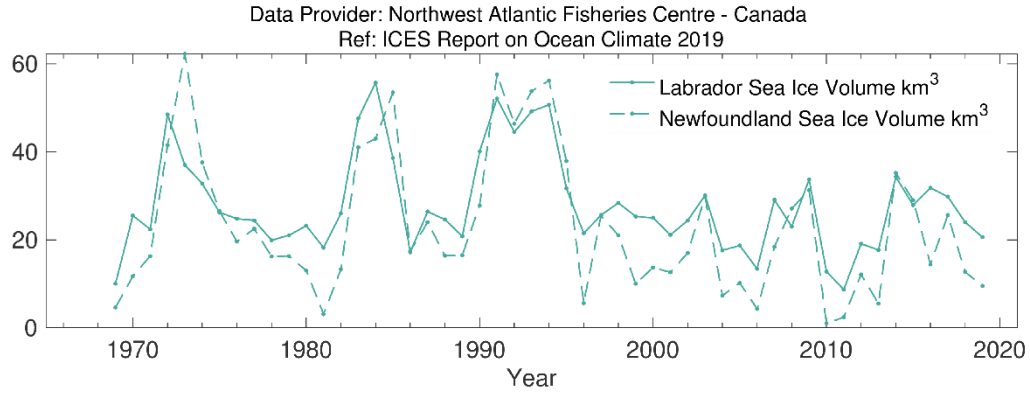

Figure 4.9. Northwest Atlantic: Newfoundland–Labrador Shelf. Winter and spring sea ice areas off Newfoundland–Labrador between 45°N and 55°N.

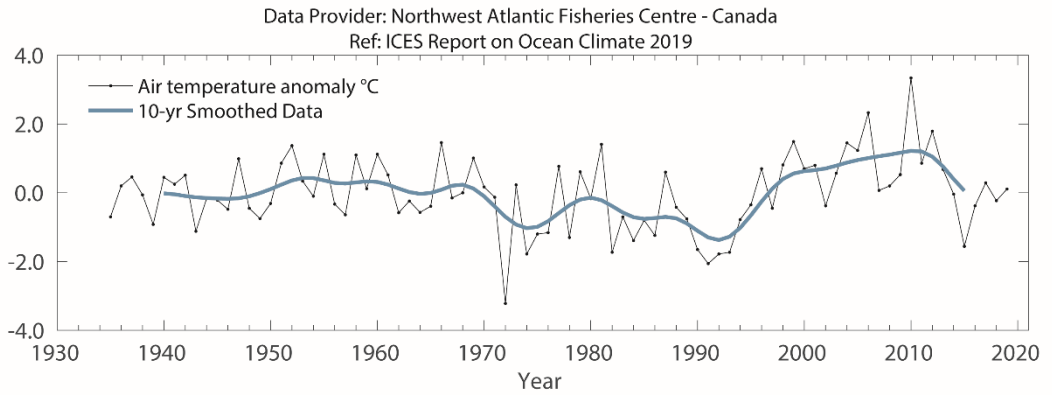

Figure 4.10. Northwest Atlantic: Newfoundland–Labrador Shelf. Annual air temperature anomalies at Cartwright on the Labrador coast.

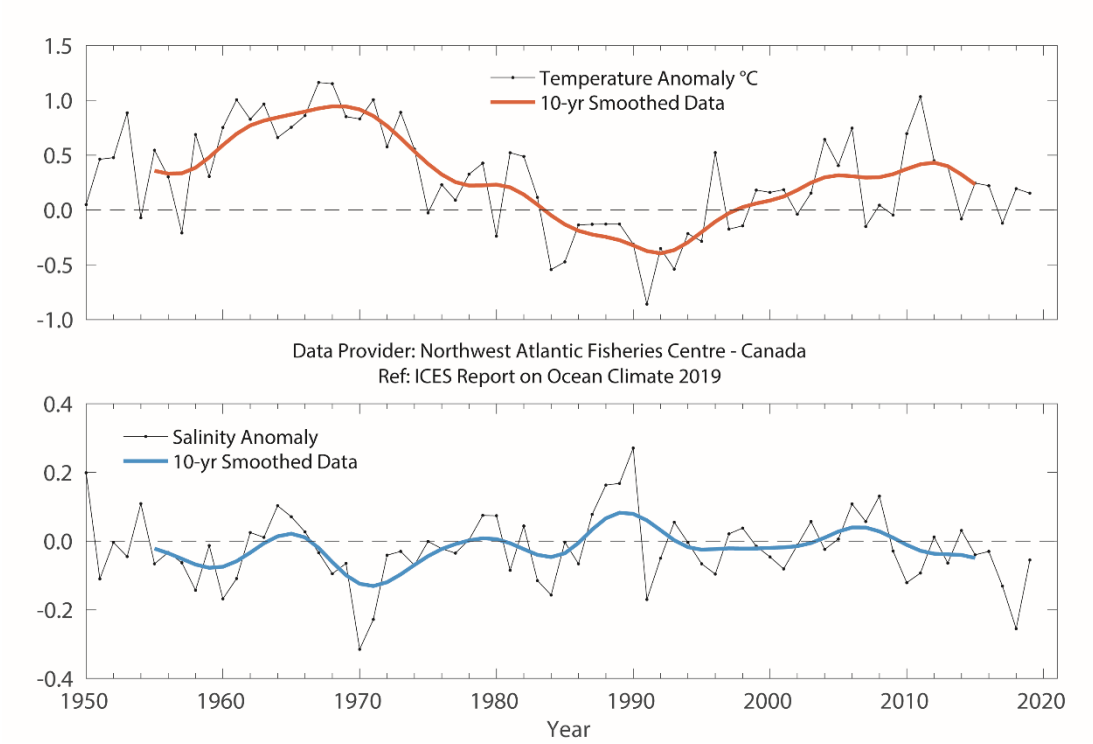

Figure 4.11. Northwest Atlantic: Newfoundland–Labrador Shelf. Annual depth-averaged Newfoundland Shelf temperature (top panel) and salinity (bottom panel) anomalies at Station 27 (47.55°N 52.59°W).

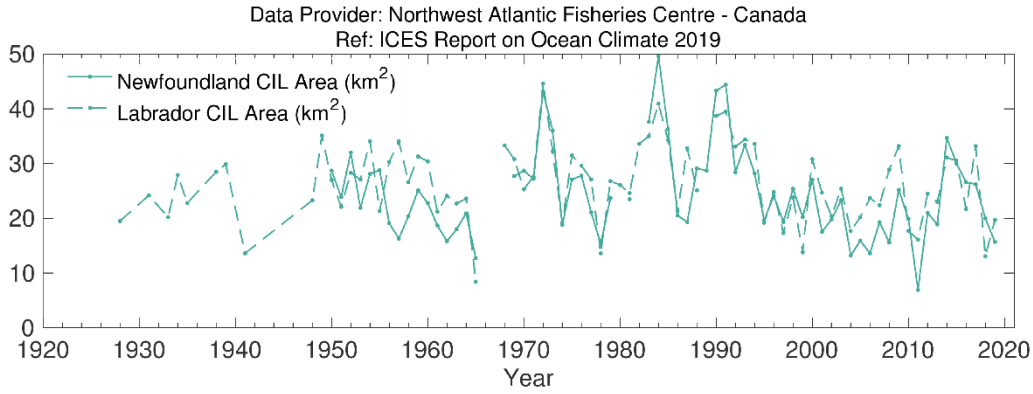

Figure 4.12. Northwest Atlantic: Newfoundland–Labrador Shelf. Spatial extent of CIL.

4.4 Gulf of St Lawrence

P. Galbraith

DEEP-WATER TEMPERATURE (300 M) IN THE GULF OF ST LAWRENCE WAS AT A RECORD HIGH. THE LAST FIVE YEARS WERE THE WARMEST ON RECORD.

The Gulf of St. Lawrence is a semi-enclosed Canadian sea covering an area of about 235 000 km^2 and containing 35 000 km^3 of water. It opens to the Atlantic Ocean through Cabot Strait (104 km wide and 480 m at its deepest) and the Strait of Belle Isle (17 km wide and 60 m deep at its sill). In winter, it can become completely covered by sea ice, and nearly half of its volume of water gets cooled to temperatures below 0°C within the winter mixed layer. This creates a CIL that persists until late autumn, and that determines the bottom temperature habitat on the Magdalen Shallows.

Waters deeper than roughly 150–200 m are entrained inwards from the continental slope by estuarine circulation, taking several years to reach the heads of the Gulf deep channels while mixing and diffusion occurs. This layer has been warming since 2009, up to 7°C in places in recent years.

The sea ice maximum volume reached during winter was near normal at 77 km^3 (+0.3 s.d.; Figure 4.13). In the 10-year span since 2010, seven of the ten lowest maximum ice volumes of the time-series have occurred, although this does not include 2019. In 2019, the sea ice cover formed much earlier than normal in the Estuary, the western portion of the Gulf, and along the coast of the lower north shore, but later than normal in offshore regions of the Gulf. It was the earliest first occurrence of ice on record in the Upper Estuary, and the first time it has occurred in November.

In winter, a near-freezing mixed layer is formed in the Gulf of St Lawrence that averages 75 m in depth. The layer has been sampled every March since 1996 using a unique helicopter-based survey, which now samples over 100 stations to 200 m depth from stationary flight. The mixed layer volume of 15 200 km^3, observed in March 2019, was the highest of the time-series (Figure 4.14). This record was aided by a large inflow of Labrador Shelf water into the Gulf, as determined from the same survey using water mass characteristics.

SST was greatly affected by the passage of tropical storm Dorian over the Gulf on September 7–8, 2019. A Viking oceanographic buoy (AZMP-ESG, East Southern Gulf) recorded a 60 mBar drop of atmospheric pressure to 960 mBar, 13 m waves, winds of 120 km h^{-1}, and a remarkable 8°C drop in surface water temperature. However, the ocean did not lose any heat. Temperature and salinity profiles from the Viking buoy done before the storm on August 23 and after the storm on September 10 show evidence of mixing down to a depth of 45 m and nearly identical 0–45 m depth-averaged temperature. The May–November SST average was below normal at −0.53 s.d., but would have been near-normal had it not been for the effect of tropical storm Dorian (Figure 4.15).

The volume of CIL (defined here as water masses with a temperature below 1°C) present in August and September is estimated from temperature profiles taken mostly during multispecies surveys since the mid-1980s (Figure 4.16). The volume in 2019 of 9100 km^3 was near-normal (−0.2 s.d.) for the first time since 2014, with the intervening years having volumes below normal (i.e. warmer-than-normal conditions).

Deep-water temperatures have been increasing overall in the Gulf since 2009, with inward advection from Cabot Strait (Figure 4.17). The Gulf-wide average temperature at 300 m has been at a new 100+ year record high every year since 2015, reaching 6.5°C (+1.0°C, +6.6 s.d.) in 2019.

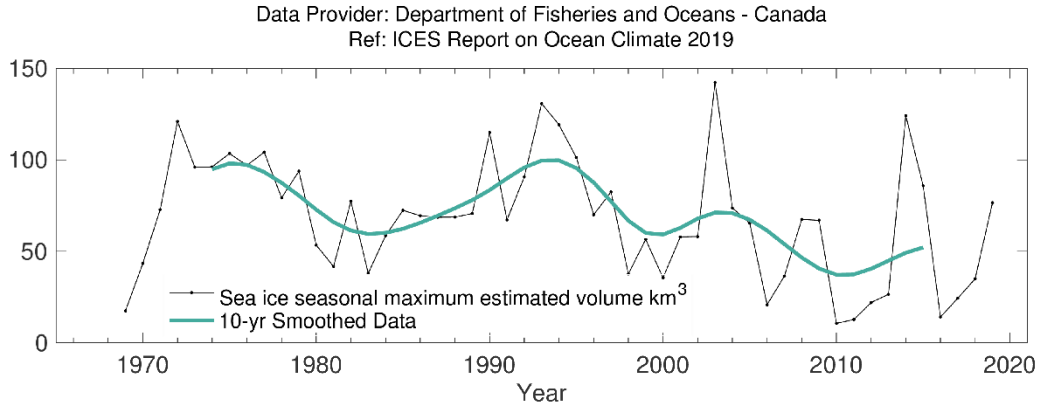

Figure 4.13. Gulf of St Lawrence. Seasonal maximum sea ice volume in the Gulf of St Lawrence estimated from weekly ice charts.

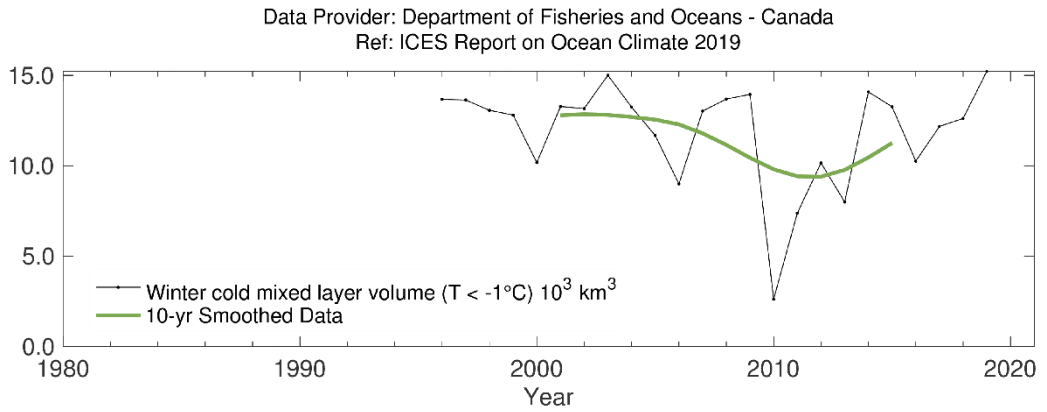

Figure 4.14. Gulf of St Lawrence. Winter mixed layer (T < –1°C) volume in the Gulf of St Lawrence.

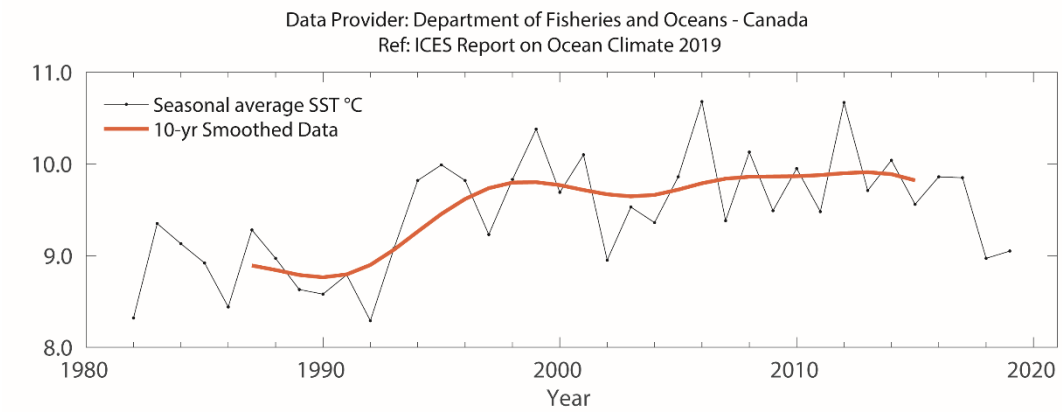

Figure 4.15. Gulf of St Lawrence. Seasonally averaged sea surface temperature (May–November) in the Gulf of St Lawrence.

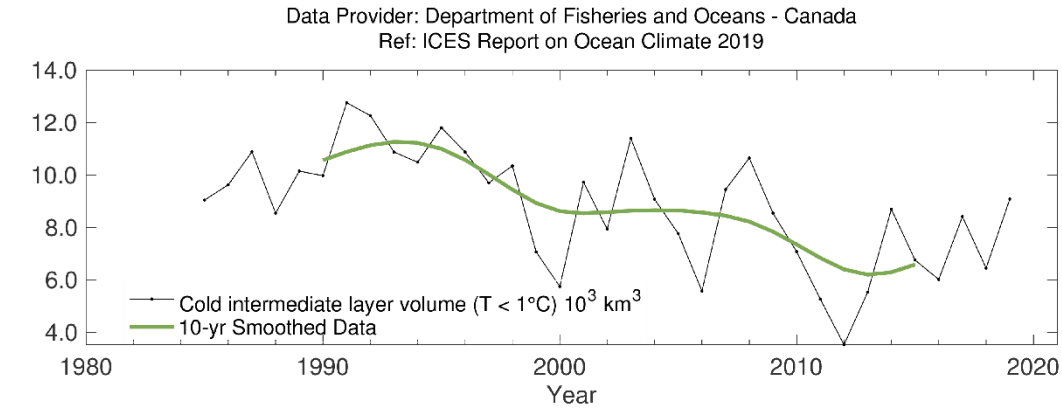

Figure 4.16. Gulf of St Lawrence. CIL volume (T < 1°C) present in August and September in the Gulf of St Lawrence.

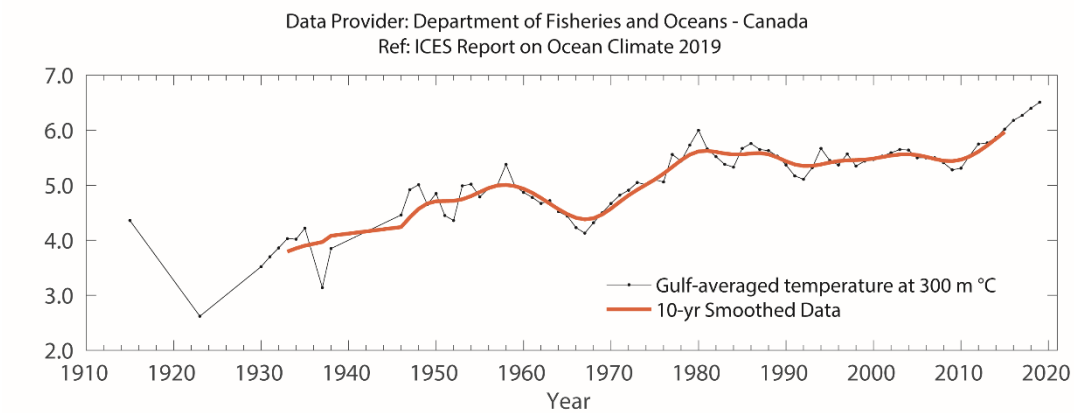

Figure 4.17. Gulf of St Lawrence. Averaged temperature at 300 m in the Gulf of St Lawrence.

4.5 Scotian Shelf

D. Hebert, C. Layton, and P. Galbraith

The Scotian Shelf is the continental shelf off the coast of Nova Scotia, and it is identified as a NOAA LME. It is characterized by complex topography consisting of many offshore shallow banks and deep mid-shelf basins. It is separated from the Newfoundland Shelf in the northeast by the Laurentian Channel and borders the Gulf of Maine to the southwest. Surface circulation is dominated by a general flow towards the southwest, interrupted by a clockwise movement around the banks and an anticlockwise movement around the basins, which vary in strength seasonally.

Hydrographic conditions on the Scotian Shelf are determined by heat transfer between ocean and atmosphere, inflow from the Gulf of St Lawrence and the Newfoundland Shelf, and exchange with offshore slope waters. Water properties have large seasonal cycles and are modified by freshwater run-off, precipitation, and melting of sea ice. Temperature and salinity exhibit strong horizontal and vertical gradients that are modified by diffusion, mixing, currents, and shelf topography.

In 2019, annual mean air temperature over the Scotian Shelf, represented by Sable Island observations, was −0.4°C (–0.6 s.d.) below the 1981–2010 long-term mean (Figure 4.18). The linear trend (and 95% confidence limits) from 1900 to 2019 is +1.3°C (+1.0°C, +1.6°C). The 2019 January–April seasonal average of sea ice on the Scotian Shelf, measured seaward of Cabot Strait between Nova Scotia and Newfoundland, was 8400 km^2, slightly above the 1981–2010 long-term mean of 6700 km^2. The maximum weekly area of 33 200 km^2 was well above the 20 900 km^2 long-term mean (Figure 4.19). This is the first year with above-average sea ice conditions since 2015.

Topography separates the northeastern Scotian Shelf from the rest of the shelf. In the northeast, the bottom tends to be covered by relatively cold water (2–5°C), whereas the basins in the central and southwestern regions typically have bottom temperatures of 6–10°C. The origin of the latter is the offshore slope waters, whereas water in the northeast comes principally from the Gulf of St Lawrence. The interannual variability of the two water masses differs.

Measurements of temperatures at 100 m at the Misaine Bank Station capture the changes in the northeast (Figure 4.20). They revealed near-average annual temperatures in 2019 (–0.2°C; –0.3 s.d.) and below-normal salinity (–0.2; –1.5 s.d.). The deep Emerald Basin anomalies represent slope-water intrusions onto the shelf that are subsequently trapped in the inner basins. In 2019, the 250 m annual temperature was a record high at +1.8°C (+2.2 s.d.), making it the sixth consecutive warmest year on record. Similarly, the salinity anomaly was well above normal at +0.30 (+2.0 s.d.). The last six years contain the five saltiest years on record, with 2019 being only slightly below the record in 2016 (Figure 4.21). Model simulations of the region showed a large flux of warm salty water from the slope region. Ocean temperatures and salinity in the deep basins of the Scotian Shelf were well above normal in 2019, even reaching record

highs or near-record highs, reflective of warm salty conditions in the slope region offshore.

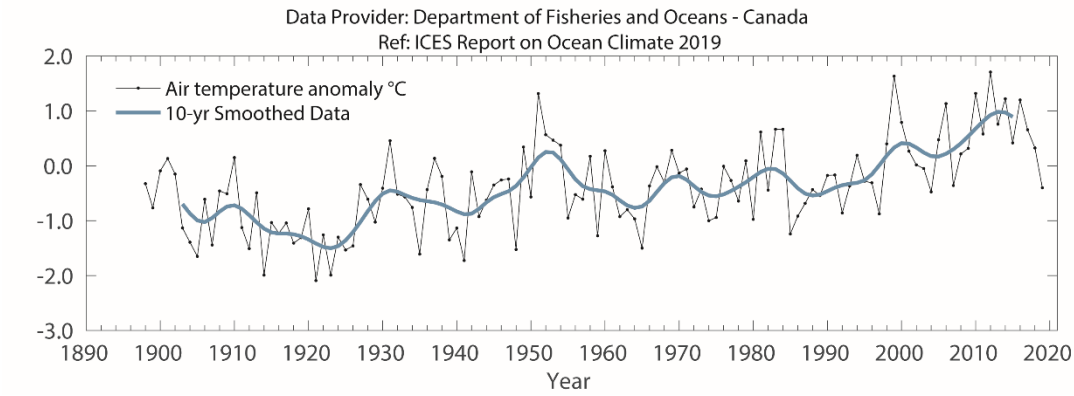

Figure 4.18. Northwest Atlantic: Scotian Shelf. Air temperature anomalies at Sable Island on the Scotian Shelf.

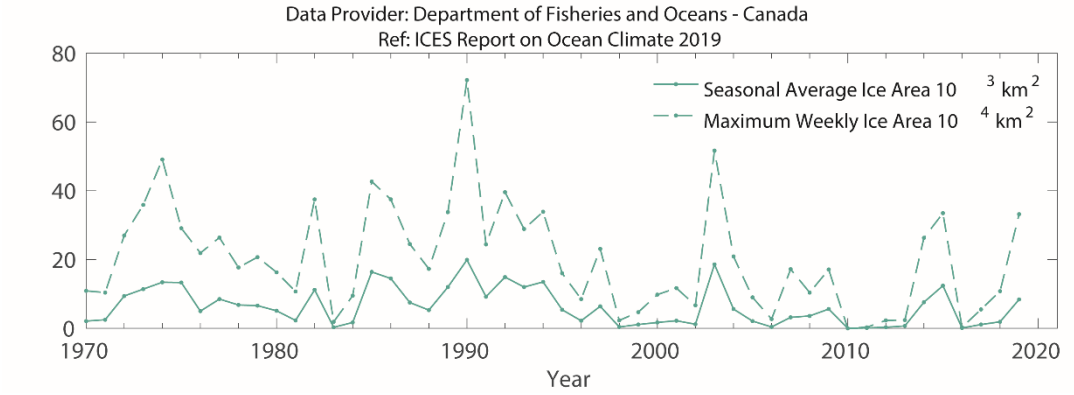

Figure 4.19. Northwest Atlantic: Scotian Shelf. Monthly means of ice area seaward of Cabot Strait.

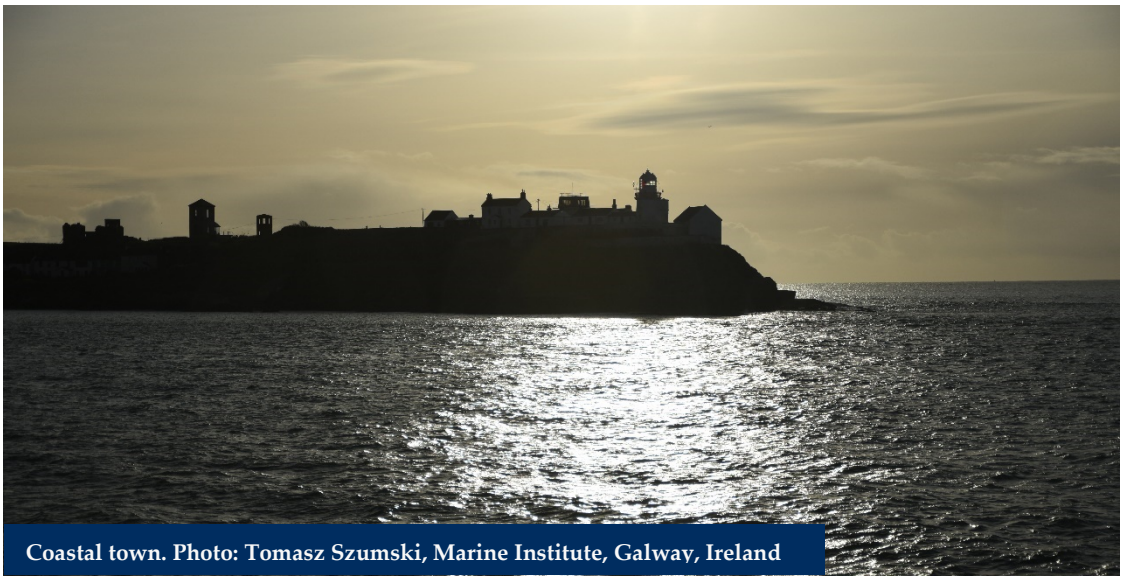

Coastal town. Photo: Tomasz Szumski, Marine Institute, Galway, Ireland

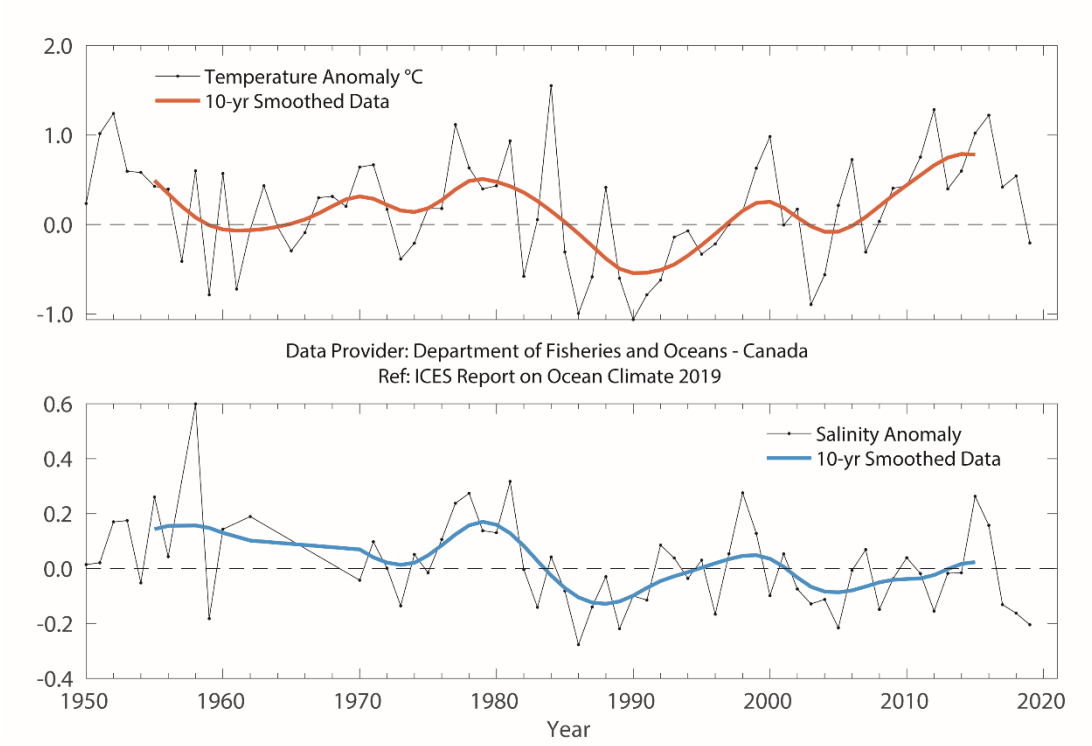

Figure 4.20. Northwest Atlantic: Scotian Shelf. Near-bottom temperature (upper panel) and salinity (lower panel) anomalies at Misaine Bank (100 m).

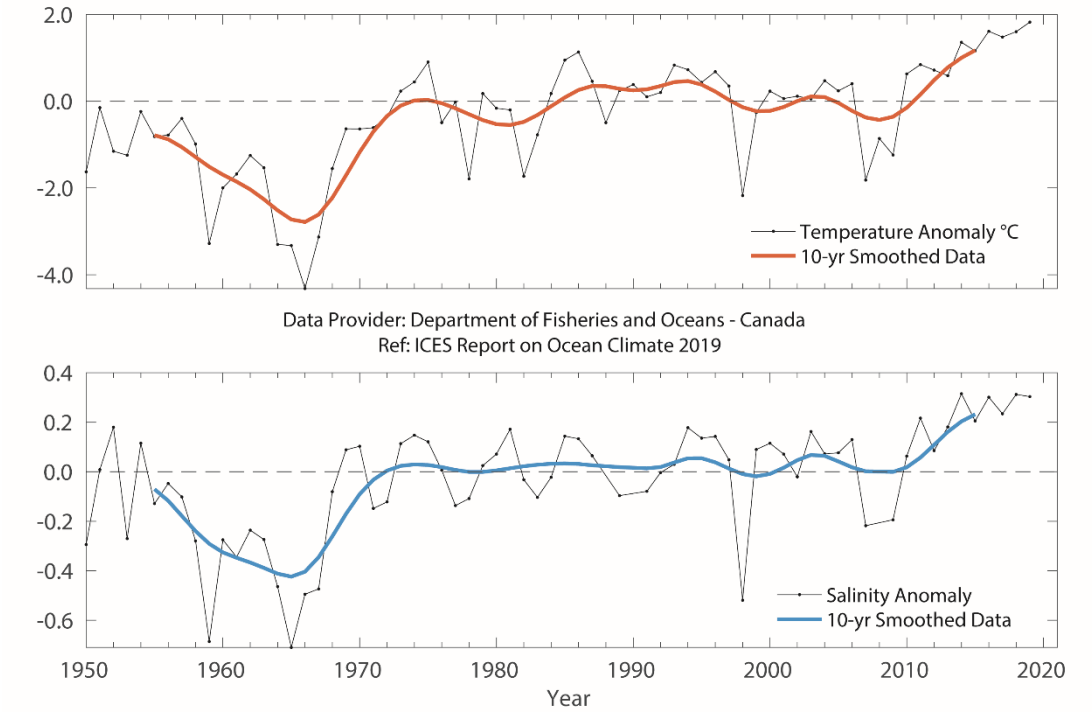

Figure 4.21. Northwest Atlantic: Scotian Shelf. Near-bottom temperature (upper panel) and salinity (lower panel) anomalies in the central Scotian Shelf (Emerald Basin, 250 m).

4.6 Northeast US continental shelf

P. Fratantoni

WATERS ON THE NORTHEAST US SHELF WERE WARMER THAN NORMAL, WITH ENHANCED WARMING OBSERVED IN SUMMER DUE TO AN INCREASE IN THE NUMBER OF GULF STREAM WARM CORE RINGS FORMED OFFSHORE.

The northeast US continental shelf extends from the southern tip of Nova Scotia, Canada, southwest through the Gulf of Maine and the Middle Atlantic Bight, to Cape Hatteras, North Carolina (Figure 4.22). Contrasting water masses from the Subtropical and Subpolar gyres influence the hydrography in this region. Located at the downstream end of an extensive interconnected coastal boundary current system, the northeast US continental shelf is the direct recipient of cold and fresh Arctic-origin water, accumulated coastal discharge, and ice melt that has been advected thousands of kilometres around the boundary of the subpolar North Atlantic. Likewise, subtropical water masses advected by the Gulf Stream, slope currents, and associated eddies also influence the composition of water masses within this shelf region. The western boundary currents of the Subpolar and Subtropical gyres respond to variations in basin-scale forcing through changes in position, volume transport, and/or water mass composition, and it is partly through these changes that basin-scale climate variability is communicated to the local northeast US continental shelf. Shelf-wide, hydrographic conditions have been monitored annually in this region since 1977 as part of quarterly ecosystem monitoring and through twice-yearly bottom-trawl surveys conducted by the US National Marine Fisheries Service, Northeast Fisheries Science Center.

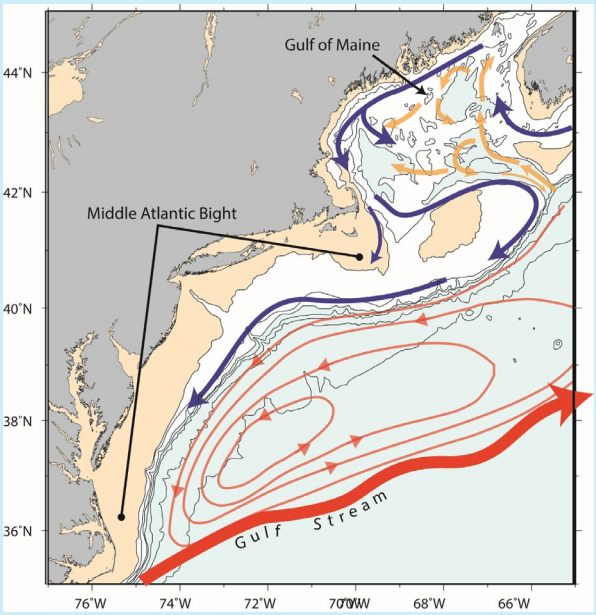

Figure 4.22. Northeast US continental shelf. Circulation schematic for the northeast US Shelf region, where blue arrows represent shelf water circulation and orange arrows represent deeper slope-water circulation pathways. Water depths deeper than 200 m are shaded blue. Water depths shallower than 50 m are shaded tan.

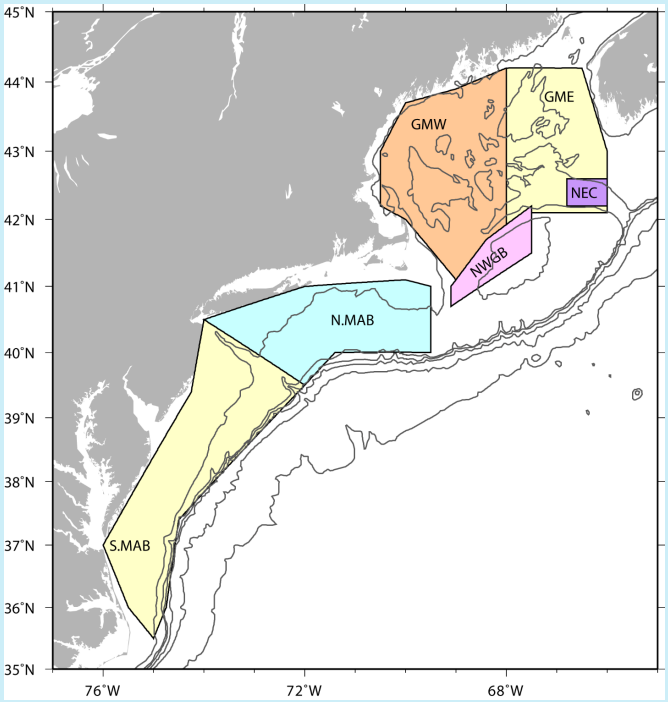

Figure 4.23. Northeast US continental shelf. The six regions within which CTD observations are used to compute regional average time-series. Eastern and western Gulf of Maine: GME and GMW, respectively; northern and southern Middle Atlantic Bight: N.MAB and S.MAB, respectively; Northeast Channel: NEC; Northwest Georges Bank: NWGB. The 50, 200, 500, 1 000, 2 000, and 3 000 m isobaths are also shown.

Observations indicate that the majority of the northeast US continental shelf was warmer in 2019 than the 1981–2010 mean. Annually, 0–30 m temperatures were between 0.5–1.1°C warmer than normal everywhere (Figure 4.24, Figure 4.25, Figure 4.26, Figure 4.27, and Figure 4.28). Of the seasons sampled, warming was most pronounced during summer in the Middle Atlantic Bight, Georges Bank, and eastern Gulf of Maine, where regional temperature anomalies approached 2°C (e.g. Figure 4.29). Extremely warm conditions were also observed near the bottom across the entire region, with anomalies exceeding those at the surface. Most notably, anomalies reached 2.7°C during October in the northern Middle Atlantic Bight, well outside the typical range of variability. Similarly, bottom temperatures measured more than one standard deviation above normal throughout the year in the Gulf of Maine.

In 2019, waters in the upper 30 m were saltier than normal in the northern Middle Atlantic Bight (Figure 4.25) and eastern Gulf of Maine (Figure 4.27), and near normal elsewhere. Seasonally, large positive anomalies (>1 s.d.) were observed during September and October in the northern Middle Atlantic Bight. Similar patterns were observed near the bottom, with more saline conditions than normal observed in the northern Middle Atlantic Bight and eastern Gulf of Maine. Seasonally, bottom waters in the eastern Gulf of Maine were saltier than normal throughout the year, whereas bottom waters in the northern Middle Atlantic Bight were anomalously salty in October relative to the rest of the year.

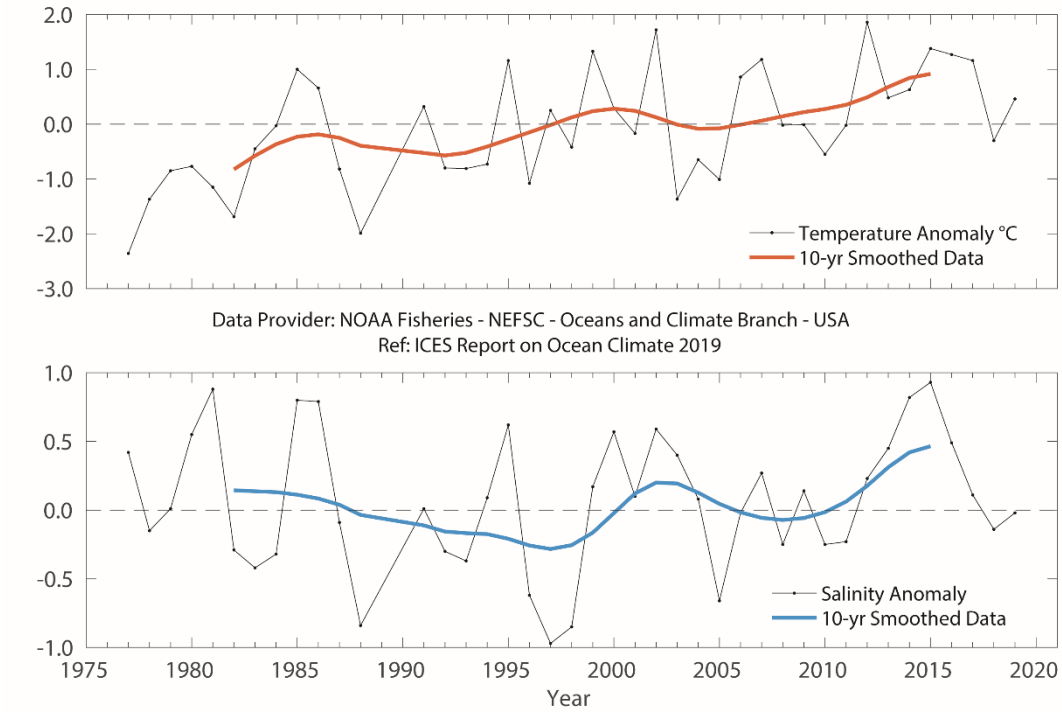

Figure 4.24. Northeast US continental shelf. Time-series plots of 0–30 m averaged temperature anomaly (upper panel) and salinity anomaly (lower panel) in the region between Cape Hatteras, North Carolina and Hudson Canyon. Anomalies are calculated relative to the period 1981–2010 using hydrographic data from shelf-wide surveys.

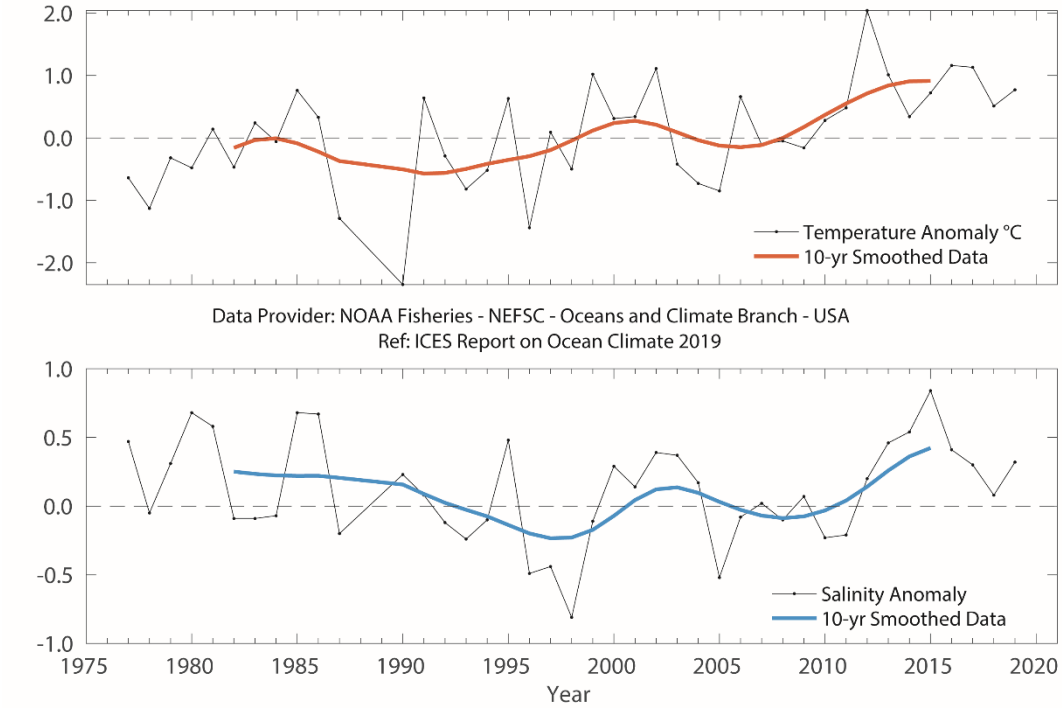

Figure 4.25. Northeast US continental shelf. Time-series plots of 0–30 m averaged temperature anomaly (upper panel) and salinity anomaly (lower panel) in the region between Hudson Canyon and Cape Cod, Massachusetts. Anomalies are calculated relative to the period 1981–2010 using hydrographic data from shelf-wide surveys.

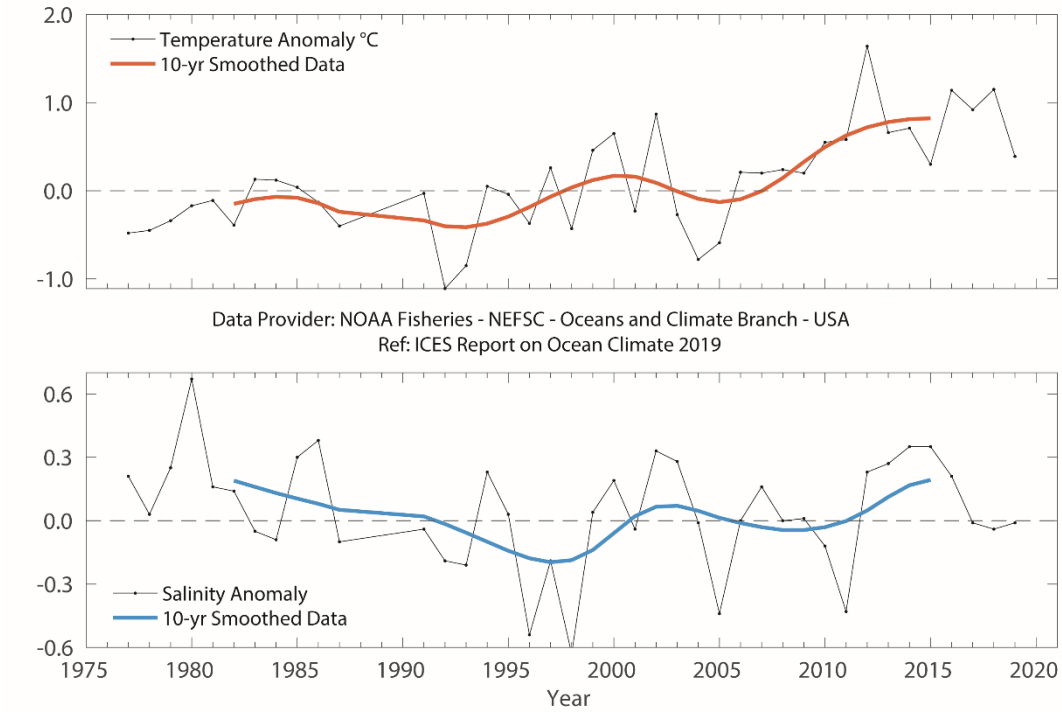

Figure 4.26. Northeast US continental shelf. Time-series plots of 0–30 m averaged temperature anomaly (upper panel) and salinity anomaly (lower panel) in the western Gulf of Maine. Anomalies are calculated relative to the period 1981–2010 using hydrographic data from shelf-wide surveys.

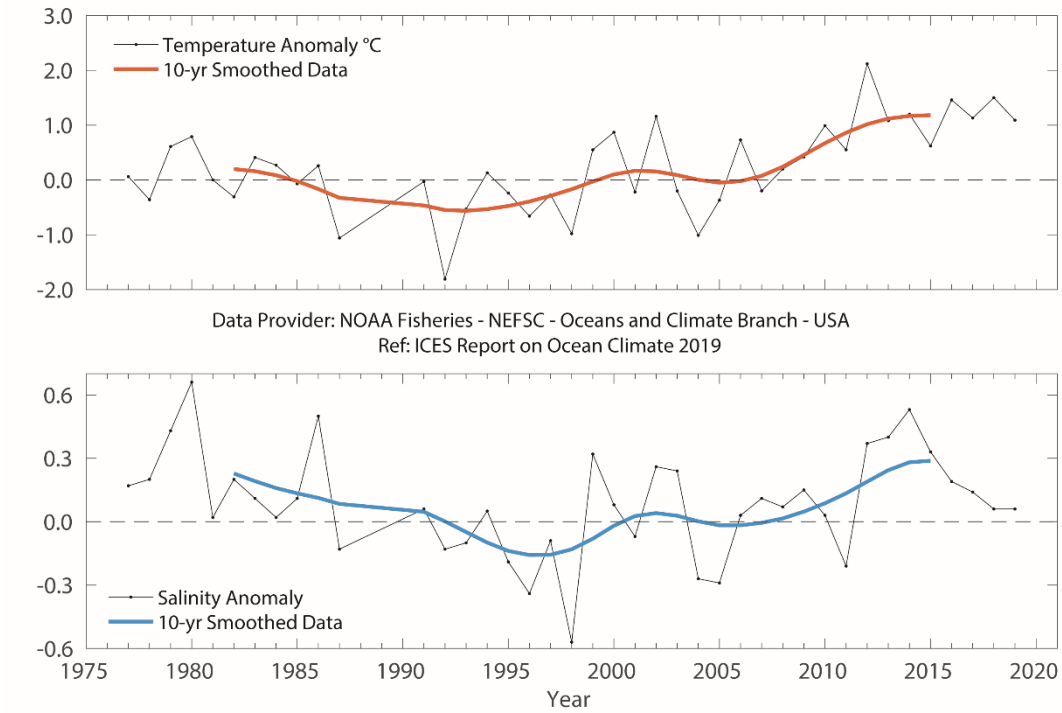

Figure 4.27. Northeast US continental shelf. Time-series plots of 0–30 m averaged temperature anomaly (upper panel) and salinity anomaly (lower panel) in the eastern Gulf of Maine. Anomalies are calculated relative to the period 1981–2010 using hydrographic data from shelf-wide surveys.

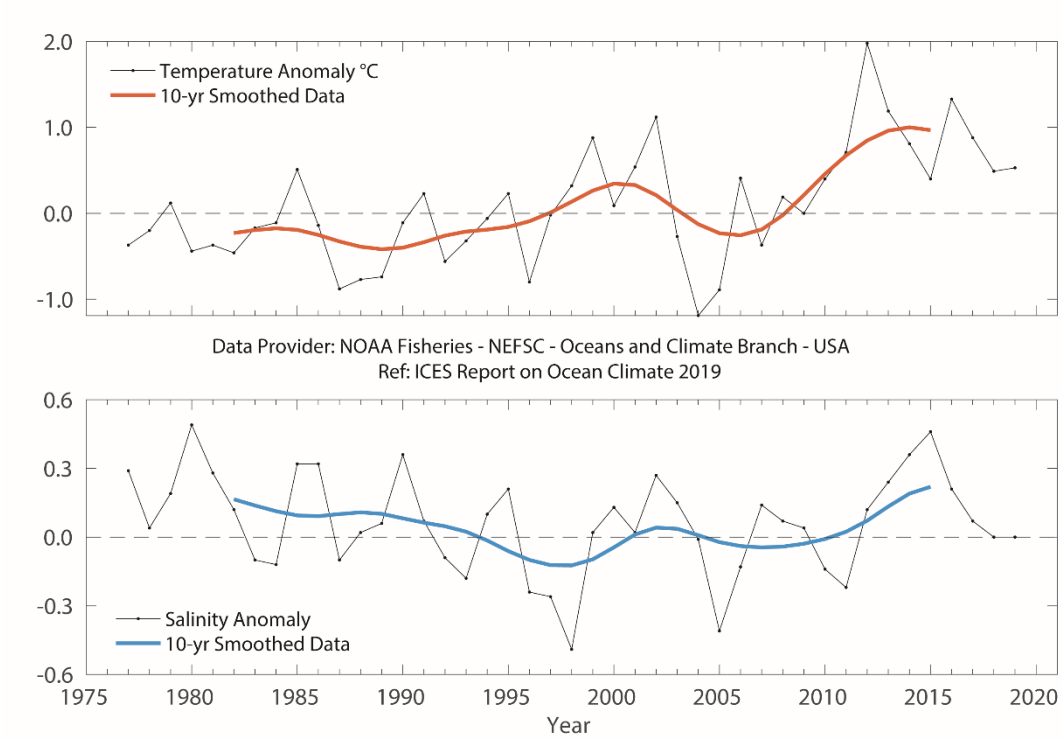

Figure 4.28. Northeast US continental shelf. Time-series plots of 0–30 m averaged temperature anomaly (upper panel) and salinity anomaly (lower panel) on George Bank. Anomalies are calculated relative to the period 1981–2010 using hydrographic data from shelf-wide surveys.

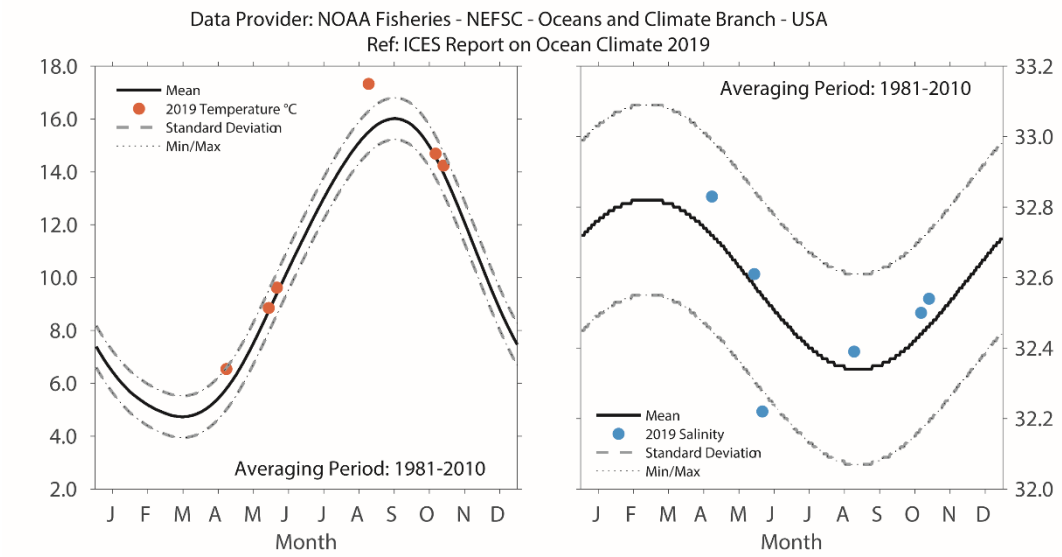

Figure 4.29. Northeast US continental shelf. 2019 temperature (left) and salinity (right) averaged over 0–30 m at northwest Georges Bank, relative to the annual cycle calculated 1981–2010. The envelope corresponding to the monthly range and one standard deviation are shown.

In the Gulf of Maine, slope waters entering through the Northeast Channel represent one of the dominant water mass sources at depth (Mountain, 2012). These deep waters, lying between 150 and 200 m, are uninfluenced by seasonal atmospheric forcing. Deep inflow to the Gulf of Maine was very warm and salty in 2019 compared with the long-term mean (Figure 4.30).

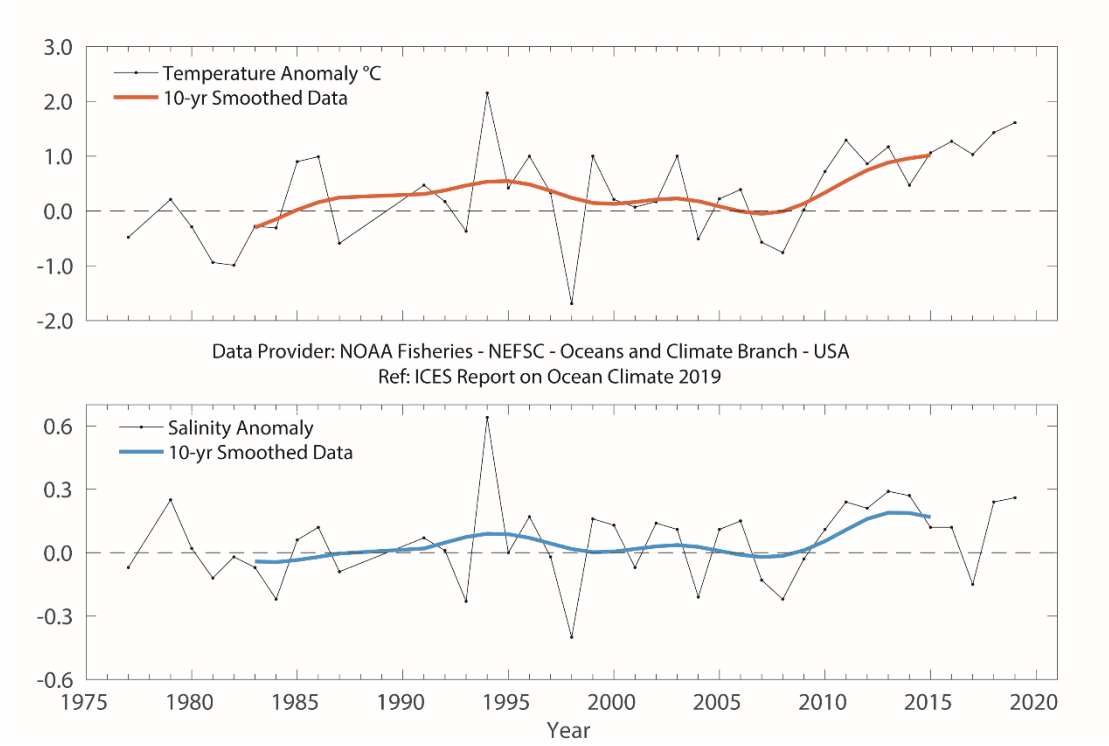

Figure 4.30. Northeast US continental shelf. Time-series plots of 150–200 m averaged temperature anomaly (upper panel) and salinity anomaly (lower panel) in the Northeast Channel. Anomalies are calculated relative to the period 1981–2010 using hydrographic data from shelf-wide surveys.

Salinity measurements. Photo: Svanhildur Egilsdottir, Marine and Freshwater Institute, Iceland

4.7 Icelandic waters

S. R. Ólafsdóttir and M. Danielsen

The Iceland Shelf and sea are identified as a NOAA LME and an ICES ecoregion. In Icelandic waters, mixing of different water masses occurs. The different water masses converge in an area of submarine ridges (Greenland–Scotland Ridge, Reykjanes Ridge, Kolbeinsey Ridge) that form natural barriers to the main ocean currents (Figure 4.31). The warm Irminger Current (6–8°C), a branch of the NAC, flows from the south, and the cold East Greenland and East Icelandic currents (–1°C to 2°C) flow from the north. Deep and bottom currents in the seas around Iceland have their principal source in the overflow of cold water from the Nordic seas and the Arctic Ocean over the submarine ridges into the North Atlantic

Hydrographic conditions in Icelandic waters are generally closely related to atmospheric or climatic conditions in and over the country and the surrounding seas, mainly through the Icelandic low-pressure and Greenland high-pressure systems. These conditions in the atmosphere and the surrounding seas affect biological conditions and impact the marine food chain and the recruitment and abundance of commercially important fish stocks.

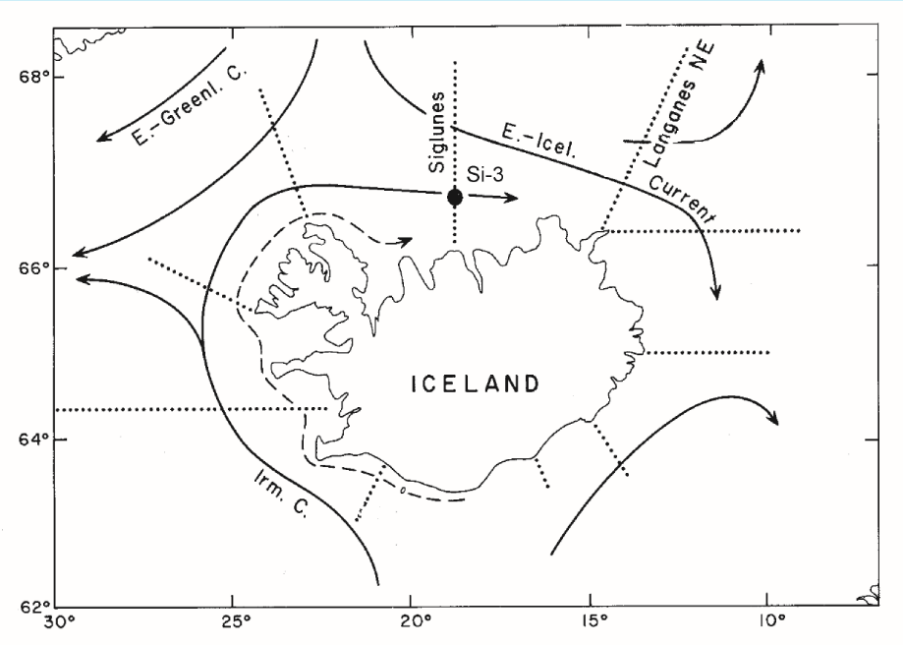

Figure 4.31. Main currents and location of standard sections in Icelandic waters.

The average air temperature for 2019 was somewhat lower than average in the south (Reykjavik), but continued to be higher than average in the north (Akureyri; Figure 4.32). The temperature of AW south of Iceland was slightly above average, while salinity increased by 0.04, but was still well below the average, as it has been since 2016 (Figure 4.34). North and northeast of Iceland, temperature continued to be above average, and the surface layer salinity rose to slightly above average (Figure 4.33 and Figure 4.35).

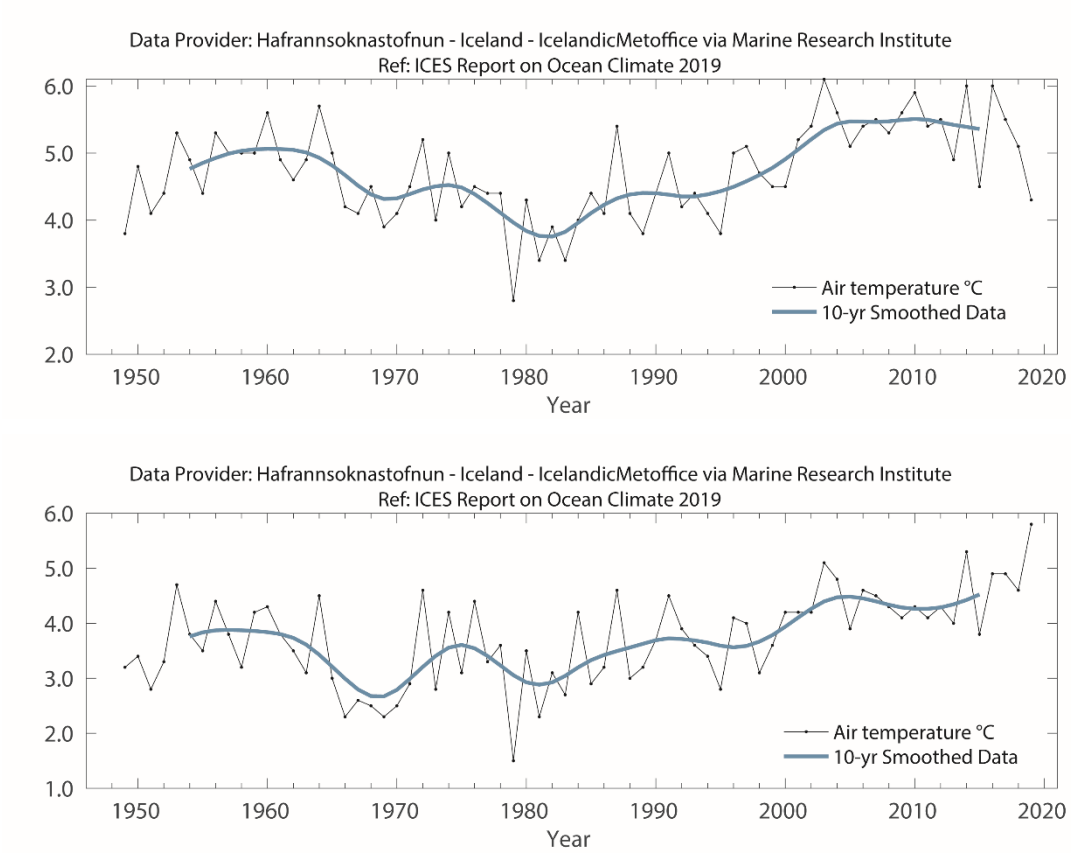

Figure 4.32. Icelandic waters. Mean annual air temperature at Reykjavik (upper panel) and Akureyri (lower panel).

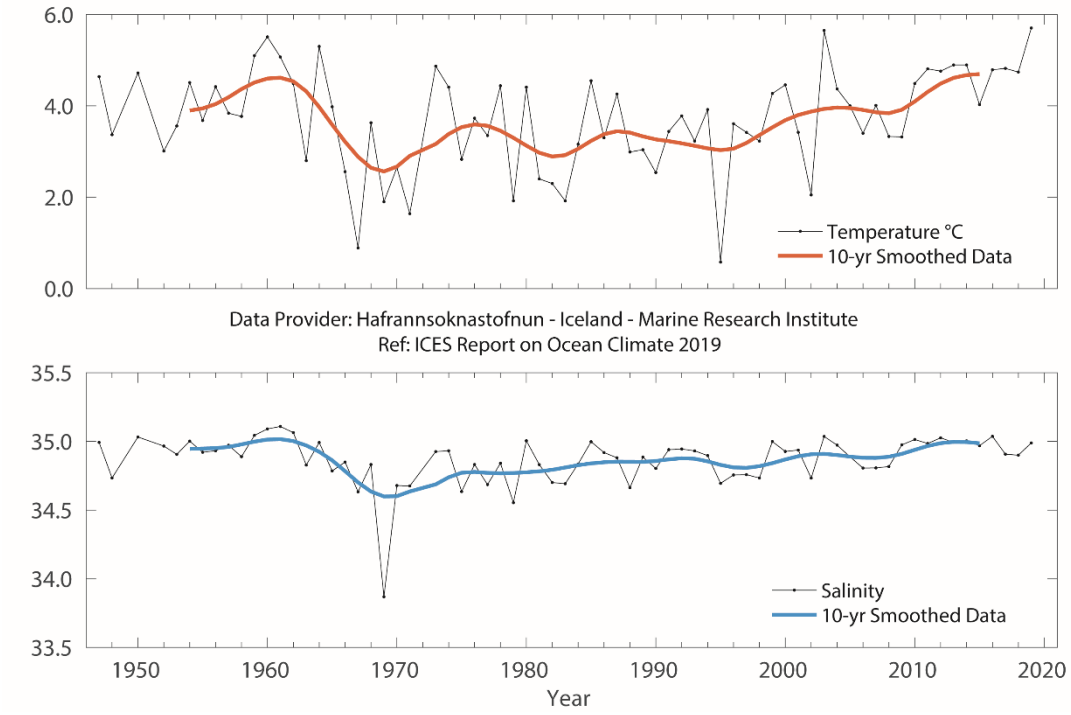

Figure 4.33. Icelandic waters. Temperature (upper panel) and salinity (lower panel) at 50–150 m at Siglunes Stations 2–4 in North Icelandic waters.

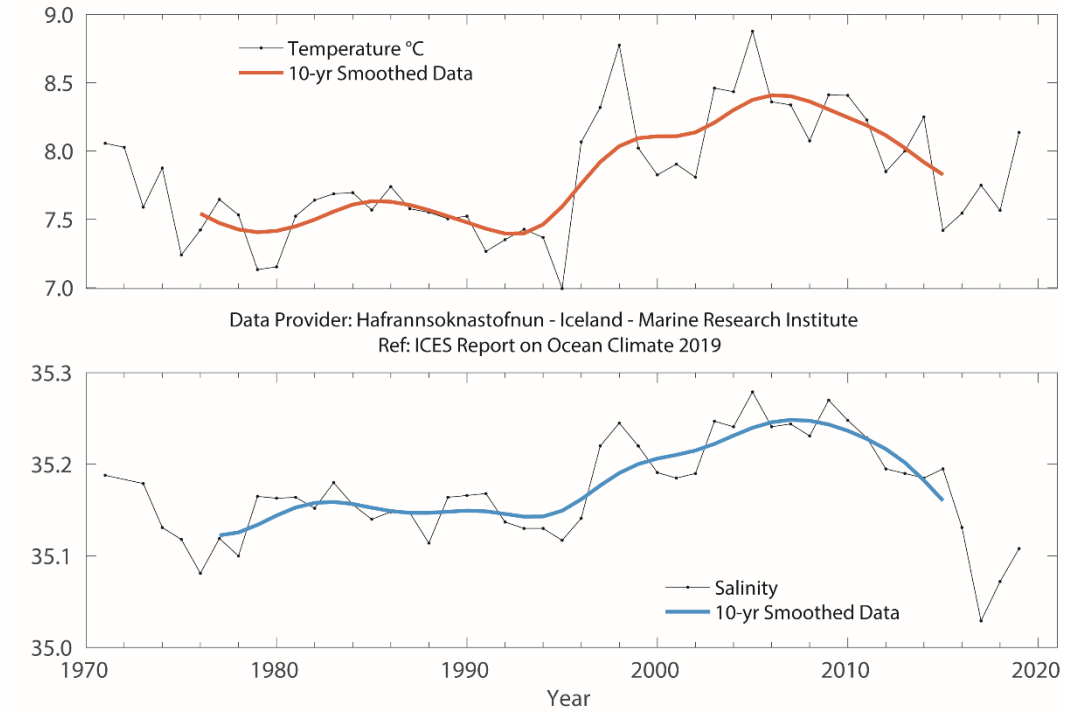

Figure 4.34. Icelandic waters. Temperature (upper panel) and salinity (lower panel) at 0–200 m at Selvogsbanki Station 5 in South Icelandic waters.

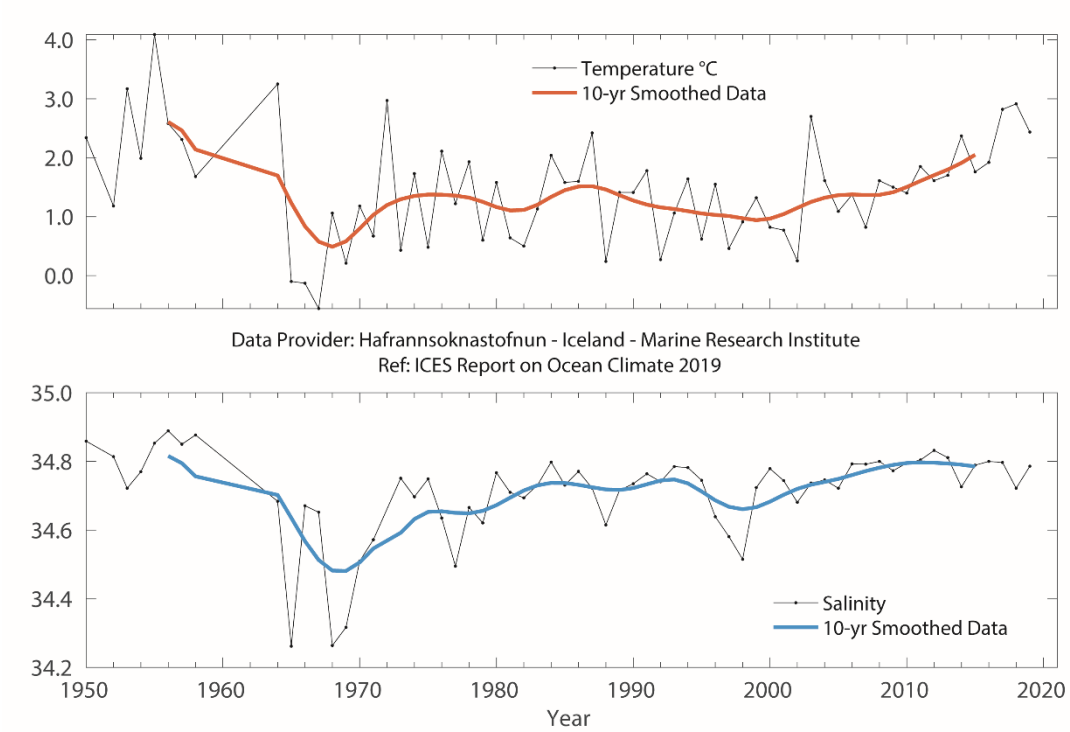

Figure 4.35. Icelandic waters. Temperature (upper panel) and salinity (lower panel) at 0–50 m in the East Icelandic Current (Langanes Stations 2–6).

4.8 Bay of Biscay and Iberian coast

A. Fontán, C. González-Pola, and V. Valencia

SHELF AND OPEN OCEAN UPPER WATERS REMAINED FRESH FOR A SIXTH CONSECUTIVE YEAR, WHILE TEMPERATURES ROSE, ESPECIALLY AT UPPERMOST LEVELS.

The western Iberian coast is located at the northeastern edge of the subtropical anticyclonic gyre, sometimes referred to as the intergyre region. It is characterized by a weak upper ocean circulation, with a mean southward flow of a few cm s^{-1} (e.g. Paillet and Mercier, 1997). The Bay of Biscay is considered an adjacent sea, with weak anticyclonic circulation (Pingree, 1993; van Aken, 2002). The area also encompasses the northern tip of the northwest Africa Upwelling system. Coastal upwelling events dominate in spring/summer, and a geostrophically balanced poleward flow known as the Iberian Poleward Current develops in autumn and winter (Pingree and Le Cann, 1990). Regional modal waters, which make up the upper permanent thermocline, are known as Eastern North Atlantic Central Waters (ENACW). Below them, Mediterranean Water (MW) spreads northwards from its source in the Gulf of Cadiz, mostly as a slope current. Further below, the Labrador Sea Water can be identified at approximately 1800 m, while the deep ocean is occupied by a mixture of cold polar waters known as North Atlantic Deep Water (NADW).

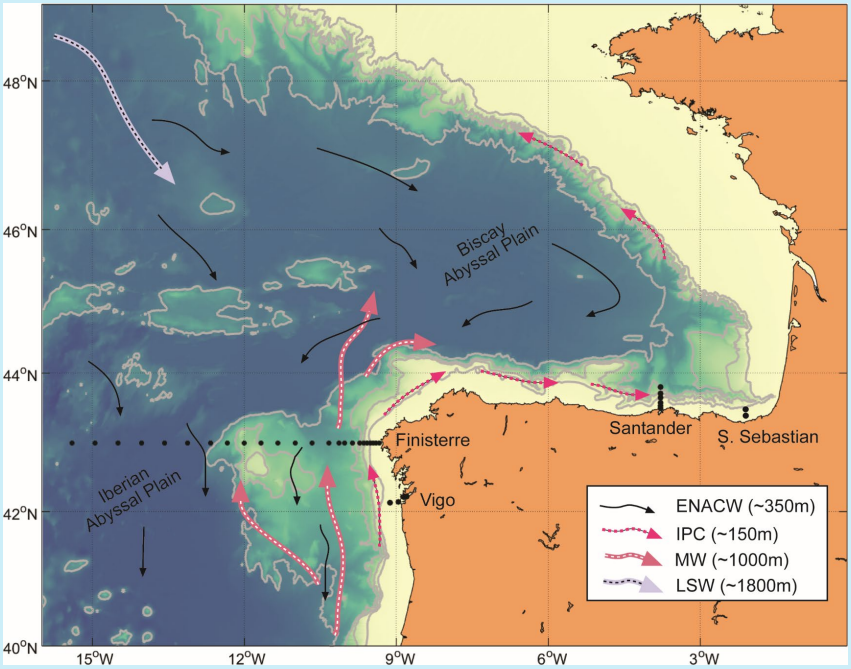

Figure 4.36. Circulation schematic for northwest Iberia and the Bay of Biscay. Black thin arrows show the dominant southward flow in the upper ocean carrying mainly ENACW. The Iberian Poleward Current and the MW pathways are also shown. Black dots show the repeated hydrographic stations, occupied monthly at Vigo, Santander and San Sebastian and 1–2 times per year at the Finisterre section.

In 2019, atmospheric conditions were spatially highly variable, ranging from warm to extremely warm at the Iberian Peninsula and the Balearics and slightly warm at the Canaries. Overall, annual atmospheric temperatures were around 0.6°C in the southern Bay of Biscay (1 s.d. above the 1981–2010 long-term average; Figure 4.37). The air temperature seasonal cycle in the southern Bay of Biscay was characterized by the prevalence of normal to very warm conditions, with the exception of January, which was very cold. In terms of precipitation, 2019 can be considered very wet in the southern Bay of Biscay, resulting from anomalously high precipitation in autumn. The annual continental run-off was near the 1981–2010 long-term average, resulting from the balance between a below-average river flow from January to October, and an above-average flow (> 1 s.d.) in November/December.

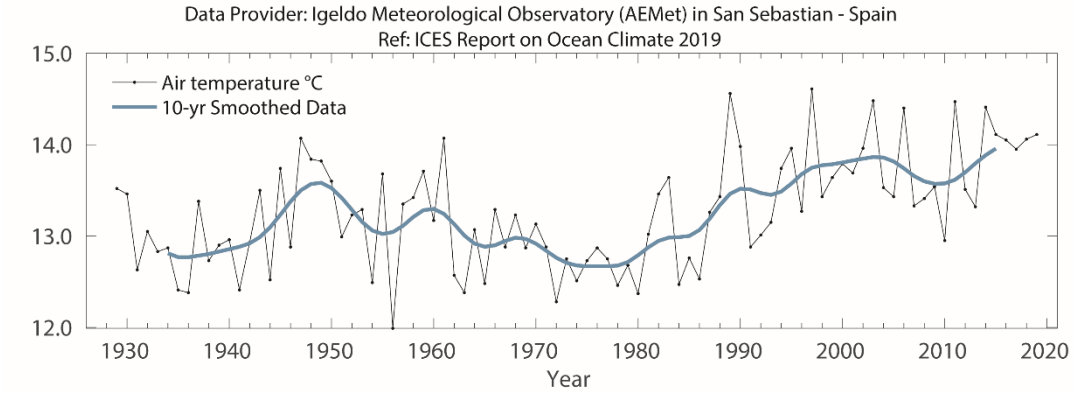

Figure 4.37. Bay of Biscay and Iberian Coast. Air temperature at San Sebastian (43°18.50´N 2°2.37´W).

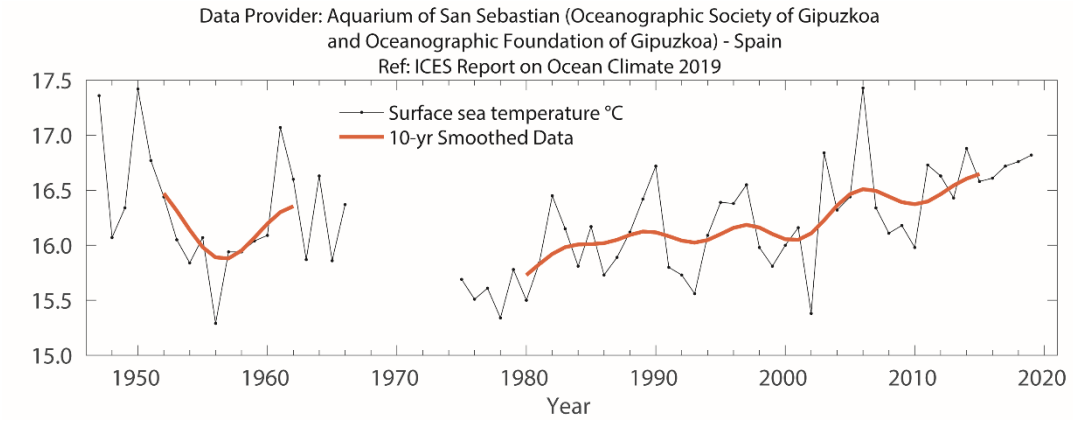

Figure 4.38. Bay of Biscay and Iberian Coast. Sea surface temperature at San Sebastian (43°18.50´N 2° 2.37´W).

SST responded to the local atmospheric forcing, with conditions ranging from normal to very warm in the second half of the year. The annual SST anomaly in 2019 was similar to previous years (> 0.6°C, > 1 s.d. above the long-term average; Figure 4.38). Upper water salinity measured closer to normal in the long-term reference series, which lacked sampling in the last quarter of the year (Figure 4.39). However, complementary records at the Basque Country shelf indicate further freshening at this time of year. Subsurface waters, below the winter development of the mixing layer (150 to 300 m depending on the year), were also fresher in 2019. This marked the sixth year

in a row with negative anomalies in salinity. Temperature rose to near long-term average values. The observed ocean conditions are the combination of warmer-than-normal atmospheric conditions, high precipitation, a weak signature of southern origin waters, and ongoing influence of fresher and colder waters currently spreading across the eastern North Atlantic. The status of deeper waters in the region is described in Section 5.2.6.

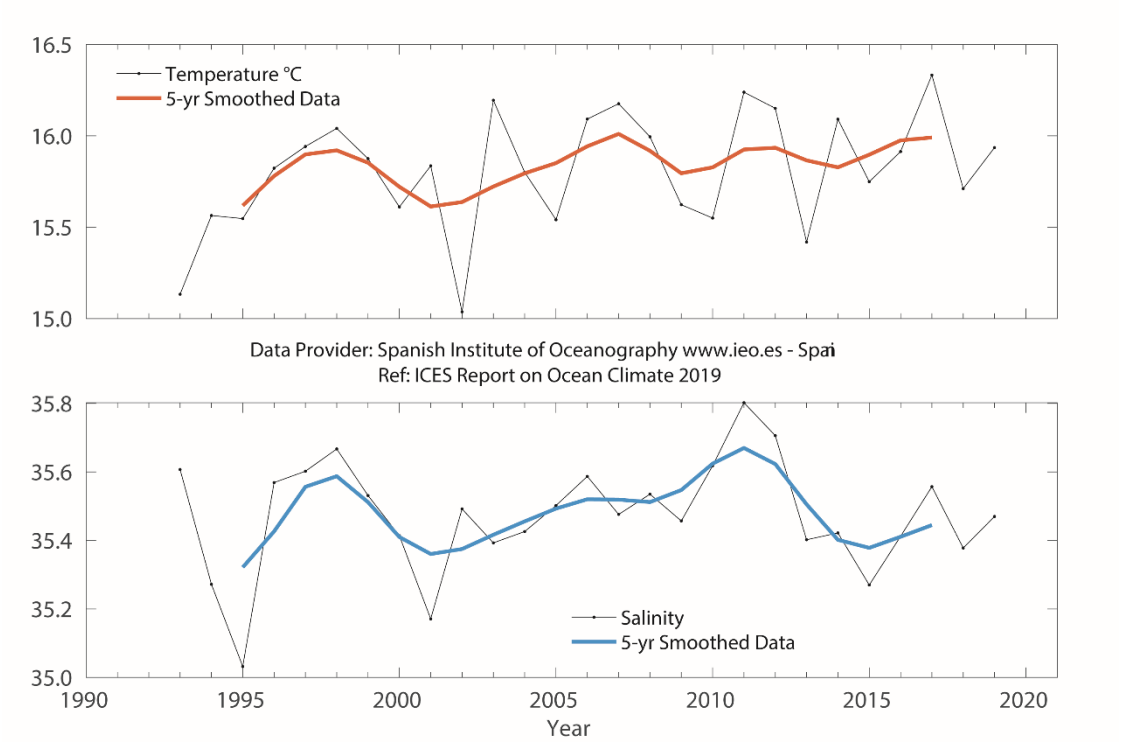

Figure 4.39. Bay of Biscay and eastern North Atlantic. Temperature (upper panel) and salinity (lower panel) at Santander Station 6, 0–30 m (43°42.50′N 3°47.00′W).

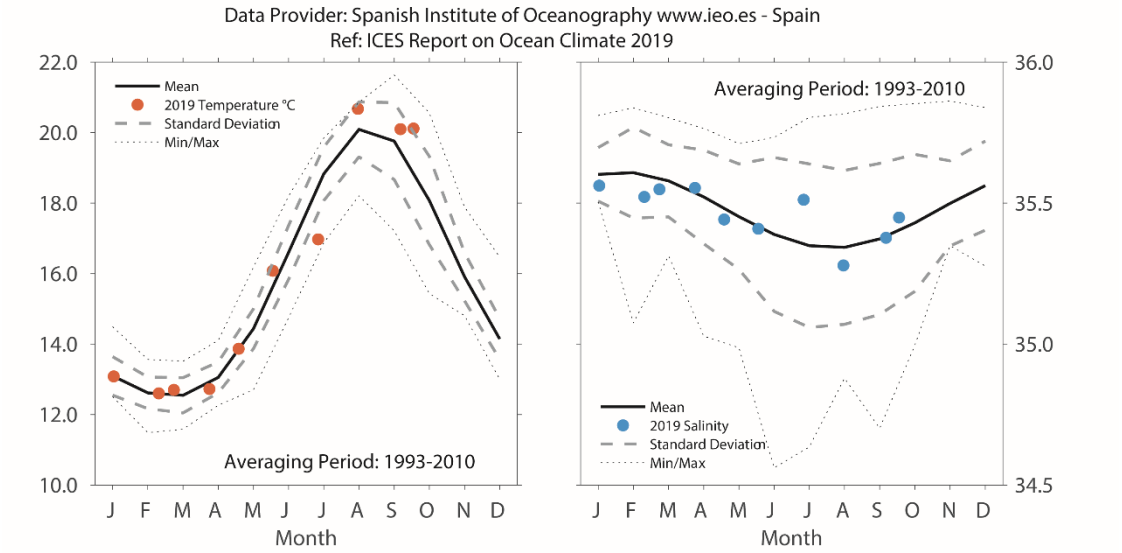

Figure 4.40. Bay of Biscay and eastern North Atlantic. 2018 monthly temperature (left panel) and salinity (right panel) at Santander Station 6, 0–30 m (43°42.50′N 3°47.00′W).

4.9 Gulf of Cadiz

R. Sánchez-Leal

IN 2019, AW FROM THE SURFACE DOWN TO 300 M WERE COLDER THAN THE AVERAGE AND SET THE HISTORIC (2009–2019) LOW-SALINITY RECORD.

The Gulf of Cadiz is located off the southwestern Iberian Peninsula. The circulation dynamics are largely governed by water exchange through the Strait of Gibraltar, the ocean gateway between the Atlantic Ocean and the Mediterranean Sea. The two-layered inverse estuarine circulation features MW flowing into the Gulf of Cadiz under AW flowing into the Mediterranean Sea. Dominant features include: (i) the baroclinic Gulf of Cadiz Current, that advects relatively fresh and cool waters from the Portuguese Coastal Transition Zone (CTZ) to feed the Atlantic Inflow (AI) in the Mediterranean basin; (ii) the meridional branch of the Azores Current, a largely barotropic flow that brings warmer more saline AW to supplement the AI into the Mediterranean; (iii) an inshore current system linked with coastal runoff like the Guadalquivir River plume; and (iv) the Trafalgar cyclonic cell, an upwelling hotspot generated by tidal stirring over the Trafalgar Banks. The subsurface circulation is given by the Mediterranean Overflow, a branched, warm, saline, and dense gravity current along the seabed that follows the intricate bottom topography (Figure 4.41).

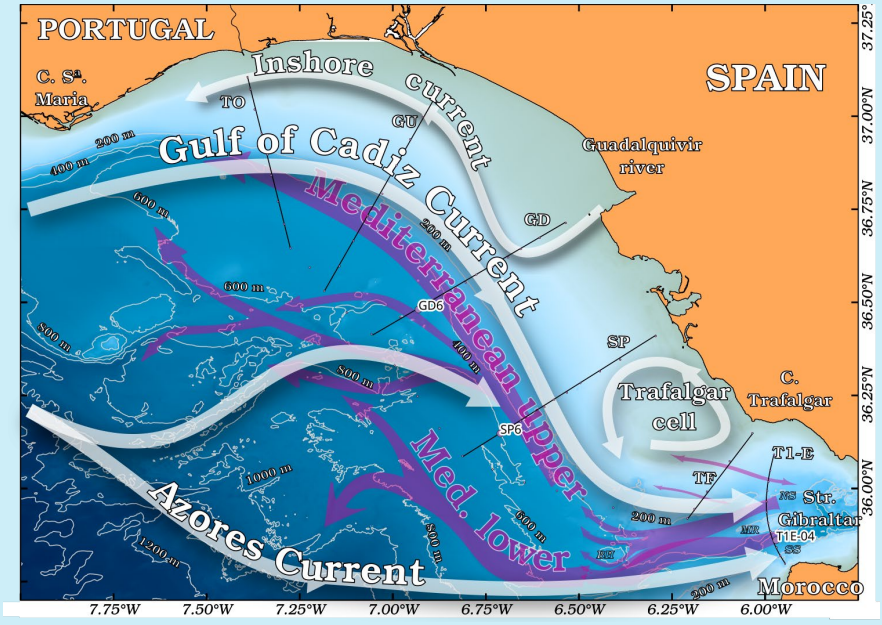

Figure 4.41. Sketch of the main currents in the Gulf of Cadiz. White arrows depict the surface circulation. Cyan arrows depict the subsurface circulation. We also include the STOCA project standard sections (black lines) and fixed oceanographic station under the responsibility of the Spanish Institute of Oceanography, Cadiz, whose data are presented in this report (GD6 and SP6). Puertos del Estado provides data from a weather buoy located at GD6.

The instrumental record in the Gulf of Cadiz suggests a statistically significant warming trend (0.15°C decade^{-1}) of air and ocean sea surface temperature over the last two decades. The smoothed time-series indicate interannual variability, with colder-than-average temperatures in 2009, 2013, 2018, and 2019 and warmer-than-average temperatures in 2010/2011 and 2016/2017. After a relative temperature maximum at the end of 2016, temperatures dropped from 2017 to a record low in 2019 (around 0.5°C, cooler than average). Salinities reached record-low values during the 2009–2019 period (36.13).

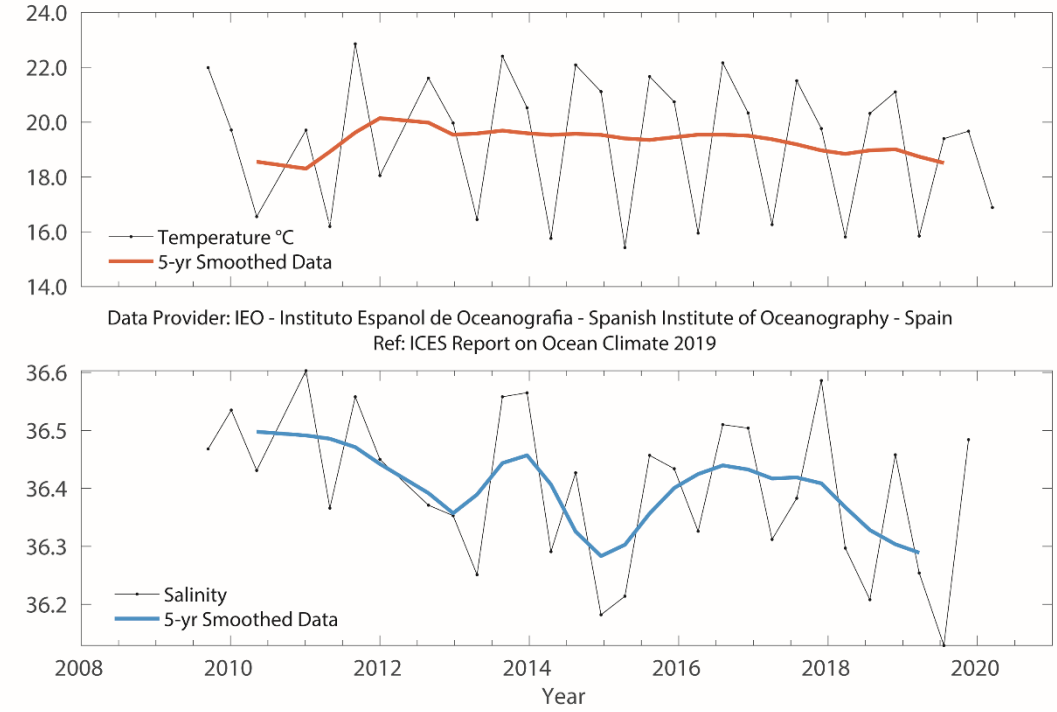

Figure 4.42. Gulf of Cadiz. Potential temperature (upper panel) and salinity (lower panel) for the 0–20 m water column at the station SP6 (36°8.68´N 6°42.76´W) of the STOCA programme.

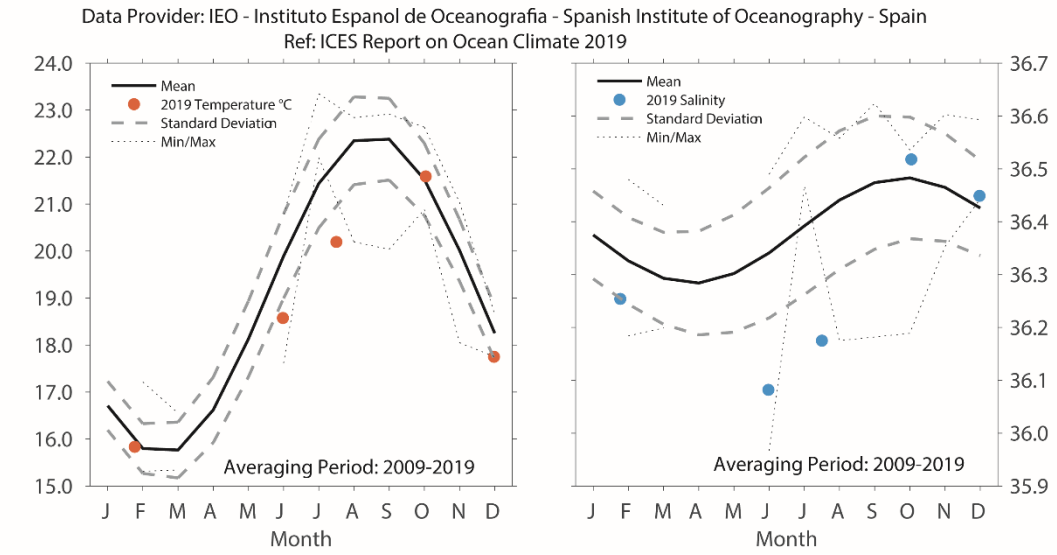

Figure 4.43. Gulf of Cadiz. 2019 monthly temperature (left panel) and salinity (right panel) at STOCA SP6 station, 10 m (36°8.68´N 6°42.76´W).

The monthly time-series for the surface layer (0–20 m) show the seasonal cycle of temperature and salinity computed from observations collected at SP6 between 2009 and 2019 (Figure 4.43). Mean and 95% confidence intervals are reconstructed from the harmonic fit of all available observations from 2009 to 2019. The time-series illustrate that seasonal variability dominates at all depth levels of the water column (Figure 4.42). In 2019, winter near-surface temperature and salinity values were close to the expected mean values, while summer was anomalously cold and fresh. In August, temperature and salinity were 2.15°C and 0.27, respectively, below the seasonal average.

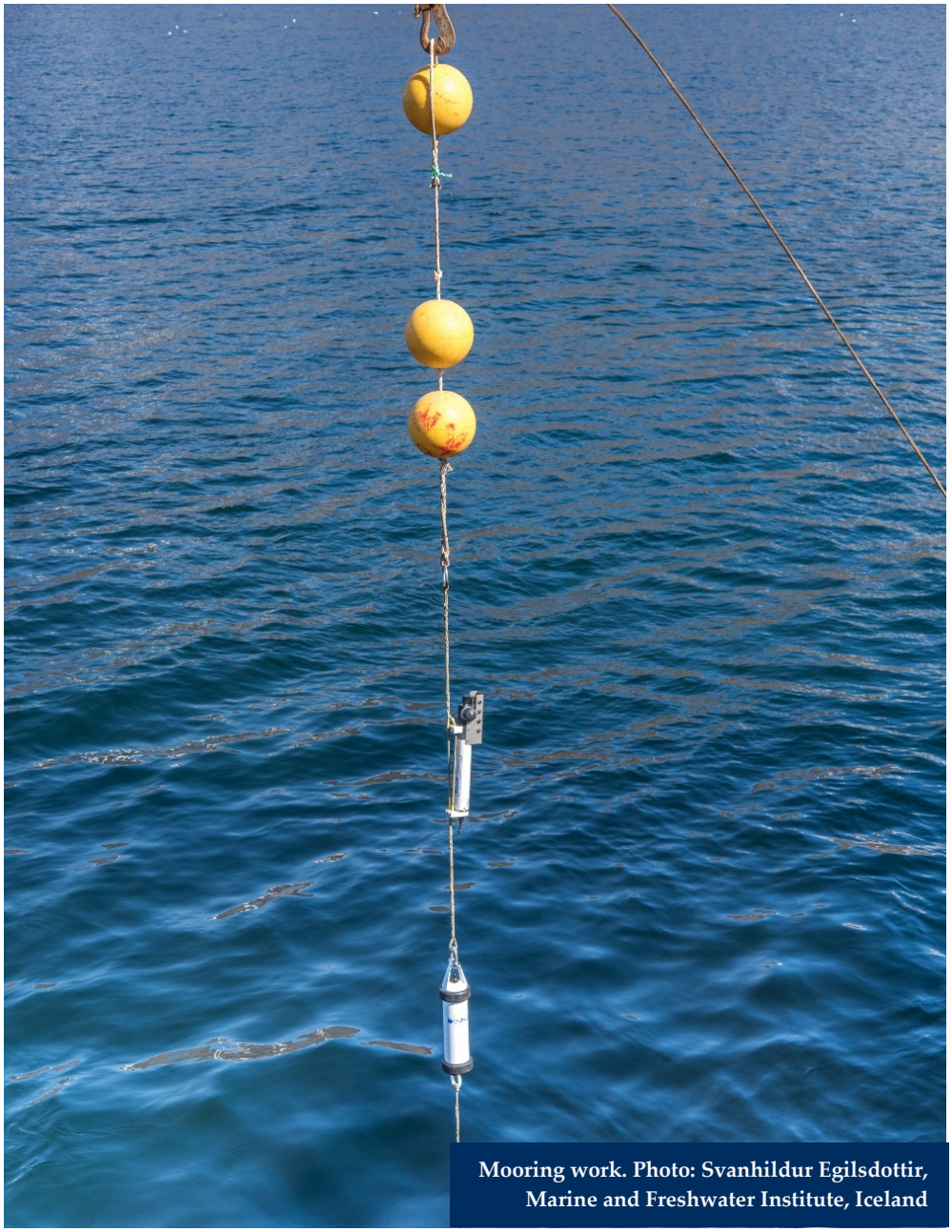

Mooring work. Photo: Svanhildur Egilsdottir, Marine and Freshwater Institute, Iceland

4.10 Canary Basin

P. Vélez-Belchí

COOLING AND FRESHENING CONTINUED IN 2019 FOLLOWING THE PEAK IN 2014 WHEN THE NORTH ATLANTIC CENTRAL WATERS (NACW) WERE AT THEIR SALTIEST AND WARMEST ON RECORD. THE AVERAGE VALUES IN THE 200–800 DBAR LAYER WERE SIMILAR TO THOSE FOUND AT THE BEGINNING OF THE 2000S.

The Canary Basin sits at the boundary between the oceanic waters of the subtropical Atlantic gyre and the upwelling waters from the Canary Current Large Marine Ecosystem (CCLME) off the coast of northwest Africa. Since the early 2000s, the Canary Islands archipelago region has been monitored by the Spanish Institute of Oceanography (Tel *et al.*, 2016). They monitor the oceanic waters west of Lanzarote (Stations 11–23, Figure 4.44) and the CTZ of the upwelling region of the CCLME (Stations 1–10, Figure 4.44). At the upper levels, the area is under the influence of the southward flowing Canary Current and the Canary Upwelling Current, associated with the upwelling front (Figure 4.44). At intermediate levels, the region is influenced by the tongue of slowly propagating MW and the slope current known as the Canary Intermediate Poleward Current (Hernández-Guerra *et al.*, 2017; Vélez-Belchí *et al.*, 2017).

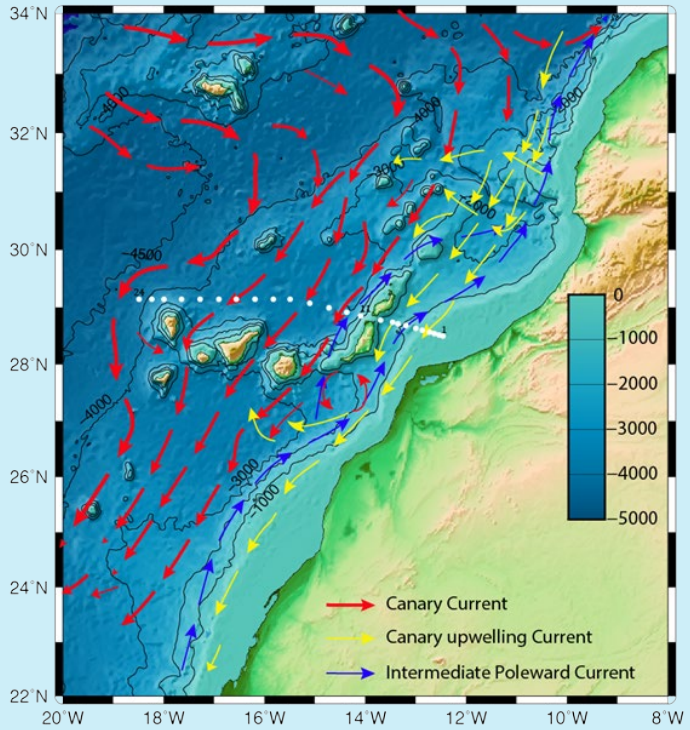

Figure 4.44. Circulation schematic for the Canary Basin. Red arrows show the southward Canary Current of, mainly, NACW and intermediate waters. Yellow arrows show the Canary Upwelling current that flows in the thermocline waters. The white dots represent the distribution of the 24 hydrographic stations sampled in the Canary Islands archipelago region since 1997. Stations 5–10 are used to estimate changes in the CTZ and stations west of Lanzarote (112–114) the oceanic waters.

The waters above the seasonal thermocline, are characterized on the θ/S diagram by scattered temperature and salinity values due to seasonal heating and evaporation. These surface waters occupy the upper 300 m in the oceanic region and the upper 100 m in the region influenced by coastal upwelling. NACW occupy the water column below the seasonal thermocline and through the permanent thermocline, roughly between 300 m and 700 m depth. These waters are characterized on the θ/S diagram by an approximately straight-line relationship between potential temperature ($11.4°C < \theta < 14.9°C$) and salinity ($35.6 < S < 36.1$). Two distinct water masses occupy intermediate levels, roughly 700–1200 m in the Canary Islands region, including the fresher ($S < 35.3$) and slightly lighter Antarctic Intermediate Waters, and the saltier ($S > 35.4$) and heavier MW.

Between the 1990s and the early 2000s, a decrease in the temperature and salinity of all upper-layer waters was observed. This was followed in the mid-2000s by a marked increase in both temperature and salinity, which peaked in 2014 in the hottest and saltiest year on record. Since that year, both temperature and salinity have decreased. As of 2019, the mean temperature and salinity was lower than that observed in the late 1990s (Vélez-Belchí *et al.*, 2015). Overall, the warming observed in oceanic surface waters ($0.19 \pm 1.35°C$ decade^{-1}) is consistent with satellite-based sea surface temperature observations, although the *in situ* time-series does not fully resolve the seasonal cycle.

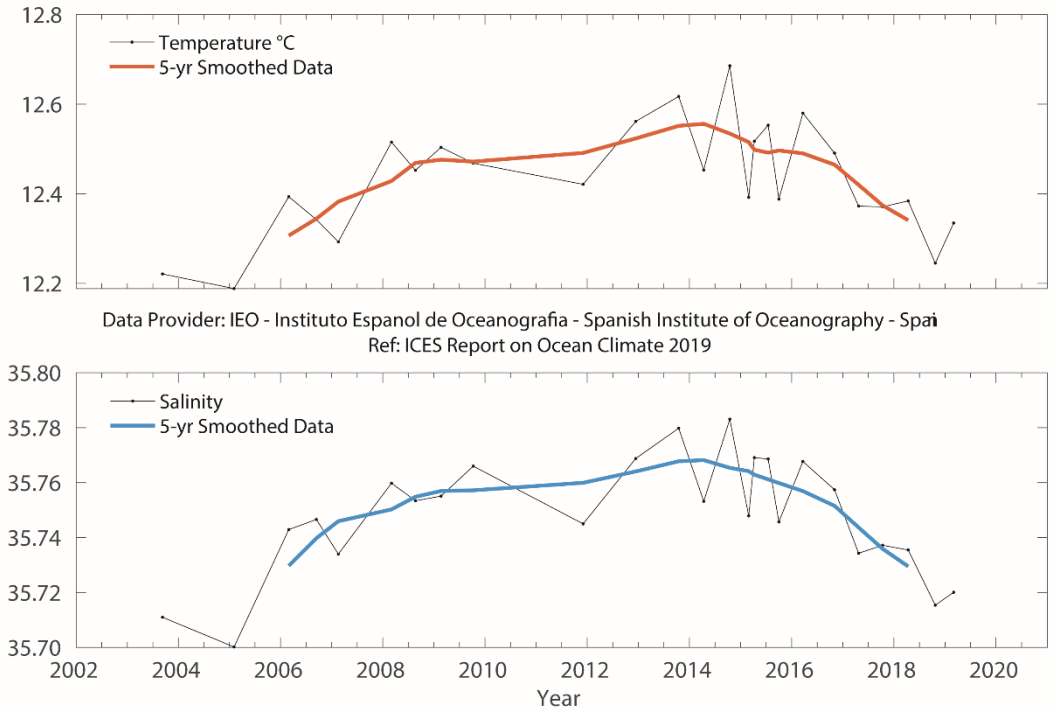

Figure 4.45. Canary Basin. Potential temperature (upper panel) and salinity (lower panel) for the 200–800 m layer in the oceanic waters of the Canary Basin.

In the depth stratum occupied by NACW waters (200–800 dbar), there is an overall statistically significant warming of $0.07 \pm 0.06°C$ decade^{-1} and an increase in salinity of $0.007 \pm 0.012°C$ per decade^{-1} (Figure 4.45). The overall increase in temperature and salinity almost compensate in density, confirming that the observed trends are due to

deepening of the isoneutral surfaces rather than changes along these surfaces. This general increasing trend in NACW salinity and temperature was also observed in the CTZ, although at a slightly lower rate due to the influence of upwelling.

The variability of the CTZ and the uncertainty in trend estimates are higher due to the proximity of the upwelling region and the frequent intrusions by upwelling filaments. CTZ surface waters show a non-statistically significant cooling of -0.29 ± 0.43°C decade^{-1}, and a non-statistically significant decrease in salinity of -0.057 ± 0.058 decade^{-1}, both coherent with an increase in the upwelling in the CCLME. The upwelling of the CCLME continues to strengthen in the long-term, with 2015 being the coolest and freshest year on record for the upwelling-influenced surface waters. Satellite-based sea surface temperature observations corroborate changes in the upwelling regime inferred from *in situ* observations, with different areas showing increases in upwelling strength. However, the magnitude of the observed trend in the satellite SST is different, due to the thin layer of ocean that the satellite observes.

Nutrient sampling. Photo: Svanhildur Egilsdottir, Marine and Freshwater Institute, Iceland

4.11 Southwest Approaches

T. Smyth

The datasets presented here are from the western end of the English Channel and the boundary of the Celtic Sea and the Bay of Biscay ecoregions. The area is commonly referred to as the Southwest Approaches, which relates to the passage of shipping through the English Channel. As these data come from a boundary between different ecoregions, this name has also been adopted here, as it relates to the region forming a pathway for AW to enter the southern North Sea.

Station E1 (50.03°N 4.37°W) is situated on the southern UK coast in the western English Channel. The water depth is 75 m, and the station is tidally influenced by a 1.1-knot maximum surface stream at mean spring tide. The seabed is mainly sand, resulting in a low bottom stress (1–2 ergs cm^{-2} s^{-1}). The station may be described as oceanic with the development of a seasonal thermocline. Stratification typically starts in early April, persists throughout summer, and is eroded by the end of October. The typical depth of the summer thermocline is around 20 m. The station is greatly affected by ambient weather.

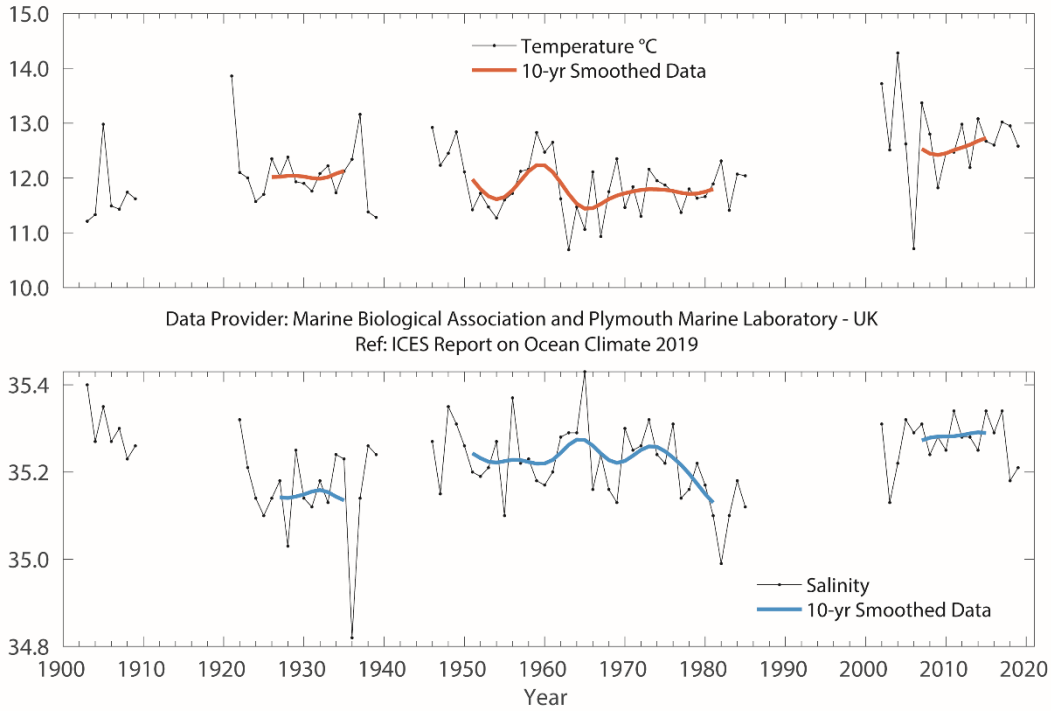

Figure 4.46. Southwest Approaches. Temperature (upper panel) and salinity (lower panel) anomalies of surface (0–40 m) water at Station E1 in the western English Channel (50.03°N 4.37°W).

Measurements have been taken at station E1 since the end of the 19th century, with data currently available since 1903 (Figure 4.46). The series is unbroken, apart from gaps for the two world wars and a hiatus in funding between 1985 and 2002. The data take the form of vertical profiles of temperature and salinity. Early measurements were

obtained with reversing mercury-in-glass thermometers and discrete salinity bottles. More recently, electronic equipment (Seabird CTD) has been utilized. The time-series demonstrates considerable interannual variability in temperature.

E1 was sampled on 18 occasions during 2019: approximately fortnightly in summer and monthly in winter. There was no sampling during October due to a ship refit.

With regard to temperature, 2019 was overall warmer than average, with notably warm conditions in January and during the late summer. This was manifested throughout the water column, with all observations being above the long-term mean for the entire year.

Salinity was below the long-term mean by up to 0.1–0.2 PSU for the first six months of 2019. During summer, salinity was slightly above the long-term mean throughout the water column by approximately 0.1 and then returned to near-average conditions in late autumn.

Storm on Grand Banks. Photo: Frederic Cyr, Fisheries and Oceans Canada

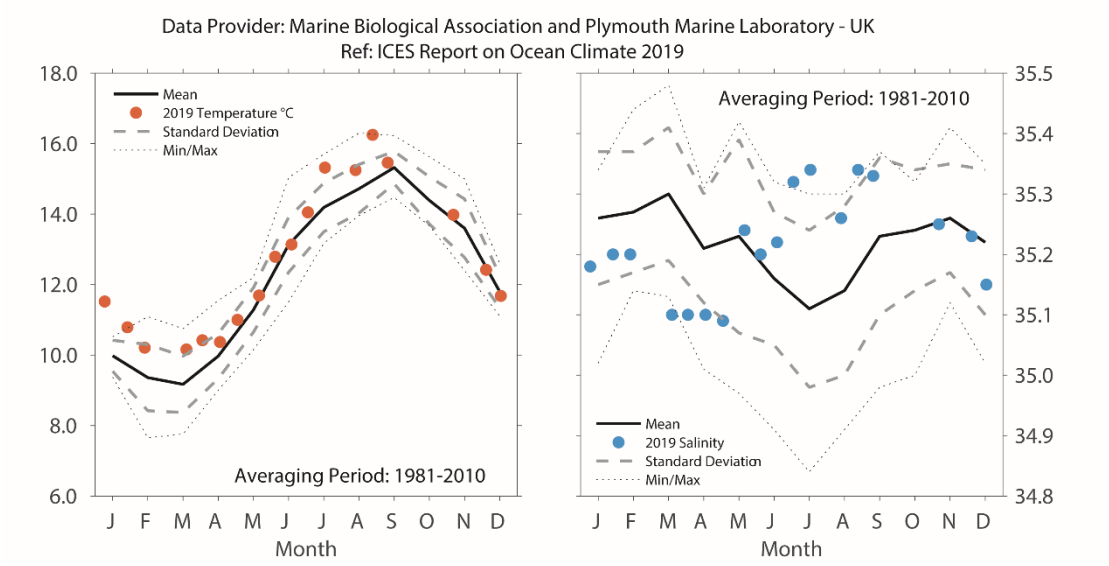

Figure 4.47. Southwest Approaches. Monthly average seasonal cycle with 2019 temperature (left panel) and salinity (right panel) observations of surface (0–40m) water at Station E1 in the western English Channel (50.03°N 4.37°W).

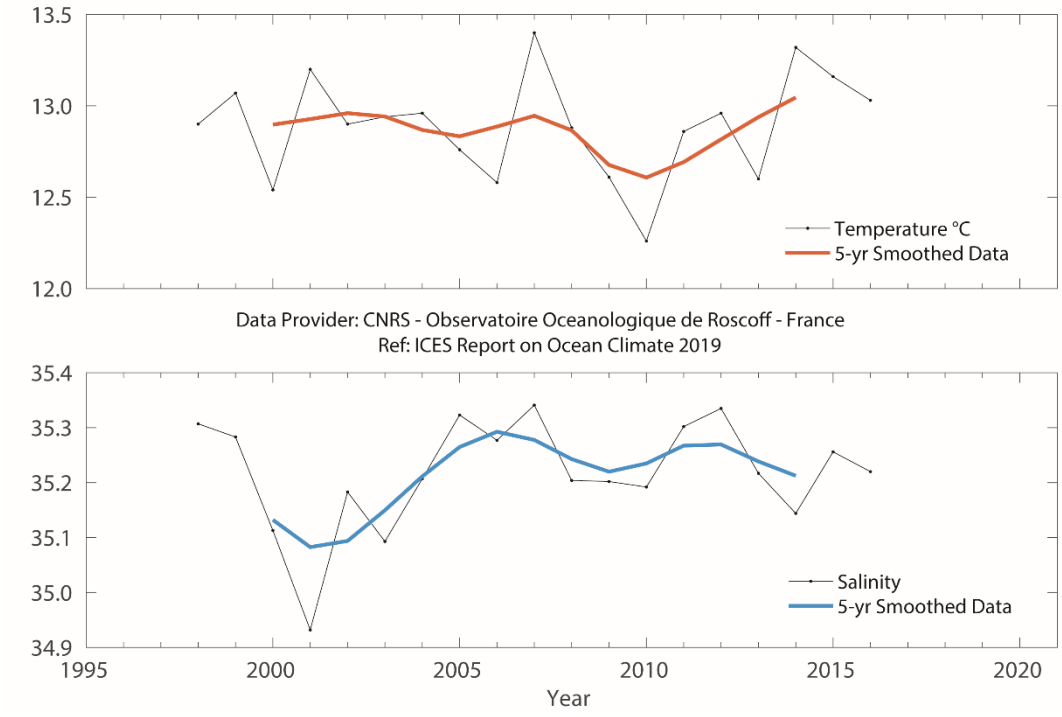

Figure 4.48. Southwest Approaches. Temperature (upper panel) and salinity (lower panel) of surface water at the Astan station (48.77°N 3.94°W) base period 1998–2010. Data until 2016.

4.12 Celtic Seas

K. Lyons and C. Cusack

RECORD SEA SURFACE TEMPERATURE AT MALIN HEAD STATION.

The Celtic Seas are defined as an ICES ecoregion and are included in NOAA LME 24 (Celtic–Biscay Shelf). The Celtic Seas region contains the shelf seas of northwestern Europe and part of the Rockall Trough. The shelf seas are mainly relatively shallow (< 100 m). The structure of the water column on the shelf is primarily driven by (i) vertical mixing caused by tides and wind and (ii) the seasonal variation of solar heating, leading to seasonal (summer) density-driven currents (e.g. Irish Coastal Current). In addition to the influence of coastal waters on the shelf, the area is strongly influenced by the poleward transport of AW and the continental slope current that brings waters northward from the Biscay region.

The mean sea surface temperature recorded at Malin Head for 2019 was 0.89°C above the 1981–2010 mean (Figure 4.50). Malin Head monthly mean temperatures for 2019 were all above the average (Figure 4.49).

For the short M3 buoy sea surface temperature time-series, the mean in 2019 was 0.21°C below the 2003–2010 mean (Figure 4.49).

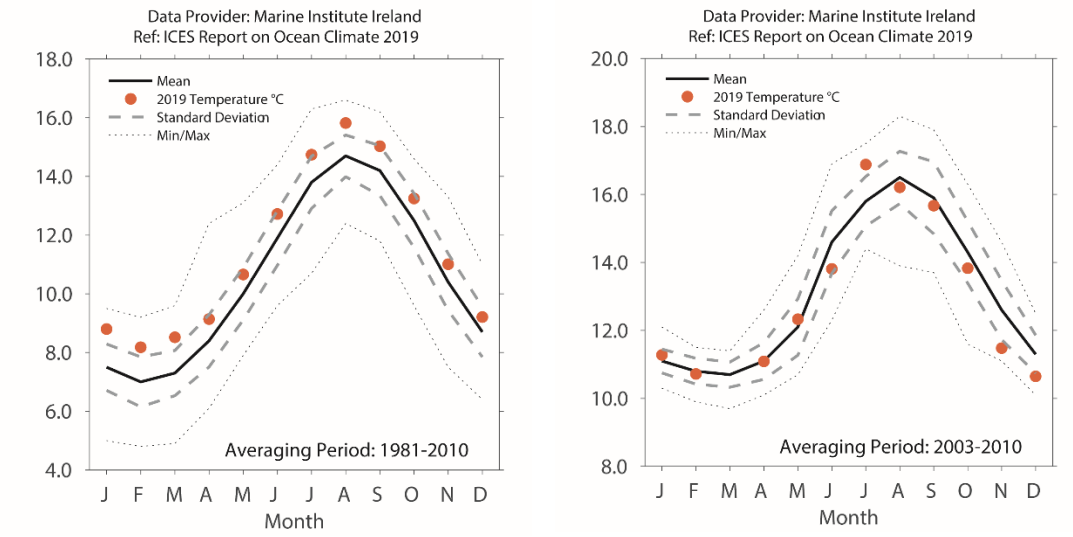

Figure 4.49. Celtic Seas. Monthly average seasonal cycle with 2019 monthly temperature at (left) Malin Head and (right) the M3 Weather Buoy southwest of Ireland (51.22°N 10.55°W).

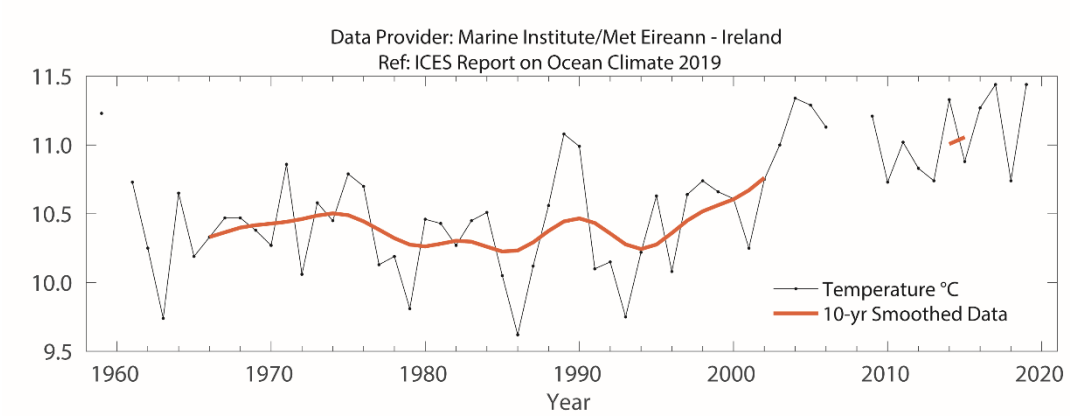

Figure 4.50. Celtic Seas. Temperature at the Malin Head coastal station (55.39°N 7.38°W).

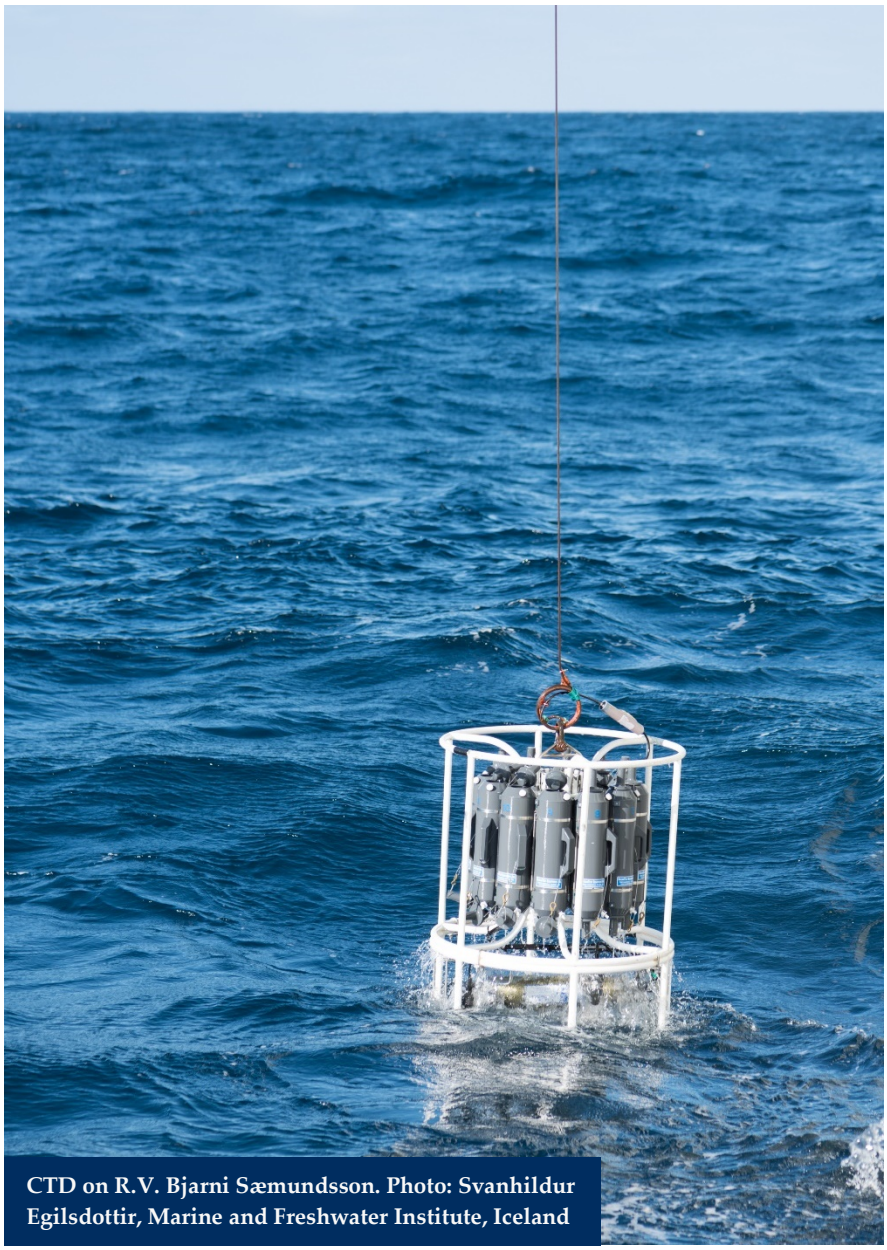

CTD on R.V. Bjarni Sæmundsson. Photo: Svanhildur Egilsdottir, Marine and Freshwater Institute, Iceland

4.13 Rockall Trough

S. Jones and N.P. Holliday

FRESH AND NEAR-AVERAGE TEMPERATURE CONDITIONS IN THE ROCKALL TROUGH UPPER OCEAN IN 2019, BUT WITH SIGNS OF INCREASING SALINITY.

Rockall Trough is a deep ocean basin situated west of the UK and Ireland within the Celtic Seas and Oceanic Northeast Atlantic ecoregions. It has significantly different oceanographic characteristics than the shallower shelf sea areas. Rockall Trough is separated from the Iceland Basin by Hatton and Rockall banks and from the Norwegian Sea by the shallow (500 m) Wyville–Thomson Ridge. It is a route for warm North Atlantic upper water to reach the Norwegian Sea, where it is converted into cold, dense overflow water as part of the thermohaline overturning in the North Atlantic. The upper water column is characterized by poleward-moving eastern North Atlantic Water (NAW), which is warmer and more saline than the Iceland Basin waters that also contribute to the Norwegian Sea inflow (Figure 4.51).

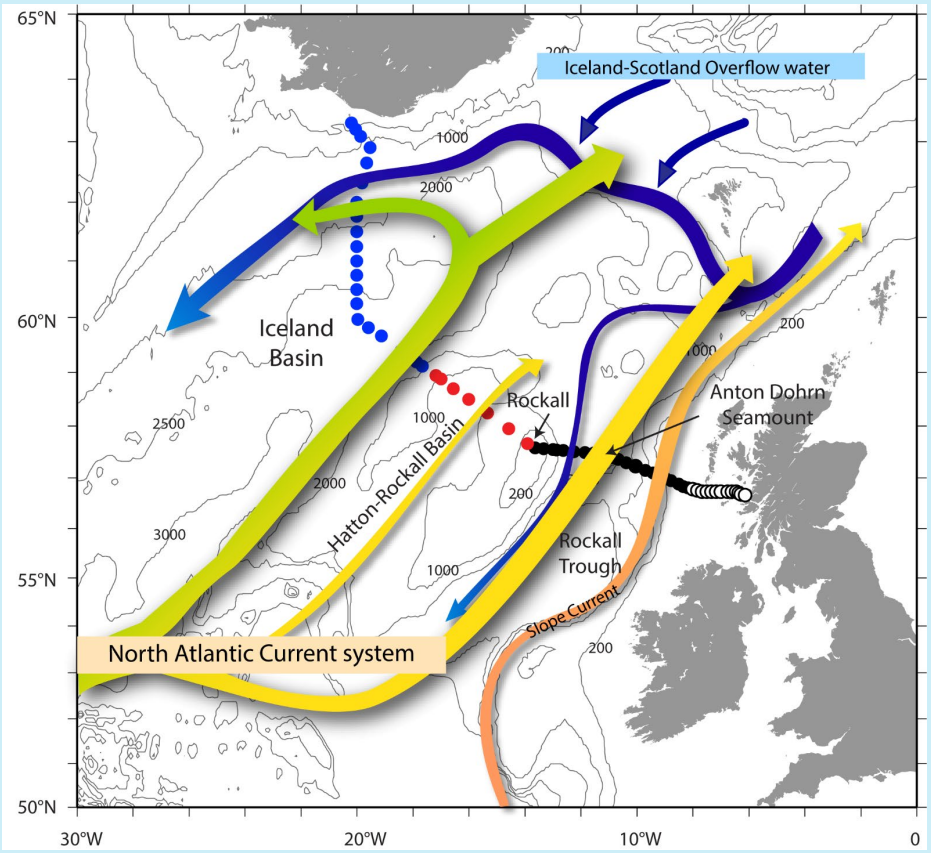

Figure 4.51. Circulation schematic for the Rockall Trough, Hatton–Rockall Basin, and Iceland Basin. Green, yellow, and orange colours indicate the upper waters of the NAC and the slope current. Dark blue arrows show the approximate locations of the main overflow currents.

The temperature of the upper 800 m was close to the 1981–2010 mean in 2019. In general, the upper ocean has been cooling relative to a peak of 9.8°C in 2007, although there have been early signs of a reversal in 2019. The salinity of the upper 800 m has been decreasing since the end of the 2000s, with a sharp freshening between 2015 and 2016. Upper-ocean salinity increased slightly from this deep minimum in 2019. The Ellett Line transect was not occupied in 2019, but equivalent data points in the time-series were generated using Argo profiles from within the basin, supported by moorings deployed by the OSNAP project for that year.

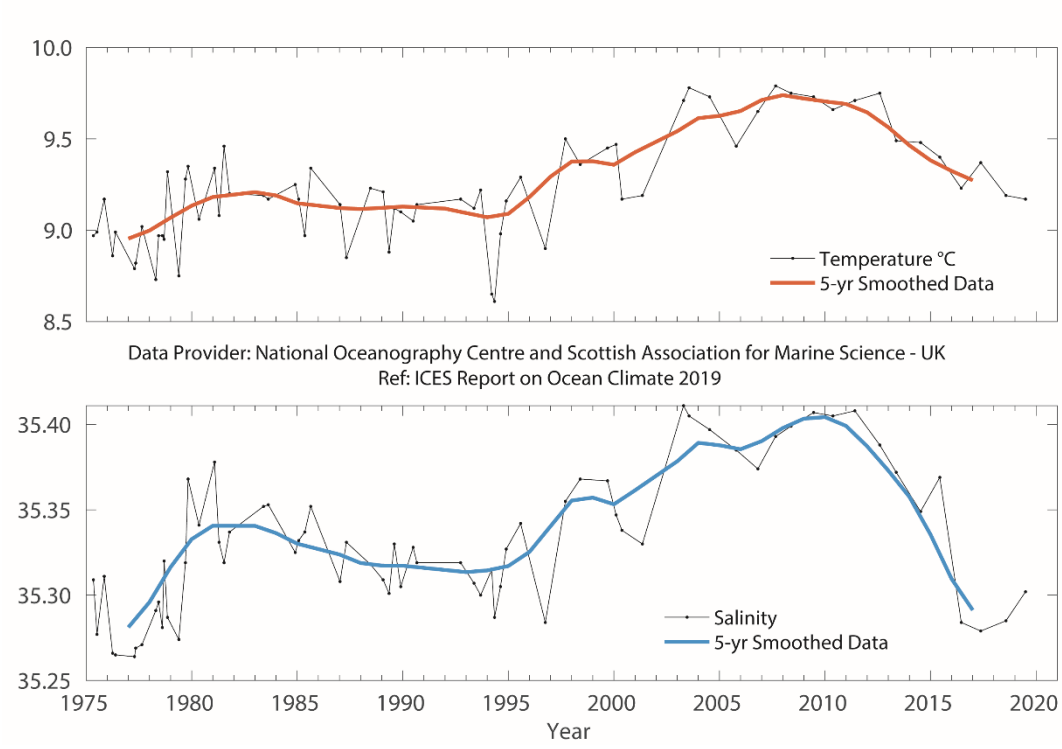

Figure 4.52. Rockall Trough. Temperature (upper panel) and salinity (lower panel) for the upper ocean (potential density 27.2–27.50 kg m^{-3}, representing the top 800 m, but excluding the seasonally warmed surface layer).

Waves in the Atlantic. Photo: Tomasz Szumski, Marine Institute, Galway, Ireland

4.14 Hatton–Rockall Basin

S. Jones and N.P. Holliday

The shallow Hatton–Rockall Basin (1000 m) lies between the Iceland Basin to the west and Rockall Trough to the east and is bounded by the Hatton and Rockall banks. The Basin is filled with well-mixed subpolar-mode water moving northward as part of the NAC complex. Winter mixing reaches 800–1000 m. Temperature and salinity vary considerably depending on the type of NAC water that enters the basin. The region is in the transition zone between cold, fresh, central subpolar water and warm, saline, eastern subpolar water.

The range in Basin mean temperature and salinity in the upper 1000 m is more than 1°C and 0.1 higher than the Iceland Basin to the west and Rockall Trough to the east. The lowest values were seen at the start of the time-series in 1996, followed by a steady rise to maximum values in the late 2000s. Since 2010, there has been a decrease in temperature and salinity. In 2018, salinity increased by 0.06, but remained lower than the 1996–2010 average. The temperature has risen since 2016 to a value close to the long-term mean. No updates were made to this time-series in 2019 due to the discontinuation of the Ellett Line transect and lack of Argo coverage.

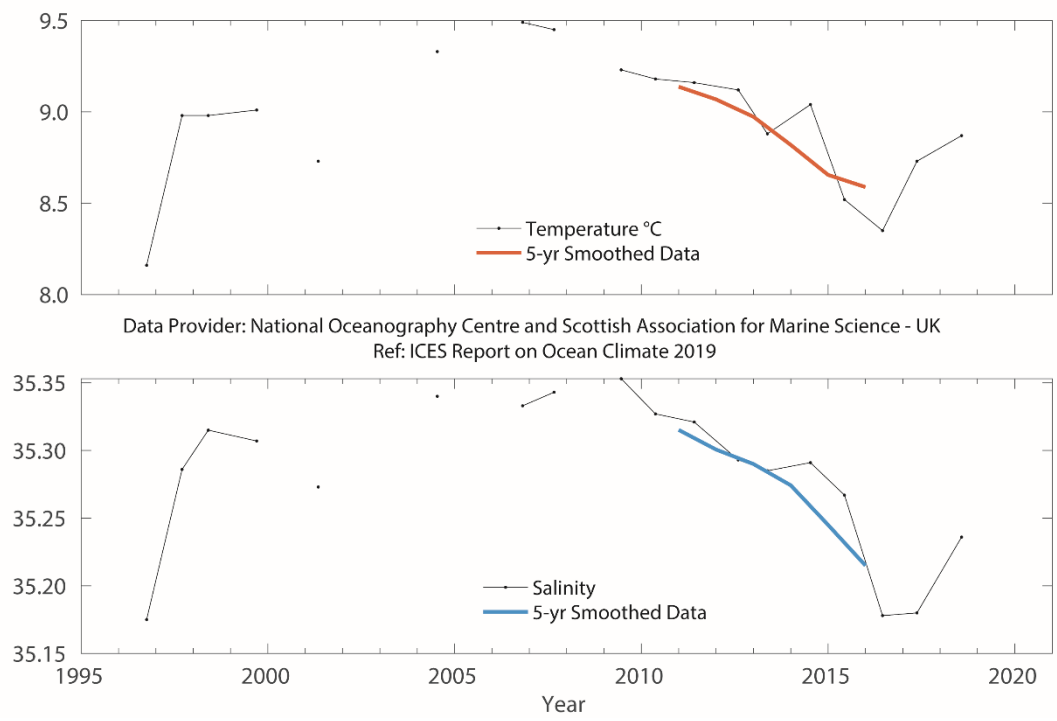

Figure 4.53. Hatton–Rockall Basin. Temperature (upper panel) and salinity (lower panel) for the upper ocean (potential density 27.20–27.50 kg m^{-3}) representing the top 600 m and excluding the seasonally warmed surface layer. Data until 2018.

4.15 Iceland Basin

S. Jones and N.P. Holliday

A major part of the NAC flows into the Iceland Basin, adjacent to the shallow Hatton Bank on the southeast side of the Basin (Figure 4.51). The NAC typically consists of one or two fronts between warmer, more-saline water in the east and colder, fresher water to the north and west. The region is rich in eddy activity, and the water properties are quite variable in time and space. Most of the water entering the Iceland Basin from the south flows through into the Norwegian Sea over the Iceland–Scotland Ridge. A smaller fraction of the NAC water recirculates south of Iceland in the boundary currents of the main anticlockwise circulation of the Subpolar Gyre.

The temperature and salinity of the upper ocean (ca. upper 500–600 m) vary from year-to-year, but also exhibit multiyear changes. From 1996 to the late 2000s, both temperature and salinity were increasing, but have since been decreasing (Holliday *et al.*, 2015). In 2016/2017, temperature and salinity values were the lowest recorded since 1996. The freshening since 2010 implies that the Basin is receiving more water originating in the west and central subpolar region and less warm, saline water from the eastern intergyre regions. Superimposed on that multiyear trend is a rapid cooling, observed in 2014/2015, which is caused by a high flux of heat from the ocean to the atmosphere (Duchez *et al.*, 2016), and a rapid freshening in 2015–2017 (Holliday *et al.*, 2020). These deep minima have recovered towards the long-term mean in 2018 and 2019. The Ellett Line transect was not occupied in 2018 or 2019, but equivalent datapoints in the time-series were generated using Argo profiles from within the Basin for that year.

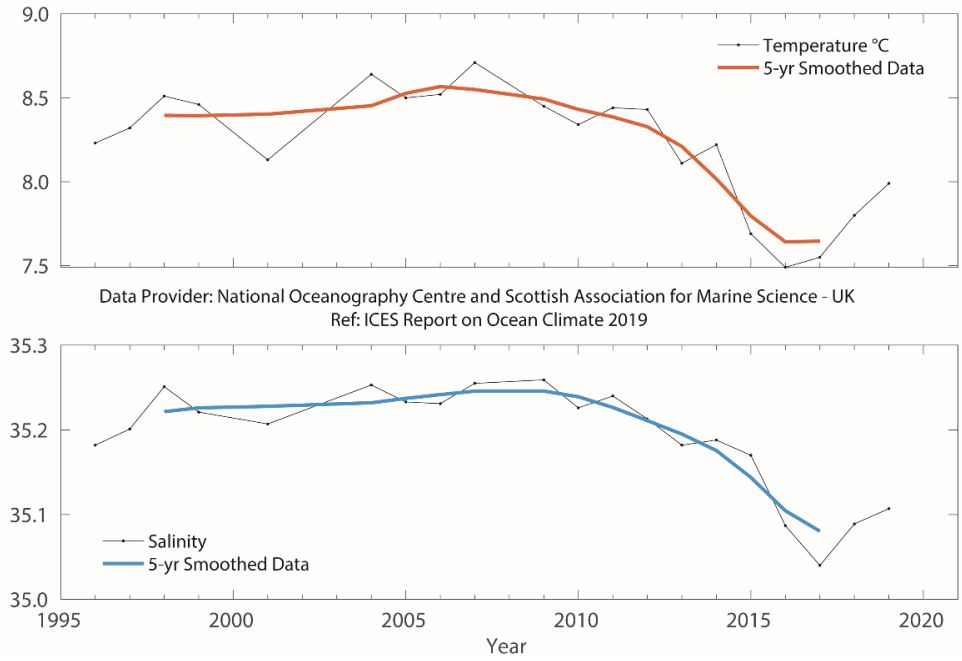

Figure 4.54. Iceland Basin. Temperature (upper panel) and salinity (lower panel) for the upper ocean (potential density 27.20–27.50 kg m^{-3}, representing the top 500 m and excluding the seasonally warmed surface layer).

4.16 Irminger Sea

M.F. de Jong

THERE IS NO 2019 UPDATE FOR THE IRMINGER SEA.

For the most recent regional overview, please see Section 4.15 in the IROC 2018 (González-Pola *et al.*, 2018).

The Irminger Sea is the ocean basin between South Greenland, the Reykjanes Ridge, and Iceland. This area forms part of the North Atlantic Subpolar Gyre. Due to this gyre, the exchange of water between the Irminger and the Labrador seas proceeds relatively fast. In the bottom layers of the Irminger Sea, cold water originating in the (sub) Arctic seas flows from Denmark Strait and to the south over the continental slope of Greenland.

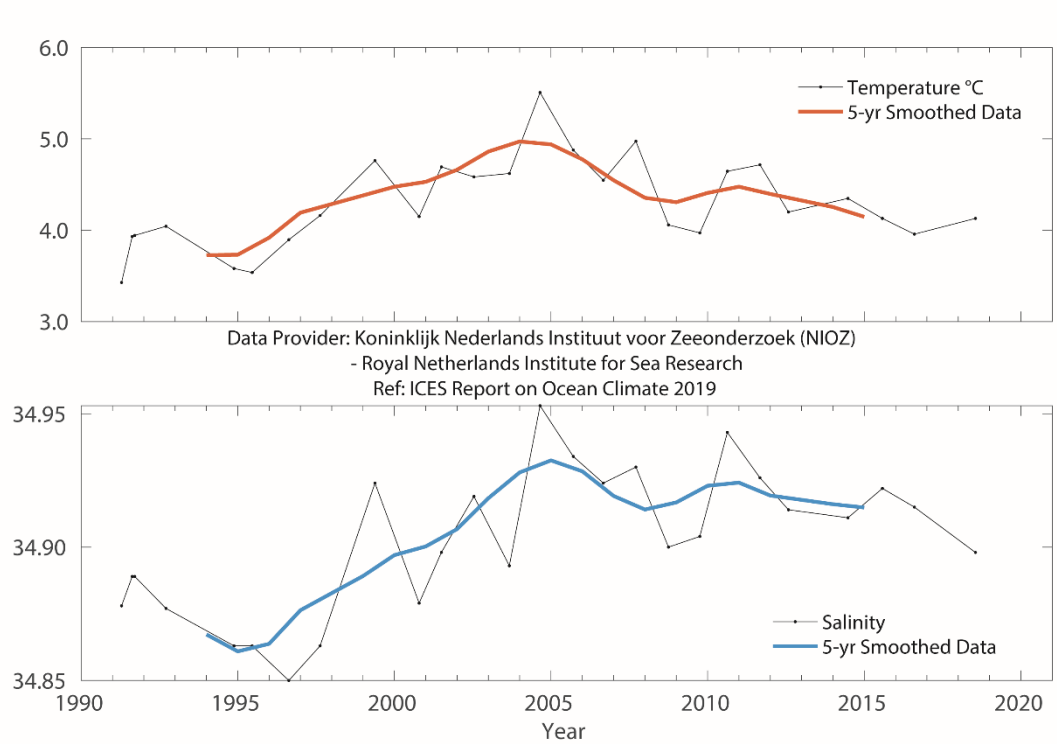

Figure 4.55. Irminger Sea. Temperature (upper panel) and salinity (lower panel) of Subpolar Mode Water in the central Irminger Sea (averaged over 200–400 m). Data until 2018.

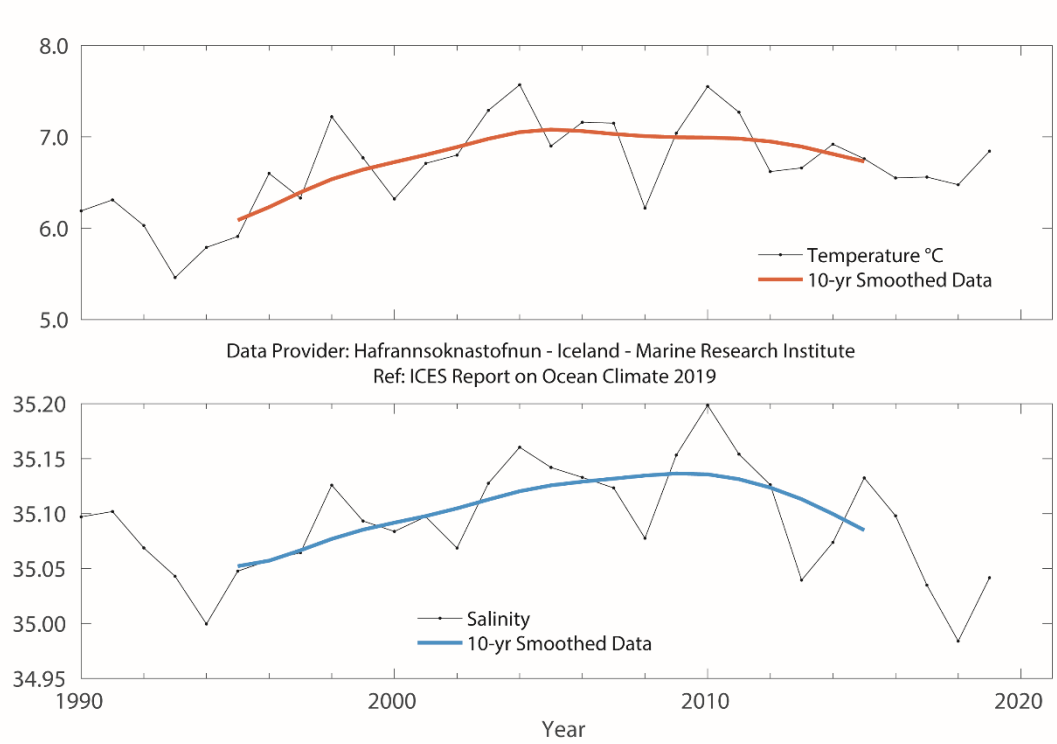

Figure 4.56. Irminger Sea. Temperature (upper panel) and salinity (lower panel) of Subpolar Mode Water in the northern Irminger Sea (Station FX9, 64.33°N 28°W) from winter observations averaged over 200–500 m).

R.V. Celtic Explorer. Photo: Tomasz Szumski, Marine Institute, Galway, Ireland

4.17 Faroese Waters and the Faroe–Shetland Channel

K.M.H. Larsen, B. Berx, and J. Hindson

SALINITIES OBSERVED IN THE NAW AND MODIFIED NORTH ATLANTIC WATER (MNAW) IN THE REGION ARE STILL VERY LOW, BUT GENERALLY INCREASING. TEMPERATURES IN THE WHOLE REGION WERE CLOSE TO THE LONG-TERM MEAN.

Data from the Faroese Waters ecoregion are grouped together here with data from the Faroe–Shetland Channel. This small region sits at the boundary between the Celtic Seas, North Sea, and Norwegian Sea ecoregions and also at the boundary between the North Atlantic Ocean and Nordic Seas.

One of the NAC branches crosses the Greenland–Scotland ridge (Figure 4.57) on either side of the Faroes. Its properties are sampled in the Faroe Bank Channel before it crosses the ridge, and in the Faroe Current after it crosses the ridge. Some of this water recirculates and is sampled within the Faroe–Shetland Channel as MNAW.

Further to the east, the continental slope current flows along the edge of the northwest European continental shelf. Originating in the Southern Rockall Trough, the slope current carries warm, saline AW into the Faroe–Shetland Channel. A proportion of this AW crosses onto the shelf itself and enters the North Sea, where it is diluted with coastal water and eventually leaves in the Norwegian Coastal Current. The remainder enters the Norwegian Sea and joins the water coming from north of the Faroes to become the Norwegian Atlantic Water.

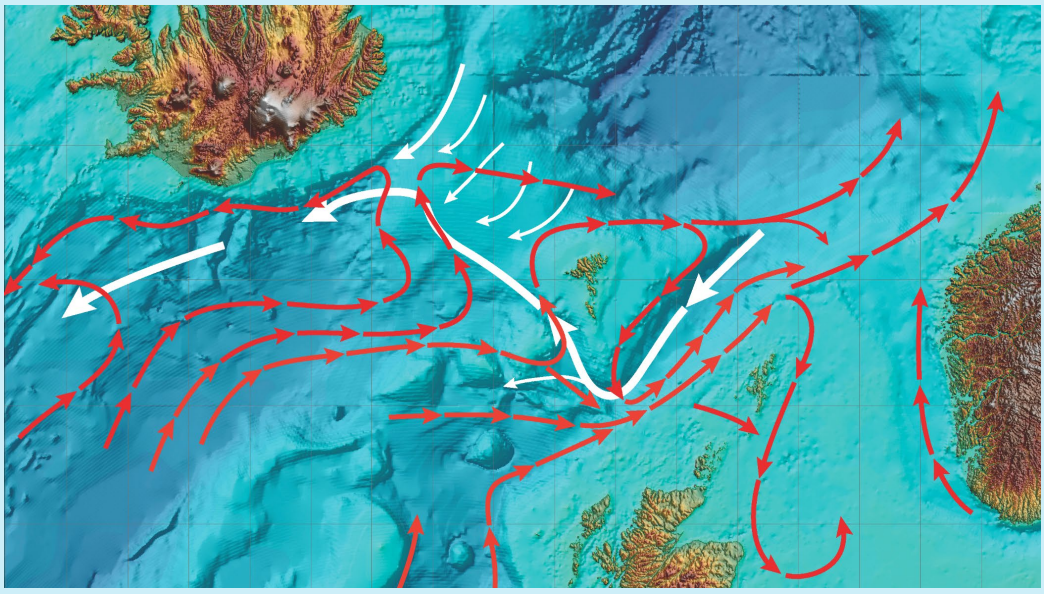

Figure 4.57. Circulation schematic for Faroese Waters and the Faroe–Shetland Channel. Red lines show the poleward movement of AW. Thick White lines show the return circulation (at depth) of waters from the Nordic Seas.

Generally, both temperature and salinity in all upper-layer waters around the Faroes and in the Faroe–Shetland Channel increased markedly during the 1990s and 2000s. Both temperature and salinity decreased during the first half of the 2010s, with record-low salinity values observed in the second half of the 2010s.

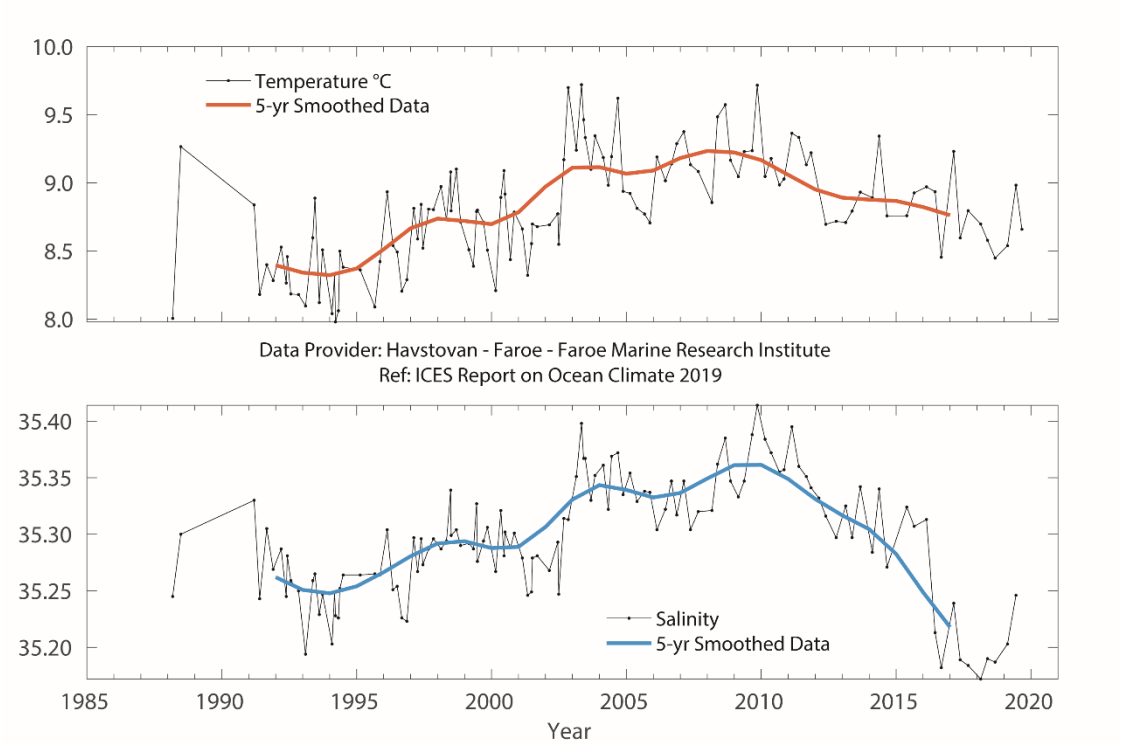

Figure 4.58. Faroese waters. Temperature (upper panel) and salinity (lower panel) in the high salinity core of AW over the Faroe Bank Channel (maximum salinity averaged over a 50 m deep layer).

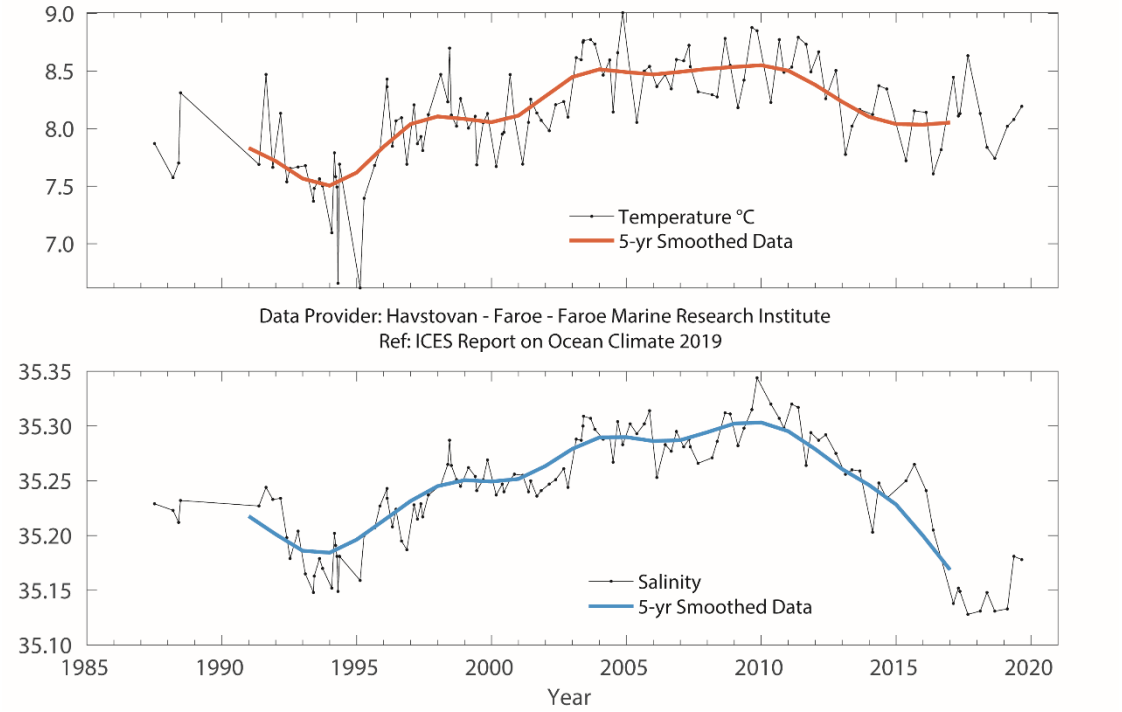

Figure 4.59. Temperature (upper panel) and salinity (lower panel) in the high salinity core of the Faroe Current north of the Faroes (maximum salinity averaged over a 50 m deep layer).

After the record-high salinities observed in the Faroe Bank Channel (Figure 4.58) and the Faroe Current (Figure 4.59) in November 2009, salinities decreased at both locations. In autumn and winter 2016/2017, salinity in both areas decreased abruptly and continued to decrease in 2017 and 2018, but at a slower rate. In 2019, salinities increased slightly compared to recent years. Temperatures in the Faroe Bank Channel and the Faroe Current were relatively high and stable during most of the 2000s. In 2012, they decreased, have been close to the long-term mean in recent years, and did not accompany the decrease in salinity. In 2019, temperatures increased slightly compared to 2018.

On the Faroe Shelf, the annual average temperature has been relatively high since the early 2000s, but it decreased in 2015 and was the lowest observed since 2000. Since 2015, temperatures have been slightly higher, and the recent four years have all been warmer than the long-term mean (not shown). The 2019 monthly mean temperatures where close to the mean throughout most of the year (Figure 4.60, left panel). The long-term trend in salinity on the Faroe Shelf follows the trend observed in off-shelf waters. Salinities increased from the start of the observations in 1995 to record-high values in 2010. Since 2010, salinities have been decreasing, and the record-low values observed in the Faroe Bank Channel in autumn 2016 were evident in the Faroe Shelf salinities already in late summer 2016. The freshening continued off-shelf in 2017, 2018, and even into 2019. Record-low salinity values were observed on the shelf in the first three months of 2019, but the annual mean in 2019 was slightly higher than in 2017 and 2018 (Figure 4.60, right panel).

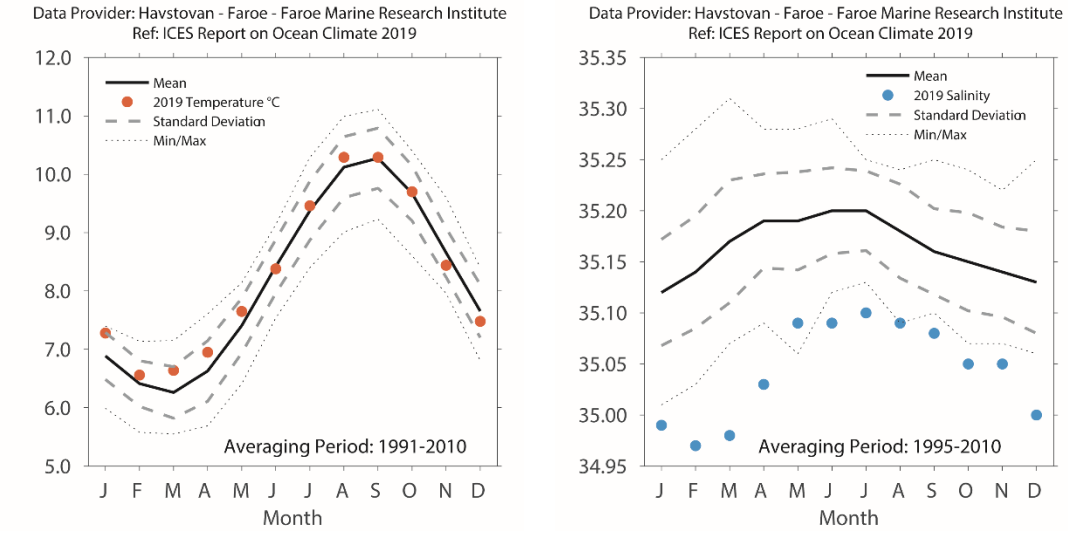

Figure 4.60. Faroese waters. 2019 monthly temperature (left) from the Faroe coastal station at Oyrargjogv (62.12°N 7.17°W) and monthly salinity (right) from the Faroe coastal station at Skopun (61.91°N 6.88°W). Note the different averaging periods.

The temperature and salinity of the surface waters of the Faroe–Shetland Channel increased from the early 1990s. However, over the past nine years, there has been a reduction in both parameters. Salinities of both AW types distinguished in the Channel, NAW, and MNAW showed significant freshening in 2017 and 2018 (Figure 4.61 and Figure 4.62). While temperatures of the AW masses on both sides of the Faroe–Shetland

Channel have decreased significantly since the record-high temperatures of 2010, these remain close to the long-term mean. Salinities of the Atlantic Water masses are now significantly lower than the long-term mean, although both NAW and MNAW salinities have increased slightly since 2018.

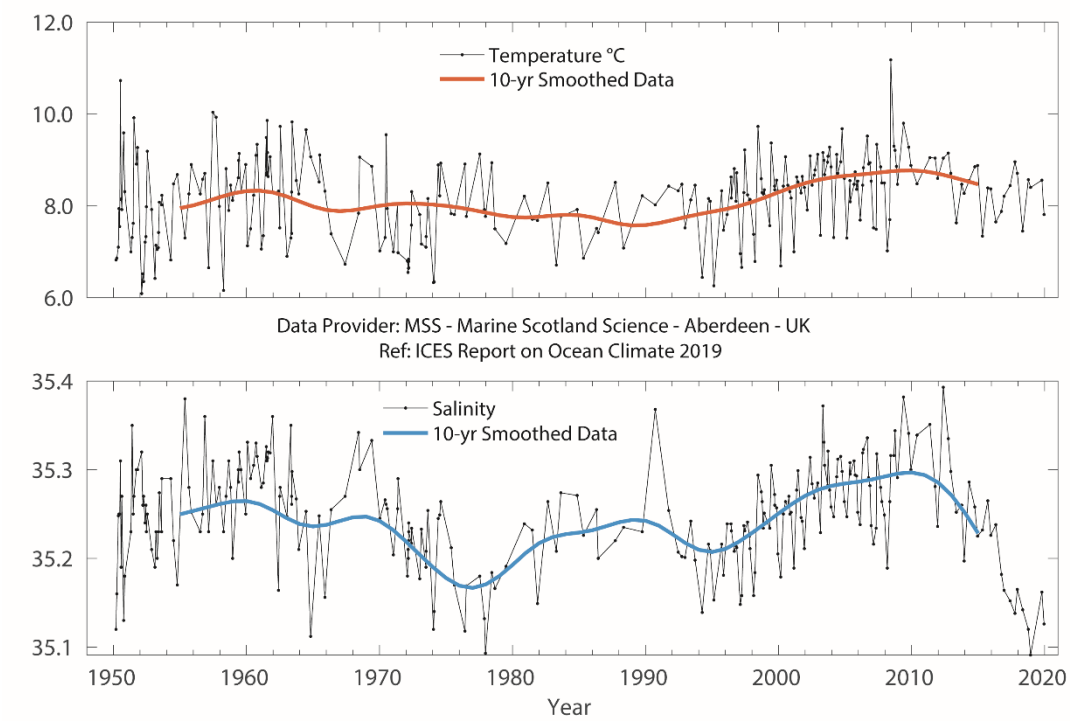

Figure 4.61. Faroe–Shetland Channel. Temperature (upper panel) and salinity (lower panel) in the modified AW entering the Faroe–Shetland Channel from the north after circulating around the Faroes.

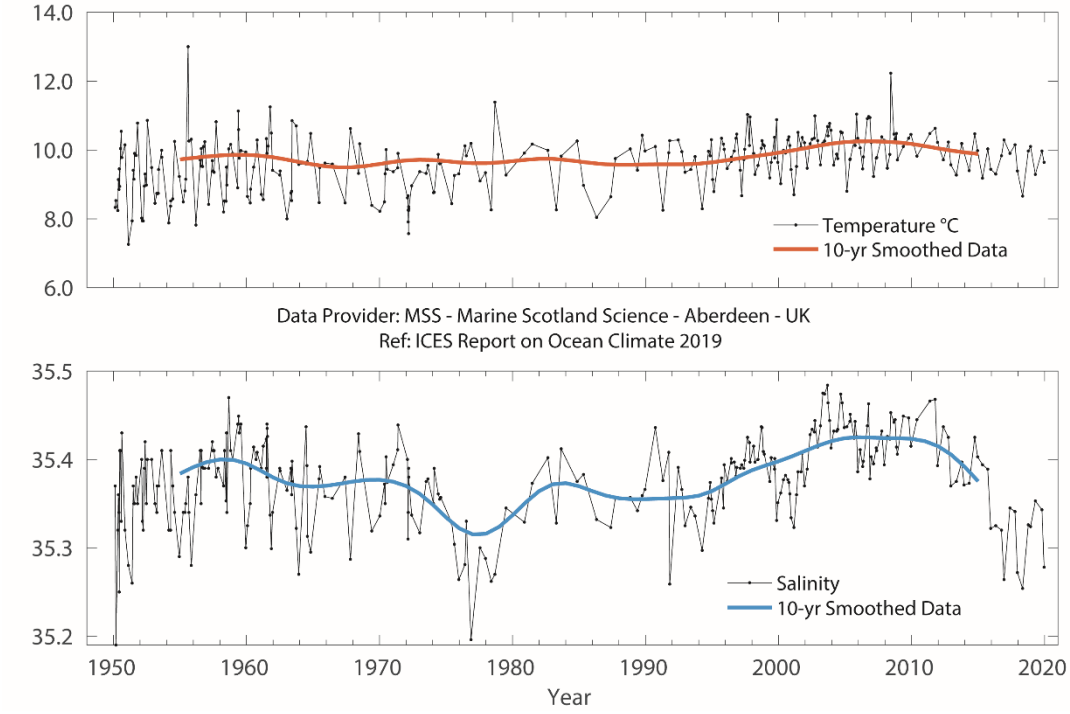

Figure 4.62. Faroe–Shetland Channel. Temperature (upper panel) and salinity (lower panel) in the AW in the slope current.

4.18 North Sea

H. Klein, P. Loewe, K. Latarius, M. Köllner, K.A. Mork, and J. Albretsen

North Sea oceanographic conditions are determined by the inflow of saline AW (Figure 4.63) and the ocean–atmosphere heat exchange. Inflow through the northern entrances and, to a lesser degree, through the English Channel can be strongly influenced by the NAO. Numerical model simulations also demonstrate strong differences in the North Sea circulation, depending on the state of the NAO. The AW mixes with river run-off and lower-salinity Baltic outflow along the Norwegian coast. A balance of tidal mixing and local heating forces the development of a seasonal stratification from April/May to September in most parts of the North Sea.

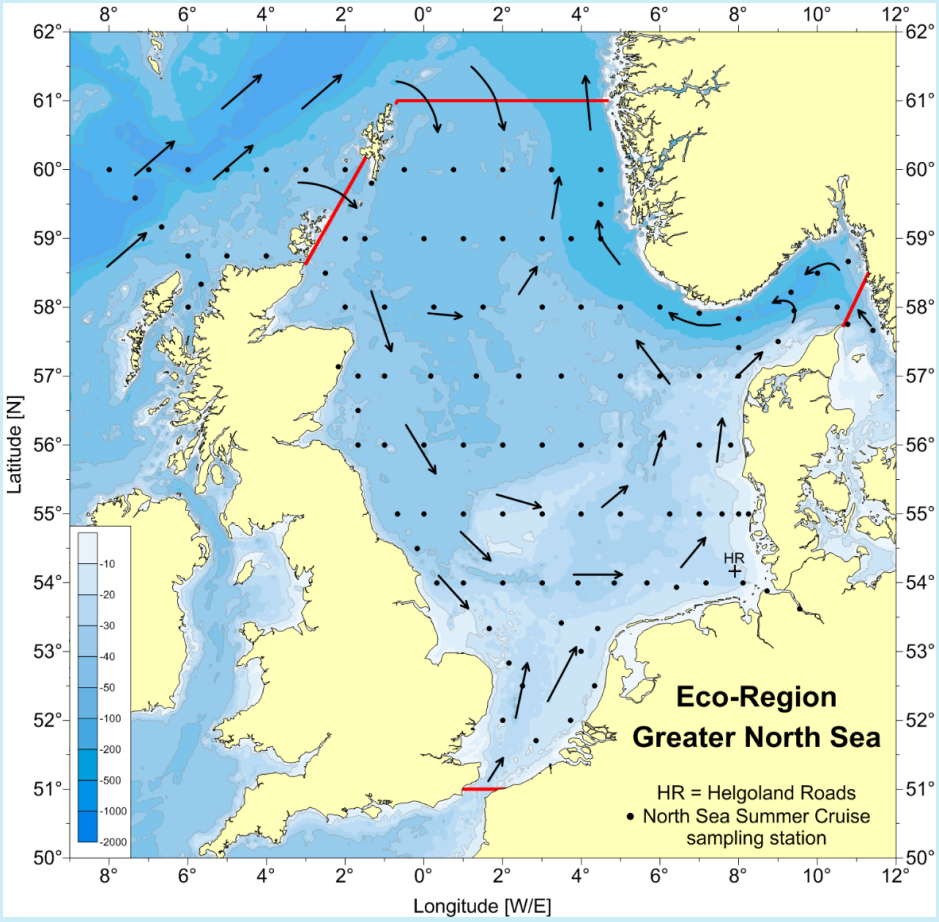

Figure 4.63. Schematic representation of North Sea circulation. Red lines show extent of the North Sea region. The sampling station at Helgoland Roads is marked with a HR+. Black arrows indicate mean residual circulation patterns. Black dots show the summer sampling undertaken in the North Sea by Bundesamt fûr Seeschiffahrt und Hydrographie (German Federal Maritime and Hydrographic Agency; BSH).

During the first four months of 2019, the area-averaged monthly North Sea SST were 0.7–1.0°C above the 1981–2010 long-term mean. For the rest of the year, with the exception of August (+1.0°C), the values were relatively close to the seasonal long-term

average (Figure 4.64). The same pattern occurred at Helgoland, in the southern North Sea, but with higher amplitude in the temporal variations (Figure 4.65).

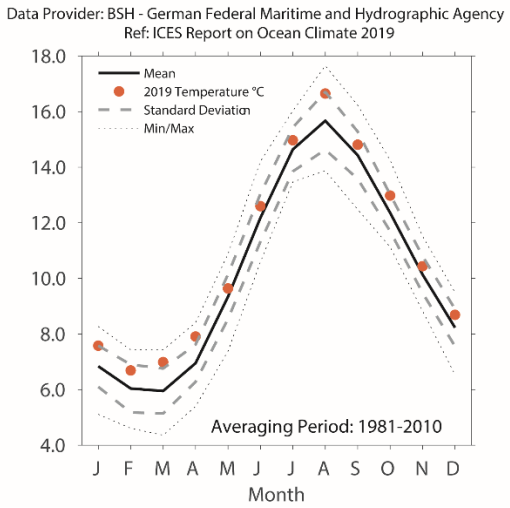

Figure 4.64. North Sea. Monthly means of area-averaged North Sea SST.

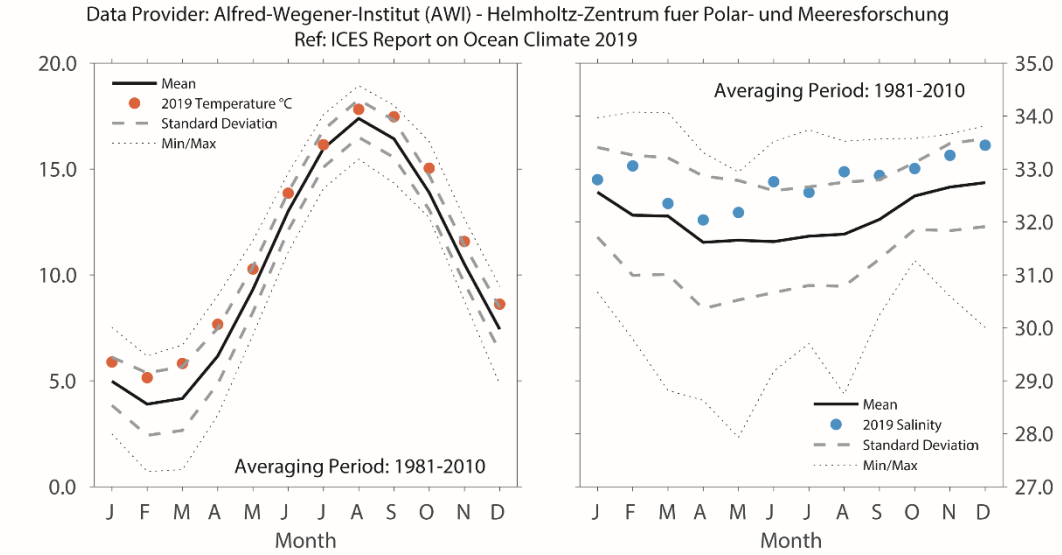

Figure 4.65. Southern North Sea. Monthly surface temperature (left panel) and salinity (right panel) at Station Helgoland Roads.

The 2019 annual mean of area-averaged North Sea SST in 2019 was 10.8°C (+0.6°C, Figure 4.66). The annual average at Helgoland Roads in the southern North Sea was 11.3°C (+1.0°C). Both time-series show the same variability over time, but there is a greater temperature range at Helgoland Roads due to shallower water depth in the German Bight.

Besides the inflow of warmer AW at the northern boundary and through the English Channel, much of North Sea SST variability is caused by local ocean–atmosphere heatflux. The annual sea surface salinity (SSS) means at Helgoland Roads (Figure 4.65 and Figure 4.67) have been relatively high in recent years, which corresponds to low Elbe River run-offs into the German Bight.

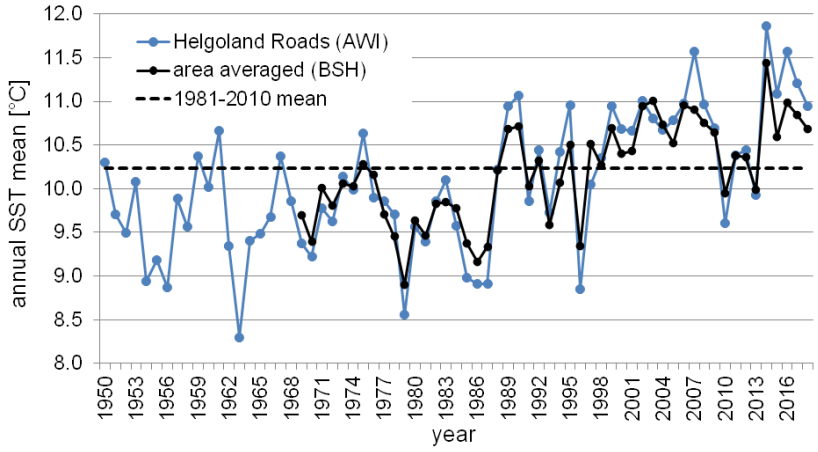

Figure 4.66. Annual average of the area-averaged North Sea SSTs.

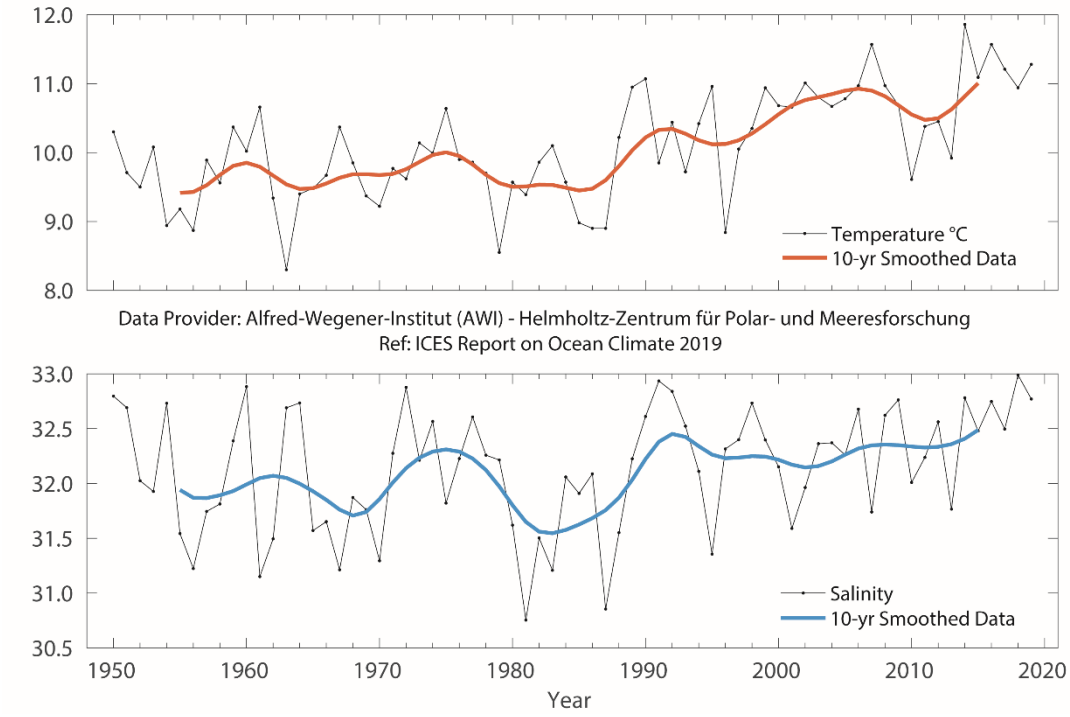

Figure 4.67. Southern North Sea. Annual mean surface temperature anomaly (upper panel) and salinity anomaly (lower panel) at Station Helgoland Roads.

During summer 2019, the area north of 56°N showed negative anomalies up to –2°C in the surface layer at the open boundary to the North Atlantic, while to the south, positive anomalies of up to +2°C were recorded along the German and Dutch coasts. The majority of bottom-water temperatures showed positive anomalies of up to +4°C in the southeastern North Sea and over Dogger Bank. Only a few small areas showed negative anomalies, with the largest of them being –1°C west of Dogger Bank. The differences between surface and bottom temperature exceeded 8°C in the central North Sea and over the Norwegian Trench. The area-averaged summer SST (J, A, S) of 15.5°C equals the climatological mean and ranks as the 13th warmest since 1969. Nevertheless, due to high air temperatures before the survey, for the first time since 1998, there was

a notable thermal stratification along the 54°N section between 2 and 7°W, with vertical gradients of 0.6 to 1.5°C m^{-1}. Normally, this section is vertically well mixed in summer, owing to shallow-water depths. All northern sections up to 60°N showed a sharp thermocline, with gradients up to 3°C m^{-1} and a maximum depth of 101 m at 58°N over the Norwegian Trench. Compared to 2018, the total heat content increased slightly reaching 1.707 x 10^{21} J, which is 0.9 s.d. above the reference mean of 1.631 x 10^{21} J.

During summer, there was an inflow of AW (S > 35) between 2°W and 2°E over the East Shetland Shelf and the Fair Isle Channel, reaching southward to about 57.5°N. In the bottom layer, there was a broad inflow across the entire North Sea reaching southward, with a small tip to 56°N. At the southern connection between the North Sea and Atlantic, AW was detected at the eastern approach to the Strait of Dover.

At the surface, there were slightly positive salinity anomalies in the eastern part of the North Sea, with small local maxima, up to +2, in the German Bight and over the Norwegian Trench. In the western part of the North Sea, there were only minor positive deviations from the long-term mean. In the bottom layer, there were only small anomalies up to ±0.5, which were positive south of a line from Lowestoft to Kristiansand in the Skagerrak and negative in the northern part. The positive anomalies in the southern and eastern North Sea are, at least partly, caused by low river discharge during the last three years. Compared to 2018, the total salt content decreased slightly to 1.099 x 10^{12} t, which is 1.9 s.d. below the 2000–2010 mean. This general decline correlates to low net inflows of saline AW from the north. The ocean circulation model NORWECOM is conducted to calculate transports of inflowing AW through a transect between Utsira, Norway, and the Orkneys. The model results for 2019 indicate that the AW inflows were low in all quarters of the year compared with the 1985–2010 reference period. The annual net inflow was the fourth lowest of all years in the 1985–2019 period. The overall supplement of AW to the North Sea and the Skagerrak thus remains low, following the trend of the last 6–7 years (Figure 4.68). Furthermore, the salinity data from the Fair Isle Current confirm a continued freshening of AW entering the North Sea from the North Atlantic (Figure 4.69).

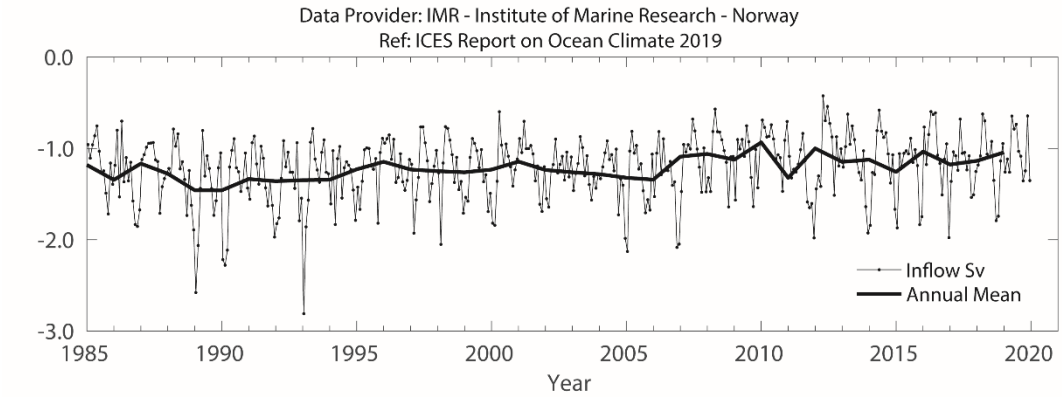

Figure 4.68. Northern North Sea. Modelled annual mean (bold) and monthly mean volume transport of AW into the northern and central North Sea southwards between the Orkney Islands and Utsire, Norway.

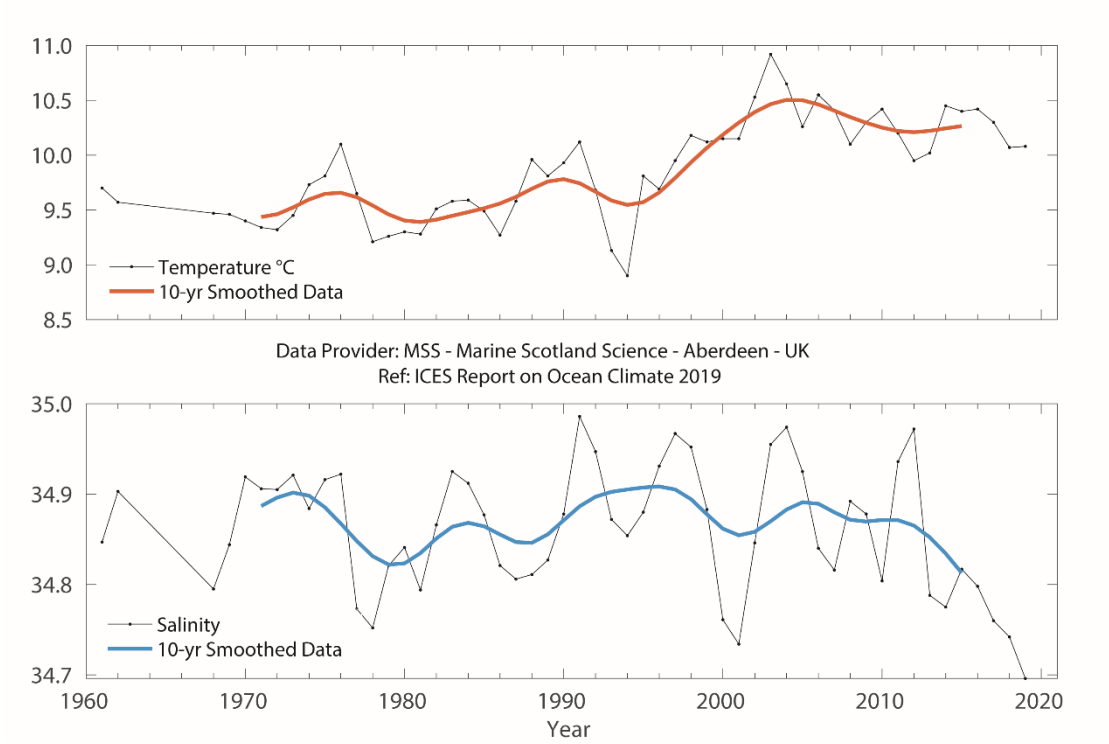

Figure 4.69. Northern North Sea. Temperature anomaly (upper panel) and salinity anomaly (lower panel) in the Fair Isle Current entering the North Sea from the North Atlantic.

Cobh, Co. Cork, Ireland. Photo: Tomasz Szumski, Marine Institute, Galway, Ireland

4.19 Skaggerak, Kattegat, and the Baltic Sea

K. Wesslander, T. Wodzinowski, and T. Liblik

The Skaggerak, Kattegat, and Baltic Sea are characterized by large salinity variations. In the Skagerrak, water masses from different parts of the North Sea are present. The Kattegat is a transition area between the Baltic and the Skagerrak. The water is strongly stratified, with a permanent halocline. The deep water in the Baltic Sea proper, which enters through the Belts and the Sound, can be stagnant for long periods. In the relatively shallow area in the southern Baltic, smaller inflows pass relatively quickly, and conditions in the deep water are highly variable. Surface salinity is very low in the northern, central, and eastern Baltic. The Gulf of Bothnia and the Gulf of Finland are at least partly ice covered during winter.

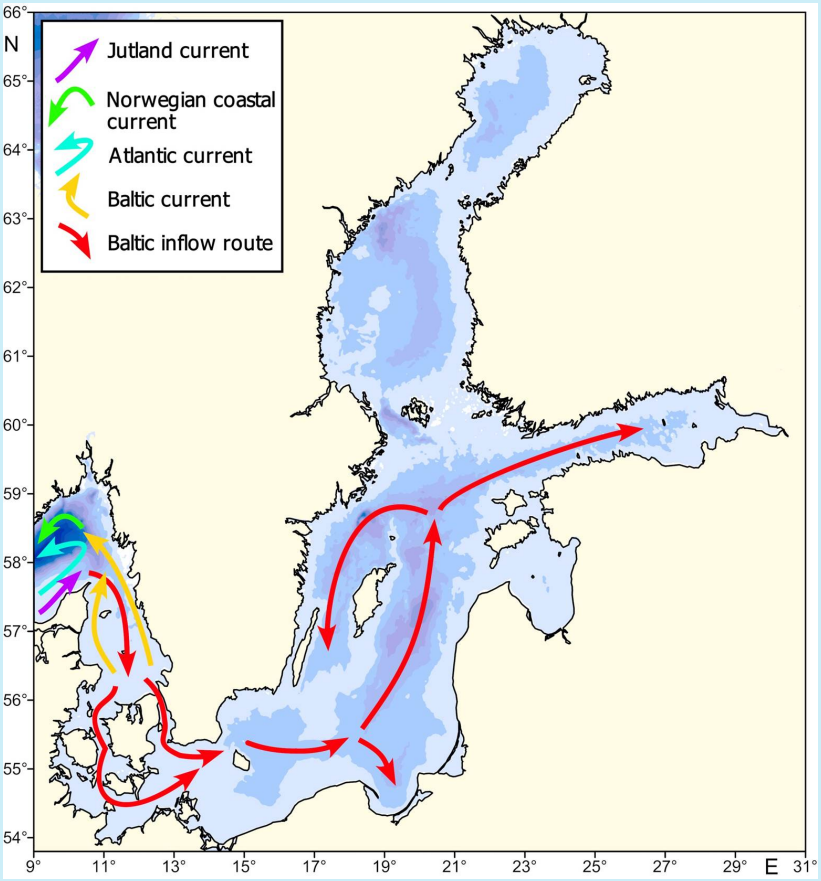

Figure 4.70. Skagerrak, Kattegat, and the Baltic. Circulation map of water masses.

Owing to its central location relative to the Skagerrak, Kattegat, and the Baltic, the weather in Sweden can be taken as representative for the area. Mean air temperature in Sweden was above normal in 2019, especially in the southern parts, with a warm summer and a warm December, which raised the mean air temperature. Mean precipitation was higher than normal in large parts of Sweden during 2019. The number of sun hours was also above normal.

In general, temperatures in the surface water in the Skagerrak and the Baltic Sea were close to normal in 2019. In the Skagerrak, temperatures were warmer than normal in winter and slightly cooler in summer. In the Baltic Sea proper, surface water was somewhat warmer than normal during summer. Surface salinity was close to normal in the Skagerrak and the Kattegat during most of the year, with the exception of some instances of higher salinity during spring. Surface salinities in the Baltic Sea were close to normal during 2019.

The severe oxygen deficiency conditions in Baltic Sea proper deep waters continued in 2019, with values similar to those in 2018. Areal calculations are presented in relation to the area of the Baltic Sea proper, including Arkona Basin, Bornholm Basin, Gulf of Gdańsk, eastern, western, and northern Gotland Basin, Gulf of Riga, and Gulf of Finland. Around 22% of the bottom area in the Baltic Sea proper was affected by anoxic conditions (< 0 ml l^{-1}), and 32% by a combination of both hypoxic (< 2 ml l^{-1}) and anoxic conditions. These two latest years may indicate a new trend, where new areas are affected regularly by anoxic conditions, and hence a larger total area is affected. A major Baltic inflow can significantly refresh the deep water along its route into the Baltic Sea proper. However, no major Baltic inflow was detected in 2019, and the last one occurred in 2016. A smaller inflow into the Baltic was detected during late November to mid-December, estimated at roughly 40 km^3.

The 2018/2019 ice season started in late October, ended in May, and was mild. A cold period in January made most of the Bay of Bothnia, the Quark, and the northern part of the Bothnian Sea ice covered. Also, in the eastern part of the Gulf of Finland and the West Estonian Archipelago, a thin ice cover was present at that time. The maximum ice extent of 88 000 km^2 was reached on January 27, earlier than usual.

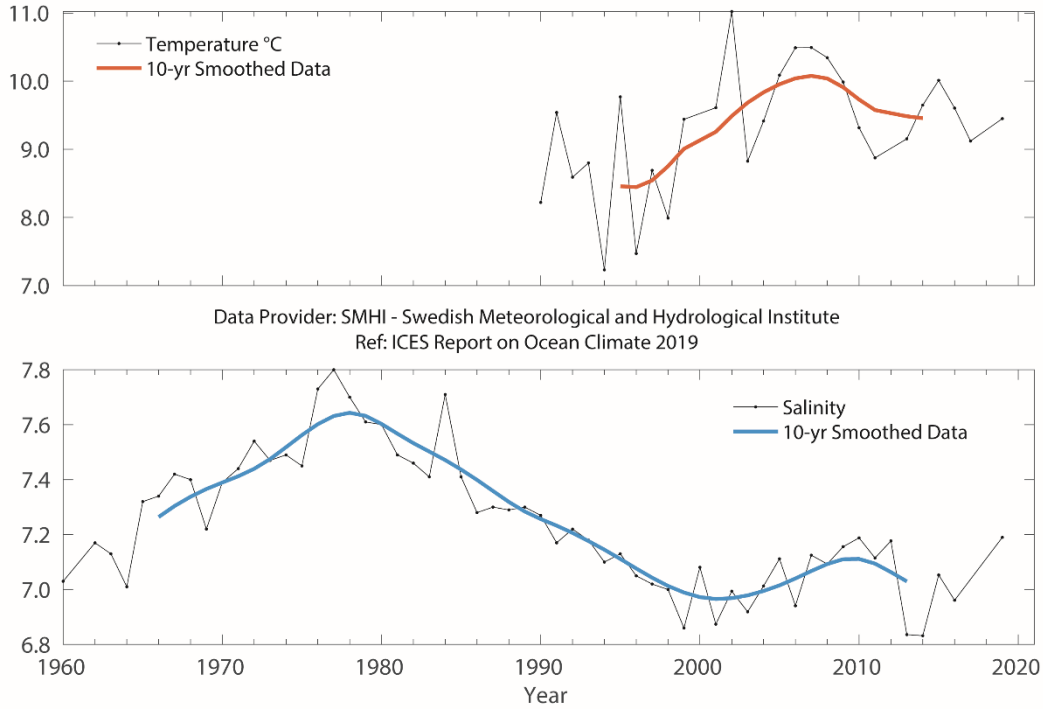

Figure 4.71. Skagerrak, Kattegat, and the Baltic. Surface temperature, yearly mean (upper panel), and surface salinity, yearly mean (lower panel) at Station BY15 (east of Gotland) in the Baltic proper.

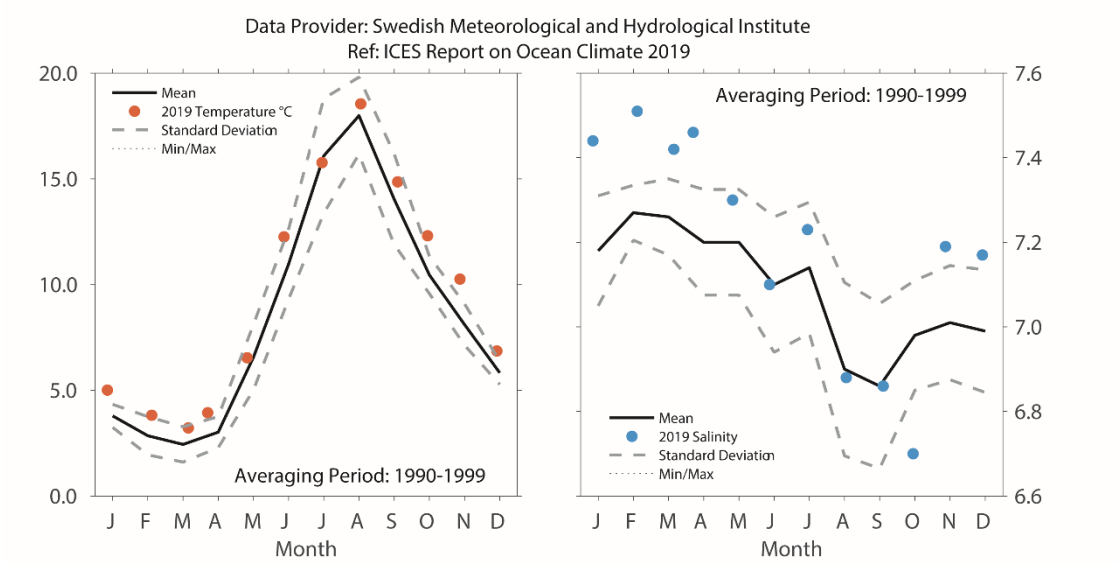

Figure 4.72. Skagerrak, Kattegat, and the Baltic. Monthly surface temperature (left panel) and salinity (right panel) at Station BY15 (east of Gotland) in the Baltic proper.

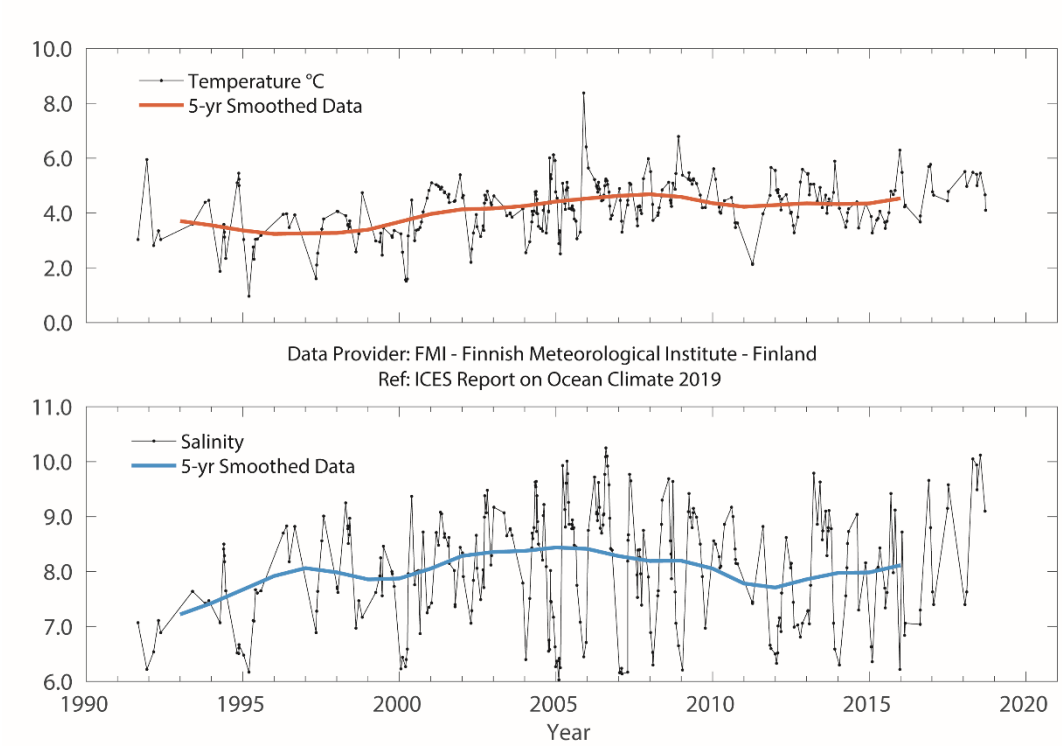

Figure 4.73. Skagerrak, Kattegat, and the Baltic. Temperature (upper panel) and salinity (lower panel) at Station LL7 in the Gulf of Finland. Data until 2018.

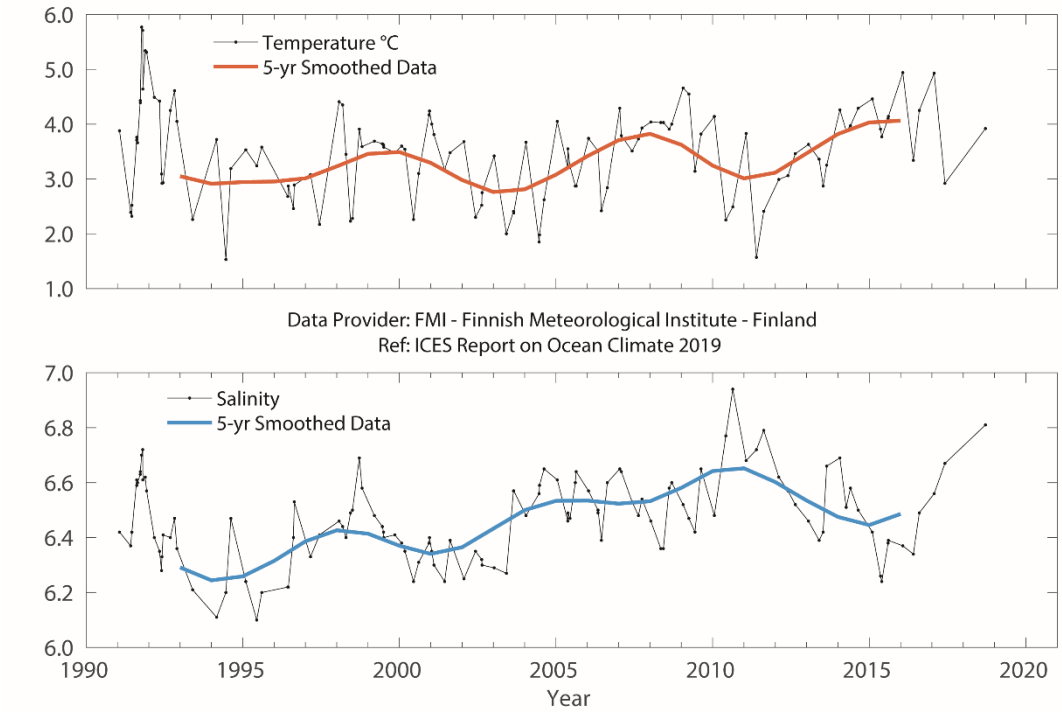

Figure 4.74. Skagerrak, Kattegat, and the Baltic. Temperature (upper panel) and salinity (lower panel) at Station SR5 in the Bothnian Sea. Data until 2018.

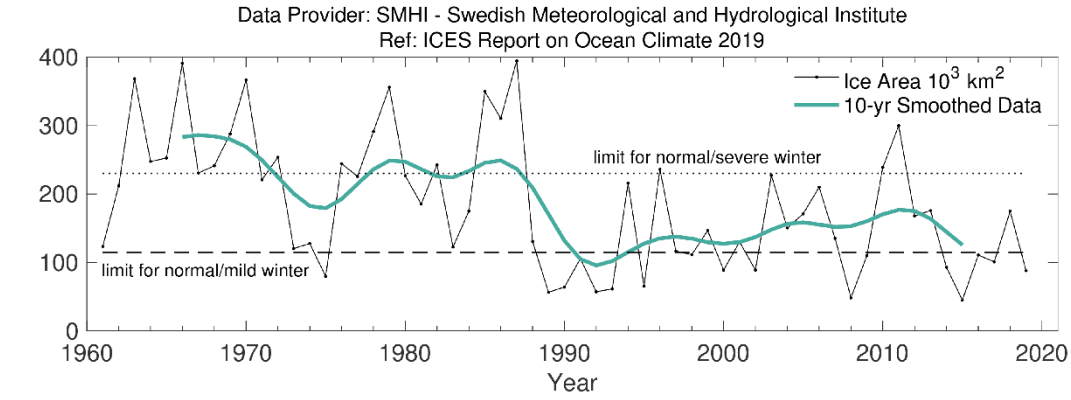

Figure 4.75. Skagerrak, Kattegat, and the Baltic. The maximum ice extent in the Baltic starting from 1960.

4.20 Norwegian Sea

K.A. Mork

CONTINUED FRESHENING AND HIGH HEAT CONTENT IN THE NORWEGIAN SEA, ALTHOUGH TEMPERATURES DECREASED SLIGHTLY WITH RESPECT TO 2018.

The Norwegian Sea is characterized by warm AW on the eastern side and cold Arctic water on the western side, separated by the Arctic front (Figure 4.76). AW enters the Norwegian Sea through the Faroe–Shetland Channel and between the Faroes and Iceland via the Faroe Front. A smaller branch, the North Icelandic Irminger Current, enters the Nordic seas on the western side of Iceland. AW flows north as the Norwegian Atlantic Current, which splits when it reaches northern Norway; some enters the Barents Sea, whereas the rest continues north into the Arctic Ocean as the West Spitsbergen Current.

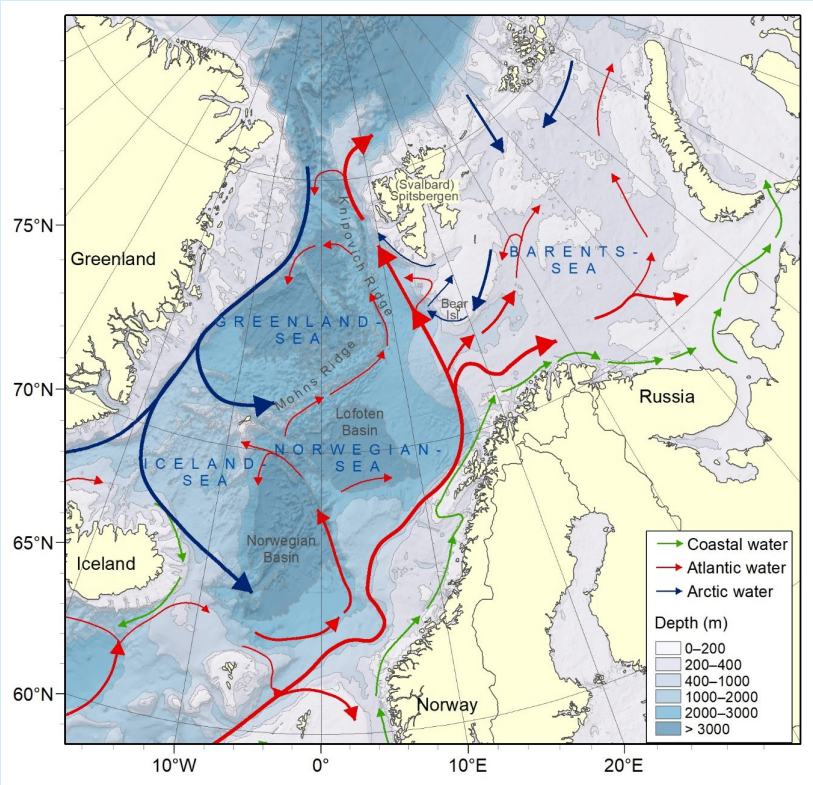

Figure 4.76. Circulation schematic for the Norwegian Sea and Barents Sea. Red lines show the poleward movement of AW. Blue lines show the circulation of Arctic Water. Green lines show the circulation of coastal waters.

The development of temperature and salinity in the core of the AW can be observed at three sections, from south to north in the eastern Norwegian Sea: Svinøy-NW (Figure 4.77), Gimsøy-NW (Figure 4.79), and Sørkapp-W (Figure 4.80). In general, there has been an increase in temperature in all three sections since the mid-1990s, except during the most recent years, when temperature declined at the Svinøy-NW and Gimsøy-NW

sections. Annual temperature averages in 2019 were close to the long-term means at both the Svinøy-NW and Gimsøy-NW sections (0.1°C below the long-term means at both sections). At the Sørkapp-W section, the average temperature in 2019 was still 0.5°C above the long-term mean.

Salinity increased until around 2010 at all three sections and then decreased in recent years. In both the Svinøy-NW and Gimsøy-NW sections, the 2018/2019 salinity was the lowest observed since the end of the 1970s. Annual salinity averages in 2019 were 0.08, 0.09, and 0.04 below the long-term means at the Svinøy-NW, Gimsøy-NW, and Sørkapp-W sections, respectively.

The AW ocean heat and freshwater content, using hydrographic data during spring from 1951 to the present, describe the climate variability of the Norwegian Sea (Figure 4.81). Heat content in the Norwegian Sea has been above the long-term mean since 2000, reaching a record-high in 2017. Freshwater content has increased since 2000, and was above the long-term mean in 2019, while heat content was still relatively high in 2019.

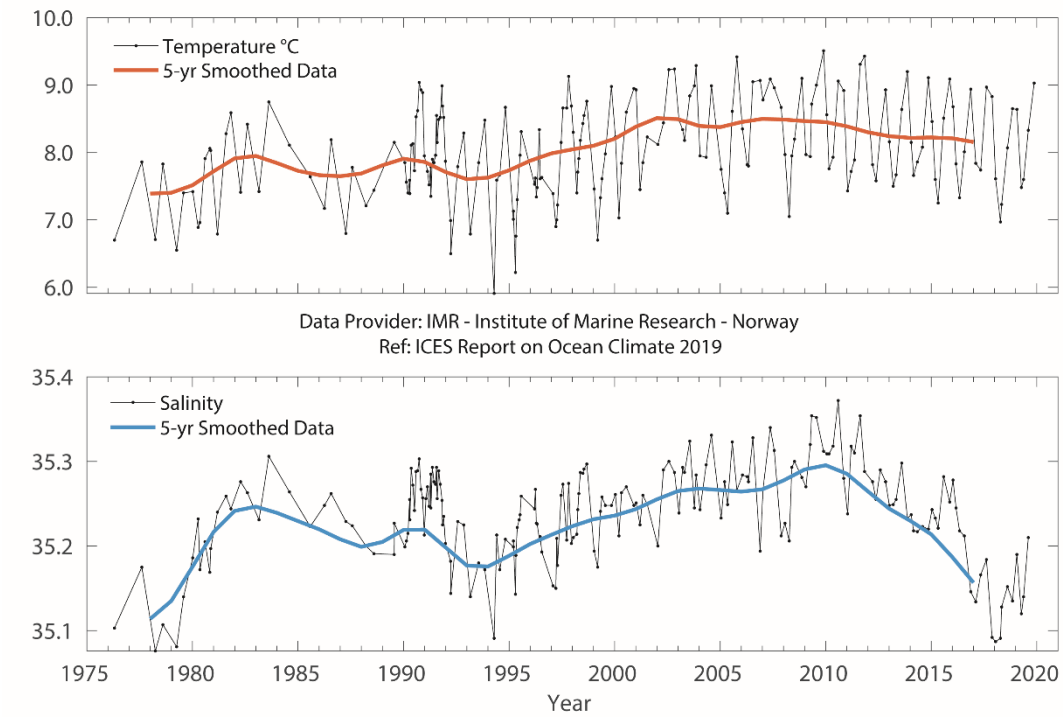

Figure 4.77. Norwegian Sea. Temperature (upper panel) and salinity (lower panel) above the slope at Svinøy Section (63°N).

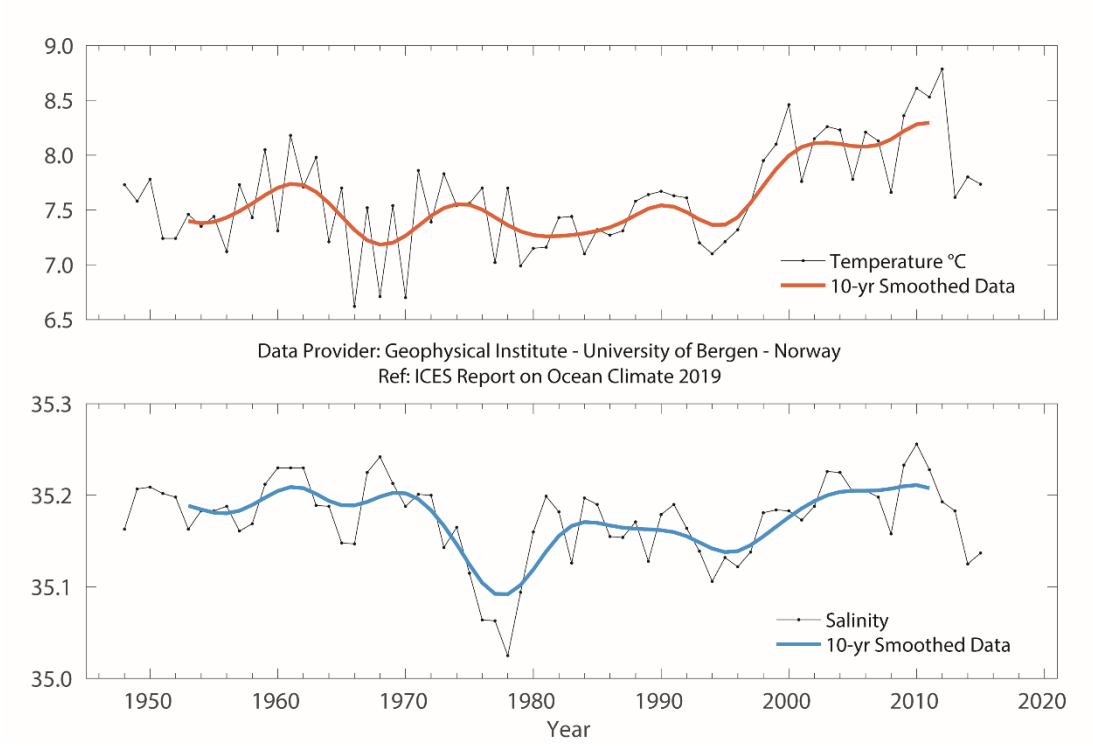

Figure 4.78. Norwegian Sea. Temperature (upper panel) and salinity (lower panel) at 50 m at Ocean Weather Station "M" (66°N 2°E). Data until 2015.

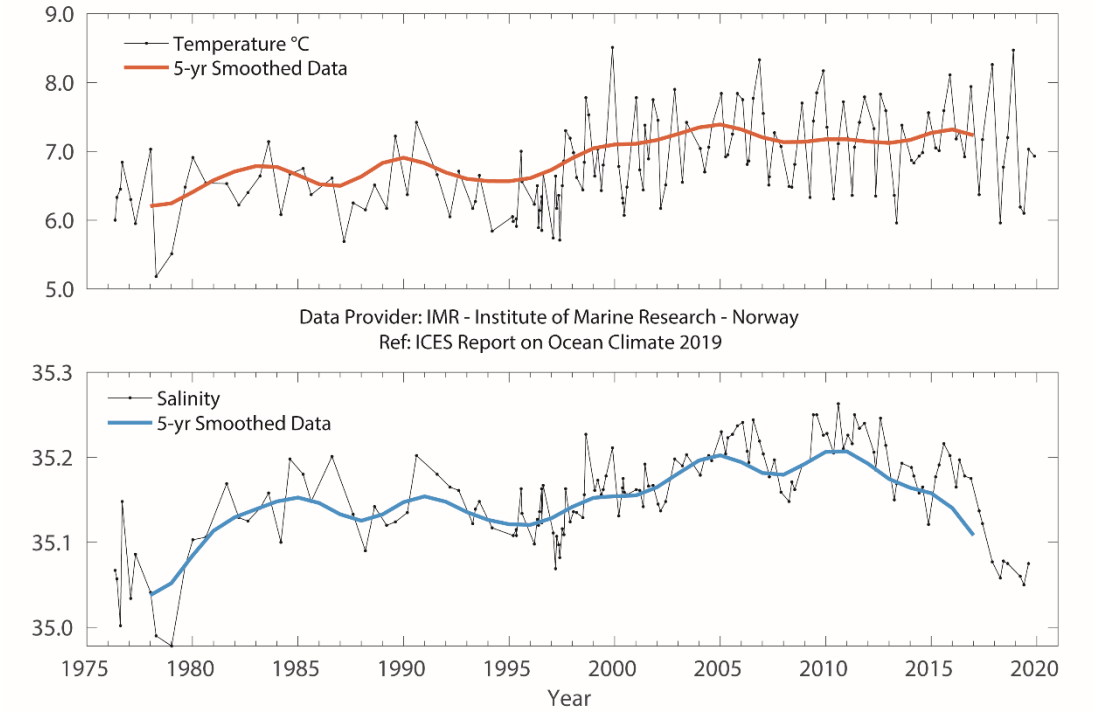

Figure 4.79. Norwegian Sea. Temperature (upper panel) and salinity (lower panel) above the slope at Gimsøy Section (69°N).

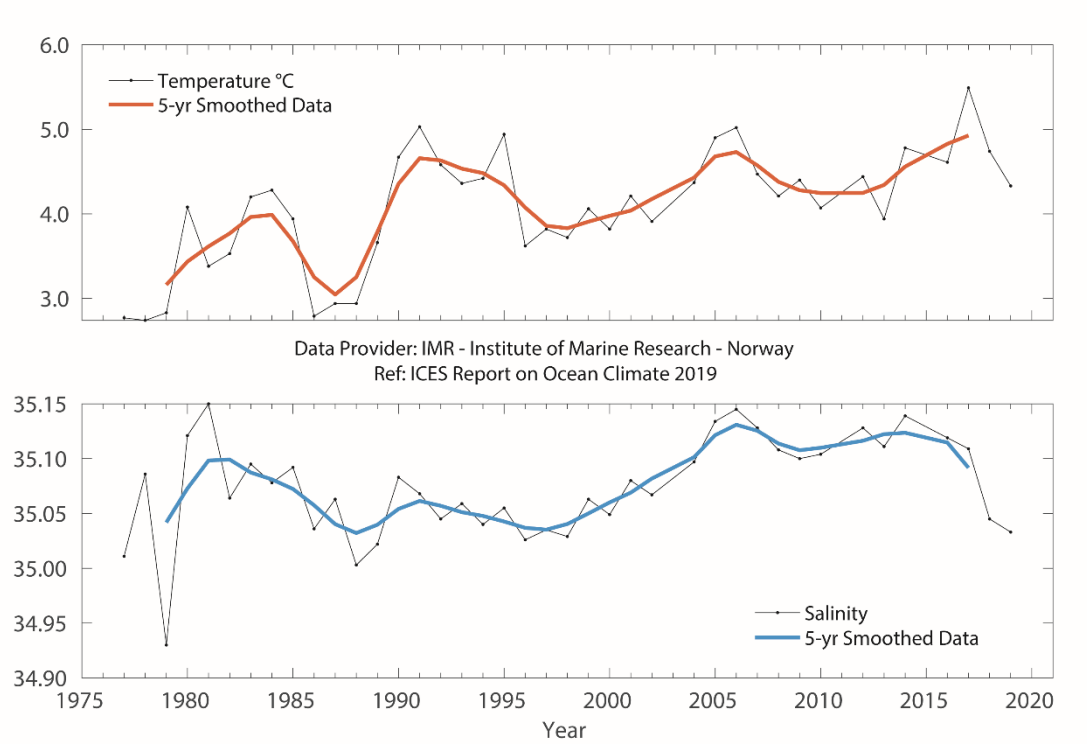

Figure 4.80. Norwegian Sea. Temperature (upper panel) and salinity (lower panel) above the slope at Sørkapp Section (76°N).

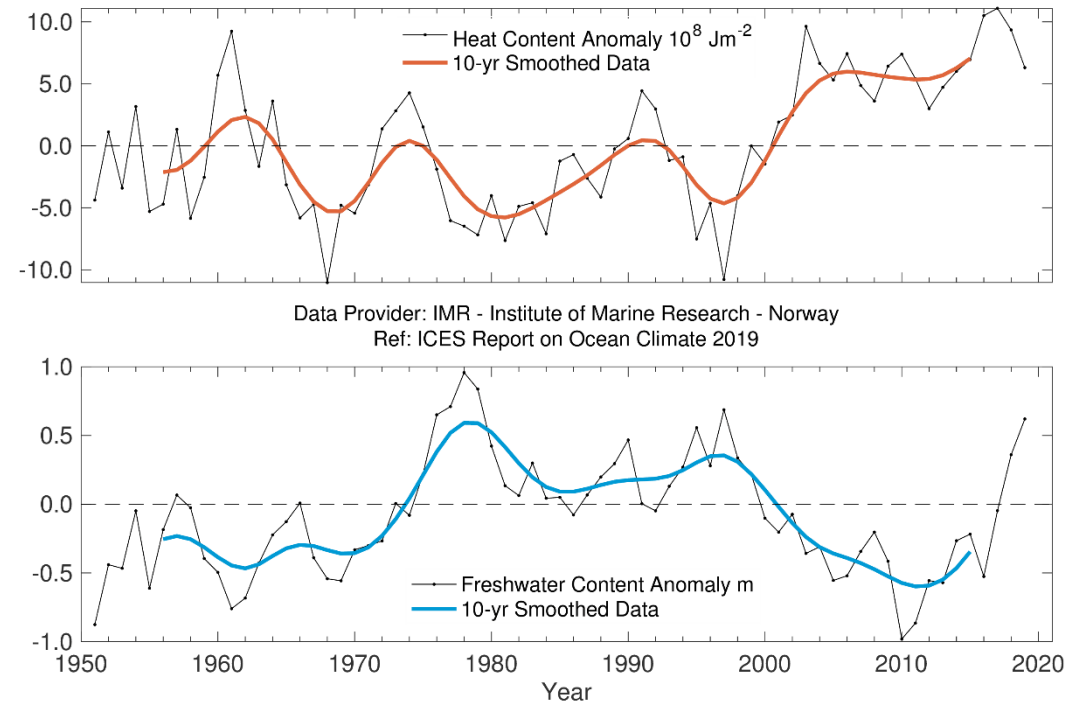

Figure 4.81. Norwegian Sea. Heat (upper panel) and freshwater (lower panel) contents of AW in the Norwegian Sea.

4.21 Barents Sea

A. Trofimov and R. Ingvaldsen

STILL WARM AND LOW-ICE CONDITIONS IN THE BARENTS SEA IN 2019, BUT WITH A COOLING TREND SINCE 2016.

The Barents Sea is a shelf sea that receives an inflow of warm AW from the west (Figure 4.76). The inflow exhibits considerable seasonal and interannual fluctuations in volume and water mass properties causing high variability in heat content and ice coverage of the region.

In 1996 and 1997, after a period with high temperatures in the first half of the 1990s, temperatures in the Barents Sea dropped to slightly below the long-term average. From March 1998, temperature in the western Barents Sea increased to just above average, but remained below average in the eastern part during 1998. From the beginning of 1999, there was a rapid temperature increase in the western Barents Sea that spread to the eastern part. Since then, temperature has remained above average.

The Fugløya–Bear Island section covers the inflow of AW and coastal water masses from the Norwegian Sea into the Barents Sea, while the Kola Section covers the same waters in the central Barents Sea. Since 2015, AW temperature in the western Barents Sea (Fugløya–Bear Island Section) has decreased by more than 1°C (Figure 4.82). In 2019, it was at the same level as in the early 2000s. The decrease in temperature is linked to lower temperatures upstream in the Norwegian Sea. AW salinity in the Fugløya–Bear Island Section has been decreasing since 2011, and was at the same level in 2019 as during a very fresh and cold period in the late 1970s (Figure 4.82).

In the central Barents Sea (Kola Section), air and water temperatures in 2019 were still above the 1981–2010 average, but were far lower than in 2018. In March–December, the observation period in the Kola Section (0–200 m) in 2019, coastal waters in the inner part of the section and AW in its central part (Murman Current) had positive temperature anomalies, decreasing from +0.7°C in March to close to zero in autumn and early winter. In the outer part of the section (central branch of the North Cape Current), the AW temperature anomaly first increased from close to zero in March to +0.4°C in June, then decreased to –0.3°C in November, increasing again to +0.2°C in December. The 2019 annual AW mean temperature in the central Kola Section (0–200 m) was 0.4°C above average and 0.4°C lower than in 2018 (Figure 4.83).

Throughout the observation period in 2019, coastal and AW salinity in the Kola Section (0–200 m) was lower than the 1981–2010 average and, in general, close to that observed in 2018. In coastal waters, a negative salinity anomaly was observed, which decreased from –0.18 in March–May to close to zero in December. The AW in the Murman Current also decreased from –0.13 in March to –0.03 in December, but with a less-pronounced trend. The AW in the central branch of the North Cape Current was fresh, with a negative salinity anomaly varying from –0.02 to –0.09. The seasonal (March–

December) average salinity was fresher than normal, with anomalies decreasing along the section from –0.10 in coastal waters to –0.05 in the AW offshore. The 2019 annual mean salinity in AW (0–200 m) in the central Kola Section was 0.07 below average and the second lowest, after 2018, observed since 1990 (Figure 4.83).

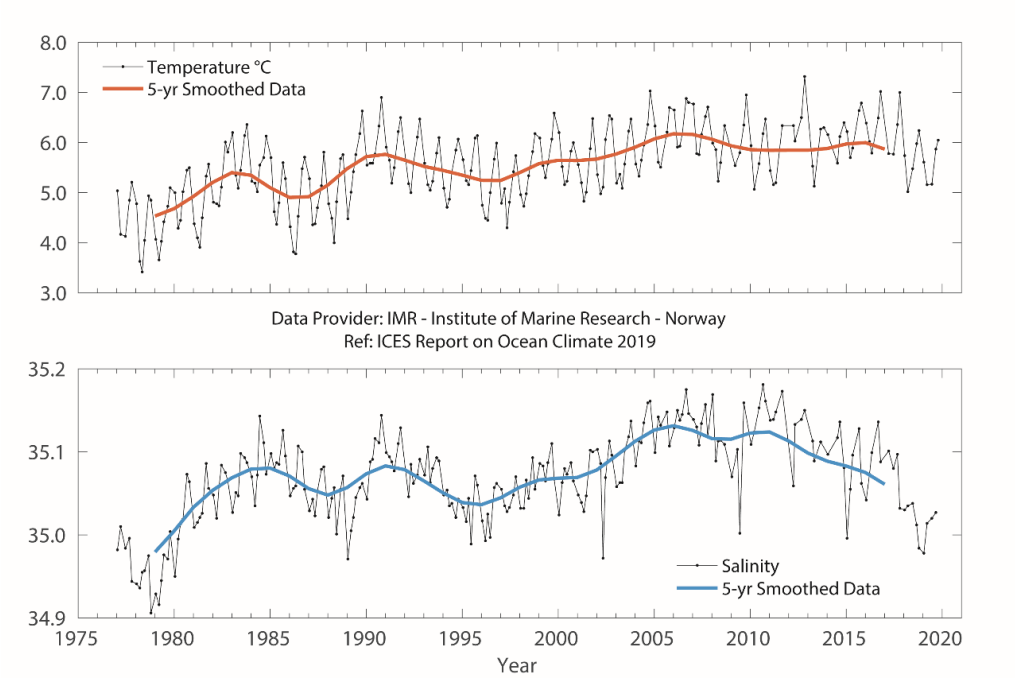

Figure 4.82. Barents Sea. Temperature (upper panel) and salinity (lower panel) in the Fugløya–Bear Island Section.

According to data from the Barents Sea Ecosystem Survey carried out in August/September 2019, surface, deeper, and bottom waters in most of the Barents Sea (about two-thirds of the covered area) were still warmer than the long-term average. The largest positive anomalies were predominantly observed in the southeast, especially near bottom. Negative anomalies were mainly observed in the southwestern part of the sea at the surface and in the northern part at all depths, especially near bottom. Compared to 2018, the water was 0.6–0.9°C colder in most of the Barents Sea (75–85% of the surveyed area). The coldest temperature anomalies between 2019 and 2018 were mainly found in the north at all depths and in the south at the surface, while the warmest anomalies were mostly observed in the southeastern part of the sea near the bottom.

In August/September 2019, surface waters were saltier than the long-term average in almost half of the surveyed area, mainly in its central and northern parts, with the largest positive anomalies in the northern Barents Sea. Negative surface salinity anomalies were mostly observed in the western, southern, and southeastern parts of the Sea. Bottom salinity was slightly lower than the long-term average in two thirds of the surveyed area, with the largest negative anomalies in the southeastern and northernmost Barents Sea. Positive bottom salinity anomalies were mainly found south and southeast of the Spitsbergen Archipelago, as well as in shallow waters in the most southeastern part of the Sea. Compared to 2018, surface waters were, on average, 0.4 fresher over 87% of the surveyed area, with the largest negative differences east of the Spitsbergen Archipelago and in the southeastern Barents Sea. Bottom waters were

slightly fresher than in 2018 in 80% of the surveyed area. Only coastal waters in the southwestern part of the Sea and waters around the Spitsbergen Archipelago were somewhat saltier than in the previous year.

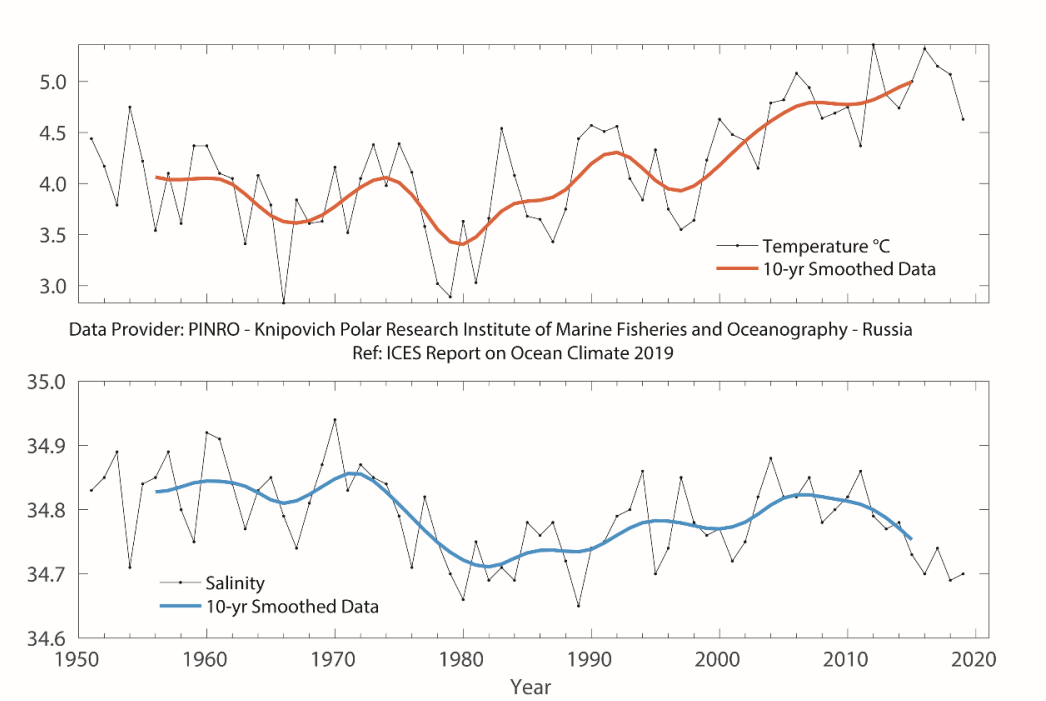

Figure 4.83. Barents Sea. Temperature (upper panel) and salinity (lower panel) in the Kola Section (0–200 m).

In autumn 2019, the area occupied by AW (> 3°C) decreased slightly but remained higher than normal; the area occupied by Arctic waters (< 0°C) increased slightly but remained relatively small; and the area occupied by warm bottom waters (> 1°C) was nearly halved compared to the previous year. The area of cold bottom waters has been increasing since a record-low value in 2016.

During recent years, lower temperatures, in combination with lower AW inflow during winter, have caused increases in winter sea ice in the Barents Sea. In 2019, the sea ice extent was still below the 1981–2010 average, but higher than in 2018. The ice-covered area reached a seasonal maximum of 51% in March, a month earlier than usual, and was close to average. During the low-ice season from August to October, ice coverage equalled 1 to 4%, with the minimum occurring at the usual time in September (1% of coverage).

The volume flux into the Barents Sea varies with a period of several years. The annual volume flux was relatively high during 2003–2006. From 2006 to 2014, inflow was relatively stable before it increased substantially in 2015 to about 1 Sv above the long-term average. A relatively low inflow was measured in 2016. Since 2017, the annual inflow to the Barents Sea has decreased. Since 2015, quarterly volume fluxes have been decreasing during winter and spring and increasing during summer and autumn. The inflow in spring 2019 was about 1 Sv lower than in 2018, but this number might change when the time-series (which currently stops in May 2019) is updated.

4.22 Fram Strait

A. Beszczynska-Möller and W.J. von Appen

SIGNIFICANTLY LOWER TEMPERATURE AND SALINITY OF AW CARRIED POLEWARD ALONG THE EASTERN RIM OF THE GREENLAND SEA AND FRAM STRAIT, WITH TEMPERATURE CLOSE TO AND SALINITY FAR BELOW THE LONG-TERM AVERAGE.

Fram Strait (Figure 4.76) is the northern border of the Nordic seas. It is the only deep passage connecting the Arctic to the rest of the world oceans and is one of the main routes whereby AW enters the Arctic (the other is the Barents Sea). The AW flows along the eastern rim of the Greenland Sea and is carried north in Fram Strait by the West Spitsbergen Current. AW temperature, salinity, volume, and heat fluxes exhibit strong seasonal and interannual variations. A significant part of the AW also recirculates within and shortly north of Fram Strait and joins the flow to the south as the Return Atlantic Water (RAW). Polar Water from the Arctic Ocean flows south in theEGC and affects water masses in the Nordic seas.

AW temperature at the eastern rim of the Greenland Sea (along the 75°N section, between 10° and 13°E) reached its highest value in 2005–2007 with a peak in 2006. After this period, AW temperature decreased significantly in 2008/2009 and remained below its long-term mean value until 2011. In 2012, AW temperature in the eastern Greenland Sea recovered and remained relatively stable until 2018, exceeding its long-term mean by 0.25–0.55°C, with small variations (up to 0.5 s.d.). Since 2018, AW temperature has decreased compared to previous years, reaching 4.37°C in 2019 (0.2°C below the long-term average).

A significant increase in AW salinity in the eastern Greenland Sea was observed in 2005/2006, with the maximum of 35.16 in 2006 (0.07 above the long-term average). This peak was followed by a sharp decrease in 2007 and a further slow descent until 2009 when AW salinity returned to its long-term average. In 2010, salinity started to rise again and reached its second peak in 2012 (0.06 above its long-term mean). It remained relatively steady until 2014 (with a slight decrease in 2013). Since 2015, a notable decrease in salinity has been observed and reached the lowest value in the last 20 years (35.042, i.e. 0.05 below its long-term average) in 2019. In the preceding 14 years (2004–2017), AW salinity in the eastern Greenland Sea was above its long-term average, but was 1.3 s.d. below in 2019.

The western and central parts of the Greenland Sea section at 75°N have not been measured since 2010. RAW temperature at the Greenland Sea western rim reached its maximum in 2006 (2.9°C) and slowly decreased until the end of the observation period in 2010. The 2008–2010 RAW temperature was slightly below the long-term average. The temperature maximum in 2006 was accompanied by a very strong peak in RAW salinity (0.13 above the long-term mean, > 3 s.d. of RAW salinity). In 2007, RAW salinity dropped, remained slightly higher than its long-term average until 2008, and decreased

to close to the average in 2009 and 2010. Temperature and salinity in the upper layer of the central Greenland Basin, within the Greenland Gyre, were modified by the advection of AW and winter convection.

In the southern Fram Strait, at the standard section along 76.50°N (at the level of 200 dbar, spatially averaged between 9° and 12°E), a record-high summer AW temperature was observed in 2006 (maximum of 4.5°C, exceeding the long-term average by 1.3°C), accompanied by the highest AW salinity (35.13) in the observation period. After that peak, temperature and salinity decreased rapidly in 2007 and 2008, before increasing again in summers 2009–2012. In 2011–2015, AW temperature in the southern Fram Strait remained relatively constant (3.7–3.8°C, exceeding its average by ca. 0.6°C), except in summer 2013 when it dropped to 3.22°C and levelled out at its long-term mean. A moderate increase has been observed since 2015, and AW temperature reached its decadal maximum of 4.1°C in 2017, the second largest value after the 2006 maximum of 4.5°C. Generally, in 2016–2018, AW temperature remained nearly constant (between 4.03°C and 4.08°C). In 2019, AW temperature dropped significantly to 3.36°C (only 0.2°C above its long-term average). In 2011, 2012, and 2014, AW salinity in the southern Fram Strait was the same (35.13) as during the 2006 maximum, exceeding its long-term mean by 0.07. After recovering from a drop in 2015, the AW salinity remained the same in 2016 and 2017 (about 1 s.d., i.e. 0.04, above its long-term mean of 35.06). Since 2018, salinity has been notably decreasing and reached a minimum of 35.02 (the lowest value observed in the last 20 years, 1 s.d below its long-term average) in 2019.

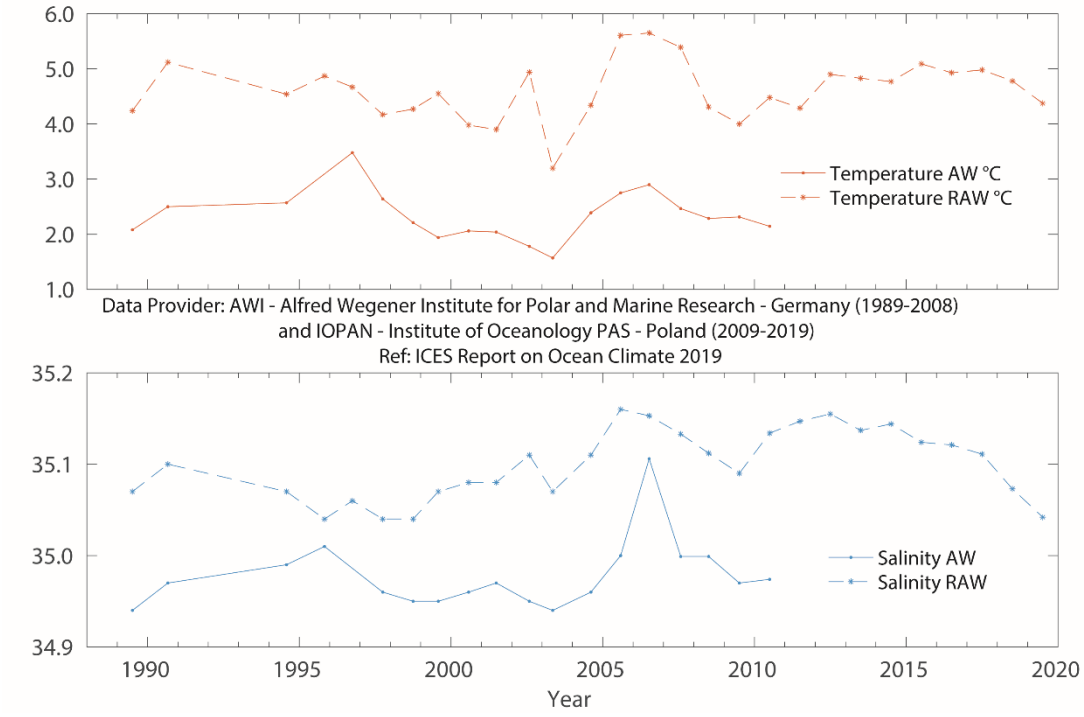

Figure 4.84. Greenland Sea and Fram Strait. Temperature (upper panel) and salinity (lower panel) of AW and RAW in the Greenland Sea Section at 75°N. AW properties are 50–150 m averages at 10–13°E. The RAW is characterized by temperature and salinity maxima below 50 m averaged over three stations west of 11.5°W. RAW has not been measured since 2010.

In the northern Fram Strait, at the standard section along 78.83°N, three characteristic areas can be distinguished in relation to the main flows: the West Spitsbergen Current (WSC) between the shelf edge and 5°E, the Return Atlantic Current (RAC) between 3°W and 5°E, and the Polar Water in the East Greenland Current (EGC) between 3°W and the Greenland Shelf.

The spatially averaged mean temperature of the upper 500 m layer in the WSC reached its peak in 2006 (4.54°C) and decreased afterwards. In 2007–2011, it varied ±0.4°C with respect to the long-term average. In 2012–2013, WSC temperature dropped further, reaching 0.7–0.8°C below its long-term mean. Since 2014, it has been rising again and reached the second highest value in the observation period (4.24°C, 1.13°C above the long-term mean) in 2015. Until 2017, temperature in the WSC remained high, exceeding its long-term average by about 1 s.d. Since 2018, temperature has started to decrease and dropped to 3.28°C (0.2°C warmer than its long-term average) in 2019.

The highest salinity in the upper 500 m of the WSC was observed in 2006 (35.11), followed by a decrease to the long-term average in 2007/2008. Since 2009, WSC salinity increased again until it reached 0.5 above the long-term mean in 2011. After a slight decrease in 2012/2013, salinity in the WSC reached its second maximum (35.09) in 2014, followed by slightly lower values in 2015 and 2016. In 2017, AW salinity in the WSC increased again to 35.07, remaining below the 2014 maximum, but still 0.05 above the long-term average. Since 2018, WSC salinity has been significantly decreasing. It dropped slightly below its long-term average in 2018, and the lowest salinity in the last 21 years (35.001) was observed in the WSC (0.7 s.d. below the long-term average) in 2019.

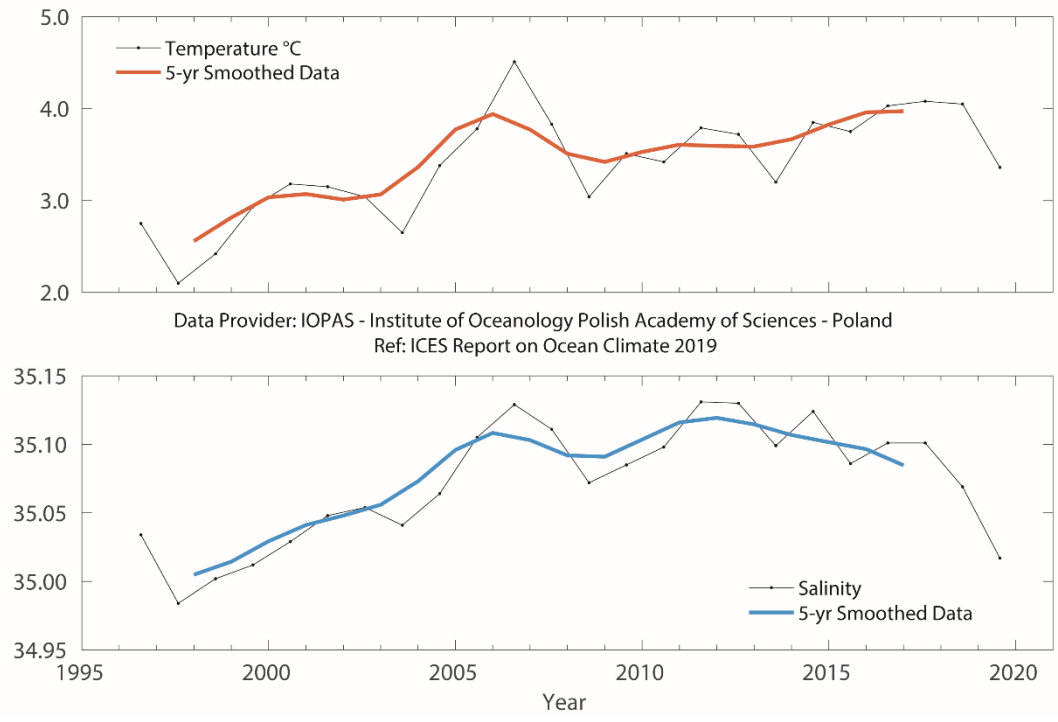

Figure 4.85. Greenland Sea and Fram Strait. Temperature (upper panel) and salinity (lower panel) at 200 dbar in the southern Spitsbergen Section (76.50°N).

At the standard section along 78.83°N, the AW in the WSC core located over the upper shelf slope reached down to about 700–800 m in 2017 and 2018 (the AW lower boundary is represented by the isotherm of 2°C), while in 2016, it was found slightly shallower at the depth of about 500–600 m. In 2019, AW occupied the core of the WSC and was slightly shallower than in the two previous years, reaching down to 500–600 m, similar to that in 2016. The offshore branch of the WSC, located over the lower shelf slope, was less pronounced and slightly shallower in 2019 than in 2017 and 2018, with the isotherm of 2°C found at the depth of about 400–450 m. In 2019, it was also occupied by colder and significantly less saline water than in the previous years. The low salinity surface layer over the WSC core, which covered the upper 20–30 m in 2017, was absent in 2018 and 2019. In 2019, the low salinity surface layer in the offshore WSC branch was found west of 6°E, reaching down to 50 m.

The RAC and EGC domains were not measured in 2017–2019. The RAC temperature in 2016 remained close to that in previous years, while the temperature difference between AW in the WSC, and AW recirculating in the RAC was half of that observed in 2015 (0.7°C and 1.5°C, respectively). The highest RAC temperatures were observed in 2005 (3°C) and 2009/2010 (slightly above 2.9°C). In 2011/2012, it remained close to the long-term average of 2.2°C, after which it increased slowly and reached 2.8°C in 2016. The maximum RAC salinity was observed in 2010. In the subsequent years (2011, 2012, and 2014), it exceeded its long-term mean by about 0.05, after which it levelled out in 2015 before increasing again in 2016.

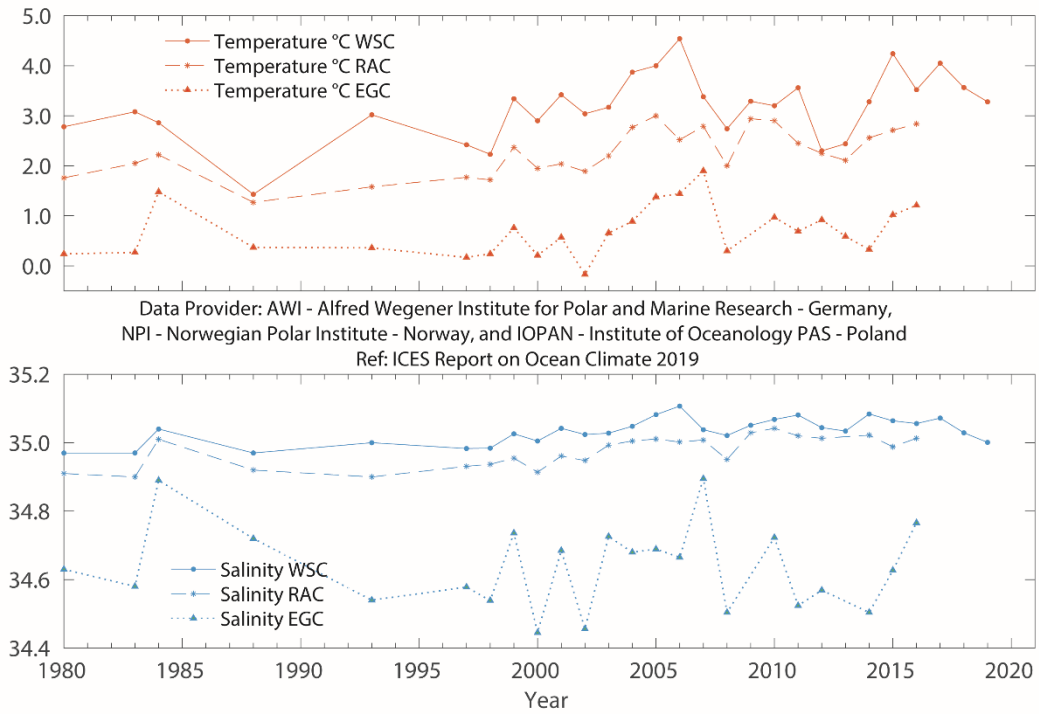

Figure 4.86. Greenland Sea and Fram Strait. Temperature (upper panel) and salinity (lower panel) in Fram Strait (78.83°N) at 50–500 m: in the AW in the West Spitsbergen Current (WSC; between the shelf edge and 5°E), in the RAC (between 3°W and 5°E), and in the Polar Water in the EGC(between 3°W and the Greenland Shelf). RAC and EGC were not measured in 2017–2019.

In the EGC domain, temperature reached its peak in 2007 (1.9°C), decreased significantly to 0.3°C in 2008, and since then remained relatively stable (within ±0.3°C from its long-term mean), with a slight decrease to 0.3°C in 2014 and a return to 1.0°C in 2015. In 2016, the EGC temperature was slightly higher than in the previous year. Salinity in the EGC was highest in 2007 (34.90) and then dropped below its long-term average, with the exception of an intermediate peak (34.72) in 2011. In 2008 and 2014, EGC salinity reached the lowest value observed during the last decade (34.50, compared to the record low minimum of 34.45 observed in 2000 and 2002). Since 2014, salinity steadily increased and was slightly above its long-term mean in 2016.

5 Detailed area descriptions, Part II: The intermediate and deep ocean

This section focuses on the deeper waters of the Nordic seas and the North Atlantic, typically below 1000 m. The general circulation scheme and dominant water masses can be seen in Figure 5.1.

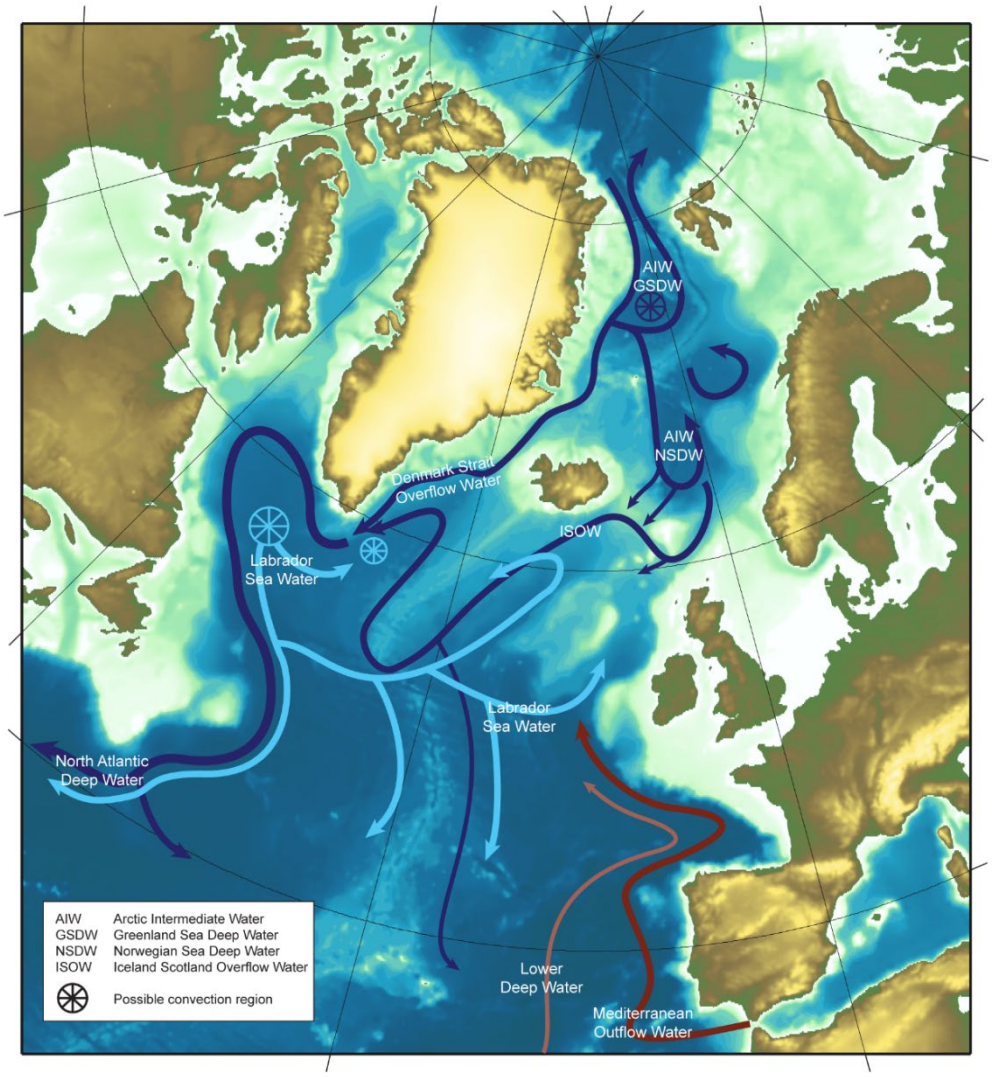

Figure 5.1. Schematic circulation of the intermediate to deep waters in the Nordic seas and North Atlantic.

At the northern boundary of the region of interest, cold and dense outflow from the Arctic Ocean enters the Fram Strait along its western side and reaches the Greenland Sea. The outflow is a mixture of Eurasian Basin and Canadian Basin deep waters and Upper Polar Deep Water (UPDW). The Eurasian Deep Water feeds the densest water of all Nordic seas: the Greenland Sea Bottom Water. The Canadian Basin Deep Water and UPDW supply the Arctic Intermediate Water (AIW) in the Greenland Sea. The UPDW also includes products of winter convection. The deep southward outflow from the North Atlantic in the deep western boundary current is fed by the cold and dense overflow waters. The deepest and densest is the Denmark Strait Overflow Water (DSOW). This water mass originates in the AIW produced in the Greenland and

Iceland seas by winter convection and mixing with surrounding water masses. The DSOW sinks to the bottom as it passes over the Denmark Strait sill, vigorously entraining ambient water. Downstream, it is overlain by LSW, an intermediate water mass formed by deep-winter convection in the Labrador Sea. The middle layer of the deep, cold water export in the deep western boundary current is supplied by the Iceland–Scotland Overflow Water (ISOW), which originates in water masses formed in the Norwegian Sea (AIW and Norwegian Sea Deep Water). Passing through the Iceland Basin, ISOW also entrains upper ocean water and LSW. The deep Antarctic Bottom Water enters the North Atlantic on the western side, but its signature is also present in eastern Atlantic abyssal basins. At intermediate levels, MW originates from vigorous mixing of Atlantic central waters and Mediterranean Overflow Waters at the Gulf of Cadiz. This water mass spreads at about 1000 m depth in all directions, with a main vein progressing northward along the European margin. Around the Canaries, MW encounters the northern limit of Antarctic Intermediate Waters.

5.1 Nordic seas

The deep waters of the Greenland, Iceland, and Norwegian seas are all warming. The source of the warming is the deep outflow from the Arctic Ocean, a southward-flowing current of the Eurasian and Canadian Basin Deep Waters and the UPDW found on the western side of Fram Strait at ca. 2000 m depth. The Greenland Sea Deep Water (GSDW) is warming fastest owing to its direct contact with this Arctic outflow, whereas the Iceland and Norwegian seas are warming more slowly because they are products of the mixing of their own ambient waters with GSDW and Arctic outflow water.

5.1.1 Greenland Sea

A. Beszczynska-Möller

Continuous warming has been observed in the Greenland Sea deep layer at 3000 m, both in the Greenland Sea Gyre (not measured since 2011) and in the eastern part of the deep basin (at 5°E, measured since 2001), Figure 5.2, upper panel. GSDW temperature is similar at both locations, and a relatively steady temperature increase from –1.18°C to –0.87°C has been observed between 1993 and 2019. In 2019, the deep-water temperature exceeded its long-term average by 0.14°C (3.3 s.d.). The strongest temperature increase of 0.03°C was found between 2010 and 2011, while more recently, year-to-year temperature changes have been lower (between 0 and 0.02°C). Between 2018 and 2019, the deep water in the eastern Greenland Sea warmed by 0.006°C. For the entire 1993–2019 observation period, the average warming rate in the deep Greenland Sea can be estimated as 0.11°C per decade.

Warming of deep waters in the Greenland Sea has been accompanied by an increase in salinity, albeit its interannual variability differs between the central Greenland Sea Gyre (observed in 1993–2010) and the eastern Greenland Sea (measured since 2001), Figure 5.2, lower panel. A relatively steady increase in salinity from 34.901 in 1993 to 34.916 in 2010 was observed in the Greenland Sea Gyre. In the eastern part of the deep Greenland Sea, the year-to-year changes are much stronger than in the central gyre, but

the overall 2001–2019 trend is positive and similar to that in the central basin. The salinity increase is of the order of 0.01 per decade. The maximum salinity of 34.919 was found in the eastern Greenland Sea in 2015, 2017, and 2019, with a slight drop in 2018 to 34.916. In the last decade, salinity in the deep layers of the eastern Greenland Sea remained above its long-term average (1.8 s.d. above the long-term average in 2019).

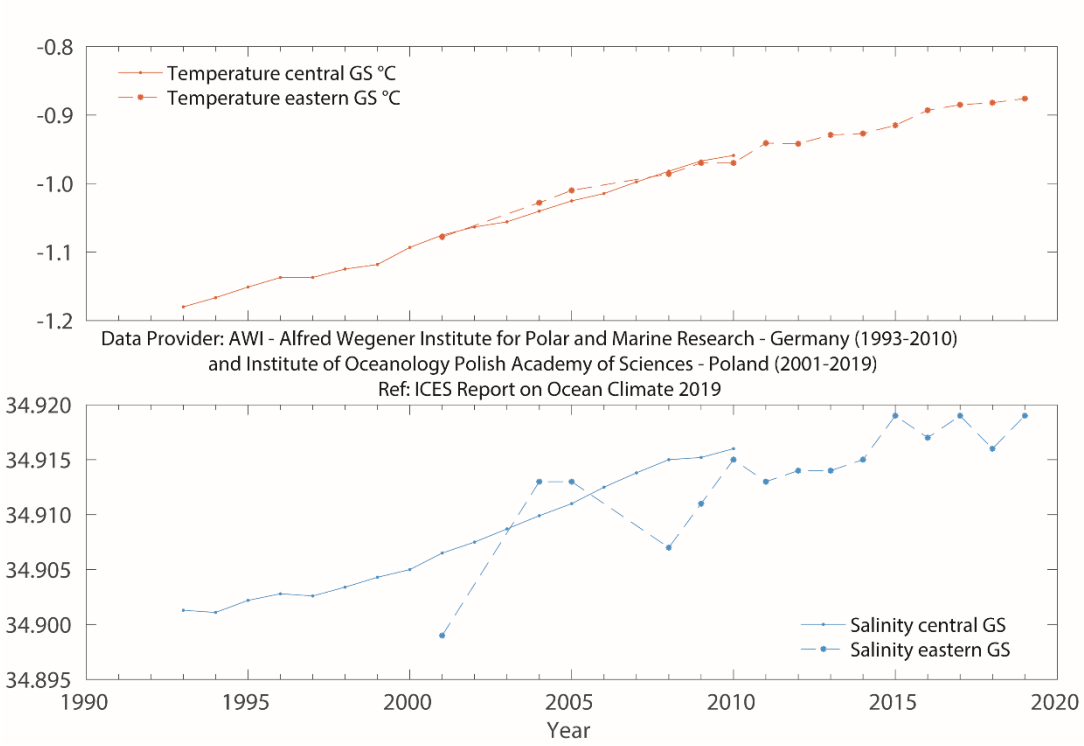

Figure 5.2. Greenland Sea and Fram Strait. Temperature (upper panel) and salinity (lower panel) at 3000 m in the Greenland Sea Section at 75°N (solid line in the central Greenland Sea Gyre, dashed line in the eastern Greenland Sea at 5°E).

After a cessation of deep convection, the doming structure in the Greenland Sea Gyre is being replaced by a two-layered water mass arrangement. During the 1993–2010 measurement period, the winter convection depth varied between 700 and 1600 m and was only significantly deeper in small-scale convective eddies. In winter 2007/2008, the maximum convection depth was estimated to be 1700 m, deeper than the previous year (1200 m) and similar to the maxima observed during 2001/2002 and 2002/2003. The import of warm and saline AW to the Greenland Sea is currently not balanced by an import of cool and fresh Polar Water from the north. The AW dominates changes in the upper ocean and tends to prevent ice formation and to vertically homogenize the waters ventilated by convective processes. GSDW formerly included a small admixture of surface freshwater through the convective process and, therefore, had a lower salinity than the Arctic outflow waters. The observed increase in GSDW salinity may be the result of an adjustment to the Arctic outflow in the continued absence of deep convection and an increased presence of AW in the upper layer.

5.1.2 Norwegian Sea

S. Østerhus

The longest time-series in the Nordic seas is from the Ocean Weather Ship M in the Norwegian Sea. It reveals persistent warming from the mid-1980s; although slight decreases in temperature occurred in 2001–2011, 2013–2015, and again in 2019 (Figure 5.3). The long warming trend for the 1981–2010 period was 0.06°C per decade. However, in the recent decade (2010–2019), the trend has been slightly lower.

It is unclear whether there has been any corresponding salinity trend in the Norwegian Sea deep waters in recent decades. After a slight decrease in the early 1990s, salinity in the Norwegian Sea deep basins has remained relatively stable over the 2000s and until 2019, although a relatively high value was recorded in 2000 and a record-low value in 2012. The salinity in 2019 was the lowest since 2012 (Figure 5.3).

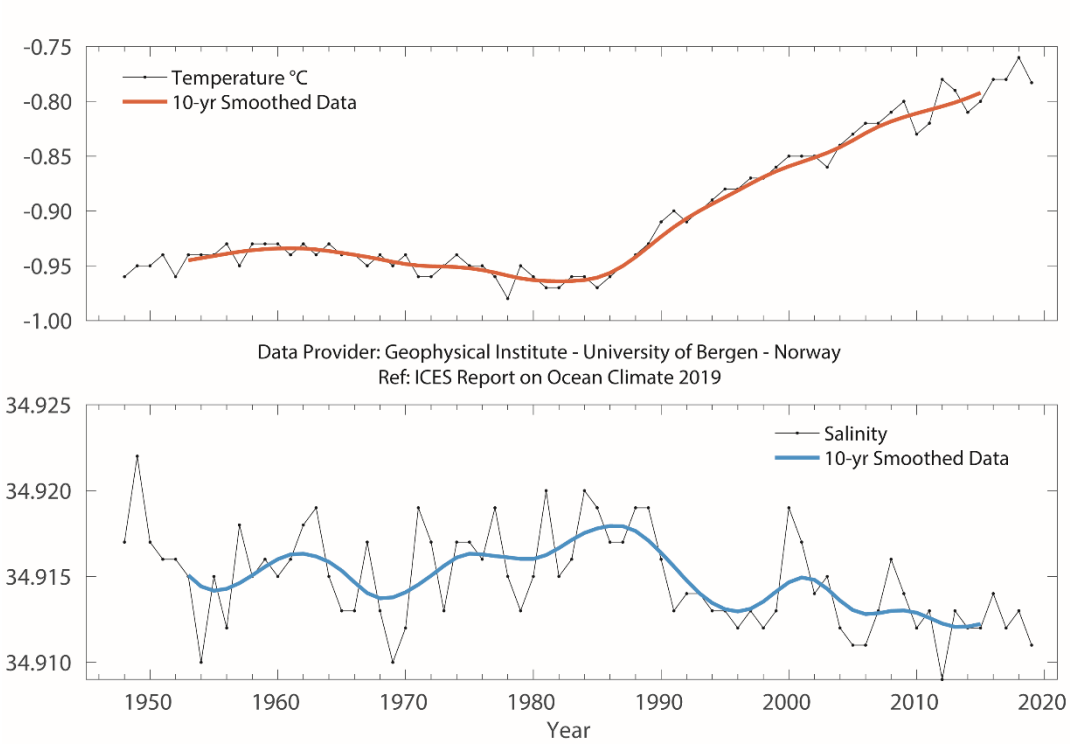

Figure 5.3. Norwegian Sea. Temperature (upper panel) and salinity (lower panel) at 2000 m at Ocean Weather Station "M" (66°N 2°E).

5.1.3 Iceland Sea

S. R. Ólafsdóttir and M. Danielsen

In the Iceland Sea, an increase in temperature in the depth range 1500–1800 m has been observed almost continuously since the beginning of the time-series in the early 1990s and continued until the end of 2019 (Figure 5.4). Deep water in the eastern part of the Iceland Sea has warmed 0.2°C in 29 years.

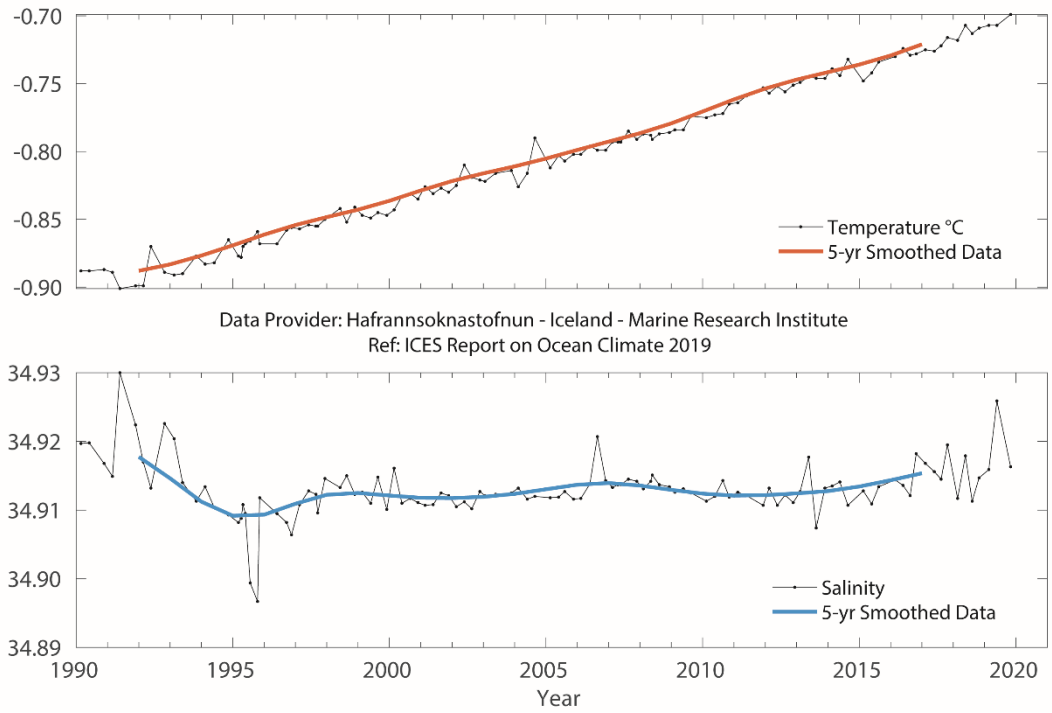

Figure 5.4. Icelandic waters. Temperature (upper panel) and salinity (lower panel) at 1500–1800 m in the Iceland Sea (68.00°N 12.67°W).

5.2 North Atlantic

5.2.1 Iceland–Scotland Ridge overflow waters

B. Berx and J. Hindson

In the deep layers of the Faroe–Shetland Channel, the properties at 800 m are the same as those of the Norwegian Sea Deep Water as it passes through the Channel back into the North Atlantic.

The temperature at this depth has relatively strong variability, but the overall trend was for decreasing temperature from the 1950s to the 1990s (Figure 5.5). Following a period of fluctuations, with both increasing and decreasing temperatures, there has been an increasing trend since about 2000. This warming trend continues in 2019, with temperatures coming close to the highest observed since the early 1980s. The relatively stable salinity in the first period of measurements (1950 to mid-1970s) was followed by a slow decline. The lowest annual mean salinity values were observed in 1997; since then, there has been a slow, but gradual, increase in salinity (Figure 5.5).

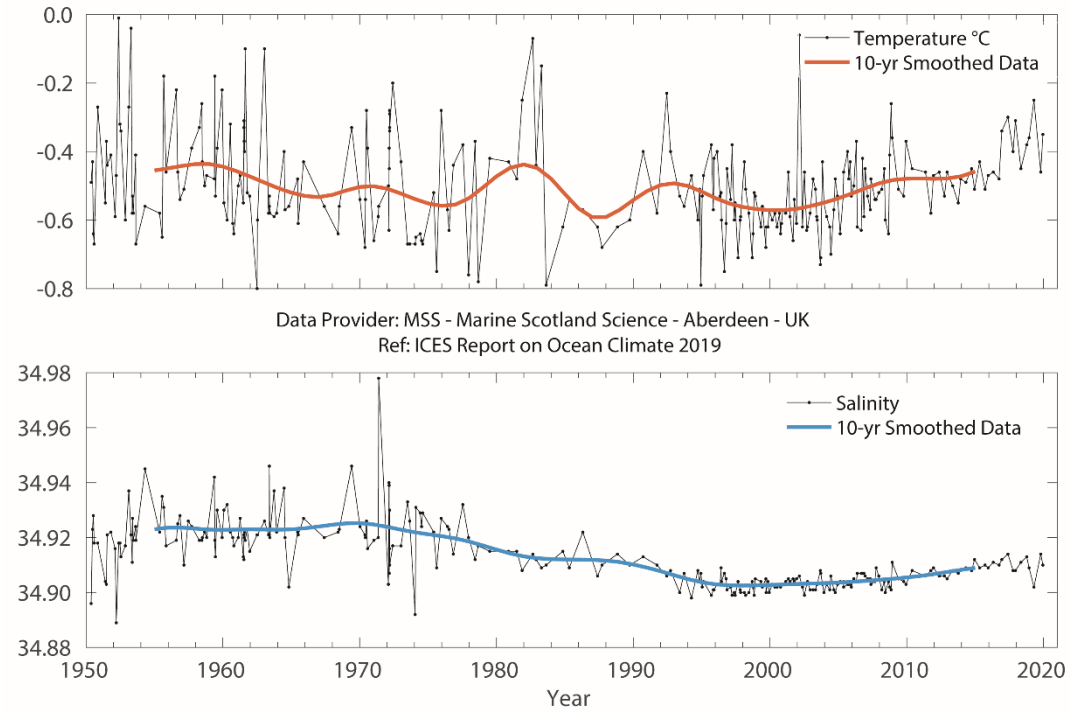

Figure 5.5. Faroe–Shetland Channel. Temperature (upper panel) and salinity (lower panel) at 800 m.

5.2.2 Iceland Basin

S. Jones and N. P. Holliday

In the Iceland Basin, LSW is the dominant water mass below about 1000 m, evident as a large recirculating body of relatively fresh and low stratified water with a core which lies between 1700 and 2000 m (Holliday *et al.*, 2015), Figure 5.6. After the Norwegian Sea deep water flows through the Faroe–Shetland Channel and Faroe Bank Channel and into the Iceland Basin, it becomes known as ISOW (Figure 4.51, Figure 5.1 and Figure 5.7). The dense water, supplemented by a small amount of additional flow over the sill between Iceland and the Faroes, mixes rapidly with the upper ocean and intermediate water of the Iceland Basin, entraining the lighter water and increasing the volume of the overflow plume. Thus, the properties of the ISOW measured at 20°W in the Iceland Basin are a product of the properties of the dense water at the sill and the entrained ambient water. ISOW temperature and salinity vary closely with the LSW and upper ocean water in the Iceland Basin. Since 1996, the water has warmed and increased in salinity, although there has been a slight decrease in both since 2011. The Ellett Line transect was not occupied in 2018 and 2019, and Argo floats do not adequately sample the deepest waters in Iceland Basin, so no observations were possible for the deep-water time-series (Figure 5.7). However, for the intermediate water time-series (Figure 5.6), observations from Argo floats show that temperature and salinity remained near average in 2019, with no evidence of the deep freshening observed in the upper waters.

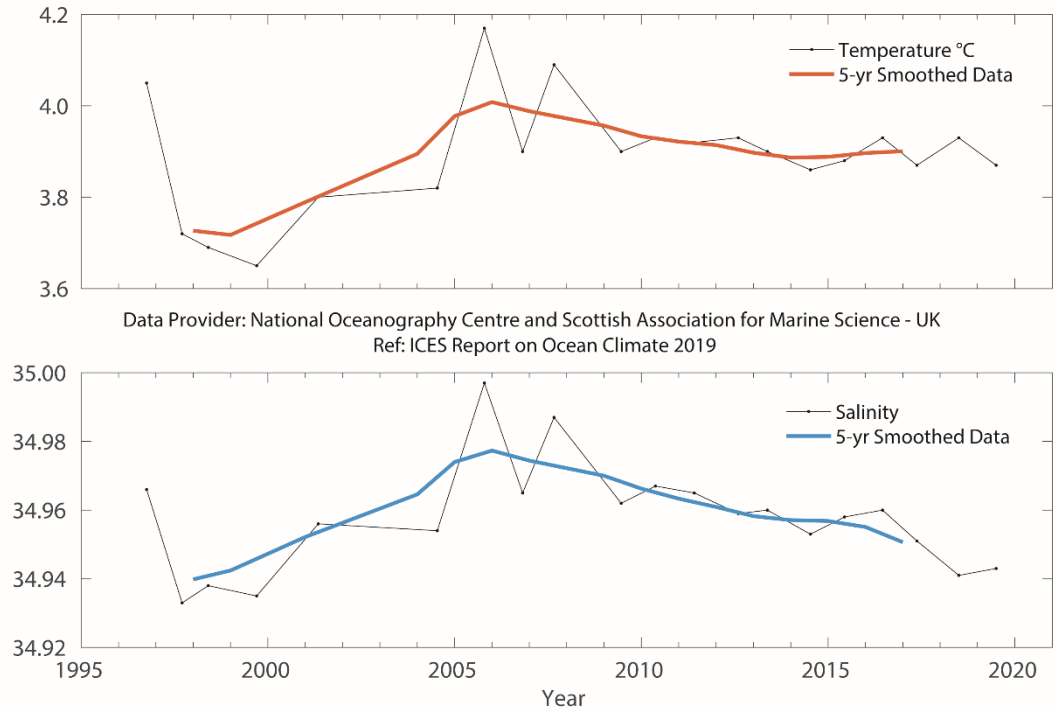

Figure 5.6. Iceland Basin. Temperature (upper panel) and salinity (lower panel) of Labrador Sea Water ($27.70 \leq \sigma_\theta \leq 27.85$ kg m^{-3}, approx. 1200–2000 m).

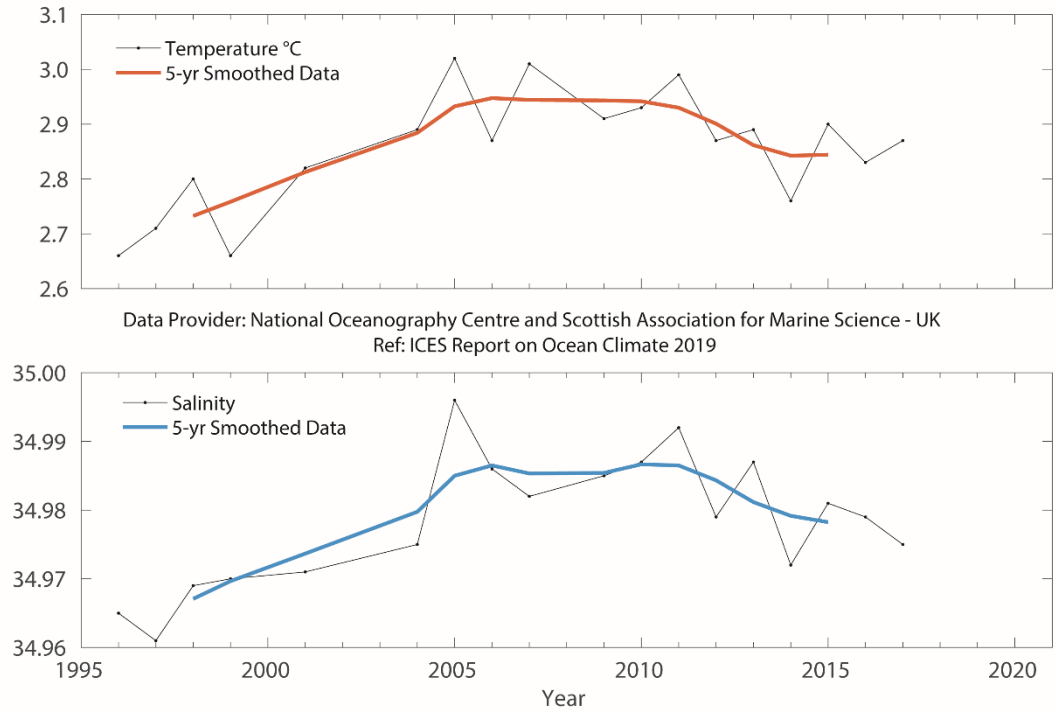

Figure 5.7. Iceland Basin. Temperature (upper panel) and salinity (lower panel) of Iceland–Scotland Overflow Water ($\sigma_\theta > 27.85$ kg m^{-3}, approx. 2000–2600 m). Data until 2017.

5.2.3 Rockall Trough

S. Jones and N. P. Holliday

LSW is the dominant water mass below about 1500 m in Rockall Trough and usually has its maximum concentration between 1700 and 2000 m. East of the Anton Dohrn seamount, this peak tends to be characterized by a minimum in salinity and potential vorticity, although its patchy temporal distribution (possibly due to aliasing of mesoscale eddies) results in a noisy year-on-year signal. Over the time-series, there is no significant long-term trend. From 1975 to the mid-1990s, there was a cooling and freshening trend, which was followed by gradual warming and increase in salinity. In 2019, the LSW potential temperature and salinity were close to the long-term means.

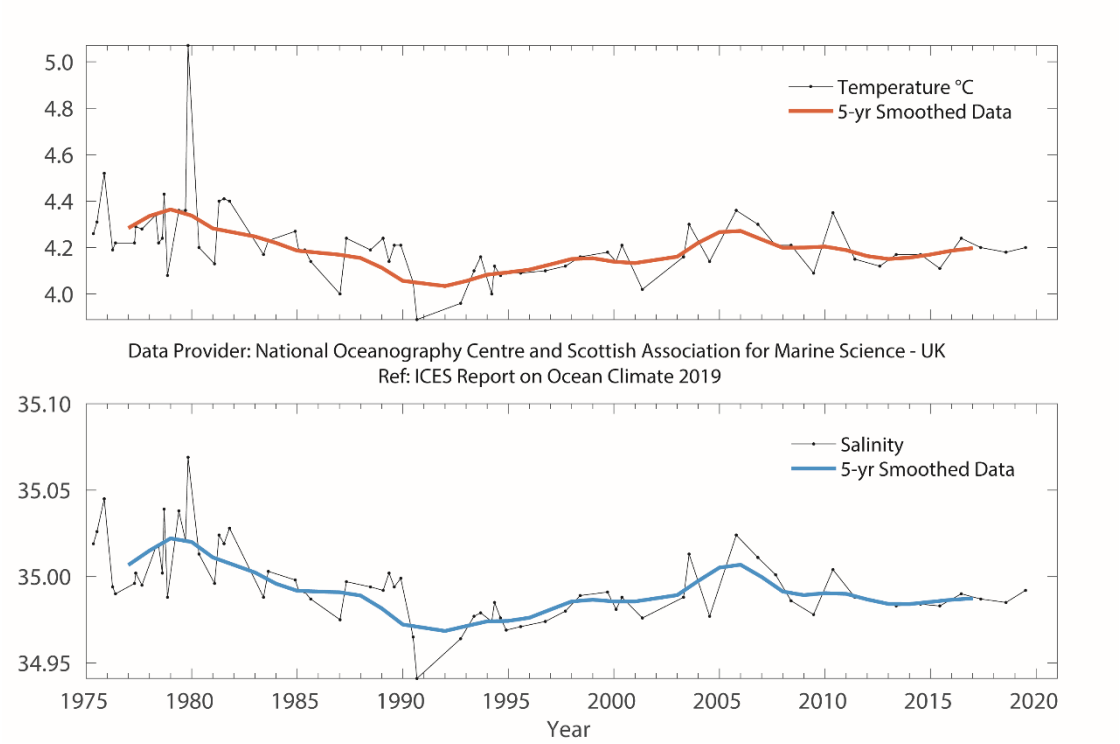

Figure 5.8. Rockall Trough. Temperature (upper panel) and salinity (lower panel) of Labrador Sea Water ($27.70 \leq \sigma_\theta \leq 27.85$ kg m^{-3}, approx. 1500–2000 m).

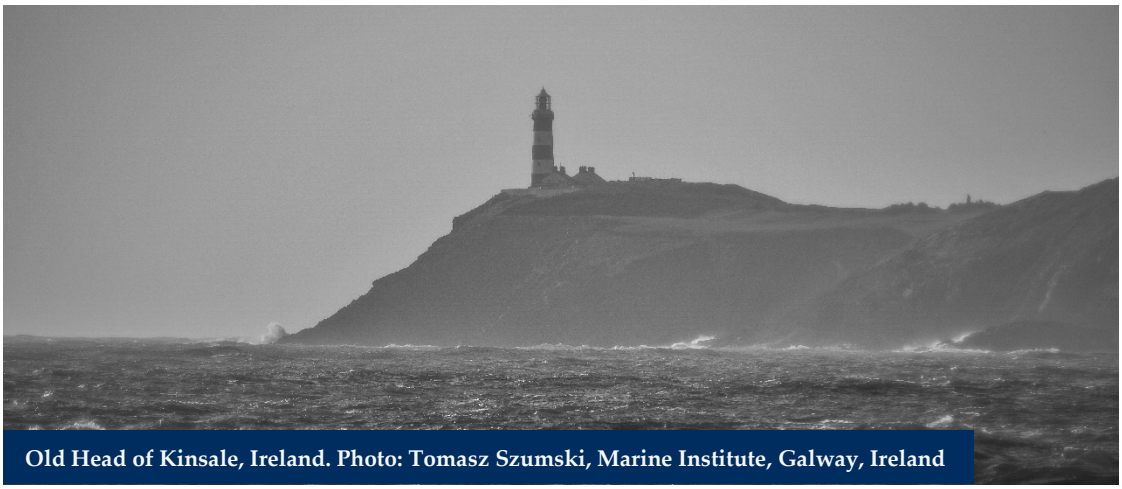

Old Head of Kinsale, Ireland. Photo: Tomasz Szumski, Marine Institute, Galway, Ireland

5.2.4 Irminger Basin

There is no 2019 update for the Irminger Basin. For the most recent regional overview, please see Section 5.2.4 in the IROC 2018 (González-Pola *et al.*, 2018).

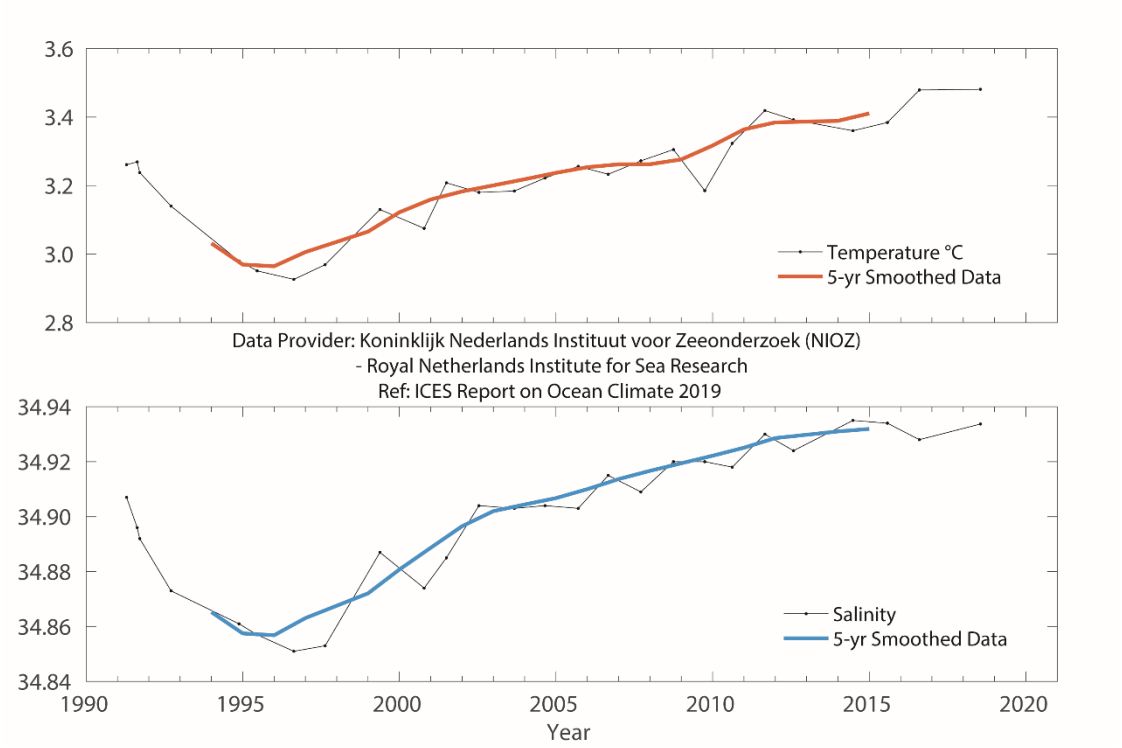

Figure 5.9. Irminger Sea. Temperature (upper panel) and salinity (lower panel) of Labrador Sea Water (averaged over 1600–2000 m). Data until 2018.

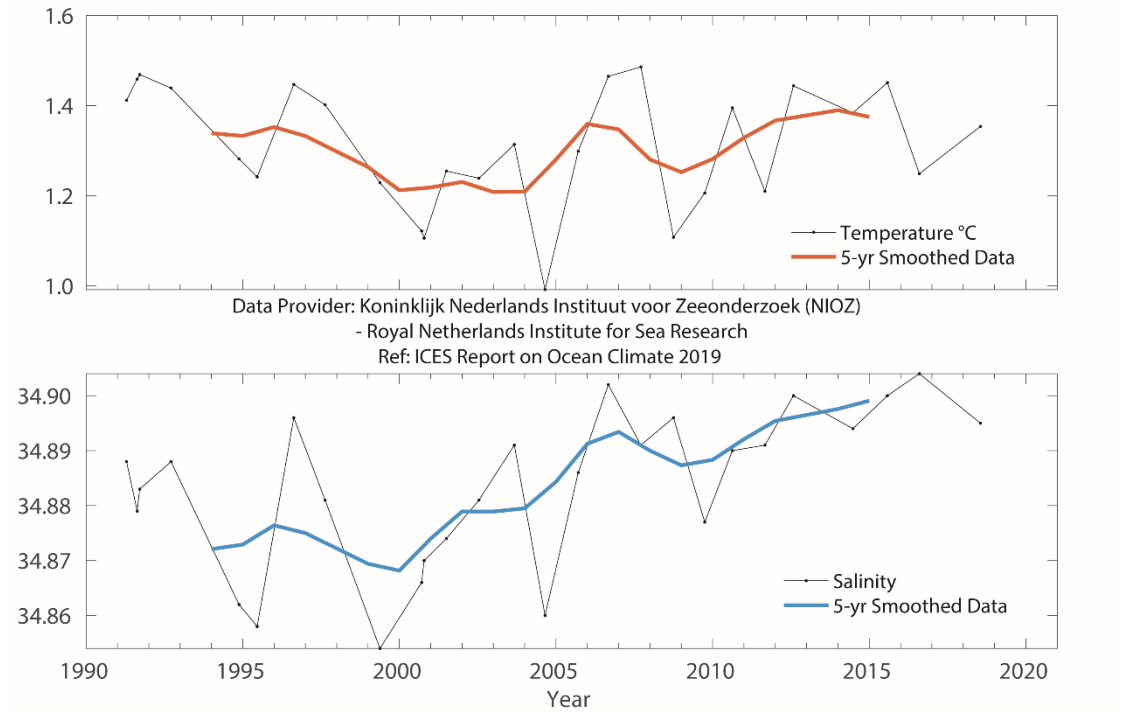

Figure 5.10. Irminger Sea. Temperature (upper panel) and salinity (lower panel) in DSOW on the East Greenland Slope. Data until 2018.

5.2.5 Labrador Basin

I. Yashayaev and B. Cisewski

The properties of the North Atlantic Deep Water (NADW) in the deep boundary current west of Greenland are monitored at 2000 m depth at Cape Desolation Station 3 (Figure 5.12). During the 1990s, both temperature and salinity decreased and reached their minimum values in 1998 and 1997, respectively. After that, NADW temperature showed a positive trend until 2019, whereas salinity has remained relatively unchanged between 2007 and 2019. In 2019, temperature and salinity of the NADW were 3.11°C and 34.92 (anomalies 0.22°C and 0.01) above the long-term mean, respectively.

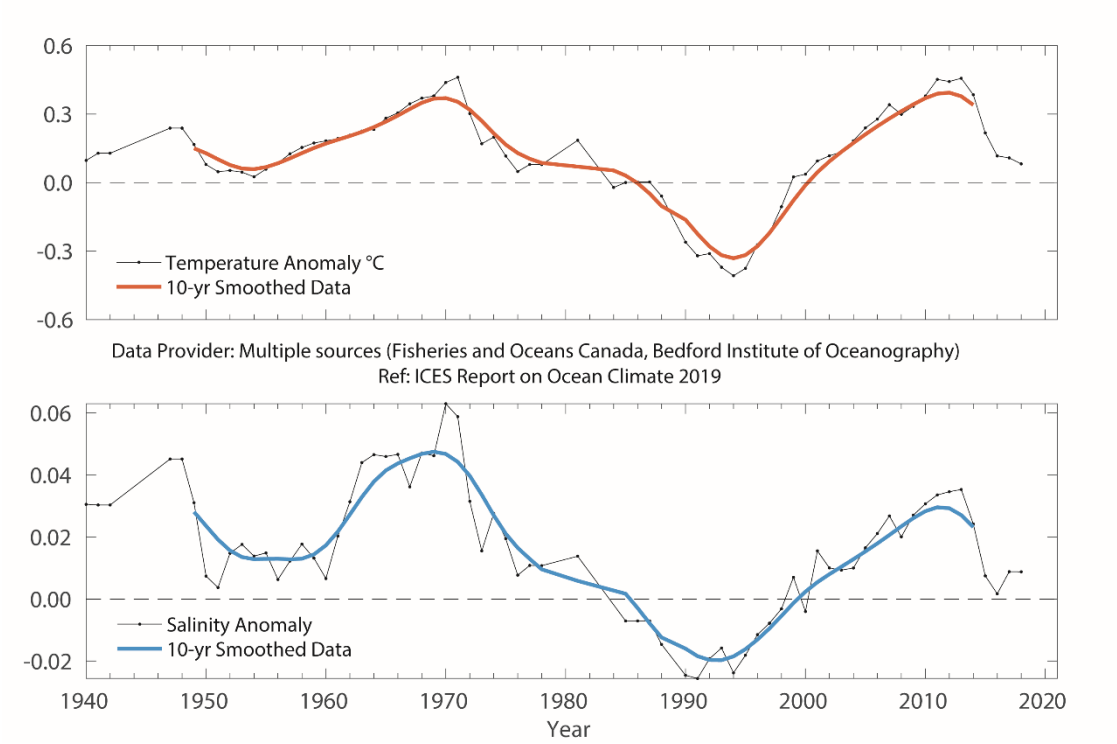

Figure 5.11. Labrador Sea. Temperature (upper panel) and salinity (lower panel) anomalies in the deep intermediate layer of the Labrador Sea. Vertical profile data to 2017 were averaged over 1000–1800 m and then over calendar years. Data until 2018.

Northern gannets. Photo: Holger Klein, Federal Maritime and Hydrographic Agency, Hamburg, Germany

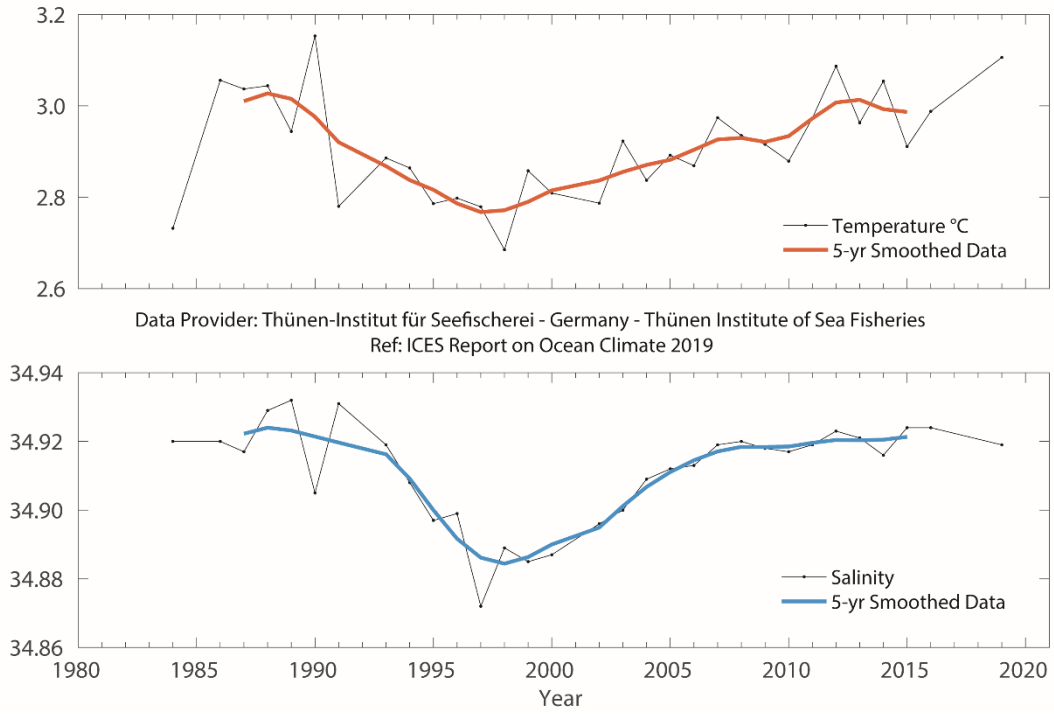

Figure 5.12. West Greenland. Temperature (upper panel) and salinity (lower panel) at 2000 m water depth at Cape Desolation Station 3 (60.47°N 50.00°W).

5.2.6 Western Iberian Margin

C. González-Pola

The whole water column down to 1000 m (core MW) has been sampled at the outer slope stations in Santander (Figure 4.36) on a monthly basis since the early 1990s (González-Pola *et al.*, 2005). Overall, warming over the previous 20 years is evident at most layers, corresponding to the ENACW (300–600 m (Figure 5.13) and upper MW (600–1000 m; Figure 5.14).

The evolution of the water masses has been strongly influenced by a significant shift in the salinity of the lower ENACW (ca. 400 m) in 2005 after the occurrence of very strong winter mixing (Somavilla *et al.*, 2009). In 2014, the upper central waters showed freshening and cooling for the first time in about a decade. In 2015, salinity values fell continuously throughout the year, ending the year ca. 0.05 units below 2014 values. During 2016 and 2017, salinity remained at 2015 levels, i.e. fresher and colder than in recent years. Temperature and salinity decreased further in 2018 and 2019, reaching minimum values at 400 m. Meanwhile, temperature and salinity remained high below this depth. Deeper water masses (at the level of the MW, ca. 1000 m) became gradually fresher following a maximum reached in 2007–2009, and have rebounded somewhat in 2019.

Since 2003, a programme designed to supplement the monthly monitoring of the upper ocean in the area has monitored waters deeper than 1000 m and the full water column (> 5500 m) at the Western Iberian Margin deep (Prieto *et al.*, 2015). Cruises were carried

out semi-annually during 2003–2010 and annually after that. The Finisterre section, measuring roughly 400 km long, starts west of the Iberian Peninsula (43.0°N 9.3°W) and reaches the centre of the Iberian Abyssal Plain (43.0°N 15.5°W).

The Finisterre section provides information about upper, intermediate, and deep waters. The limit of intermediate waters is considered to be near 2000 m depth, where the core of LSW and the base of the permanent thermocline are typically centred. From the core of MW to the core of LSW, there is a strong gradient and some coherence in variability, indicating the influence of large-scale atmospheric patterns. The main highlight of the series is the passage of a cold and fresh anomaly between 2008 and 2010. An upward swing in temperature and salinity was observed in 2015/2016, but trends reversed again towards colder and fresher conditions in 2017 (Figure 5.15), consistent with expectations for positive NAO conditions. 2019 was characterized by an upward swing in temperature and salinity at the MW level, between 800 and ca. 1600 m.

The abyssal waters in this basin are NADW (composed of a mixture of all Arctic water masses) and what is known as Lower Deep Water, which reflects a signature of Antarctic-origin waters. Interannual variability for these abyssal waters within the monitored period has been weak (< 0.1°C and 0.01 in salinity). A weak, but progressive, pattern of cooling and freshening has begun to emerge recently near ca. 2500 to ca. 3000 m. Potential temperature and salinity anomalies at this depth are currently roughly –0.06°C and –0.01 relative to 2003–2010 mean values. On average, temperature and salinity in the water layers between 2000 m and the bottom are currently close to long-term mean values (Figure 5.16).

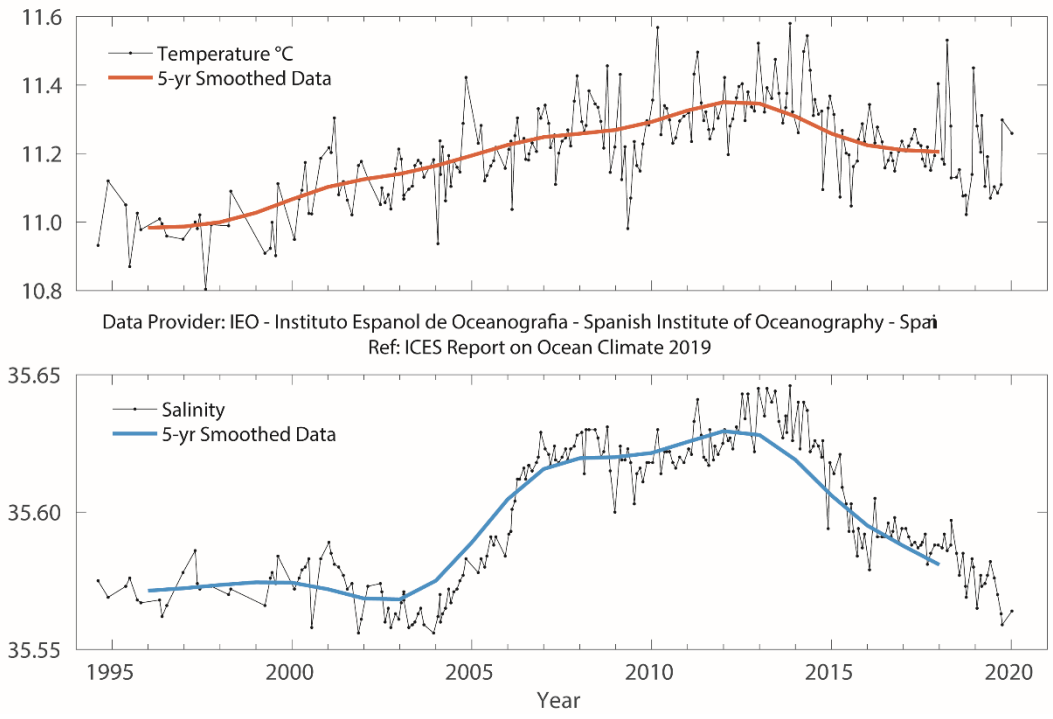

Figure 5.13. Bay of Biscay. Potential temperature (upper panel) and salinity (lower panel) for the 300–600 m layer at Santander station 7.

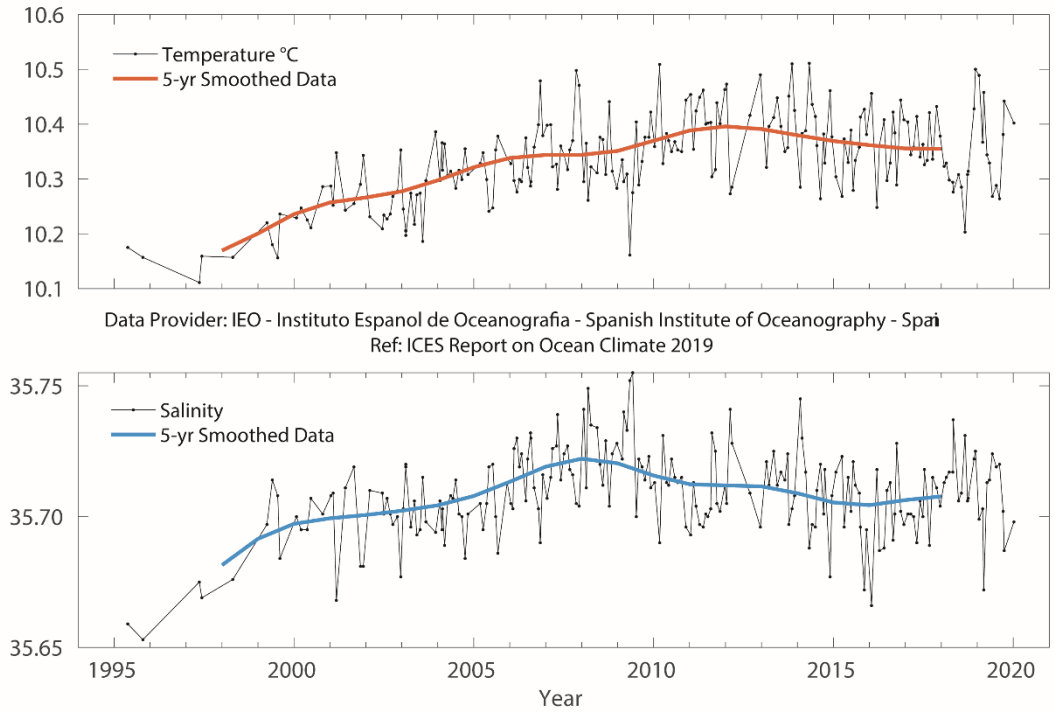

Figure 5.14. Bay of Biscay. Potential temperature (upper panel) and salinity (lower panel) for the 600–1000 m layer at Santander station 7.

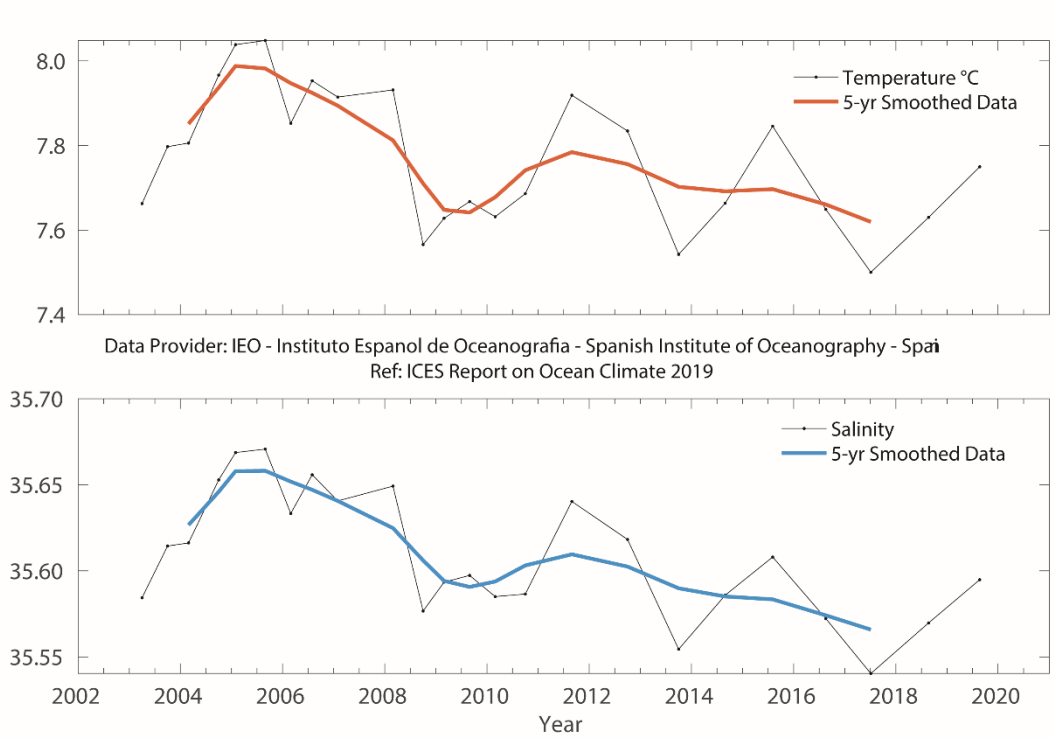

Figure 5.15. Western Iberian Margin. Potential temperature (upper panel) and salinity (lower panel) for the 800–2000 m layer averaged across the Finisterre section.

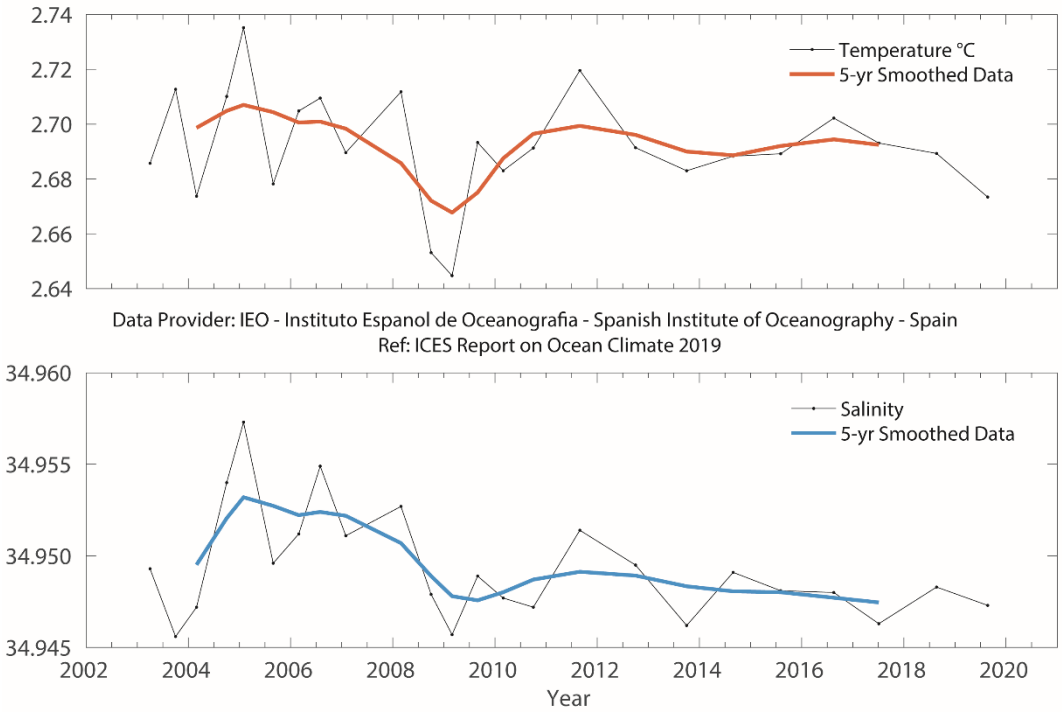

Figure 5.16. Western Iberian Margin. Potential temperature (upper panel) and salinity (lower panel) for the 2000–5500 m layer averaged across the Finsiterre section.

North of Faroes. Photo: Karin M. H. Larsen, Faroe Marine Research Institute, Faroe islands

5.2.7 Gulf of Cadiz

R. Sánchez-Leal

The outer stations in the STOCA sections (Figure 4.41) sample the ENACW (100–300 m; Figure 5.17) and the Mediterranean Overflow Water (300 m–bottom; Figure 5.18).

The ENACW layer has been showing a statistically significant freshening trend since 2009 (0.13 decade^{-1}). This freshening coincides with a non-statistically significant cooling trend (0.21°C decade^{-1}). These trends have been sustained through time and were reinforced in 2019 as cooler- and fresher-than-average conditions prevailed.

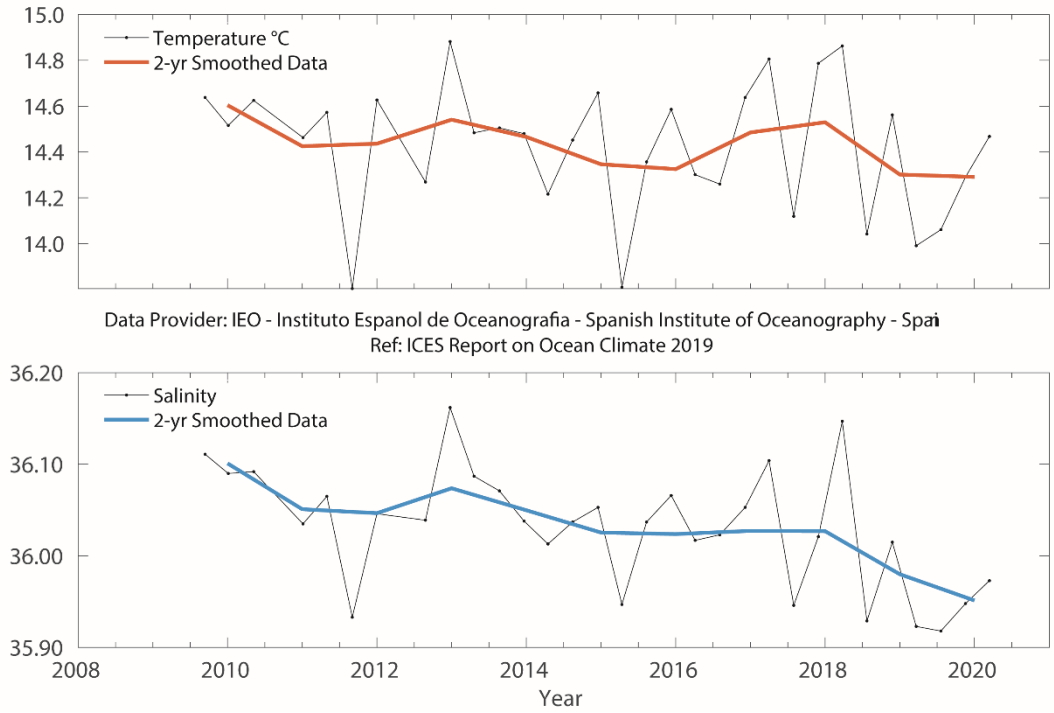

Figure 5.17. Gulf of Cadiz. Potential temperature (upper panel) and salinity (lower panel) for the 100–300 m layer at STOCA SP6.

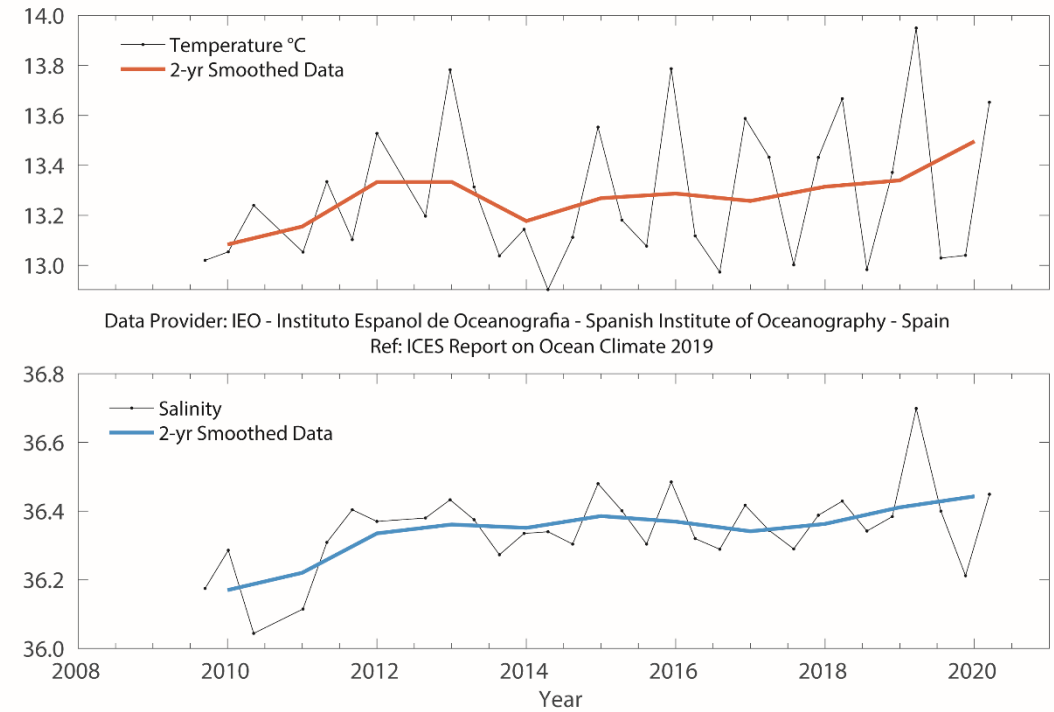

Figure 5.18. Gulf of Cadiz. Potential temperature (upper panel) and salinity (lower panel) for the 300–600 m layer at STOCA SP6.

5.2.8 Canary Basin

P. Vélez-Belchí

In the intermediate oceanic water stratum (800–1400 m), weak cooling and decreasing salinity has been observed since the 1990s (Figure 5.19). In the CTZ, the intermediate waters are dominated by Antarctic Intermediate Waters and do not show any long-term change in temperature or salinity. The time-series in both areas exhibit high variability, due to the two very different intermediate water masses present in the region, MW and the Antarctic Intermediate Waters.

In the layer corresponding to the upper NADW (1700–2600 m), there has been an overall weak warming and a decrease in salinity that is not statistically significantly different from zero. However, statistically significant freshening (–0.002 ± 0.001 decade^{-1}) is observed, coherent with observations in the upper NADW, although no trend can be confirmed for temperature (–0.005 ± 0.01°C decade^{-1}; Figure 5.20).

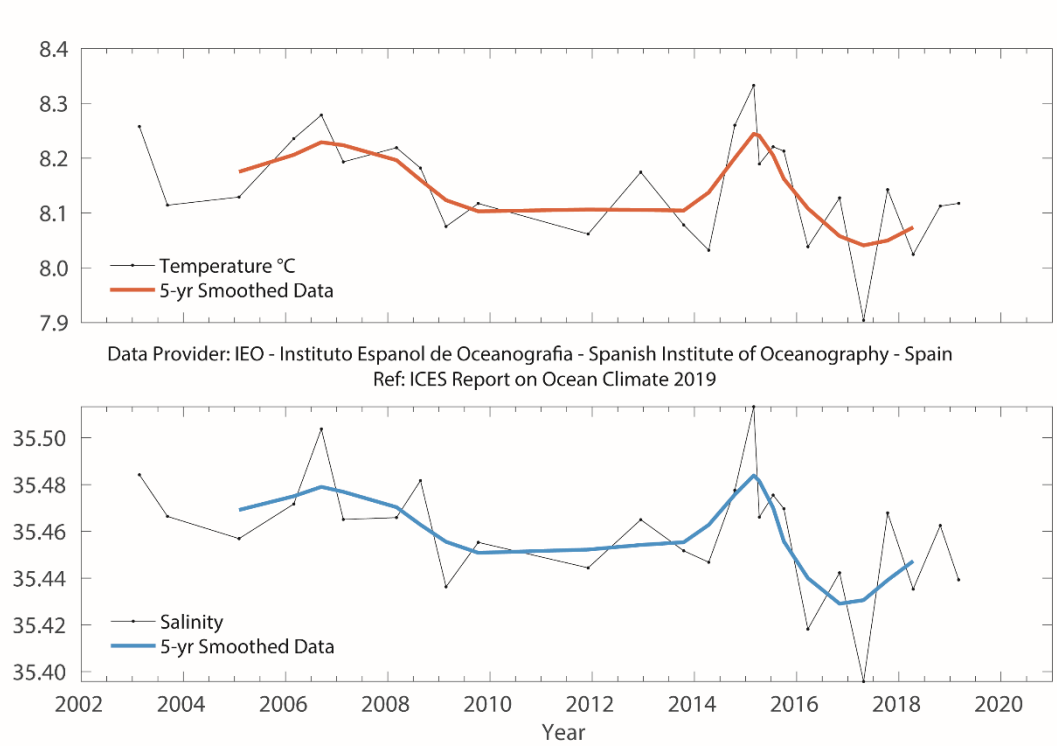

Figure 5.19. Canary Basin. Potential temperature (upper panel) and salinity (lower panel) for the 800–1400 m layer.

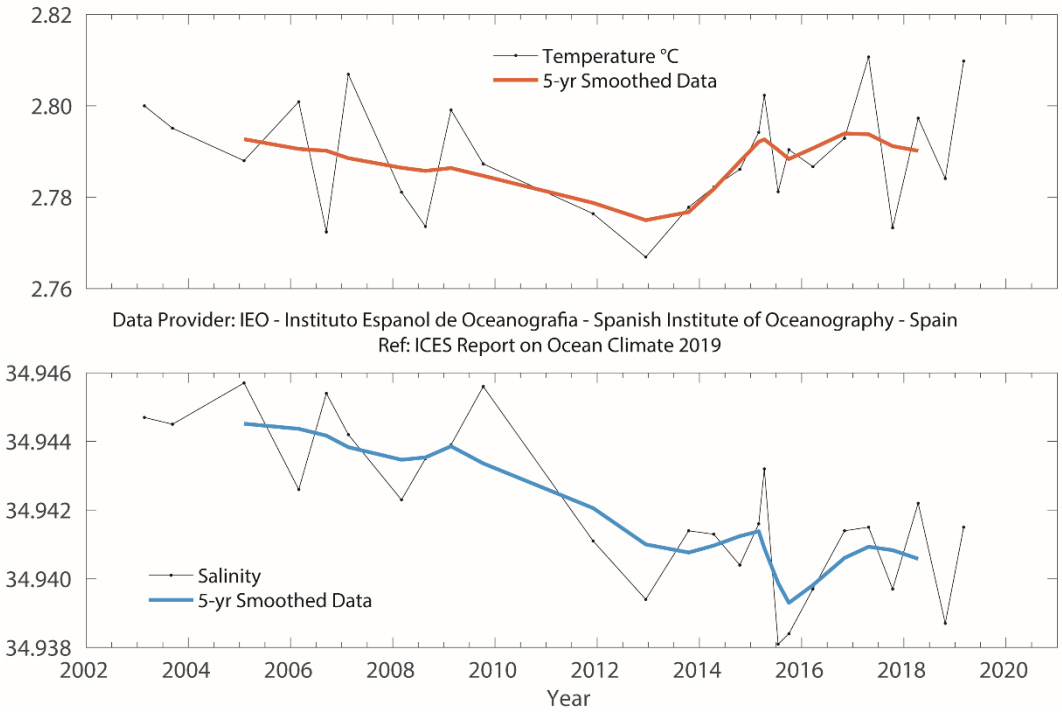

Figure 5.20. Canary Basin. Potential temperature (upper panel) and salinity (lower panel) for the 2600–3600 m layer averaged across the Canaries section.

6 References

Buckley, M. W., and Marshall, J. 2016. Observations, inferences, and mechanisms of the Atlantic Meridional Overturning Circulation: A review. Reviews of Geophysics, 54: 5–63. https://doi.org/10.1002/2015RG000493

Cappelen, J. 2020. Greenland-DMI historical climate data collection 1784–2019, DMI Technical Report 20–04.

de Boyer Montégut, C., Madec, G., Fischer, A. S., Lazar, A., and Iudicone, D. 2004. Mixed layer depth over the global ocean: An examination of profile data and a profile-based climatology. Journal of Geophysical Research: Oceans, 109 (C12). https://doi.org/10.1029/2004JC002378

Delworth, T. L., Zeng, F., Vecchi, G. A., Yang, X., Zhang, L., and Zhang R. 2016. The North Atlantic Oscillation as a driver of rapid climate change in the Northern Hemisphere. Nature Geoscience, 9: 509–512. https://doi.org/10.1038/ngeo2738

Duchez, A., Frajka-Williams, E., Josey, S. A., Evans, D. G., Grist, J. P., Marsh, R., McCarthy, G. D., *et al*. 2016. Drivers of exceptionally cold North Atlantic Ocean temperatures and their link to the 2015 European heat wave. Environmental Research Letters. 11(7): 074004. https://doi.org/10.1088/1748-9326/11/7/074004

Dunstone, N., Smith, D., Scaife, A., Hermanson, L., Eade, R., Robinson, N., Andrews, M., *et al*. 2016. Skilful predictions of the winter North Atlantic Oscillation one year ahead. Nature Geoscience, 9(11): 809–814. https://doi.org/10.1038/ngeo2824

Gaillard, F., Reynaud, T., Thierry, V., Kolodziejczyk, N., and von Schuckmann, K. 2016. In situ–based reanalysis of the global ocean temperature and salinity with ISAS: variability of the heat content and steric height. Journal of Climate. 29(4): 1305–1323. https://doi.org/10.1175/jcli-d-15-0028.1

González-Pola, C., Fratantoni, P., Larsen, K. M. H., Holliday, N. P., Dye, S., Mork, K. A., Beszczynska-Möller, A., *et al*. 2019. The ICES Working Group on Oceanic Hydrography: A bridge from *in-situ* sampling to the remote autonomous observation era. Frontiers in Marine Science, 6: 103. https://doi.org/10.3389/fmars.2019.00103

González-Pola, C., Larsen, K. M. H., Fratantoni, P., and Beszczynska-Möller, A. (Eds.). 2019. ICES Report on Ocean Climate 2018. ICES Cooperative Research Report No. 349. 122 pp. https://doi.org/10.17895/ices.pub.5461

González-Pola, C., Lavín, A., and Vargas-Yáñez, M. 2005. Intense warming and salinity modification of intermediate water masses in the southeastern corner of the Bay of Biscay for the period 1992–2003. Journal of Geophysical Research. 110: C05020. https://doi.org/10.1029/2004JC002367

Häkkinen, S., and Rhines, P. B. 2004. Decline of subpolar North Atlantic circulation during the 1990s. Science, 304(5670): 555–559. https://doi.org/10.1126/science.1094917

Hátún, H., Azetsu-Scott, K., Somavilla, R., Rey, F., Johnson, C., Mathis, M. Mikolajewicz, U., *et al*. 2017. The subpolar gyre regulates silicate concentrations in the North Atlantic. Scientific Reports, 7: 14576. https://doi.org/10.1038/s41598-017-14837-4

Hátún, H., and Chafik, L. 2018. On the Recent Ambiguity of the North Atlantic Subpolar Gyre Index, Journal of Geophysical Research: Oceans, 123(8): 5072–5076. https://doi.org/10.1029/2018JC014101

Hátún, H., Lohmann, K., Matei, D., Jungclaus, J. H., Pacariz, S., Bersch, M. Gislason, A., *et al*. 2016. An inflated subpolar gyre blows life toward the northeastern Atlantic. Progress in Oceanography, 147: 49–66. https://doi.org/10.1016/j.pocean.2016.07.009

Hátún, H., Payne, M., Beaugrand, G., Reid, P., Sandø, A., Drange, H., Hansen, B., *et al*. 2009. Large bio-geographical shifts in the north-eastern Atlantic Ocean: From the subpolar gyre, via plankton, to blue whiting and pilot whales. Progress in Oceanography, 80(3): 149–162. https://doi.org/10.1016/j.pocean.2009.03.001

Hátún, H., Sandø, A. B., Drange, H., Hansen, B., and Valdimarsson H. 2005. Influence of the Atlantic Subpolar Gyre on the Thermohaline Circulation. Science, 309(5742): 1841–1844. https://doi.org/10.1126/science.1114777

Hernández-Guerra, A., Espino-Falcón, E., Vélez-Belchí, P., Pérez-Hernández, M. D., Martínez-Marrero, A., and Cana, L. 2017. Recirculation of the Canary Current in fall 2014. Journal of Marine Systems, 174: 25–39. https://doi.org/10.1016/j.jmarsys.2017.04.002

Holliday, N. P., Cunningham, S. A., Johnson, C., Gary, S. F., Griffiths, C., Read, J. F., and Sherwin, T. 2015. Multidecadal variability of potential temperature, salinity, and transport in the eastern subpolar North Atlantic. Journal of Geophysical Research: Oceans, 120: 5945–5967. https://doi.org/10.1002/2015jc010762

Holliday, N. P., Bersch, M., Berx, B., Chafik, L., Cunningham, S., Florindo-López, C., Hátún, H., *et al*. 2020. Ocean circulation causes the largest freshening event for 120 years in eastern subpolar North Atlantic, Nature Communications, 11(1): 585. https://doi.org/10.1038/s41467-020-14474-y

Hurrell, J. W., and Deser, C. 2010. North Atlantic climate variability: the role of the North Atlantic Oscillation. Journal of Marine Systems, 79: 231–244. https://doi.org/10.1016/j.jmarsys.2009.11.002

Hurrell, J. W., Kushnir, Y., Ottersen, G., and Visbeck M. 2003. An overview of the North Atlantic oscillation. *In* The North Atlantic Oscillation: Climatic Significance and Environmental Impact. Ed. by J. W. Hurrell, Y. Kushnir, G. Ottersen, and M. Visbeck. Wiley Online Library. https://doi.org/10.1029/134GM01

Hurrell, J., and National Center for Atmospheric Research Staff (Eds). 2019. Climate Data Guide: Hurrell North Atlantic Oscillation (NAO) Index (station-based). https://climatedataguide.ucar.edu/climate-data/hurrell-north-atlantic-oscillation-nao-index-station-based. Last modified 24 Apr 2020.

Kalnay, E., Kanamitsu, M., Kistler, R., Collins, W., Deaven, D., Gandin, L., Iredell, M., *et al.* 1996. The NCEP/NCAR 40-Year Reanalysis Project. Bulletin of the American Meteorological Society, 77: 437–471. https://doi.org/10.1175/1520-0477(1996)077<0437:TNYRP>2.0.CO;2

Kolodziejczyk, N., Prigent-Mazella, A., and Gaillard, F. 2017. ISAS-15 temperature and salinity gridded fields. SEANOE. https://doi.org/10.17882/52367

Moffa-Sánchez, P., and Hall, I. R. 2017. North Atlantic variability and its links to European climate over the last 3000 years. Nature Communications, 8: 1726. https://doi.org/10.1038/s41467-017-01884-8

Mountain, D. 2012. Labrador slope water entering the Gulf of Maine–response to the North Atlantic Oscillation. Continental Shelf Research, 47: 150–155. https://doi.org/10.1016/j.csr.2012.07.008

NOAA. 2018. National Centre for Environmental Information, State of Climate: Annual National Climate Report for 2018. https://www.ncdc.noaa.gov/sotc/national/201813. Accessed 30 April 2019.

Paillet, J., and Mercier, H. 1997. An inverse model of the eastern North Atlantic general circulation and thermocline ventilation, Deep Sea Research Part I: Oceanographic Research Papers, 44(8): 1293–1328. https://doi.org/10.1016/s0967-0637(97)00019-8

Pingree, R. D. 1993. Flow of surface waters to the west of the British Isles and in the Bay of Biscay. Deep Sea Research Part II: Topical Studies in Oceanography, 40(1–2): 369–388. https://doi.org/10.1016/0967-0645(93)90022-f

Pingree, R. D., and Le Cann, B. 1990. Structure, strength and seasonality of the slope currents in the Bay of Biscay region. Journal of the Marine Biological Association of the UK, 70(4): 857–885. https://doi.10.1017/S0025315400059117

Prieto, E., González-Pola, C., Lavín, A., and Holliday, N. P. 2015. Interannual variability of the northwestern Iberia deep ocean: Response to large-scale North Atlantic forcing. Journal of Geophysical Research: Oceans, 120: 832–847. https://doi.org/10.1002/2014jc010436

Scaife, A. A., Arribas, A., Blockley, E., Brookshaw, A., Clark, R. T., Dunstone, N. Eade, R., *et al*. 2014. Skillful long-range prediction of European and North American winters. Geophysical Research Letters, 41: 2514–2519. https://doi.org/10.1002/2014gl059637

Scaife, A. A., Karpechko, A. Y., Baldwin, M. P., Brookshaw, A., Butler, A. H., Eade, R., Gordon, M., *et al*. 2015. Seasonal winter forecasts and the stratosphere. Atmospheric Science Letters, 17: 51–56. https://doi.org/10.1002/asl.598

Somavilla, R., Gonzalez-Pola, C., Rodriguez, C., Josey, S. A., Sanchez, R. F., and Lavin, A. 2009. Large changes in the hydrographic structure of the Bay of Biscay after the extreme mixing of winter 2005. Journal of Geophysical Research: Oceans, 114(C1). https://doi.org/10.1029/2008jc004974

Taburet, G., Sanchez-Roman, A., Ballarota, M., Pujol, M-I., Legeais, J-F., Fournier, F., Faugere, Y., and Dibarboure, G. 2019. DUACS DT2018: 25 years of reprocessed sea level altimetry products. Ocean Science 15(5): 1207-1224 https://doi.org/10.5194/os-15-1207-2019

Tel, E., Balbin, R., Cabanas, J-M., Garcia, M-J., Garcia-Martinez, M. C., Gonzalez-Pola, C., Lavin, A., *et al*. 2016. IEOOS: the Spanish Institute of Oceanography Observing System. Ocean Science, 12(2): 345–353, https://doi.org/10.5194/os-12-345-2016.

van Aken, H. M. 2002. Surface currents in the Bay of Biscay as observed with drifters between 1995 and 1999. Deep Sea Research Part I: Oceanographic Research Papers, 49(6): 1071–1086. https://doi.org/10.1016/s0967-0637(02)00017-1

Vélez-Belchí, P., González-Carballo, M., Pérez-Hernández, M. D., and Hernández-Guerra, A. 2015. Open ocean temperature and salinity trends in the Canary Current Large Marine Ecosystem. *In* Oceanographic and biological features in the Canary Current Large Marine Ecosystem, pp. 201–213. Ed. by L. Valdés, and I. Déniz-González. IOC Technical Series No. 115. IOC-UNESCO, Paris. 383 pp.

Vélez-Belchí, P., Pérez-Hernández, M. D., Casanova-Masjoan, M., Cana, L., and Hernández-Guerra, A. 2017. On the seasonal variability of the Canary Current and the Atlantic Meridional Overturning Circulation. Journal of Geophysical Research: Oceans, 122(6): 4518–4538. https://doi.org/10.1002/2017jc012774

Yashayaev, I., and Loder, J. W. 2017. Further intensification of deep convection in the Labrador Sea in 2016. Geophysical Research Letters, 44(3): 1429–1438. https://doi.org/10.1002/2016gl071668

Annex 1: Database providers contact information

AREA	SECTION	FIGURES	TIME-SERIES	CONTACT	INSTITUTE
Barents Sea	4.21	4.82	Fugløya–Bear Island section, Western Barents Sea	Randi Ingvaldsen randi.ingvaldsen@imr.no	Institute of Marine Research (IMR), Bergen, Norway
	4.21	4.83	Kola section, Eastern Barents Sea	Oleg V. Titov titov@pinro.ru	Knipovich Polar Research Institute of Marine Fisheries and Oceanography (PINRO), Russian Federation
Baltic Sea	4.19	4.71 4.72 4.73	Station BY15, Baltic Proper, east of Gotland, and observed ice extent	Johanna Linders johanna.linders@smhi.se	Swedish Meteorological and Hydrological Institute (SMHI), Norrköping, Sweden
		4.74 4.75	Stations LL7 and SR5	Pekka Alenius pekka.alenius@fimr.fi	Finnish Institute of Marine Research (FIMR), Helsinki, Finland
Bay of Biscay and western Iberian margin	4.8 5.2.6	4.37 4.38 4.39 4.40 5.13 5.14 5.15 5.16	Santander and Finisterre sections	César González-Pola cesar.pola@ieo.es	Instituto Español de Oceanografía (IEO, Spanish Institute of Oceanography), Gijón Oceanographic Centre, Gijón, Spain Aquarium of San Sebastian (SOG) and Igeldo Meteorological Observatory (AEMet), San Sebastian, Spain
Canary Basin	4.10 5.2.8	4.45 5.19 5.20	Canary Basin Oceanic Waters Section	Pedro Vélez-Belchí pedro.velez@ieo.es	Instituto Español de Oceanografía (IEO, Spanish Institute of Oceanography), Canary Islands Oceanographic Centre, Tenerife, Spain
Faroese Waters	4.17	4.58 4.59 4.60	Faroe Bank Channel–West Faroe Islands, Faroe Current – North Faroe Islands, Faroe Shelf	Karin Margretha H. Larsen KarinL@hav.fo	Havstovan (Faroe Marine Research Institute, FAMRI), Faroe Islands

Faroe–Shetland Channel	4.17 5.2.1	4.61 4.62 5.5	Faroe–Shetland Channel, Faroe Shelf and Shetland Shelf deep waters (800 m)	Barbara Berx B.Berx@marlab.ac.uk	Marine Scotland Science (MSS), Aberdeen, UK
Greenland Sea and Fram Strait	4.22 5.1.1	4.85	Greenland Sea section N, west of Spitsbergen (76.5°N)	Agnieszka Beszczynska-Möller abesz@iopan.gda.pl	Institute of Oceanology, Polish Academy of Sciences (IOPAN), Sopot, Poland
		4.84 5.2	Greenland Sea section 75°N, Greenland Sea deep waters	Gereon Budeus Gereon.Budeus@awi.de	Alfred Wegener Institute, Helmholtz Centre for Polar and Marine Research (AWI), Bremerhaven, Germany
	4.22	4.86	Fram Strait (78.83°N), West Spitsbergen Current and East Greenland Current	Wilken-Jon von Appen Wilken-Jon.von.Appen@awi.de	Alfred Wegener Institute, Helmholtz Centre for Polar and Marine Research (AWI), Bremehaven, Germany
Gulf of Cadiz	4.9	4.42 4.43	STOCA Station SP6 – Gulf of Cadiz time-series	Ricardo F. Sánchez-Leal rleal@ieo.es	Instituto Español de Oceanografía (IEO, Spanish Institute of Oceanography), Cadiz Oceanographic Centre, Cadiz, Spain
Gulf of St Lawrence	4.5	4.13 4.14 4.15 4.16 4.17	Gulf of St. Lawrence time-series	Peter Galbraith peter.Galbraith@dfo-mpo.gc.ca	Maurice Lamontagne Institute, Fisheries and Oceans Canada
Icelandic waters	4.7 5.1.3	4.32 4.33 4.34 4.35 5.4	Reykjavik and Akureyri air temperature, Siglunes stations 2–4, Selvogsbanki Station 5, Langanes stations 2–6, Faxafloi Station 9, Icelandic deep water (1800 m)	Sólveig R. Ólafsdóttir solveig.rosa.olafsdot-tir@hafogvatn.is Magnus Danielsen magnus.danielsen@hafog-vatn.is	Hafrannsóknastofnun (Marine and Freshwater Research Institute), Reykjavik, Iceland

Irminger Sea	4.16	4.56	Station FX9 (64.33°N 28°W)	Sólveig R. Ólafsdóttir solveig.rosa.olafsdot-tir@hafogvatn.is	Hafrannsóknastofnun (Marine and Freshwater Research Institute), Reykjavik, Iceland
	4.16 5.2.4	4.55 5.9 5.10	Central Irminger Sea, East Greenland slope	M. Femke de Jong Femke.de.Jong@nioz.nl	Koninklijk Nederlands, Instituut voor Zeeonderzoek (NIOZ, Royal Netherlands Institute for Sea Research), Texel, Netherlands
Labrador Sea	4.2 5.2.5	4.8, 5.11	Section AR7W	Igor Yashayaev Igor.Yashayaev@dfo-mpo.gc.ca	Ocean Monitoring and Observation Section, Oceans and Ecosystem Division, Bedford Institute of Oceanography, Fisheries and Oceans, Bedford, Canada
North Sea	4.18	4.68	North Sea Utsira, modelled North Sea inflow	Jon Albretsen jon.albretsen@imr.no Solfrid Hjollo solfrids@imr.no	Institute of Marine Research (IMR), Bergen, Norway
		4.69	Fair Isle Current water	Barbara Berx B.Berx@marlab.ac.uk	Marine Scotland Science (MSS, Aberdeen), UK
		4.65 4.66 4.67	Helgoland Roads coastal waters, German Bight, North Sea	Karen Wiltshire Karen.Wiltshire@awi.de	Alfred Wegener Institute for Polar and Marine Research (AWI)/Biologische Anstalt Helgoland (BAH), Germany
		4.64 4.66	area-averaged North Sea SST	Peter Loewe peter.loewe@bsh.de	Federal Maritime and Hydrographic Agency (BSH)
Northeast US continental shelf	4.6	4.24 4.25 4.26 4.27 4.28 4.29 4.30	MAB, Gulf of Maine, Georges Bank, Northeast Channel	PaulaFratantoni paula.fratantoni@noaa.gov	NOAA Fisheries, NEFSC, Oceans and Climate Branch, Woods Hole, MA, USA

Northwest Atlantic	4.5	4.18 4.20 4.21	Sable Island air temperature, Cabot Strait sea ice, Misaine Bank, Emerald Bank	David Hebert David.Hebert@dfo-mpo.gc.ca Chantelle Layton Chantelle.Layton@dfo-mpo.gc.ca	Ocean Monitoring and Observation Section, Oceans and Ecosystem Division, Bedford Institute of Oceanography, Fisheries and Oceans, Bedford, Canada
		4.19	Calbot Strait ice	Peter Galbraith Peter.Galbraith@dfo-mpo.gc.ca	Maurice Lamontagne Institute, Fisheries and Oceans Canada
	4.3	4.10 4.11 4.12	Newfoundland and Labrador sea ice, Cartwright air temperature, Station 27 CIL	Frederic Cyr frederic.cyr@dfo-mpo.gc.ca	Northwest Atlantic Fisheries Centre, St Johns, Newfoundland, Canada
		4.9	Sea ice areas off Newfoundland–Labrador between 45°N and 55°N	Peter Galbraith Peter.Galbraith@dfo-mpo.gc.ca	Maurice Lamontagne Institute, Fisheries and Oceans Canada
Northwest European continental shelf	4.11	4.48	Astan Section, Point 33	Pascal Morin pmorin@sb-roscoff.fr	CNRS–UPMC, Observatoire Oceanologique de Roscoff, Roscoff, France
		4.46 4.47	Western Channel Observatory, Station E1	Tim J. Smyth tjsm@pml.ac.uk	Marine Biological Association and Plymouth Marine Laboratory, Plymouth, UK
	4.12	4.49 4.50	Malin Head Weather Station, M3 Weather Buoy	Caroline Cusack Caroline.Cusack@Marine.ie	Marine Institute/Met Eireann, Ireland
Norwegian Sea	4.20	4.77 4.79 4.80 4.81	Svinøy, Gimsøy, and Sørkapp sections	Kjell Arne Mork kjell.arne.mork@imr.no	Institute of Marine Research (IMR), Bergen, Norway

	4.19 5.1.2	4.78 5.3	Ocean Weather Station Mike (50 and 2000 m)	Svein Østerhus svos@norceresearch.no	NORCE Norwegian Research Centre, Institute of Marine Research (IMR) and University of Bergen (UiB), Norway
Rockall Trough and Iceland Basin	4.13 4.14 4.15 5.2.2 5.2.3	4.52 4.53 4.54 5.6 5.7 5.8		N. Penny Holliday nph@noc.soton.ac.uk Sam Jones Sam.Jones@sams.ac.uk	National Oceanography Centre, Southampton and Scottish Association for Marine Science, Southampton, UK Scottish Association for Marine Science (SAMS), Oban, UK
West Greenland	4.1	4.4	Nuuk air temperature	Boris Cisewski boris.cisewski@thuenen.de	Danish Meteorological Institute, Copenhagen, Denmark
	4.1 5.2.5	4.5 4.6 5.12	Fylla andCape Desolation section	Boris Cisewski boris.cisewski@thuenen.de	Thünen-Institut für Seefischerei (Thünen Institute of Sea Fisheries), Bremehaven, Germany

Annex 2: Author contact information by section

SECTION	AREA/TOPIC	AUTHORS	E-MAIL	AFFILIATION
2. Summary of upper ocean conditions in 2018				
2.3	Argo gridded temperature and salinity fields	Nicolas Kolodziejczyk	Nicolas.Kolodziejczyk@univ-brest.fr	University of Brest (UBO), CNRS, IRD, Ifremer, Laboratoire d'Océanographie Physiqueet Spatiale (LOPS, Laboratory for Ocean Physics and Satellite remote sensing), Brest, France
		Damien Desbruyères	Damien.Desbruyeres@ifremer.fr	Ifremer, University of Brest, CNRS, IRD, Laboratoire d'Océanographie Physique et Spatiale, Plouzané, France
2.4	Subpolar Gyre Index	León Chafik	leon.chafik@misu.su.se	Department of Meteorology (MISU), Stockholm University
		Hjálmar Hátún	hjalmarh@hav.fo	Faroe Marine Research Institute (FAMRI), Tórshavn, Faroe Islands
		Barbara Berx	b.berx@marlab.ac.uk	Marine Scotland Science (MSS). Aberdeen, UK
3. The North Atlantic atmosphere				
All		Stephen Dye	stephen.dye@cefas.co.uk	Centre for Environment, Fisheries and Aquaculture Science (Cefas), Lowestoft, UK
4. Detailed Area Descriptions, Part I: The upper ocean				
4.1	West Greenland	Boris Cisewski	boris.cisewski@thuenen.de	Thünen-Institut für Seefischerei (TI-SF, Thünen Institute of Sea Fisheries), Bremerhaven, Germany
		Jon Mortensen	jomo@natur.gl	

4.2	Labrador Sea	Igor Yashayaev	Igor.Yashayaev@dfo-mpo.gc.ca	Fisheries and Oceans Canada (DFO), Bedford, Canada
4.3	Newfoundland–Labrador Shelf	Frédéric Cyr	Frederic.Cyr@dfo-mpo.gc.ca	Fisheries and Oceans Canada (DFO), StJohn's, Newfoundland, Canada
		Peter Galbraith	Peter.Galbraith@dfo-mpo.gc.ca	Maurice Lamontagne Institute, Fisheries and Oceans Canada
4.4	Gulf of Saint Lawrence	Peter Galbraith	Peter.Galbraith@dfo-mpo.gc.ca	Maurice Lamontagne Institute, Fisheries and Oceans Canada
4.5	Scotian Shelf	David Hebert	David.Hebert@dfo-mpo.gc.ca	Fisheries and Oceans Canada (DFO), Bedford, Canada
		Chantelle Layton	Chantelle.Layton@dfo-mpo.gc.ca	
		Peter Galbraith	Peter.Galbraith@dfo-mpo.gc.ca	Maurice Lamontagne Institute, Fisheries and Oceans Canada
4.6	Northeast US continental shelf	Paula Fratantoni	paula.fratantoni@noaa.gov	NOAA Fisheries, NEFSC, Oceans and Climate Branch, Woods Hole, MA, USA
4.7	Icelandic waters	Sólveig R. Ólafsdóttir	solveig.rosa.olafsdottir@hafogvatn.is	Hafrannsóknastofnun (Marine and Freshwater Research Institute, MFRI), Hafnarfjörður, Iceland
		Magnus Danielsen	magnus.danielsen@hafogvatn.is	
4.8	Bay of Biscay and Iberian coast	Almudena Fontán	afontan@azti.es	AZTI. Aquarium of San Sebastian (SOG) and Idalgo Meteorological Observatory (AEMet), San Sebastian, Spain
		Victor Valencia	vvalencia@azti.es	
		Cesar González-Pola	cesar.pola@ieo.es	Instituto Español de Oceanografía (IEO, Spanish Institute of Oceanography), Gijón Oceanographic Centre, Gijón, Spain
4.9	Gulf of Cadiz	Ricardo Sánchez-Leal	rleal@ieo.es	Instituto Español de Oceanografía (IEO, Spanish Institute of Oceanography), Cádiz Oceanographic Centre, Cádiz, Spain

4.10	Canary Basin	Pedro Vélez-Belchí	pedro.velez@ieo.es	Instituto Español de Oceanografía (IEO, Spanish Institute of Oceanography), Canary Islands Oceanographic Centre, Tenerife, Spain
4.11	Southwest Approaches	Tim J. Smyth	tjsm@pml.ac.uk	Marine Biological Association and Plymouth Marine Laboratory (PML), Plymouth, UK
4.12	Celtic Seas	Kieran Lyons	Kieran.lyons@Marine.ie	Marine Institute/Met Eireann, Galway, Ireland
		Caroline Cusack	caroline.cusack@Marine.ie	
4.13	Rockall Trough	N. Penny Holliday	penny.holliday@noc.ac.uk	National Oceanography Centre (NOC), Southampton UK
4.14	Hatton–Rockall Basin			
4.15	Iceland Basin	Sam Jones	Sam.Jones@sams.ac.uk	Scottish Association for Marine Science (SAMS), Oban, UK
4.16	Irminger Sea	M. Fremke de Jong	Femke.de.Jong@nioz.nl	Koninklijk Nederlands, Instituut voor Zeeonderzoek (NIOZ, Royal Netherlands Institute for Sea Research), Texel, Netherlands
4.17	Faroese waters and the Faroe–Shetland Channel	Karin Margretha H. Larsen	karinl@hav.fo	Havstovan (Faroe Marine Research Institute, FAMRI), Tórshavn, Faroe Islands
		Barbara Berx	B.Berx@MARLAB.AC.UK	Marine Scotland Science (MSS), Aberdeen, UK
		Jenny Hindson	J.Hindson@MARLAB.AC.UK	
4.18	North Sea	Holger Klein	Holger.Klein@bsh.de	Bundesamt für Seeschifffahrt und Hydrographie (BSH, Federal Maritime and Hydrographic Agency, Hamburg, Germany
		Peter Loewe	peter.loewe@bsh.de	
		Manuela Köllner	manuela.koellner@bsh.de	
		Katrin Latarius	katrin.latarius@bsh.de	
		Kjell Arne Mork	kjell.arne.mork@hi.no	Institute of Marine Research (IMR), Bergen, Norway
		Jon Albretsen	jon.albretsen@hi.no	

4.19	Skaggerak, Kattegat, and the Baltic Sea	Johanna Linders	johanna.linders@smhi.se	Swedish Meteorological and Hydrological Institute (SMHI), Göteborg, Sweden
		Tycjan Wodzinowski	tycjan@mir.gdynia.pl	National Marine Fisheries Research Institute (MIR-PIB), Gdynia, Poland
		Taavi Liblik	taavi.liblik@taltech.ee	Tallinn University of Technology, Estonia.
4.20	Norwegian Sea	Kjell-Arne Mork	kjell.arne.mork@hi.no	Institute of Marine Research (IMR), Bergen, Norway
4.21	Barents Sea	Alexander Trofimov	trofimov@pinro.ru	Knipovich Polar Research Institute of Marine Fisheries and Oceanography (PINRO),Murmansk, Russian Federation
		Randi Ingvaldsen	randi.ingvaldsen@imr.no	Institute of Marine Research (IMR), Bergen, Norway
4.22	Fram Strait	Agnieska Beszczynska-Möller	abesz@iopan.gda.pl	Institute of Oceanology, Polish Academy of Sciences (IOPAN), Sopot, Poland
		Wilken-Jon von Appen	Wilken-Jon.von.Appen@awi.de	Alfred Wegner Institute, Hermholtz Centre for Polar and marine Research (AWI), Bremehaven, Germany
5. Detailed Area Descriptions, Part II: The intermediate and deep ocean				
5.1.1	Greenland Sea	Agnieska Beszczynska-Möller	abesz@iopan.gda.pl	Institute of Oceanology, Polish academy of sciences (IOPAN), Sopot, Poland
5.1.2	Norwegian Sea	Svein Østerhus	svos@norceresearch.no	Norwegian Research Institute (NORCE), Bergen
5.1.3	Iceland Sea	Sólveig R. Ólafsdóttir	solveig.rosa.olafsdottir@hafogvatn.is	Hafrannsóknastofnun (Marine and Freshwater Research Institute, MFRI), Hafnarfjörður, Iceland
		Magnus Danielsen	magnus.danielsen@hafogvatn.is	

5.2.1	Greenland–Scotland Ridge overflow waters	Barbara Berx	B.Berx@MARLAB.ac.uk	Marine Scotland Science (MSS), Aberdeen, UK
		Jenny Hindson	J.Hindson@MARLAB.AC.UK	
5.2.2 5.2.3	Iceland Basin Rockall Trough	N. Penny Holliday	penny.holliday@noc.ac.uk	National Oceanography Centre (NOC), Southampton UK
		Sam Jones	Sam.Jones@sams.ac.uk	Scottish Association for Marine Science (SAMS), Oban, UK
5.2.4	Irminger Basin	M. Fremke de Jong	Femke.de.Jong@nioz.nl	Koninklijk Nederlands, Instituut voor Zeeonderzoek (NIOZ, Royal Netherlands Institute for Sea Research), Texel, Netherlands
5.2.5	Labrador Basin	Igor Yashayaev	Igor.Yashayaev@dfo-mpo.gc.ca	Ocean Monitoring and Observation Section, Bedford Institute of Oceanography, Fisheries and Oceans (BIO), Bedford, Canada
		Boris Cisewski	boris.cisewski@thuenen.de	Thünen-Institut für Seefischerei (TI-SF, Thünen Institute of Sea Fisheries), Bremehaven, Germany
5.2.6	Western Iberian Basin	Cesar González-Pola	cesar.pola@ieo.es	Instituto Español de Oceanografia (IEO, Spanish Institute of Oceanography), Gijón Oceanographic Centre, Gijón, Spain
5.2.7	Gulf of Cadiz	Ricardo Sánchez-Leal	rleal@ieo.es	Instituto Español de Oceanografía (IEO, Spanish Institute of Oceanography), Cádiz Oceanographic Centre, Cádiz, Spain
5.2.8	Canary Basin	Pedro Vélez-Belchí	pedro.velez@ieo.es	Instituto Español de Oceanografia (IEO, Spanish Institute of Oceanography), Canary Islands Oceanographic Centre, Tenerife, Spain
IROC Database and IROC-online management and support				
		Hjalte Parner	hjalte@ices.dk	International Council for the Exploration of the Sea (ICES), Copenhagen, Denmark

Annex 3: List of abbreviations

AI	Atlantic Inflow
AIW	Arctic Intermediate Water
ARGO	Not an acronym, but the name of a type of instrument used to collect data. The name ARGO is a reference to Greek mythology.
Argo-GDAC	Argo - Global Data Assembly Centres
AW	Atlantic Water
BSH	Bundesamt für Seeschifahrt und Hydrographie (German Federal Maritime and Hydrographic Agency)
CCLME	Canary Current Large Marine Ecosystem
CIL	Cold Intermediate Layer
CIRES	Cooperative Institute for Research in Environmental Sciences, USA
CTD	Conductivity Temperature Depth
CTZ	Coastal Transition Zone
DSOW	Denmark Strait Overflow Water
EGC	East Greenland Current
ENACW	Eastern North Atlantic Central Waters
GSDW	Greenland Sea Deep Water
ICES	International Council for the Exploration of the Sea
Ifremer	Institut Français de Recherche pour l'Exploitation de la Mer (French Institute for Ocean Research)
IROC	ICES Report on Ocean Climate
ISAS	*In Situ* Analysis System
ISOW	Iceland-Scotland Overflow Water
LME	Large Marine Ecosystem
MNAW	Modified North Atlantic Water
MW	Mediterranean Waters
NAC	North Atlantic Current
NACW	North Atlantic Central Waters
NADW	North Atlantic Deep Waters
NAO	North Atlantic Oscillation
NAW	North Atlantic Water
NOAA	National Oceanic and Atmospheric Administration (USA)

NRT	Near Real Time
OI	Optimal Interpolation
OISST.v2	Optimum Interpolation SST dataset version 2
RAC	Return Atlantic Current
RAW	Return Atlantic Water
s.d.	Standard deviation
SLP	Sea Level Pressure
SST	Sea Surface Temperature
SSS	Sea Surface Salinity
UPDW	Upper Polar Deep Water
WGC	West Greenland Current
WGOH	ICES Working Group Oceanic Hydrography
WGWIDE	ICES Working Group on Widely Distributed Stocks
WOA5	World Ocean Atlas 05
WSC	West Spitsbergen Current